POLYMORPHS, CYCLODEXTRIN INCLUSION COMPLEXES AND SALTS OF THE BRONCHODILATOR TULOBUTEROL

By: Clive Lloyd Oliver

Thesis Presented for the Degree of

DOCTOR OF PHILOSOPHY

in the Department of Chemistry

Faculty of Science

UNIVERSITY OF CAPE TOWN

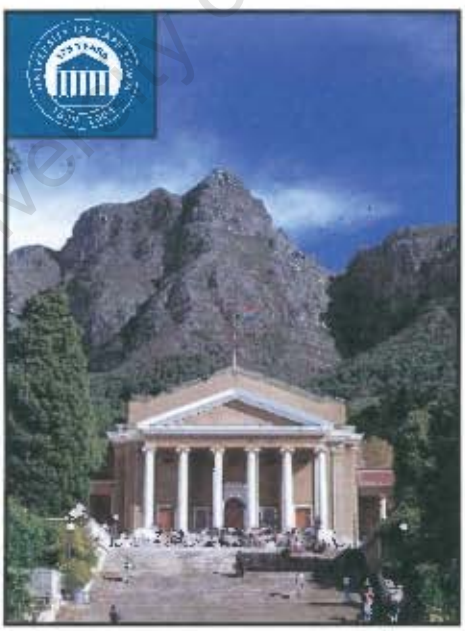

September 2004

Acknowledgements

My special thanks to:

my supervisors, Professor Mino Caira and Associate Professor Susan Bourne, for their excellent supervision and expertise that are second to none. I am truly indebted to them for pushing me beyond my limits!

the Head of the Supramolecular Chemistry Group at the University of Cape Town, Professor Luigi Nassimbeni, for being a constant source of inspiration to me

Dr J. Bacsa and Dr H. Su for single crystal X-ray diffraction data collected on the Kappa CCD diffractometer

the members of the University of Cape Town Supramolecular Chemistry Group for their assistance during my project, especially Mr V. Smith, and making my daily working environment extremely pleasant

the National Research Foundation and the University of Cape Town for financial support during my studies

my parents, Andrew and Vera, my sisters, Anthea-Lynn and Tracey-Lee, for their constant love and asking, 'So exactly what do you study?'

my dear Michellé for her love and support whilst listening to and advising me on all the daily trials and tribulations that this project has thrown my way

Journal Articles Published and Conferences Attended

Journal articles published:

1. M. R. Caira, S. A. Bourne, C. L. Oliver, Thermal and structural characterisation of two polymorphs of the bronchodilator tulobuterol, *J. Therm. Anal. Calorim.*, **2004**, 77, 597-606.

Conferences attended:

1. 2nd International Conference on Pharmaceutical and Pharmacological Sciences, 3-6 October **1999**, Cape Town, South Africa.
   Poster presentation: Inclusion of the bronchodilator tulobuterol in permethylated β-cyclodextrin
   C. L. Oliver, M. R. Caira, S. A. Bourne

2. Annual Meeting of the South African Crystallographic Society, September **1999**, University of Witwatersrand, Johannesburg, South Africa
   Poster presentation: Inclusion of the bronchodilator tulobuterol in permethylated β-cyclodextrin
   C. L. Oliver, M.R. Caira, S.A. Bourne

3. 21st Annual Congress of the Academy of Pharmaceutical Sciences, 10-13 September **2000**, Rhodes University, Grahamstown, South Africa
   Poster: Polymorphism of the bronchodilator tulobuterol
   C. L. Oliver, M. R. Caira, S. A. Bourne

4. The American Association of Pharmaceutical Scientists Annual Meeting and Exposition, 21-25 October **2001**, Denver, Colorado, U.S.A.
   Poster presentation: Polymorphism of the bronchodilator tulobuterol
   C. L. Oliver, M. R. Caira, S. A. Bourne

5. Annual Meeting of the South African Crystallographic Society, 4-5 April **2002**, University of Stellenbosch, Stellenbosch, South Africa
   Oral presentation: Polymorphism of the bronchodilator tulobuterol
   C. L. Oliver, M. R. Caira, S. A. Bourne

6. 21st European Crystallographic Meeting, ECM-21, 24-29 August **2003**, Durban, South Africa.
   Oral presentation: Polymorphism of the bronchodilator tulobuterol.
   C. L. Oliver, M. R. Caira, S. A. Bourne

7. 24th Annual Congress of the Academy of Pharmaceutical Sciences, 7-10 September **2003**, Durban, South Africa.
   Poster presentation: Inclusion of the bronchodilator tulobuterol in parent and methylated cyclodextrins
   C. L. Oliver, M.R. Caira, S.A. Bourne

Abstract

Polymorphs, Cyclodextrin Inclusion Complexes and Salts of the Bronchodilator Tulobuterol, Clive Lloyd Oliver, September 2004

The aim of this thesis was to prepare polymorphs, cyclodextrin inclusion complexes and salts of tulobuterol, a drug with bronchodilating properties. Polymorphic drugs are of interest to the pharmaceutical industry because of their varied physical properties, whilst the increase in aqueous solubilities of drugs by their inclusion within cyclodextrins or by salt formation is also an important pharmaceutical consideration.

Two polymorphs, four cyclodextrin inclusion complexes and three salts of tulobuterol free base were successfully generated in this study. The cyclodextrin hosts used for drug inclusion were β-cyclodextrin, γ-cyclodextrin, heptakis(2,6-di-O-methyl)-β-cyclodextrin and heptakis(2,3,6-tri-O-methyl)-β-CD, whilst (R,R)-tartaric acid, succinic acid and benzoic acid were used for tulobuterol salt formation.

The solid-state properties of the species were characterised by elemental analysis, thermal, X-ray diffraction and spectroscopic techniques. The stability relationship between the two polymorphs was established as monotropic, i.e. the higher melting polymorph is the thermodynamically stable form at all temperatures below the melting temperatures of the polymorphs. The structures of the polymorphs revealed a common asymmetric unit consisting of three tulobuterol molecules associated by strong, classical hydrogen bonds as a cyclic trimer. Structure solution was successful for three cyclodextrin inclusion complexes. The tulobuterol guest molecule was successfully modelled in only the heptakis(2,3,6-tri-O-methyl)-β-CD inclusion complex, whilst those for the β- and γ-cyclodextrin inclusion complexes were not modelled due to severe disorder. The salts share common structural features with each other and with other β-adrenergic agents containing an ethanolamine side chain.

The chemistry and potential pharmaceutical application of tulobuterol have been extended beyond their current scope by the novel species prepared in this study. These may serve as viable alternatives to the currently marketed hydrochloride salt.

Abbreviations and Symbols

Compounds

CD	cyclodextrin
β-CD	beta-cyclodextrin
γ-CD	gamma-cyclodextrin
DIMEB	heptakis(2,6-di-O-methyl)-beta-cyclodextrin
TRIMEB	heptakis(2,3,6-tri-O-methyl)-beta-cyclodextrin
BCDTUL	β-CD·tulobuterol inclusion complex
GCDTUL	γ-CD·tulobuterol inclusion complex
DMBTUL	DIMEB·tulobuterol inclusion complex
TMBTUL	TRIMEB·tulobuterol inclusion complex
TULTAR	tulobuterol salt of (R,R)-tartaric acid
TULSUC	tulobuterol salt of succinic acid
TULBEN	tulobuterol salt of benzoic acid

Techniques

HSM	hot stage microscopy
DSC	differential scanning calorimetry
TGA	thermogravimetric analysis
PXRD	powder X-ray diffraction
FTIR	Fourier transform infrared spectroscopy
NMR	nuclear magnetic resonance
SSNMR	solid-state NMR spectroscopy

Symbols

CSD	Cambridge Structural Database
E	normalised structure factor
S	goodness of fit (F^2)
s. o. f.	site occupancy factor
T	Temperature
T_{on}	Onset temperature
μ	linear absorption coefficient
Z	number of formula units in the unit cell

Table of Contents

Chapter 1 - Introduction

Chapter 2 - Experimental and Computational Methods

Chapter 3 - Tulobuterol Polymorphs

Chapter 4 - β-CD and γ-CD Inclusion Complexes

Chapter 5 - DIMEB and TRIMEB Inclusion Complexes

Chapter 6 - Tulobuterol Salts

Chapter 7 - Conclusion

Chapter 1 - Introduction

Supramolecular Chemistry

The scope of this thesis falls under the broad discipline of supramolecular chemistry, which was referred to by J-M. Lehn[1] in his Nobel lecture as "chemistry beyond the molecule". Simply put, supramolecular chemistry is the study of non-covalent interactions between molecules, ions or radicals. This includes, amongst others, hydrogen bonding, π···π, C-H···π, van der Waals and hydrophobic interactions. The discovery of the first inclusion compound $Cl_2{\cdot}6H_2O$ in 1810 by H. Davy[2] is considered to have initiated the discipline but it was the discovery of X-rays and their use in structure analysis in 1895 and 1912 respectively that spawned growth in this field. In this thesis the polymorphism, cyclodextrin inclusion and salt formation of tulobuterol, a drug with bronchodilating properties, will be treated. Although polymorphs and salts are not inclusion compounds, non-covalent interactions play a vital role in their respective identities and therefore their study also falls within the field of supramolecular chemistry. Dunitz has in fact referred to different modifications of a polymorphic drug as 'supramolecular isomers'.[3]

Polymorphism

Polymorphism is the solid-state phenomenon whereby a chemical compound crystallises in more than one form. These forms are chemically identical but differ in the way the molecules in each polymorph pack. If there is a remarkable difference between the conformations of the molecules in the respective forms it is referred to as conformational polymorphism.[4] Species with included solvent molecules are referred to as solvates.[5] When the material exhibits no long-range order it is referred to as amorphous. In the literature, polymorphs are labelled with Arabic (1, 2, 3,...) or Roman (I, II, III,...) numerals, lower or upper case Latin (a, b, c,... or A, B, C,...) or lower case Greek (α, β, γ,...) letters.[6] In this thesis the Arabic labelling will be used except when referring to polymorphs in the literature, which have their own specific labelling. The concept of polymorphs and solvates is illustrated graphically in Figure 1.1.

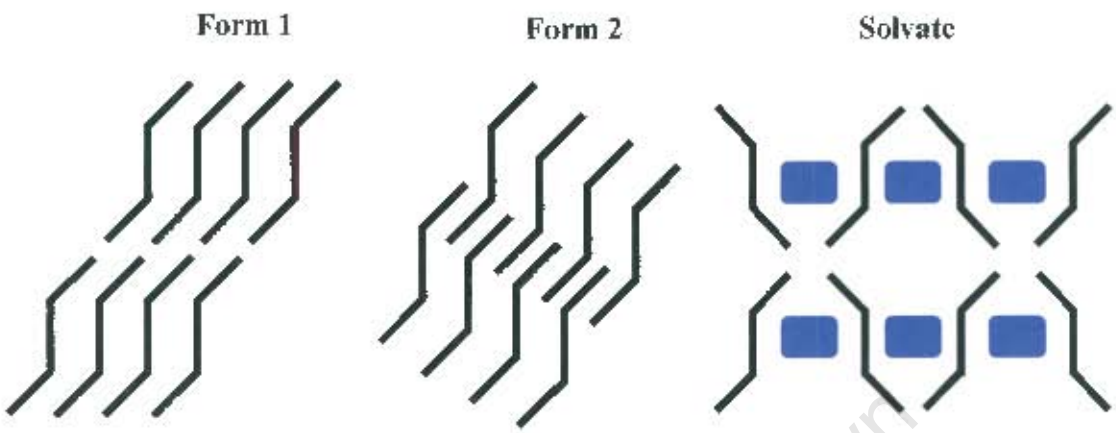

Figure 1.1 Schematic diagram illustrating the definition of polymorphism for rigid molecules. ■ represents a solvent molecule.

The importance of polymorphism in a number of industrial and commercial applications is paramount and is a direct result of differences in physical properties that accompany differences in structure.[7] Physical properties for which differences are observed include melting points, solubilities, dissolution rates and stabilities, to mention but a few.

Brief Historical Overview

The first recognition of the phenomenon of polymorphism is credited to Mitscherlich[8] who in 1822 discovered that the salt $NaH_2PO_4{\cdot}H_2O$ crystallises with different crystal morphologies. He attributed these morphological variations to differences in the internal structural arrangements of the constituent ions. This was before the dawn of X-ray crystallography and the phenomenon was then largely investigated by the microscope and subsequently also with the polarizing microscope[9] invented in 1844.[10] With the recognition of different forms of the same compound, investigations into their stability relationships naturally followed. In 1839, Frankenheim suggested principles for the transition of one polymorph into a second[10] whilst Lehman coined the irreversible and reversible transitions as *monotropic* and *enantiotropic* respectively.[11] Subsequently Ostwald, in 1897, used thermodynamics to address the relative stabilities of polymorphs, some of his important findings being that the metastable form has the higher solubility

and crystallises first, eventually transforming via a solution-mediated process into the stable form.[12] With the advent of X-ray crystallography it was Tammann that considered polymorphs as identical molecular species arranged on different lattices.[13] This serves today as the basic criterion for identifying polymorphism.

Relevance

Polymorphism may have important health and economical consequences, which have provided some of the driving forces for the study of this phenomenon. A recent dramatic example occurred when the production of the HIV protease inhibitor, ritonavir, had to be temporarily halted by Abbott in 1998, due to the appearance of an undesired form of the drug during its manufacturing process.[14] It had health consequences since the undesired form, a thermodynamically more stable polymorph than the original form, severely affected the dissolution of the semi-solid capsule. The economic consequences were that the company had to spend extra time and expense in rectifying problems arising out of the inadvertent production of an undesired form. Polymorphism also plays an especially significant role in the fat-based food industries where the melting point and melting characteristics are of particular importance.[15] Drug polymorphs have also been the cause of many litigation battles between pharmaceutical companies in recent years. The polymorphism of blockbuster drugs like ranitidine hydrochloride and cefadroxil have been the subject of these intense legal battles.[16]

Theoretical Background

Thermodynamics

The thermodynamic investigation of a polymorphic system presents valuable insight into the key question of the stability relationships and the effect that these have on phase changes. Buerger laid down the fundamentals for this investigation.[17]

Enantiotropy vs monotropy

Enantiotropy and monotropy, mentioned earlier, are terms used to describe the reversibility [or lack of reversibility] of the phase transition between polymorphs.[11] Phase

transitions are restricted thermodynamically to occur spontaneously in the direction of the stable form only. This means that an irreversible phase transition [monotropy] implies that one form is the thermodynamically stable form at all temperatures. A reversible phase transition [enantiotropy] implies the presence of a transition point where the stability order of the polymorphs is reversed. The most widely used thermodynamic relationship for the treatment of this question is:

$$G = H - TS \qquad (1)$$

where G = Gibbs free energy, H = enthalpy, T = absolute temperature and S = entropy. This relationship is used to construct diagrams that illustrate the variation of G and H with temperature to establish the stability relationship of polymorphs from 0K to just beyond their melting temperatures. Figure 1.2 illustrates these stability relationships where the subscripts '1' and '2' denote the polymorph to which the function refers [the lower melting polymorph is denoted '2'], whilst 'L' refers to the supercooled liquid. The subscripts 'f' and 'tr' refer to 'fusion' and 'transition' respectively.

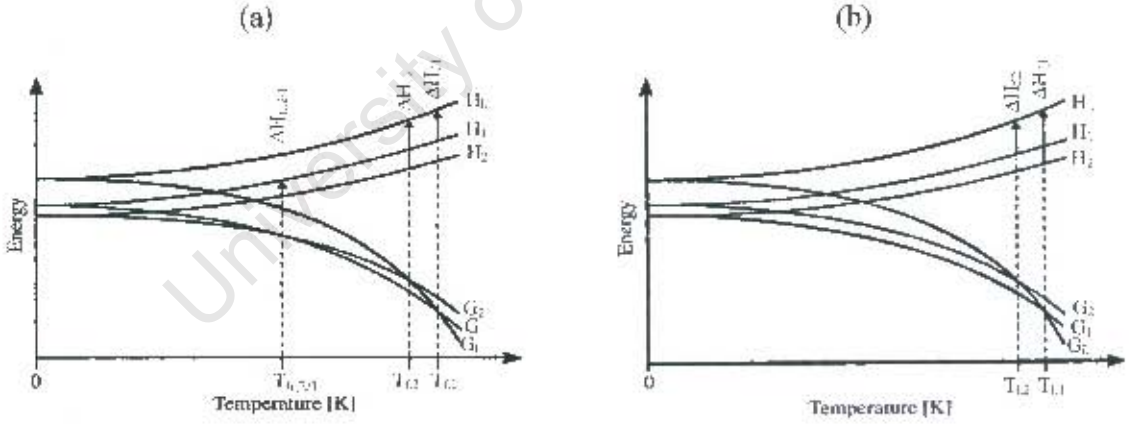

Figure 1.2 Semi-schematic diagrams showing the variation of G and H with temperature for (a) an enantiotropic and (b) a monotropic dimorphic system [adapted from reference 18]

The G curves can only have a negative slope and intersect at most once, whilst the H curves have a positive slope and it is assumed that they never intersect.[19] These conditions led to Burger and Ramberger to suggest the following rule:[20]

Heat of Transition Rule

If an endothermic phase change is observed at a particular temperature, the stability relationship is enantiotropic, otherwise it is monotropic [adapted from reference 20].

Burger and Ramberger also suggested several other rules in terms of various thermodynamic properties and these are presented in Table 1.1. The density and infrared rules must be applied with caution as exceptions to them have been found, as was pointed out by these authors.

Table 1.1 Rules for enantiotropy and monotropy[20,21,22,18]

Rule	Definition
Heat of Fusion Rule	If the higher melting polymorph has the higher heat of fusion, the stability relationship is monotropic, otherwise it is enantiotropic.
Entropy of Fusion Rule	If the higher melting polymorph has the higher entropy of fusion, the stability relationship is monotropic, otherwise it is enantiotropic.
Heat Capacity Rule	If the higher melting polymorph has the higher heat capacity at a given temperature then the stability relationship is enantiotropic, otherwise it is monotropic.
Density Rule	The more stable polymorph at 0K should have the higher density.
Infrared Rule	For polymorphs with strong hydrogen bonds the one with the larger frequency for the highest frequency infrared absorption band, will have the larger entropy.

The conclusions of Burger and Ramberger were based on statistical mechanical arguments of an ideal model of molecular crystals. Yu[23] used pure thermodynamical arguments to infer the stability relationship from melting data and derived thermodynamic formulae for calculating ΔG_0, the Gibbs free energy difference of the polymorphs, and their temperature slopes at the melting point of the lower melting polymorph. Extrapolation of the ΔG_0 temperature slopes to their point of intersection then

yields the transition temperature, T_{tr}. The advantage of Yu's treatment is that both the stability relationship and T_{tr} can be obtained from it. The equations necessary for the determination of the transition temperature for the process:

$$\textbf{Form 2 } (T_{f,2}) \rightarrow \textbf{Form 1 } (T_{f,2}) \tag{2}$$

are:

$$\Delta H_0 = \Delta H_{f,2} - \Delta H_{f,1} + (C_{p,L} - C_{p,1})\,(T_{f,1} - T_{f,2}) \tag{3}$$

$$\Delta S_0 = \Delta H_{f,2}/T_{f,2} - \Delta H_{f,1}/T_{f,1} + (C_{p,L} - C_{p,1})\,\ln(T_{f,1}/T_{f,2}) \tag{4}$$

and $$\Delta G_0 = \Delta H_{f,1}(T_{f,2}/T_{f,1} - 1) + (C_{p,1} - C_{p,1})[\,T_{f,1} - T_{f,2} - T_{f,2}\ln(T_{f,1}/T_{f,2})] \tag{5}$$

where the subscript 0 describes the function at the melting temperature of the lower melting form and $(C_{p,L} - C_{p,1})$ is the difference between the heat capacities of the supercooled liquid and Form 1 between the temperatures $T_{f,2}$ and $T_{f,1}$. If $\Delta G(T)$ has a linear dependence, then

$$\Delta G(T) = \Delta G_0 - \Delta S_0(T - T_{f,2}) \tag{6}$$

and the condition $$\Delta G(T_{tr}) = 0 \tag{7}$$

yields $$T_{tr} = \Delta H_0/\Delta S_0 \tag{8}$$

All the parameters for these equations are obtained directly from conventional differential scanning calorimetric data, except for the $(C_{p,L} - C_{p,B})$ parameter. Yu estimated the latter from the following derived equation:

$$k = (C_{p,L} - C_{p,1})/\Delta H_{f,1} \tag{9}$$

where the value of k, based on an empirical study of several polymorphic systems, is approximated to 0.003/K.[23]

Kinetic considerations

Kinetic factors may also determine the polymorphic form that crystallises from solution. Figure 1.4 illustrates a Gibbs free energy vs reaction coordinate graph for a dimorphic system. It shows that even though Form 1 is the thermodynamically stable polymorph, its higher associated Gibbs free energy of activation might prevent its formation. However, it is the rates of nucleation of the respective polymorphs that determine which one precipitates from solution and the associated Gibbs free energy of activation is merely one of the factors that determine these rates. Competitive kinetic and thermodynamic factors complicate the prediction of the form that will precipitate first. The concept of critical size is one of the key factors of kinetic nucleation as proposed by Volmer in 1939.[24] According to this concept a critical size of aggregated molecules must exist in solution before further growth is stabilised. This critical size is usually different for the respective polymorphs, which would thus account for different crystallisation rates. Some of the other factors influencing nucleation rates are molecular volume, surface free energy, temperature, degree of supersaturation and solubility.

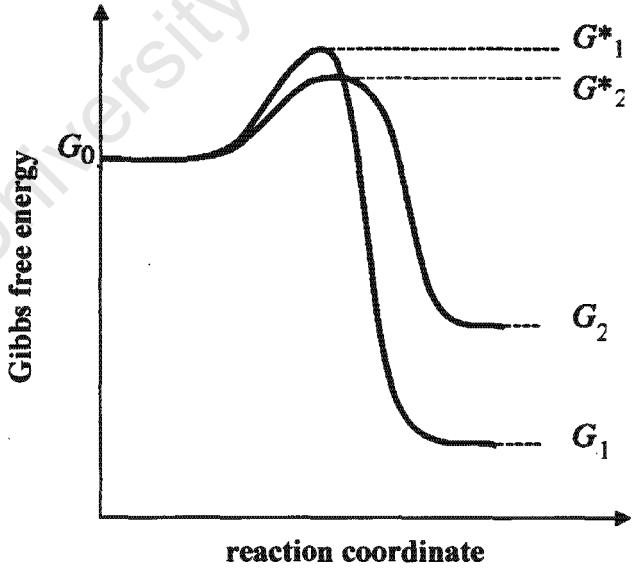

Figure 1.4 Free energy vs reaction coordinate diagram for two polymorphs [1,2] illustrating the influence of kinetics on their formation. G^*-G_0 represents the activation free energy for nucleation [adapted from reference 25]

Preparative Methods for Polymorphs

It has become incumbent upon manufacturers of pharmaceuticals to prove that they have investigated the potential polymorphism of their marketed drug so that an unwanted polymorph does not filter through to the consumer. Therefore it is important to know which methods are likely to yield polymorphs and to employ them in the search for potential polymorphs. It is commonly believed that the more time spent on attempting to produce a polymorph of a particular compound, the more likely is success. This is reflected in Walter C. McCrone's statement:

"Those who study polymorphism are rapidly reaching the conclusion that all compounds, organic and inorganic, can crystallize in different crystal forms or polymorphs. In fact, the more diligently any system is studied the larger the number of polymorphs discovered." Walter C. McCrone [1957][26]

Guillory suggested a number of methods for generating polymorphs, solvates or amorphous forms of a particular compound.[27] If none were to be found, even though it cannot be guaranteed that in future no new forms will arise, at least "due diligence" will have been exercised. Amongst these methods are sublimation, crystallisation from a single or binary solvent system, vapour diffusion, thermal treatment, crystallisation from the melt, rapid pH changes, thermal desolvation of crystalline solvates, growth in the presence of additives and grinding. Of these methods crystallisation from a variety of solvents is usually the first step in the search for polymorphic forms of a compound and has been very successful in many cases. In a review of crystal polymorphism,[28] Caira pointed out alternative methods for preparing the same polymorph, in particular desolvation of crystalline solvates, which resulted in the improvement of certain properties such as flowability and uniformity of particle size.

Polymorphic Control

Controlling the polymorphic form obtained is of obvious interest to the pharmaceutical industry. An understanding of the thermodynamic and kinetic factors discussed earlier is essential for this exercise. Bernstein pointed out a number of examples where

thermodynamic crystallisation conditions yield the stable form with kinetic conditions yielding metastable forms.[29] Once a particular form has been obtained a knowledge of the thermodynamics of the polymorphic system, e.g. in the form of energy vs temperature diagrams, is essential to provide information on the storage conditions necessary to prevent any unwanted transformations. The sophistication of the practical control of the crystallisation of a desired form may vary between simply reproducing the form with the same protocol as used before, to the rational design of auxiliaries that through selective molecular recognition may inhibit or suppress the growth of the undesired stable form, thus allowing the growth of the desired metastable form.[28] The latter strategy has enjoyed very limited success thus far, but one successful example has been the crystallisation of the metastable form of *N*-(2-acetamido-4-nitrophenyl)pyrrolidine by the addition of a small amount [0.03%] of the designed inhibitor.[30] Between these two extremes there are chemical and physical variations that have been used to produce specific polymorphs.[28] These include, amongst others, examples of polymorphs that have been produced from solutions seeded with the desired form,[31] successive chemical reactions,[32] desolvation of solvates,[33] and successive reheating and cooling strategies to produce a metastable form.[27]

Analytical Tools for the Study of Polymorphs

Once polymorphs of a compound have been found, several analytical methods are employed to characterise their individual properties as well as to see how these properties relate to each other [e.g. stability relationships]. These methods may include X-ray diffraction, thermal and spectroscopic studies, which are respectively used to characterise the polymorphs in terms of their structures, thermodynamic stabilities and spectral energies. The range of analytical techniques used should be as broad as possible as the information obtained from them is often complementary, as suggested by Bernstein.[34] Bernstein,[34] Brittain,[35] Caira[28] and Threlfall[36] have given extensive reviews on the analytical tools used in the study of polymorphs and the reader is referred to them for a more detailed discussion.

Structural Features

Structure is a fundamental property of polymorphs as it is this feature that differentiates them. Molecules in polymorphs may be fairly broadly separated into 'rigid' molecules and those with conformational 'flexibility'. In cases where different conformations of the molecules are adopted in different structures, the phenomenon is referred to as conformational polymorphism.[4]

Comparison of polymorphic structures is useful in that they might provide a structural picture of how transformation between them may be effected. However, this comparison is non-trivial and several methods have been applied in the past for this purpose. For polymorphs with no common unit cell parameters the traditional method was to prepare packing diagrams with a view down an arbitrary crystallographic axis but this usually conveyed little information about their similarities or differences. It is often more useful to choose a common molecular reference plane and orientate it the same for all the structures. This gives an indication of the immediate environment around the chosen reference plane.[38] Viewing down a common crystallographic axis, i.e. in polymorphic structures that have similar unit cell parameters and/or symmetry elements, may also allow a basis for comparison. The two polymorphic structures[37] of L-glutamic acid were compared in this manner, which revealed no similarities between them.[38]

The concept of graph set analysis has in recent years proved to be very useful in comparing polymorphic structures.[39,40] This concept is applied to hydrogen bonds which are very often a common feature of polymorphic structures. In this approach the hydrogen bonding is easily simplified and reduced to four basic patterns, viz. chains (**C**), rings (**R**), intramolecular hydrogen-bonded patterns (**S**) and other finite patterns (**D**). These designators are superscripted **a** and subscripted **d** for the number of hydrogen-bond acceptors and donors respectively. This is followed by the descriptor (**n**) which indicates the total number of atoms involved in the pattern. The general graph set descriptor is thus $\mathbf{G}_{\mathbf{d}}^{\mathbf{a}}(\mathbf{n})$ and examples of assignments are given in Figure 1.5.

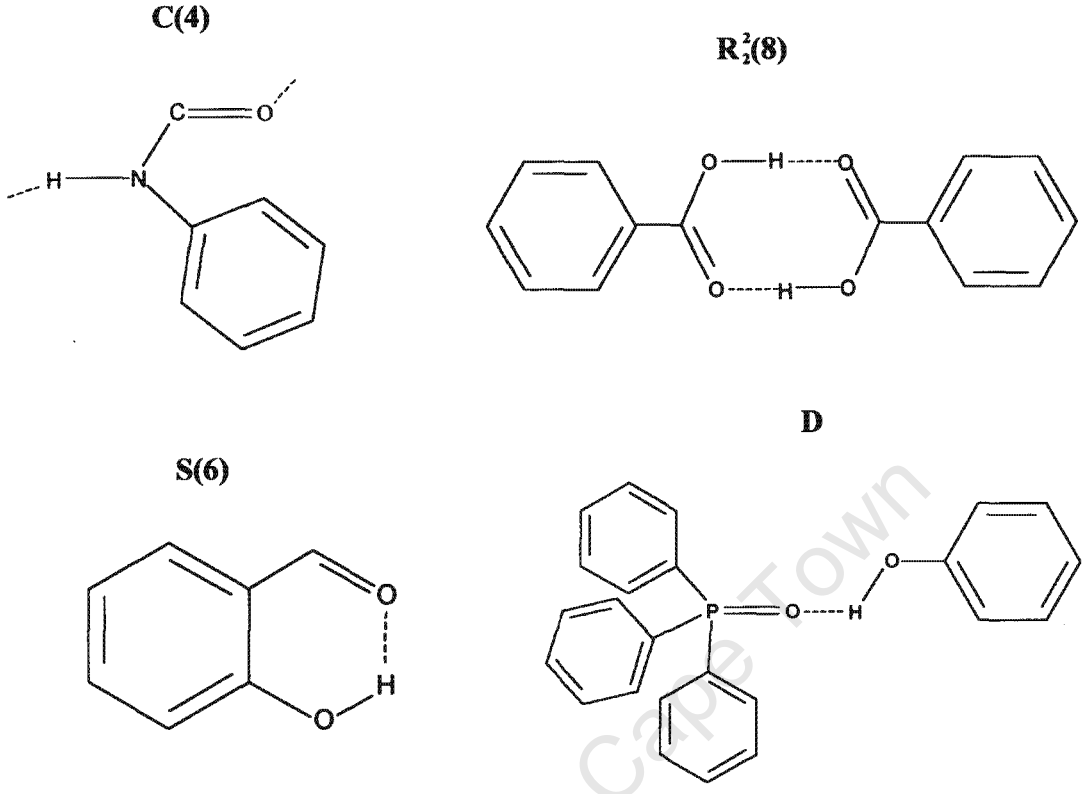

Figure 1.5 Schematic diagrams showing the four basic patterns using graph-set analysis. If no **a** , **d** or **(n)** descriptor is present, the value is assumed to be 1.

Polymorphism of pharmaceuticals, as stated earlier, may have important consequences in terms of their performance, e.g. their solubilities may have an impact on their bioavailabilities. The varying physical properties of polymorphs thus necessitate control over the form produced. However, this can prove costly. Inclusion of the drugs into cyclodextrins, effectively eliminates the need for this careful control, as 'new chemical entities' are formed and the polymorphic identity of the drug is removed. An overview of cyclodextrins in terms of their structure, properties, inclusion complexes and application in the pharmaceutical industry follows.

Cyclodextrins

Natural Origin of Cyclodextrins

Cyclodextrins [hereinafter CDs] are cyclic oligosaccharides that are the products of an enzymatic process of the degradation of amylose, a linear unbranched fraction of starch. The enzyme used in the process, cyclodextrin glucotransferase [CGTase], was first isolated from the microbe *Bacillus macerans*.[41] CDs are also known as Schardinger dextrins, cycloamyloses and cycloglucoamyloses. The cyclic oligosaccharides consist of glucopyranose units that may vary in number due to the unspecificity of the enzyme action.[41,42] However, the most commonly produced CDs are those with six, seven and eight glucopyranose units, known as α-, β- and γ-CD respectively [Figure 1.6]. Larger cyclodextrins have been prepared,[43] but it has been predicted that smaller ones cannot be formed due to severe steric strain,[44] though the synthesis of a five-membered CD[45] has been reported.

Brief Historical Overview

Villiers is credited with the first publication of a substance [he named it a 'cellulosine'] that later proved to be a cyclodextrin.[46] However, it was Schardinger with publications between 1904-1911 who is credited with laying down the fundamentals of cyclodextrin chemistry [he referred to the compounds as dextrins].[47,48,49,50] Freudenberg *et al.*[51,52,53] as a result of their own experiments as well as observations published by Karrer and Nägeli,[54] and Miekeley,[55] postulated that the dextrins contain α-1,4-glycosidic linkages which, in 1936, they proposed to be cyclic.[56] In the 1950s, French[57] and Cramer[42] were responsible for the enzymatic production of cyclodextrins and characterising their physical and chemical properties. By the end of the 1960s the physical and chemical properties of cyclodextrins had been characterised and their ability to form inclusion complexes with improved properties, such as solubility and volatility, of the included chemical had been recognised.[58] But it was only after competent toxicological studies had been performed that these compounds took off industrially to a point where at present they are used in the food, pharmaceutical, biomedical and analytical industries, to mention but a few.[58]

Structural Features

Figure 1.6 presents schematic diagrams of the glucopyranose unit atom labelling and the native CDs. The glucopyranose units are almost invariably in the $^4C_1$-chair conformation and their conformations are fairly rigid,[59,60,61] except for the rotational freedom of the O6 atom around the C5-C6 bond. The cyclodextrin molecule is therefore also fairly rigid except for the limited rotational freedom around the C1-O4'-C4' glycosidic link [primed numbers refer to the next glucopyranose unit].

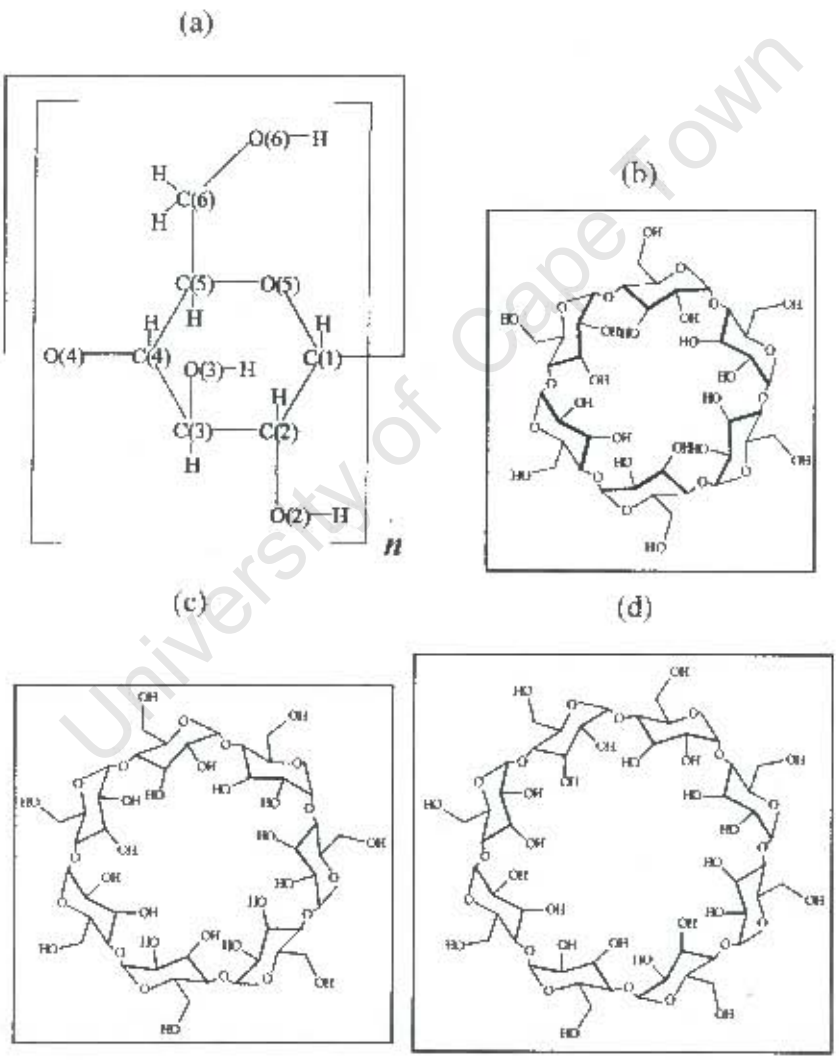

Figure 1.6 Schematic diagram of (a) glucopyranose unit labelling, (b) α-CD (c) β-CD and (d) γ-CD

Hydrogen bonding

All the glucopyranose units are orientated *cis* relative to one another and therefore intramolecular hydrogen bonding between O2 and O3 of adjacent units is observed. This hydrogen bonding has been elucidated to be of a 'flip-flop' nature by neutron diffraction studies,[62,63] i.e. they oscillate between O2-H···O3' and O2···H-O3' hydrogen bonds. The hydrogen bonding strengthens with an increase in the number of units [O···O distances of 3.05, 2.92 and 2.84Å for α, β and γ-CD respectively].[61] The hydrogen bonding is also responsible for the stabilisation of the CD on the secondary side and explains why tri-methylated β-CD, which lacks this hydrogen-bonding, is more flexible.[64]

Conformation of cyclodextrins

There are three types of torsion angles that describe important conformational aspects of the glucopyranose units of a CD molecule. These are the primary, glycosidic and pyranoid torsion angles. The primary hydroxyl torsion angle, ω [O5-C5-C6-O6], describes the rotation around the C5-C6 bond, indicating the direction of the C6-O6 bond. This angle is assigned as (+)-*gauche* or (-)-*gauche* depending on whether the C6-O6 bond points towards or away from the CD cavity respectively. The *trans* and *syn* conformations are not observed for steric reasons. There are two glycosidic torsion angles, that describe the rotation around the C1-O4'-C4' linkage, and these are defined as Φ [O5-C1-O4'-C4'] and ψ [C1-O4'-C4'-C3']. The pyranoid torsion angles Θ_1 [C2-C3-C4-C5] and Θ_2 [C3-C4-C5-O5] describe the conformational relationships around the C4 atom. The glucopyranose units of CDs are invariably in the $^4C_1$ chair conformation. Table 1.2 lists the mean values for principal torsion angles for the three most common native CDs.

Table 1.2 Mean values for principal torsion angles [°]

CD	ω[65]	Φ[66]	ψ[66]	Θ_1[66]	Θ_2[66]
α	68	108	130	52	-53
β	64	112	128	56	-56
γ	68	110	130	62	-62

Saenger[60] and Harata[61] defined parameters for describing the macrocyclic symmetry of CD molecules. The O4 atoms are used to construct polygons that define several parameters describing the macrocyclic symmetry of a CD molecule. These parameters are illustrated schematically for α-CD in Figure 1.7.

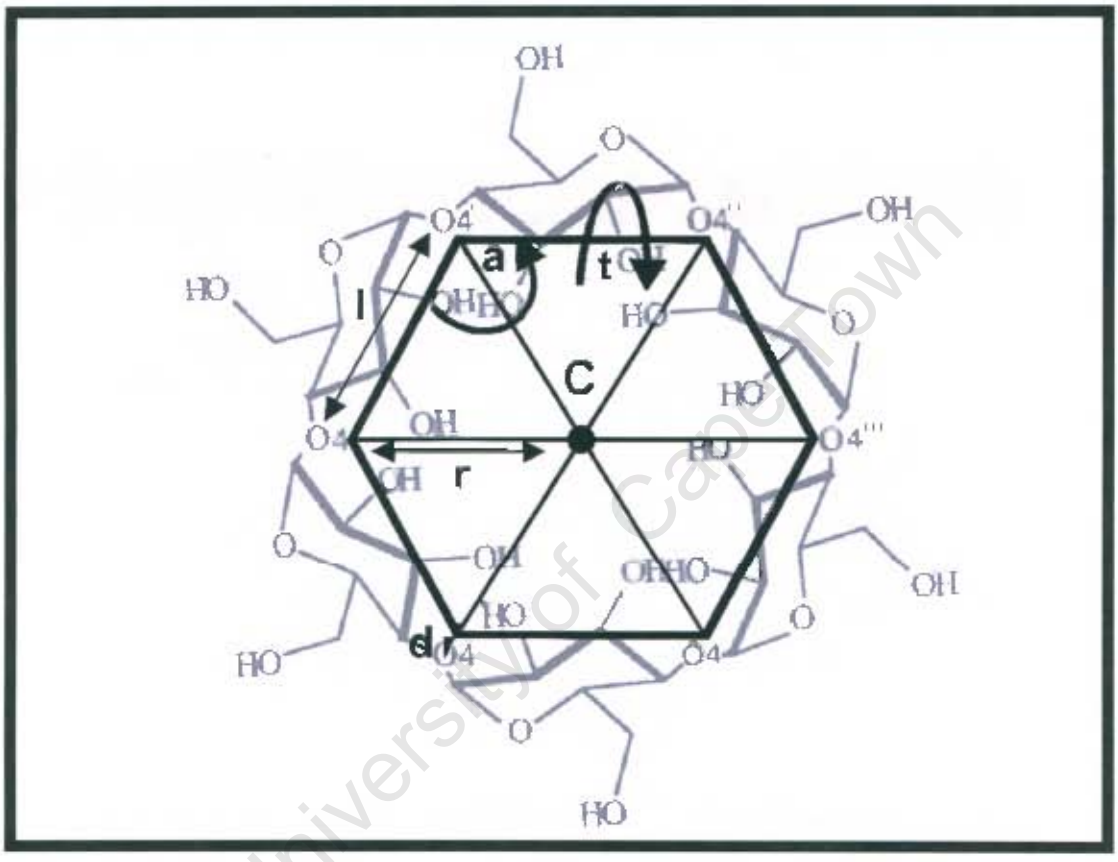

Figure 1.7 Schematic diagram of the O4 polygon for α-CD

The parameters are the O4 distance to the polygon centroid, **r** [the centroid is abbreviated as **C** in Figure 1.7], the O4···O4' distance, **l**, the O4···O4'···O4'' angle, **a**, the O4···O4'···O4''···O4''' torsion angle, **t**, and the deviation of each atom from the mean O4 plane, **d**. Other useful parameters that are not directly defined by this polygon are the O2···O3' distance, the intersaccharidic bond angle, **ϕ**, defined by C1'-O4-C4, and the tilt angle of a glucopyranose unit which can be defined in two ways. The first tilt angle definition τ_1[67] is the angle that the mean plane through atoms C1, C2, C3, C4, C5 and O5 makes with the line orthogonal to the O4 mean plane, whilst the second tilt angle

definition τ_2[68] is the angle that the mean plane through atoms O4, C4, C1 and O4' makes with the O4 mean plane. Ideally, both definitions should yield the same values but this is often not the case due to the slight distortions of the glucopyranose units. Positive values and negative values for the tilt angles indicate that the glucopyranose units on the primary side tilt towards and away from the cavity respectively. Comparisons of all the above defined parameters are listed for α, β and γ-CD in Table 1.3.

Table 1.3 Structural parameters for α-CD, β-CD and γ-CD

Parameter	α-CD	β-CD	γ-CD
O4···C / r [Å][71]	4.2	5.0	5.9
O4···O4' / l [Å][71]	4.2	4.3	4.5
O4···O4'···O4'' / a [°][65]	120	128	132
O4···O4'···O4''···O4''' / t [°][65]	5	5	2
Planarity of O4 polygon / d [Å][73]	0.07	0.08	0.02
O2···O3' [Å][67]	3.05	2.92	2.84
C1'-O4-C4 / ϕ [°][67]	118.4	117.7	115.0
Tilt angle / τ_1 [°]	−11.4	−9.5	−14.5
Tilt angle / τ_2 [°]	+13[69]	−14[70]	−17[71]

Hydrophobic and Hydrophilic Character of Cyclodextrins

Figure 1.8 is a schematic representation of the native CDs as well as their physical dimensions. The secondary and primary hydroxyl groups are on opposite sides of the CD and these sides are thus denoted the secondary and primary faces respectively. The primary face is narrower, therefore giving the CD the shape of a 'truncated cone'. This is a result of the O2-H···O3' and O2···H-O3' intramolecular hydrogen bonds which widen the secondary sides of the CDs. The presence of the hydroxyl groups on the outside of the CD is responsible for its solubility whilst the glycosidic O4 atoms and hydrogen atoms of the methine [those of C3 and C5] and methylene [those of C6] that line the inner wall of the CD are responsible for the hydrophobic character of the cavity. There is also a dipole

moment parallel to the pseudo-symmetry axis as a result of there being twice the number of hydroxyl groups on the secondary side when compared to the primary side.

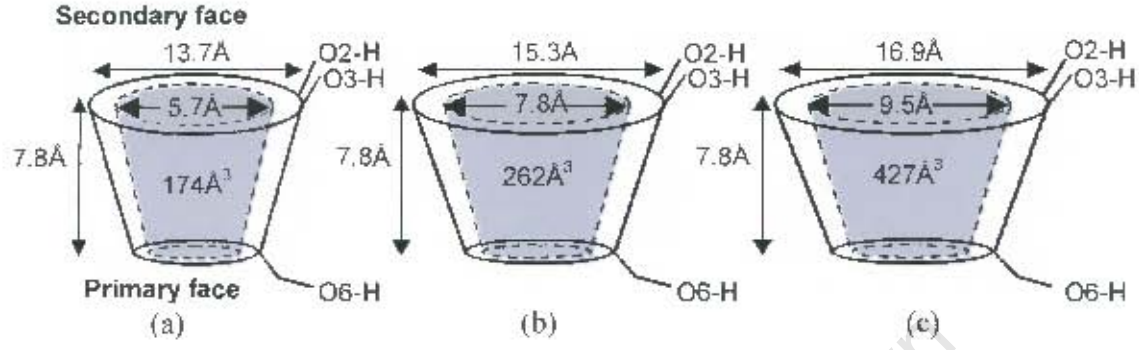

Figure 1.8 Schematic diagram illustrating physical dimensions of (a) α-CD, (b) β-CD and (c) γ-CD [adapted from reference 72]

Cyclodextrin Inclusion Complexes

Driving forces for complexation

As alluded to earlier, the formation of cyclodextrin inclusion complexes, and their associated advantages, were known by the end of the 1960s. The driving forces for inclusion are not entirely understood but there are several factors that are thought to contribute to the overall process.[73,74] One of the initially implicated factors was thought to be a replacement of 'high-enthalpy' water molecules with the relatively more hydrophobic guests, as illustrated in Figure 1.9. These apolar-apolar interactions were thought to be energetically more favourable than the polar-apolar interactions when the cavity is occupied by water. The other forces such as van der Waals, hydrogen-bonding and hydrophobic interactions as well as CD strain release on complexation were thought to be the secondary forces. However, a recent review of the driving forces in the inclusion complexation of CDs,[75] assigns more weight to the latter forces [except for the release of conformational strain] than to the exclusion of cavity-bound water, and found that enthalpy and entropy changes of complexation were not good criteria for judging the effect of a driving force, due to the enthalpy-entropy compensation that takes place.

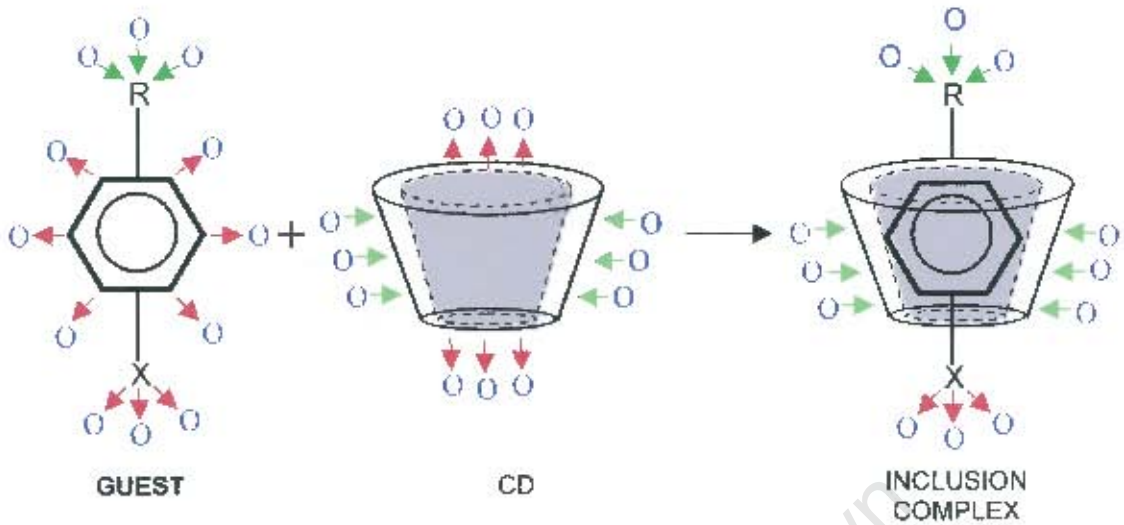

Figure 1.9 Schematic diagram of the inclusion of guest and expulsion of water [O] on inclusion complex formation. The green arrows [→]indicate attractive interactions of water with hydrophilic portions, whilst the red arrows [→] indicate repulsive interactions of water with hydrophobic portions. [adapted from reference 72]

Guest orientation

The orientation of the guest is determined by size and shape, dipole alignments and hydrophobic attractions. The end of the guest molecule that best fits into the cavity could be a determining factor in guest orientation in the CD cavity. The native CDs also exhibit dipole moments as a result of the greater number of hydroxyl groups on the secondary rim of the CD. The dipole moments of aromatic guest molecules have been observed to be anti-parallel to that of their host CDs.[76,77] Careful analyses of computer-generated molecular lipophilicity patterns [MLPs] have shown that there is a close relationship between the hydrophobic and hydrophilic regions of CDs and the guests that they include.[78] Figure 1.10 shows MLPs for the native CDs with dark blue and yellow regions representing hydrophilic and hydrophobic regions respectively. These show that the inner walls of the cavity are hydrophobic whilst the secondary rim is more hydrophilic than the primary rim. The hydrophobic part of the guest aligns with the hydrophobic cavity and the polar group is located close to the secondary hydroxyls or even on the outside of the cavity. These patterns are reversed with per-O-methylated CDs and thus the guest orientations are usually reversed within the cavities of these hosts.

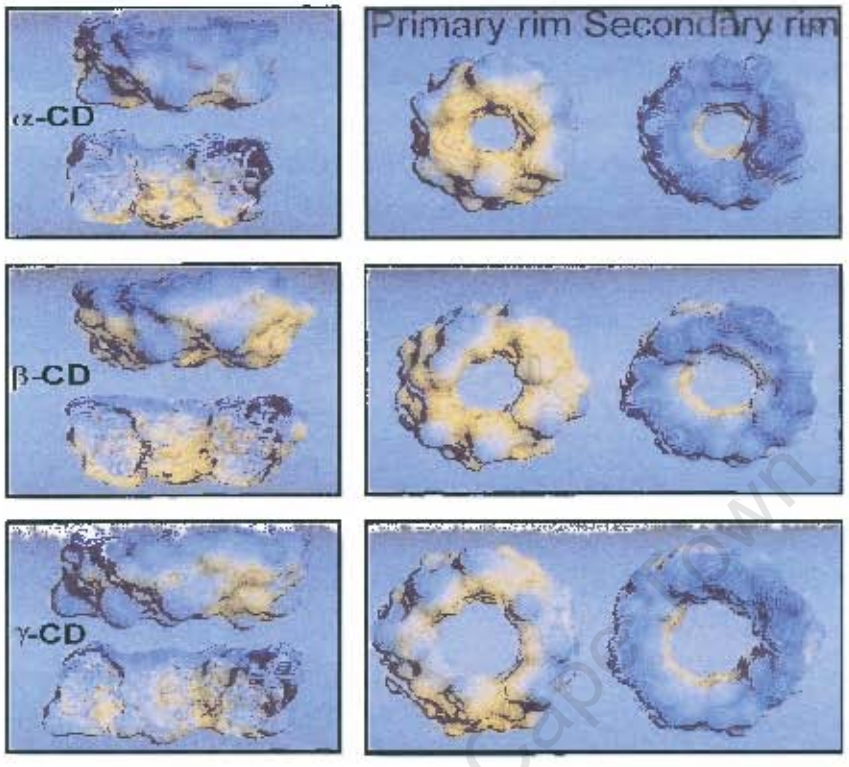

Figure 1.10 MLPs of α-CD (top), β-CD (middle) and γ-CD (bottom). Pictures on the left are views of closed and bisected CDs with the secondary rim on top. Pictures on the right are views onto the primary and secondary rims. [adapted from reference 67]

Methylated Cyclodextrins

Native cyclodextrins have low solubilities, especially in the case of β-CD,[41,79] and have been chemically modified to increase their solubilities. β-CD has been methylated for this purpose at the O2 and O6 positions to form heptakis(2,6-di-O-methyl)-β-cyclodextrin [DIMEB], and additionally at the O3 position to form heptakis(2,3,6-tri-O-methyl)-β-cyclodextrin [TRIMEB]. The structural modifications to the glucopyranose unit are presented in Figure 1.11.

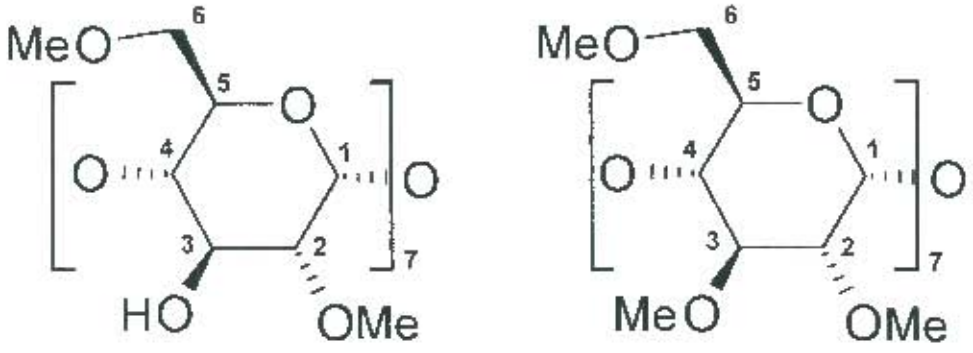

(a) (b)

Figure 1.11 The positions of methylation for the glucopyranose units of (a) DIMEB and (b) TRIMEB

Packing Arrangements in Cyclodextrin Crystal Structures

Caira has recently reviewed the phenomenon of isostructurality amongst cyclodextrin complexes.[80] Isostructurality is the phenomenon whereby two or more crystalline phases have identical or quasi-identical packing motifs[81] and thus necessarily have similar unit cell dimensions and a similar internal arrangement of molecules. As a result, common atoms of these phases thus have approximately the same three-dimensional coordinates.[82] For cyclodextrin complexes, which normally are ternary systems consisting of CD, guest and water molecules, this usually applies only to the inflexible portions of the CD molecule.[80] This gives rise to complexes with similar unit cell dimensions and packing motifs. The packing motifs for β-CD, γ-CD, DIMEB and TRIMEB are discussed next, with those for β-CD illustrated schematically because it has by far the largest number of packing motifs. The packing motifs of the other CD complexes are common to those of β-CD or variations of them.

Packing Arrangements of β-CD Species

The packing motifs of β-CD structures can broadly be categorised into monomeric, dimeric [two β-CD molecules that are linked at their secondary faces by multiple hydrogen bonds] and tetrameric structures [consisting of two dimers]. The monomeric packing arrangements are herringbone [$P2_1$], brickwork [$P2_1$], zigzag [$P2_12_12_1$], layer [$P2_1$] and helical channel [$P6_1$] which are presented schematically in Figure 1.12.

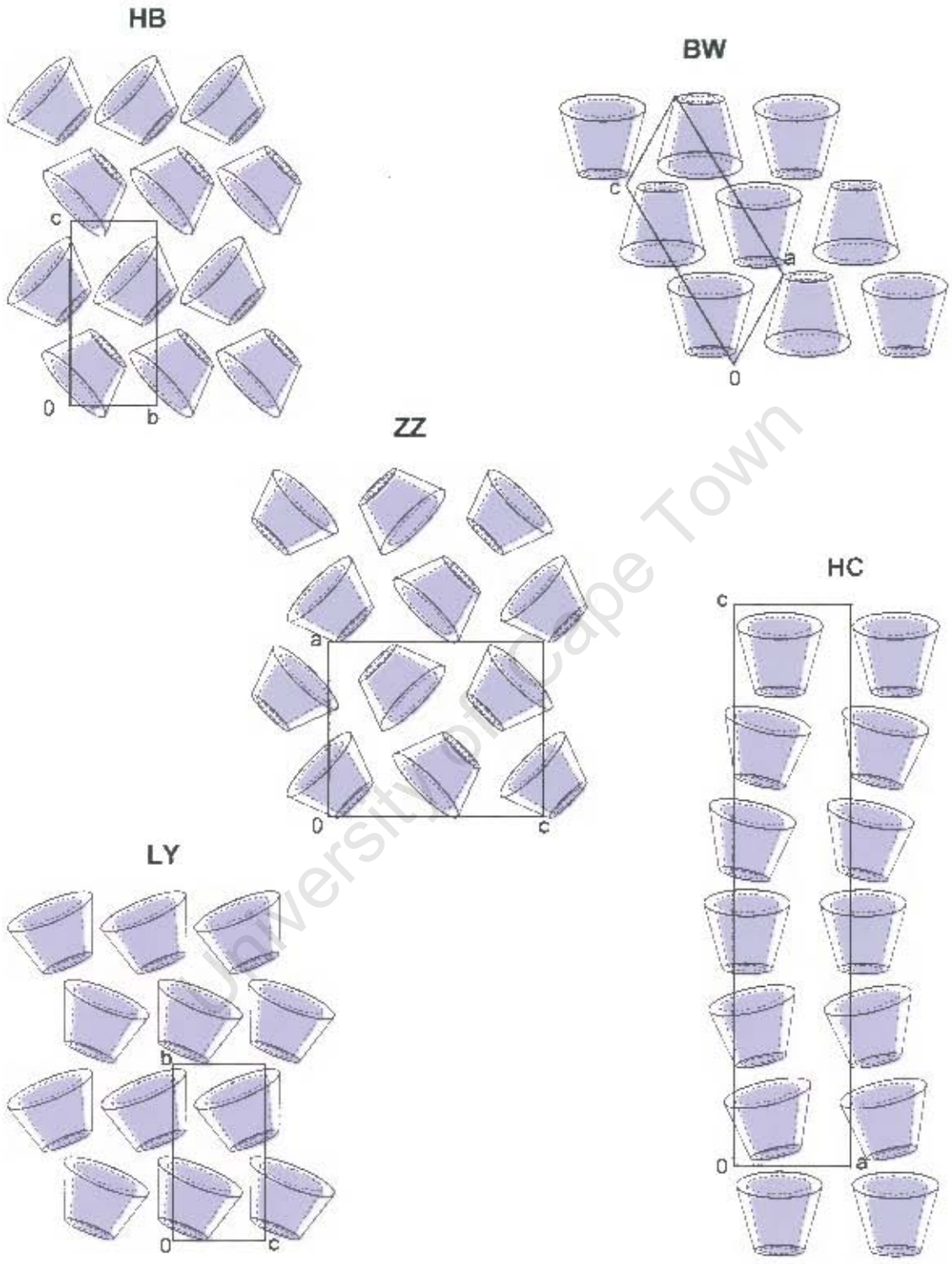

Figure 1.12 Monomeric packing arrangements for β-CD structures are of the type herringbone [**HB**], brickwork [**BW**], zigzag [**ZZ**], layer [**LY**] and helical channel [**HC**] [Adapted from reference 83]

The dimeric structures of β-CD are channel [P1 or C2], screw channel [$P2_1$], chessboard [$C222_1$] and intermediate [P1]. These are presented schematically in Figure 1.13. The majority of β-CD complexes consist of such dimers that are formed by head-to-head stacking stabilised by multiple hydrogen bonds across the secondary rims. In this manner a larger cavity is created allowing for the inclusion of bulkier guests. The tetrameric packing arrangements are tetrameric intermediate [P1] and tetrameric chessboard [$P2_1$] and are also illustrated schematically in Figure 1.13.

Packing Arrangements of γ-CD Species

The packing arrangements of γ-CD structures are herringbone type [$P2_1$] for the uncomplexed molecule and channel type [$P42_12$] for the inclusion complexes.

Packing Arrangements of DIMEB Species

The packing arrangements of DIMEB itself and its inclusion complexes vary from channel type to modified brickwork and herringbone type packing. The structures crystallise in the space groups $P2_1$ and $P2_12_12_1$. The DIMEB molecules are stacked in a head-to-tail fashion with the guest located either in the cyclodextrin cavity or in the interstitial sites.[84]

Packing Arrangements of TRIMEB Species

The majority of TRIMEB crystal structures display a screw-channel type packing crystallising in the space group $P2_12_12_1$. Two TRIMEB crystal structures have been reported in the monoclinic space group $P2_1$, namely the butamben-TRIMEB[85] and (E)-ajoene-TRIMEB[86] complexes. The former complex displays a channel-type packing with successive layers of complex units having alternating polarities, whilst the latter forms channels as a result of translated units. Each one of the monoclinic complexes is the first member of a new isostructural series.

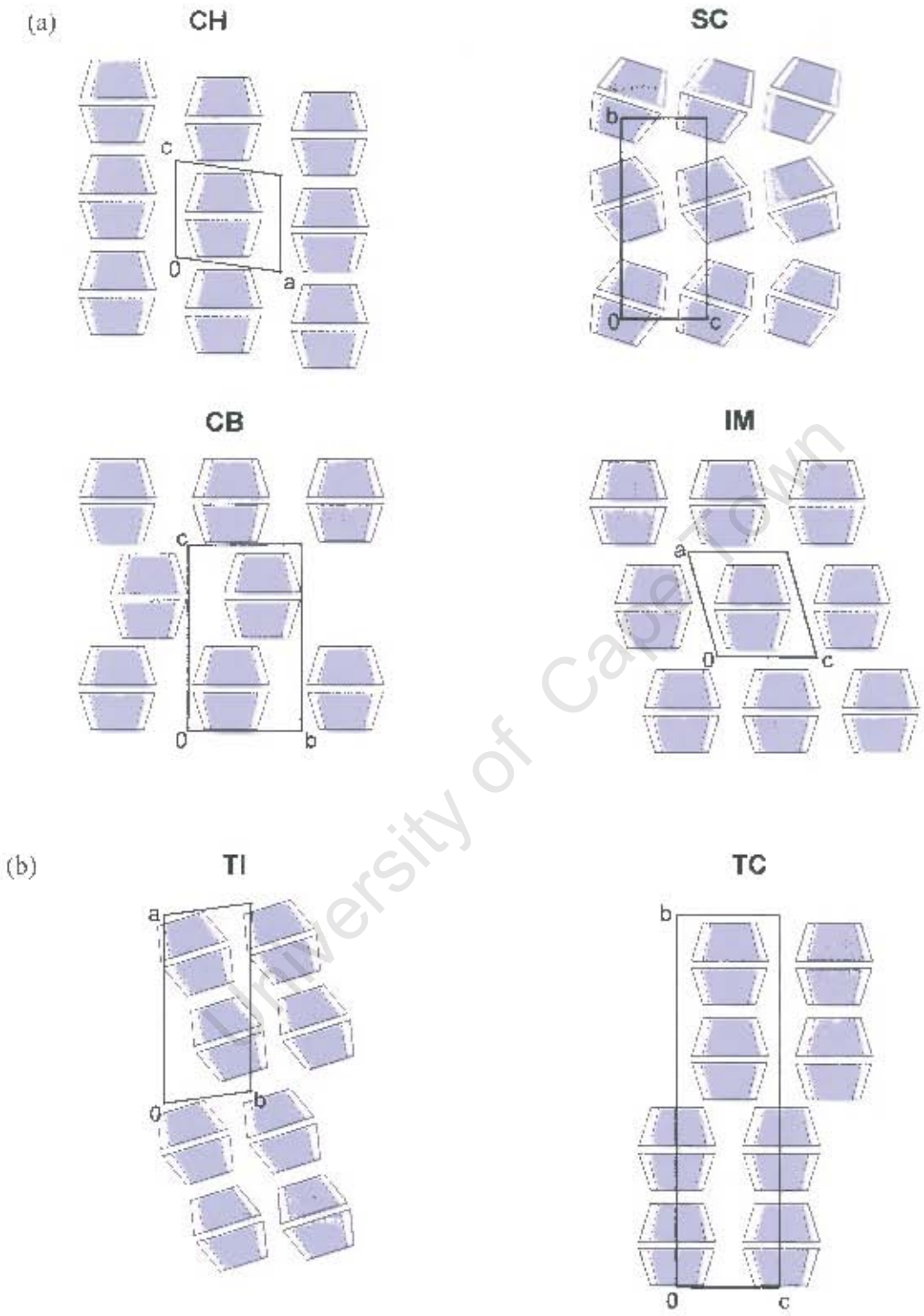

Figure 1.13 Packing arrangements of β-CD complexes that are (a) dimeric - channel **[CH]**, screw channel **[SC]**, chessboard **[CB]**, intermediate **[IM]** and (b) tetrameric - tetrameric intermediate **[TI]**, tetrameric chessboard **[TC]** [adapted from reference 83].

Application in the Pharmaceutical Industry

CDs have many applications in the food, pharmaceutical, biomedical and analytical industries, but in this section a brief summary will be given of their application in the pharmaceutical industry, as the title compound is a drug molecule. The pharmaceutical use of cyclodextrins as drug carriers has been extensively reviewed.[41,79,87,88] The encapsulation of drugs within CDs may eliminate potential problems such as photodegradation, racemisation, isomerisation, hydrolysis, oxidation, decomposition and polymorphism. The encapsulation may also mask bad odour or taste of drugs which would be advantageous in the paediatric oral application of the drug.[79] Other associated advantages of encapsulation may be the fixation of aroma-containing drugs or volatile drugs, the formulation of liquid drugs as solid formulations, increased solubility of the drug and therefore increased bioavailability.

The many applications that CDs may have in the pharmaceutical industry have also necessarily spawned studies on their toxicity, carcenogenicity, mutagenicity and teratogenicity.[89] Oral administration of the native CDs was found to be relatively safe with only very high concentrations causing damage to human erythrocytes.[90] Most of the CDs were found to be degraded by the intestinal flora in the colon. The methylated CDs have been found to have a higher toxicity, which presently limits their use in the pharmaceutical industry. However, these systems may serve as models for the mode of inclusion of the title drug, which is discussed next.

Tulobuterol

Background

Tulobuterol [2-chloro-α-[[(1,1-dimethylethyl)-amino]-methyl]benzenemethanol] falls into a category of compounds known as β-adrenoreceptors whose development over the last one hundred years towards the treatment of asthma and chronic bronchitis, has recently been reviewed.[91] Bullowa and Kaplan first reported the use of compounds of this class for the treatment of asthma in 1903[92] when they discovered that subcutaneous injections of adrenaline dramatically relieved the symptoms.[91] Adrenaline proved to be an

undesirable drug due to its many side effects such as hypertension and metabolic instability. When the structure of adrenaline became known, attempts were made to synthesise analogues with more advantageous properties. The synthesis of isoprenaline[93] was the first of many attempts that made significant progress towards eliminating the side effects associated with adrenaline. However, it was salbutamol[94,95] and terbutaline[96,97] that became the first to be in "general clinical use".[91] After the success of salbutamol and terbutaline various congeners appeared and tulobuterol forms part of this "first wave".[91] It was first prepared by Kato and Kurata in 1973.[98] Kubo *et al.* showed that tulobuterol had a sustained effect on the bronchial smooth muscle of up to ten times longer than salbutamol.[99] The drug has been administered mainly by inhalation but recently a tulobuterol patch, that administers the drug transdermally, has been introduced. The tulobuterol patch has been deemed safe and efficacious in the long-term management of childhood asthma.[100]

Salts of tulobuterol

Tulobuterol is marketed and administered as the hydrochloride salt racemate [illustrated together with the free base in Figure 1.14], which in itself exhibits polymorphism. Saito *et al.* performed studies on the relationship between the physicochemical properties and crystalline forms of the salt from a thermoanalytical[101] and crystal structure perspective.[102] Three polymorphs and a hydrate of tulobuterol hydrochloride were isolated and the thermodynamic stability relationship between the polymorphs was investigated and related to the crystal structures.

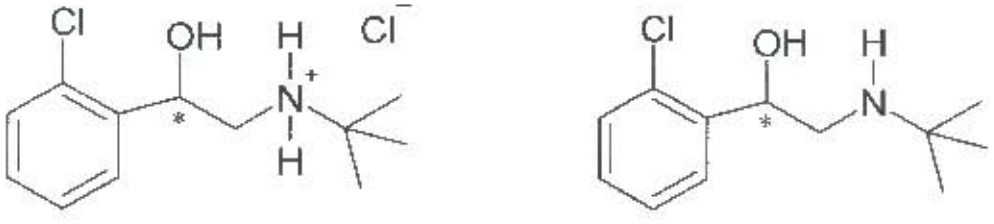

Figure 1.14 Schematic diagrams of the (a) hydrochloride salt and (b) free base of tulobuterol. The chiral centre is denoted with '*'.

Motivation and Objectives of the Study

In this study the racemic free base, prepared from the commercially available hydrochloride salt, was used. The motivation for the free base preparation was to investigate the CD inclusion of the derived species. If successful the encapsulation in CDs would present several advantages, namely (a) the provision of previously unexplored CD-tulobuterol inclusion complexes [effectively 'new chemical entities'], (b) elimination of potential problems that could arise with the current use of the hydrochloride salt, which is prone to polymorphism, and (c) possible improvement of tulobuterol performance [drug stability, enhanced dissolution rate], as illustrated for many drugs formulated as their CD complexes.[87] The polymorphism of the free base itself was also investigated, not only for academic interest, but to extend the chemistry and pharmaceutical applications of tulobuterol. Preparation of other salts of tulobuterol was also attempted in order to derive potential alternatives to the currently used hydrochloride form.

The aim of this study was to prepare and isolate polymorphs, cyclodextrin complexes and salts of tulobuterol. Polymorph preparation was attempted using as many of the methods described in this chapter as feasible. Cyclodextrin complexation was attempted using β-CD, γ-CD, DIMEB and TRIMEB as hosts. Alternative tulobuterol salt preparation was attempted using (R,R)-tartaric acid, succinic acid and benzoic acid. Isolated species were studied by thermoanalytical, spectroscopic and X-ray diffraction techniques and as far as possible correlations were drawn between them. X-ray diffraction studies included single crystal structure analyses and powder diffraction methods to complement the former. Thermal analyses were used to establish thermal stabilities and in the case of polymorphs, stability relationships. Spectroscopic studies were used to a lesser extent, but were nevertheless employed to provide additional information where relevant.

Materials

Tulobuterol hydrochloride was purchased from Sigma Chemical Company [St. Louis, Missouri, USA] and used as received for the free base preparation. The free base was prepared by the excess addition of 1.0 **M** NaOH to an aqueous solution of tulobuterol hydrochloride. The free base was then extracted from the aqueous phase using dichloromethane after which the product was obtained by fast evaporation of the solvent on a rotary evaporator. The host compounds β-cyclodextrin, γ-cyclodextrin, DIMEB and TRIMEB were obtained from Cyclolab [Budapest, Hungary] and used as received.

Preparation Methods

Slow evaporation and slow cooling were used for the preparation of crystals of polymorphs, cyclodextrin complexes and salts from their saturated solutions. Cyclodextrin complexes were initially prepared by kneading after which single crystals were obtained by the above methods. Kneading involved making a paste of the cyclodextrin with water using a mortar and pestle. An equimolar amount of drug was then added after which kneading continued for an hour. The consistency of the paste was maintained by adding an appropriate amount of water during this period. Before slow cooling and/or slow evaporation continued for all preparations, the solutions were filtered with a 0.45 μm microfilter in order to encourage the growth of larger crystals. More detail about the preparation of each species will be given in the appropriate chapters.

Microanalysis

The carbon, hydrogen and nitrogen content of prepared compounds was determined using a Fisons EA1108 CHNS-O Elemental Analyser. The polymorphic and salt compounds proved to be anhydrous from thermal analysis but were dried under vacuum before analysis to evaporate any surface solvent. Cyclodextrin inclusion complexes were dried under vacuum before analysis but due to their hygroscopic nature [specifically the β- and γ-CD complexes] still contained water on analysis. Thermal gravimetric analyses of these compounds were thus performed concurrently in order to ascertain their water content at the time of their microanalysis. In addition to microanalysis confirming the purity of the

prepared species, it also provided additional information, the nature of which depended on the species. In the case of polymorphs it confirmed whether the species were polymorphs or solvates, whilst it was used to establish the host:guest and cation:anion ratios for the cyclodextrin complexes and tulobuterol salts respectively.

Thermal analyses

Thermal analysis involves heating or cooling a sample at a controlled rate and observing the physical changes associated with the temperature changes. In this study thermal analysis comprises hot stage microscopy [HSM], differential scanning calorimetry [DSC] and thermogravimetric analysis [TGA]. All three techniques are used in conjunction to elucidate the physical changes that take place.

HSM provides a quick and sample-inexpensive means of qualitatively analysing for possible polymorphism, complexation or salt formation. Information may be also be recorded visually that may not be apparent from DSC and TGA. DSC is used to quantitatively determine onset temperatures [T_{on}] of fusion, dehydration, recrystallisation and transformation and can indicate complexation, polymorphism or salt formation. It is also used to determine the enthalpy changes associated with these events that is particularly important in the determination of stability relationships of polymorphs. TGA is used to determine mass loss of a sample on heating thus allowing for the determination of the mass percentage of included solvent. Both DSC and TGA were performed on a Perkin Elmer PC-7 Series instrument, a dual system that consists of a PE DSC7 Differential Scanning Calorimeter and a PE TGA7 Thermogravimetric Analyser. Unless specifically stated otherwise, all DSC and TGA runs were performed at 10 K/min under a nitrogen flow rate of 30 ml/min.

Hot Stage Microscopy [HSM]

A Linkam TP92 temperature control unit linked to a Linkam TH MS600 was used to heat the crystals at a controlled rate. Visual characterisation of this process was made possible by a real-time Sony Digital Hyper HAD colour video camera fitted to a Nikon SMZ-10

stereoscopic microscope. Images that were recorded were analysed by the Soft Imaging System, analySIS.[103] Silicone oil was used in appropriate cases to indicate the possible inclusion of solvent, as would be suggested by bubbling of the liquid medium on desolvation.

Differential Scanning Calorimetry [DSC]

DSC experiments measure the difference in energy input between the sample and reference pans whilst maintaining the heating rates of the two pans. Thermal events such as fusion and dehydration require a higher energy input for the sample to maintain its heating rate relative to the reference pan whilst recrystallisation of the melt requires less energy input relative to the reference pan. Prior to the analysis, 0.8-5.0 mg of the sample was placed in a crimped, vented aluminium sample pan, whilst the reference pan was left empty. Onset temperatures of thermal events [T_{on} in °C], indicated by endothermic and/or exothermic peaks, their temperature ranges as well their associated enthalpies [ΔH in J/g] were measured. The DSC analyser was calibrated against the melting points of indium (156.6°C) and zinc (419.5°C) and the fusion enthalpy of indium (28.5 J/g).

Thermal Gravimetric Analysis [TGA]

TGA yielded mass loss of the sample upon heating it at a controlled rate. An open platinum pan was used, which was connected to the hanging wire of a thermobalance. The mass loss could be used to determine qualitatively and quantitatively the presence of included solvent. Built-in procedures for furnace and mass calibration were used to calibrate the TGA analyser. The furnace was calibrated by measuring the Curie points of alumel (163°C) and nickel (354°C).

Scanning Electron Microscopy [SEM]

SEM was used to investigate visually morphological differences between polymorphic crystals, which could thus be studied to a greater magnification and detail. Morphological and crystal surface differences can account for differences in filtering and drying

behaviour, whereas using SEM to monitor the growth of one polymorphic crystal on another, could aid in the understanding of transformation between different crystal modifications.[104]

Samples were mounted on aluminium stubs coated with carbon glue. They were then sputter-coated with gold palladium, using a pulse coating technique. For polymorphic **Form 1** of tulobuterol an accelerating voltage of 10 kV, probe current of 200 pA, working distance of 16 mm and magnification of 673x were used. For polymorphic **Form 2** of tulobuterol, photographs were recorded employing an accelerating voltage of 10 kV, probe current of 20 pA, working distance of 22 mm and a magnification of 214x.

Fourier Transform Infrared Spectroscopy [FTIR]

FTIR spectroscopy was used to investigate possible differences in the N-H and O-H stretching frequencies as well as in the fingerprint region for the polymorphs of tulobuterol prepared in this work. Although it is a technique used primarily for the investigation of molecular properties, rather than solid-state properties, polymorphs often exhibit differences in the above stretching frequencies as a result of different hydrogen bonding environments. This technique is thus a possible diagnostic tool. FTIR spectra were recorded on a Perkin-Elmer 983 FTIR spectrophotometer over the range 4000-600 cm^{-1}. Samples were ground in Nujol mull and the percentage transmittance recorded against frequency.

Solid-state Nuclear Magnetic Resonance Spectroscopy [SSNMR]

SSNMR is increasingly used in polymorphic studies as it provides information on the environment of individual atoms, thus allowing for the monitoring of crystal and molecular changes.[105] This can thus serve as a diagnostic tool for polymorphism and provide information that complements that obtained by single crystal X-ray analysis. ^{13}C SSNMR spectra of polymorphs were recorded on a Varian VXR 300 MHz spectrometer equipped with a Jacobson-style CP-MAS probe. Samples were run over a period of 3.5 hours.

X-ray Crystallographic Analysis

Single crystal X-ray Diffraction

Single crystal X-ray crystallography was the main tool used in this study for structure elucidation. Single crystals were obtained for all new species reported in this study. Crystals of dimensions 0.1-0.5 mm in all dimensions were selected for X-ray analysis. Crystals were mounted on a glass fibre and covered with Paratone N oil[106] to prevent dehydration in the case of solvated crystals and to 'glue' the crystal to the glass fibre when cooling the crystal for low-temperature data collection. The glass fibres were mounted on goniometer heads.

X-ray Photography

X-ray photography was used to establish preliminary unit cell parameters and Laue symmetries. Oscillation and 0-level Weissenberg photographs usually sufficed for this purpose. X-rays were generated on a Philips PW1120/00 generator using Ni-filtered CuKα radiation [1.5418 Å] produced at 20 mA and 40 kV. The photographs were recorded on a Stoë goniometer with a film radius of 28.65 mm.

Oscillation photography

Oscillation photography was used for determination of one unit cell axis as well as to determine any symmetry associated with it.[107] A crystal was mounted on a goniometer head so that one of the cell axes was parallel to the oscillation axis and orthogonal to the X-ray beam. This alignment was done photographically with a series of short oscillation photographs and was a prerequisite for the accurate cell axis determination as well as for Weissenberg photography. The cell axis length and associated symmetry were determined from a full oscillation photograph.

Weissenberg photography

Weissenberg photography was used to determine the remaining two cell axes, their associated symmetry and the angle between them.[107] In most cases, the 0-level line on the

oscillation photograph was chosen. In order to restrict recorded reflections to this line a metal encasing with a narrow slit on the inside of the camera was used. By moving the camera at the same time as oscillating the crystal, reflections contained this line were spread over the film creating a distorted, two-dimensional diffraction pattern.

Intensity data-collection

Reflection intensity data were collected on a Nonius Kappa CCD Single Crystal X-ray Diffractometer using graphite-monochromated MoKα radiation [0.71073 Å]. A Nonius FR590 generator, operated at 23 mA and 53 kV, generated radiation. Data-collections were performed at room [~298K] and low [113-203K] temperatures, with exact temperatures for each data collection given in the appropriate chapters. Low temperatures were maintained by a constant N_2 gas flow rate of 20 cm^3/min produced by a Cryostream cooler [Oxford Cryosystems]. Cell refinement and data reduction were performed by DENZO and SCALEPACK and data were corrected for Lorentz-polarisation effects.[108] XPREP[109] was used to determine/confirm space groups by examining system absences and to prepare the SHELXS-97[110] input files.

Crystal Structure Solution and Refinement Programs

The structures presented in this thesis were solved using different structure solution programs and a variety of methods depending on the size of the structure, quality of the data and nature of the problem. SHELXS-97[110] was used to solve smaller structures, such as those of the polymorphs and salt compounds. This program was however not adequate for the CD complexes due to the poor diffraction that crystals of these compounds exhibit, as well as their larger structures. CD structures were solved by isomorphous replacement in cases where isostructural complexes existed, using the coordinates of their cyclodextrin non-hydrogen atoms. An alternative to this method was to use SHELXD,[111] a program specifically designed for solving larger structures. All structures were refined on F^2 using full-matrix least-squares in the program SHELXL-97.[112] Both SHELXS-97[110] and SHELXL-97[112] were accessed via the X-SEED[113] interface. More detail on SHELXD[111] and SHELXL-97[112] follows below.

SHELXD

SHELXD[111] is a program used to solve larger *ab initio* problems than those amenable to solution with SHELXS-97.[110] The structure solution strategy of this program is based on the dual-space iteration strategy, called 'Shake-and-Bake',[114] and has been coined the 'half-baked' method.[115] Convential 'direct methods' have successfully solved only a few structures that have more than 200 independent atoms,[115] whereas the dual-space iteration strategies have solved structures of up to 1000 independent atoms with native data to at least 1.2 Å resolution.

SHELXL-97

Model refinement was done in SHELXL-97[112] employing full-matrix least-squares minimization of the function $\sum w(F_o^2-F_c^2)^2$, the weighted sum of the squares of the differences between the observed and calculated intensities. The refinement of the model was monitored by assessing the residual index, R, defined by R_1 or wR_2. R_1 [equation (2.1)] represents the agreement between observed and calculated structure factors, whilst wR_2 [equation (2.2)] represents the agreement between the observed and calculated intensities.

$$\mathbf{R_1 = [\,\Sigma\,|\,|F_o| - |F_c|\,|\,] / \Sigma\,|F_o|} \qquad \textbf{(2.1)}$$

$$\mathbf{wR_2 = \{\,[\,\Sigma\,w(F_o^2 - F_c^2)^2\,]\,/\,[\,\Sigma\,w(F_o^2)^2\,]\,\}^{1/2}} \qquad \textbf{(2.2)}$$

The parameter w in equation 2.2 refers to the weighting scheme that was used in the final cycles of the refinement, and is defined in equation 2.3.

$$\mathbf{w = 1\,/\,[\,\sigma^2(F_o^2) + (aP)^2 + bP\,]} \qquad \textbf{(2.3)}$$

where the terms **a** and **b** are chosen to yield constant distributions of $w(F_o^2 - F_c^2)^2$ with sin 0 and $(F_o/F_{max})^{1/2}$ and **P** is defined in equation 2.4

$$\mathbf{P = [\,max(F_o^2, 0) + 2F_c^2\,]\,/\,3} \qquad \textbf{(2.4)}$$

The goodness of fit, **S**, is defined in equation 2.5

$$S = [\ \Sigma\ [w\ (F_o^2 - F_c^2)^2\ ]/\ (n-p)\ ]^{1/2} \qquad (2.5)$$

where **n** and **p** represent the number of reflections and total number of refined parameters respectively. For well behaved refinement **S** should be close to unity and the overdetermination ratio, **n/p**, should be at least ~ 10.

A measure of the agreement between all equivalent reflections is given by R_{int} defined in equation 2.6

$$R_{int} = \Sigma\ |F_o^2 - F_{o\ mean}^2\ |\ /\ \Sigma\ |F_o^2| \qquad (2.6)$$

Powder X-ray Diffraction [PXRD]

PXRD was used to determine characteristic 'fingerprint' traces of crystalline materials. This technique can uniquely identify materials thus allowing for the identification of new species of polymorphs, cyclodextrin complexes and salts. This technique is especially useful in the absence of good quality single crystals for single crystal structure determination. Polymorphism can be detected due to different packing arrangements that they exhibit. CD complexes also usually have very different traces from those of the parent CDs due to their different packing arrangements. Complexation is proven if the trace is different from that of the drug and host, as well as a physical mixture of the latter two, or if it corresponds to that of a known complex of the particular CD, the latter indicating isostructurality.

Powder patterns of ground samples were recorded on a Philips PW1050/25 vertical goniometer with Ni-filtered CuKα radiation (λ = 1.5418 Å) produced at 40 kV and 25 mA. Samples were packed in aluminium or glass sample holders and step scans of 0.1 2θ, with 2 s counting times, in the range 5-40° 2θ was employed. In cases where sample material was limited, PXRD patterns were recorded using a Huber Imaging Plate Guinier Camera 670. All samples were manually ground and packed into Lindemann capillaries

with an internal diameter of 1mm and a glass thickness of 0.01mm. The capillaries were obtained from Hilgenberg, Germany. Nickel filtered CuKα radiation [λ = 1.5418 Å], produced at 40 kV and 20 mA by a Philips PW1120/00 generator fitted with a Huber long fine focus tube PW2273/20 and a Huber Guinier Monochromator Series 611/15, was employed. For high temperature PXRD the Huber High Temperature Controller HTC 9634 unit was used with the capillary rotation device 670.2. A 2θ range of 4 to 100.0° was used with a step size of 0.005° 2θ.

For each successfully determined single crystal structure LAZY PULVERIX[116] was used to generate a computed PXRD trace. These were compared with experimental traces to establish whether any phase transformations had taken place upon grinding the material in the course of preparation for the analysis.

Computer Packages

The following computer packages were used in the crystal structure analyses of the various compounds:

- LAYER[117] was used to examine simulated graphic representations of the reciprocal lattice layers in order to confirm Laue symmetries and reflection conditions in cases where X-ray photographic data were absent.

- Pov-Ray[118] and Weblab ViewerPro[119] were used for the generation of molecular and structural diagrams.

- Ortep-3[120] was used for generating molecular diagrams with thermal ellipsoids drawn at a specified probability level.

- LAZYPULVERIX[116] was used to generate computed powder X-ray diffraction traces from single crystal X-ray structures. The input for this program included space group information, fractional atomic coordinates and thermal parameters.

Chapter 2 - Experimental and Computational Methods

- X-SEED[113] was used as a graphical interface from which LAZYPULVERIX,[116] LAYER,[117] SHELXS-97[110] and SHELXL-97[112] could be run.

- PLATON[121] was used to calculate the geometrical parameters and non-bonded interactions, together with their associated standard deviations, of each structure. The geometrical parameters included bond distances, bond angles and torsion angles, whilst the non-bonded interactions included hydrogen bonding, π···π-ring, and C-H···π-ring interactions, as well as short intermolecular contacts.

- The Cambridge Structural Database[84] was used to obtain unit cell parameters, space group information and fractional coordinates of structures where appropriate.

Additional Resources

Crystallographic information on each of the solved structures in this thesis has been stored on a compact disk, attached to the inside cover of this thesis. The files are stored in the folder Appendix A in a subfolder with the abbreviation of the structure that was used in the thesis. Table 2.1 lists the file types and the information that they contain.

Table 2.1 File types in Appendix A and the information that they contain

File extension	Information
.HKL	Reflection data
.RES	SHELX type coordinate file
.CIF	Crystallographic Information File
.FCF	Structure factor tables
.XL	SHELX output file
.LIS	PLATON output file listing all geometric parameters of a structure
.SUP	PLATON output file summarising selected information from .LIS file in tabulated form

Chapter 3 - Tulobuterol Polymorphs

Polymorph Preparation

The free base of tulobuterol was prepared by adding an excess of 0.1 **M** NaOH to an aqueous solution of the hydrochloride salt. Following this, the resulting free base was extracted into dichloromethane, after which solvent evaporation on a rotary evaporator yielded **Form 1**. Subsequent recrystallisation from a variety of solvents could also lead to **Form 1** as indicated in Table 3.1. **Form 2** preparation conditions were very specific and single crystals could only be reproducibly obtained from a solution of 20 mg of the free base [**Form 1**] in 3 ml 50:50 water:methanol. The solution was prepared at 25°C and allowed to evaporate slowly to yield crystals over a period of two weeks. Any attempt to increase the mass of the crystallised product yielded **Form 1** exclusively or a mixture of the two polymorphs. Solvents that also produced **Form 2** exclusively, but not always reproducibly, were tetrahydrofuran, 1-propanol and diethyl ether. These did not yield suitable crystals due to the high solubility of tulobuterol in these solvents and were not the solvents of choice for **Form 2** preparation.

The preferred method in the search for other polymorphs was crystallisation from various solvents due to the ease and speed of using this method, although the high solubility of tulobuterol in most organic solvents rendered the latter unsuitable for single crystal preparation. These solvents, as well as alternative preparative methods, are listed in Table 3.1. All the methods were largely unsuccessful and only resulted in the isolation of existing polymorphs, except for a third form [**Form 3**] that was prepared by recrystallisation of the melt. **Form 3** was prepared by the natural cooling of molten **Form 1** or **Form 2** in an aluminium pan after Differential Scanning Calorimetry analysis. However, many attempts to obtain a powder X-ray diffraction trace to confirm it as a new polymorph were unsuccessful. Possible reasons for this will be given later in the chapter. Attempts were also made to use **Form 3** in seeding experiments for single crystal or bulk powder preparations but these were unsuccessful. Thus, both the preparation and analysis of **Form 3** were restricted to DSC analysis and therefore are discussed in the **Thermal Analysis** section only. Reference to polymorphs of tulobuterol hereinafter pertains to **Form 1** and **Form 2** only, unless stated otherwise.

Table 3.1 Selected results of polymorph preparation using various methods

Method	Concentration (mg/ml)	Crystallising form
Crystallisation from single solvent systems*		
Water	2	**Form 1**
Pyridine	48	**Form 1**
Ethyl acetate	20	**Form 1**
Dichloromethane	10	**Form 1**
Acetone	5	**Form 1**
Hexane	25	**Form 1**
Tetrahydrofuran	10	**Form 2**
Diethyl ether	20	**Form 2**
1-Propanol	20	**Form 2**
Methanol	20	**Form 1 / Form 2** mixture
Ethanol	20	**Form 1 / Form 2** mixture
Tetrahydrofuran	75	**Form 1 / Form 2** mixture
Carbon tetrachloride	50	**Form 1 / Form 2** mixture
Isopropanol	10	**Form 1 / Form 2** mixture
Crystallisation from binary solvent systems		
Water:Butanol (1:2 v/v)	6.7	**Form 1**
Water:Methanol (1:1 v/v)	6.7	**Form 2**
Sublimation	n/a	**Form 1**
Vapor diffusion*		
Carbon tetrachloride[a]:Methanol[b] (2:5 v/v)	2.9	**Form 1**
Pyridine[a]:Water[b] (1:5 v/v)	3.3	**Form 2**
Crystallisation from the melt	n/a	**Form 3**
Grinding of either Form 1 or Form 2	n/a	No effect

* Due to the high solubility of tulobuterol in the listed solvents, all solutions were prepared at 25°C and left at that temperature for crystallisation to occur

[a] Solvent, [b] precipitant

Microanalysis

The results of C, H, N microanalysis for the two polymorphs are listed in Table 3.2. The experimental values for **Form 1** and **Form 2** agree with their respective calculated values within experimental error thus showing a high degree of purity in their preparation. The agreement of **Form 1** and **Form 2** values with the calculated values also indicates that they are polymorphs and not solvated forms.

Table 3.2 C, H, N microanalysis results [n – 2] for **Form 1** and **Form 2**

Polymorph	Experimental			Calculated for $C_{12}H_{18}ClNO$		
	%C	%H	%N	%C	%H	%N
Form 1	63.49	7.61	5.93	63.29	7.97	6.15
Form 2	63.66	8.21	6.14	63.29	7.97	6.15

Scanning Electron Microscopy

SEM photographs were recorded of a representative crystal of each polymorph to examine their respective morphologies and to establish possible differences that might exist between them. These photographs are presented in Figure 3.1. **Form 1** has an elongated, flattened, prismatic shape whilst **Form 2** has an equant, triclinic shape. These differences allow for the differentiation of the polymorphic crystals based on their morphologies.

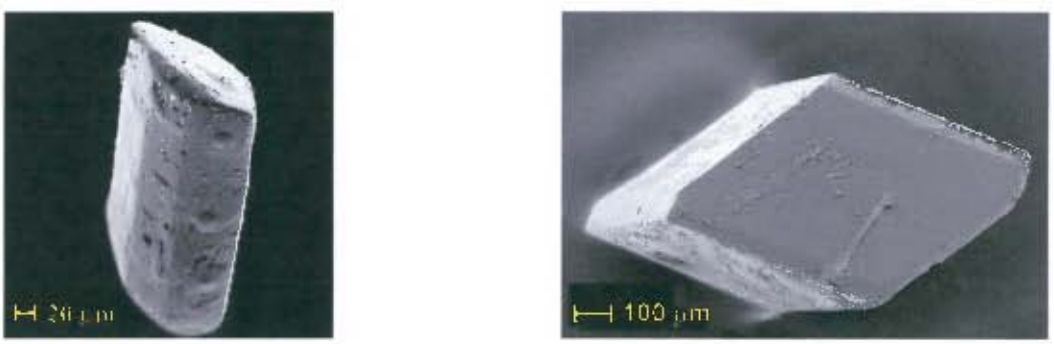

(a) (b)

Figure 3.1 SEM photographs of (a) **Form 1** and (b) **Form 2**

Thermal Analyses

Hot Stage Microscopy

HSM was performed to characterise the thermal events visually for the polymorphs on heating. Crystals of the two polymorphs were placed side by side on a glass slide and photographs were taken in the temperature range 40-100°C. These are presented in Figure 3.2. The **Form 2** crystal starts showing signs of melting at 83°C and is completely melted by 86°C. The **Form 1** crystal starts melting at 94°C and is completely melted at 95°C. The photographs indicate the distinct melting points of the two polymorphs. However, several crystals from **Form 2** batches exhibited less straightforward behaviour. In these cases the crystals opacified at ~80°C and then melted at the **Form 1** melting temperature, suggestive of a transformation of **Form 2** to **Form 1** upon melting. The **Form 2** crystals that transform or do not transform are hereinafter referred to as **Form 2(Tr)** and **Form 2(NTr)** respectively. A possible explanation for the existence of the two types of thermal behaviour is given below.

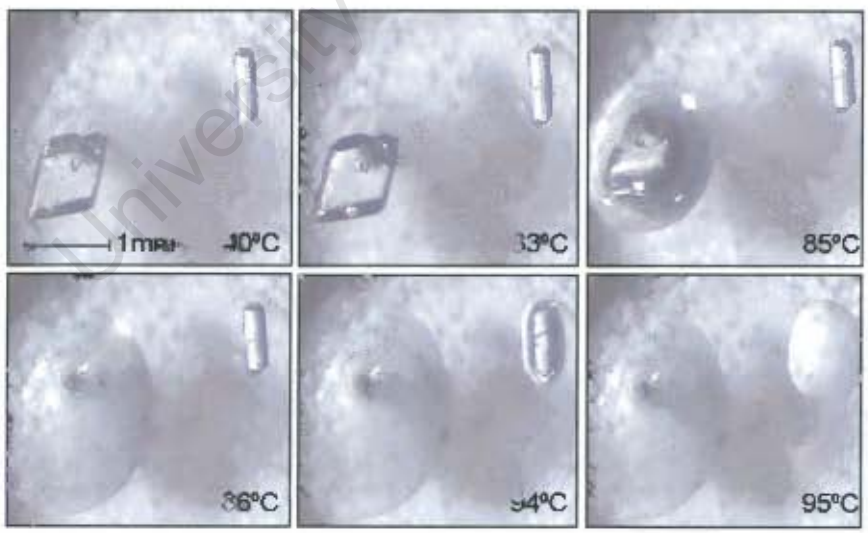

Figure 3.2 HSM photographs at various temperatures of a crystal of **Form 1** [right] and **Form 2** [left]

Differential Scanning Calorimetry and Thermogravimetric Analysis

TGA analyses [not shown] indicated negligible mass loss for both **Form 1** and **Form 2** in the range 30-100°C, thus confirming that they are not solvates. DSC analyses were also performed in the 30-100°C temperature range and proved to correlate well with HSM findings. The DSC traces for **Form 1**, **Form 2(NTr)** and **Form 2(Tr)** are presented in Figure 3.3.

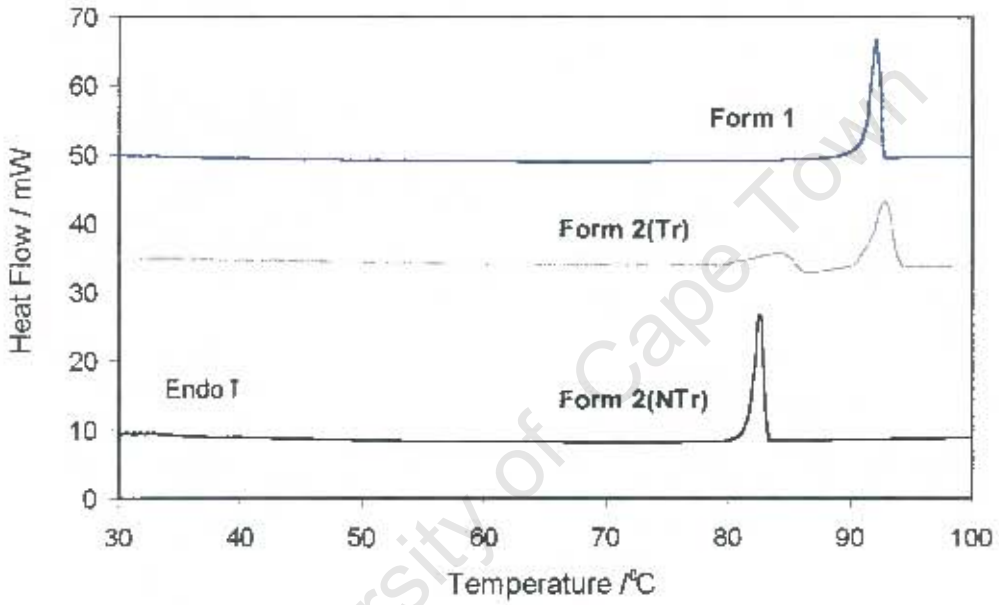

Figure 3.3 DSC traces of **Form 1**, **Form 2(Tr)** and **Form 2(NTr)**

Both the DSC traces for **Form 1** and **Form 2(NTr)** exhibit a single endotherm [**Form 1**, 90-94°C; **Form 2(NTr)**, 80-85°C] representing fusion. The DSC trace for **Form 2(Tr)** is more complicated, as was expected from the HSM analysis. Its DSC trace exhibits an initial endotherm [80-85°C], followed by an exotherm [85-90°C] and a final endotherm [90-94°C]. These respectively represent melting of **Form 2(Tr)**, recrystallisation into **Form 1** and subsequent melting of **Form 1**. These conclusions are consistent with those drawn from HSM analysis with the exotherm corresponding to the opacification of the crystals when examined by HSM. A plausible explanation for the behaviour of **Form 2(Tr)** crystals is that they are contaminated with small amounts of **Form 1**, making the only constitutional difference between **Form 2(NTr)** and **Form 2(Tr)** crystals the

presence of these **Form 1** contaminants in the latter. Thus, at the **Form 2** melting temperature, the **Form 1** contaminants are still unmelted, allowing them to act as seeds for the recrystallisation of the molten **Form 2** into **Form 1**. Due to the low level of contamination the **Form 1** contaminants are undetectable by powder X-ray diffraction analysis.

Separate DSC experiments were performed to prove that small amounts of **Form 1** contaminants in **Form 2(Tr)** crystals could be responsible for the latter's transformation behaviour. A single, large **Form 2(NTr)** crystal was halved so that one half could serve as a control and the other half sprinkled with **Form 1** granules. The DSC traces for these experiments are presented in Figure 3.4. The top trace represents the thermal behaviour of the control. The sole endotherm at ~85°C establishes the crystal identity as **Form 2(NTr)**. The bottom trace represents the thermal behaviour of the other half of the **Form 2(NTr)** crystal that was sprinkled with a small amount of **Form 1** granules [7% of total mass of analysed sample]. It is consistent with that of **Form 2(Tr)**, proving that the latter is merely **Form 2(NTr)** contaminated with small amounts of **Form 1**. The above results were reproducible down to a contamination level as low as 1%.

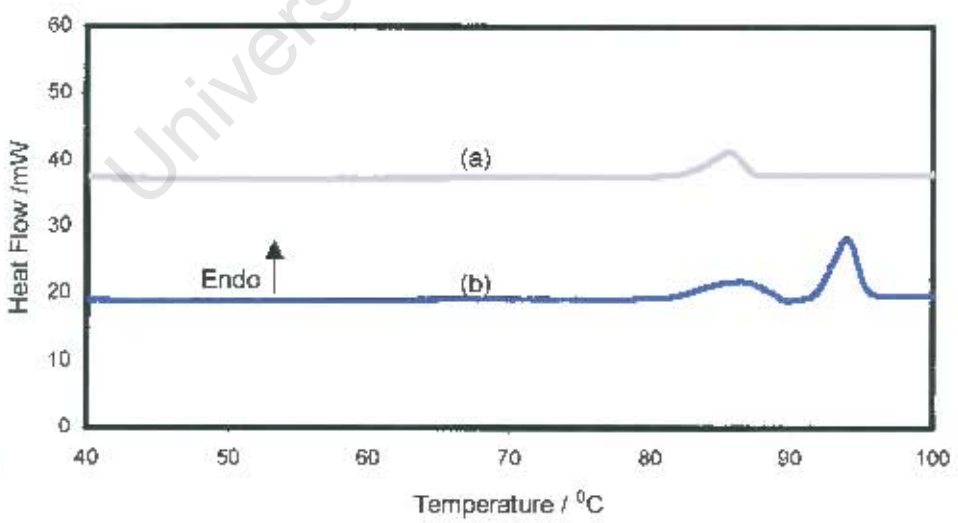

Figure 3.4 DSC traces of (a) **Form 2**(NTr) control and (b) **Form 2(NTr)** doped on the surface with **Form 1**

Factors that are known to influence thermal behaviour, such as heating rates and crystal sizes, were investigated but these were eliminated as possible explanations for the existence of both the non-transforming and transforming behaviours of **Form 2** crystals, as their variation did not change the observed behaviour of either type. Furthermore, full X-ray structure determinations carried out on **Form 2(NTr)** and **Form 2(Tr)** crystals were found to yield identical results. These are presented in the **X-ray Crystallographic Analysis** section. The sub-classification of **Form 2** into **Form 2(NTr)** and **Form 2(Tr)** crystals is thus relevant only in the context of the thermal behaviour. Interestingly, the transformation of the **Form 2** melt into **Form 1** is thermodynamically favoured [see Figure 3.6] but the existence of **Form 2(NTr)** thermal behaviour implies that there is a kinetic barrier for this to occur. The presence of the **Form 1** contaminants facilitates crossing of the kinetic barrier, enabling transformation to occur. There is the additional possibility that the presence or absence of lattice defects in **Form 2** could account for the differing behaviours displayed by **Form 2** [as manifested by **2(Tr)** and **2(NTr)**].

It was found that **Form 2** sample manipulation prior to DSC analysis could have an effect on the observed thermal behaviour. The grinding of both transforming and non-transforming **Form 2** crystals prior to DSC analysis in some cases led to only the **Form 1** melting peak being observed, possibly indicating that transformation was induced upon grinding. However, PXRD patterns of these ground materials unequivocally established their identity as **Form 2**. The transformation of the ground crystals is thus not detected by DSC analysis, indicating that prior grinding facilitates the transformation on heating as a result probably of lattice strain or defects that are introduced upon grinding.

Anomalous thermal behaviour following grinding has also been noted for the polymorphs of the tulobuterol hydrochloride salt.[101] The unground **Form III** DSC trace has a similar pattern to that of **Form 2(Tr)** of the free base, indicating transformation to the highest melting form, **Form II**, on heating. However, when ground the initial endotherm disappears and the DSC trace shows only the **Form II** endotherm. On the other hand, the unground **Form I** DSC trace resembles that of the **Form 2(NTr)** free base, showing no transformation to **Form II**. When ground prior to DSC analysis its pattern now resembles that of the unground **Form III**, indicating that it transforms to **Form II** on

heating. PXRD analysis prior to DSC analysis also showed that these forms remained unchanged, thus indicating that grinding facilitated the transformations on heating. The authors attributed this behaviour to lattice strains induced by the grinding. The above situations indicate that due care must be taken when assigning polymorph identity of ground forms to the higher melting form based on DSC analysis only and that assignment of the ground forms should always be corroborated by PXRD analysis.

It was stated earlier that methods other than recrystallisation from solvents were employed in an attempt to isolate different polymorphs. The only method to yield a positive result in this search was recrystallisation from the melt by DSC experiment of either **Form 1** or **Form 2**. Figure 3.5 presents the observed traces for **Form 2** as starting material and its reheat after cooling of the melt. Both fast and slow, controlled cooling of the melt [100 and 1 K/minute respectively, not shown] yielded no exotherm, indicating that recrystallisation did not occur. However, if the cooled material was immediately heated at a rate of 10 K/minute, a very broad exotherm [60-76°C] and two overlapping peaks [76-79°C and 79-84°C] were observed. The broad exotherm represents recrystallisation of the molten **Form 2**. It is the appearance of the first endotherm in the trace that alludes to the possible existence of a third form, **Form 3**. The second endotherm appears at 79°C, which corresponds to the **Form 2** melting temperature.

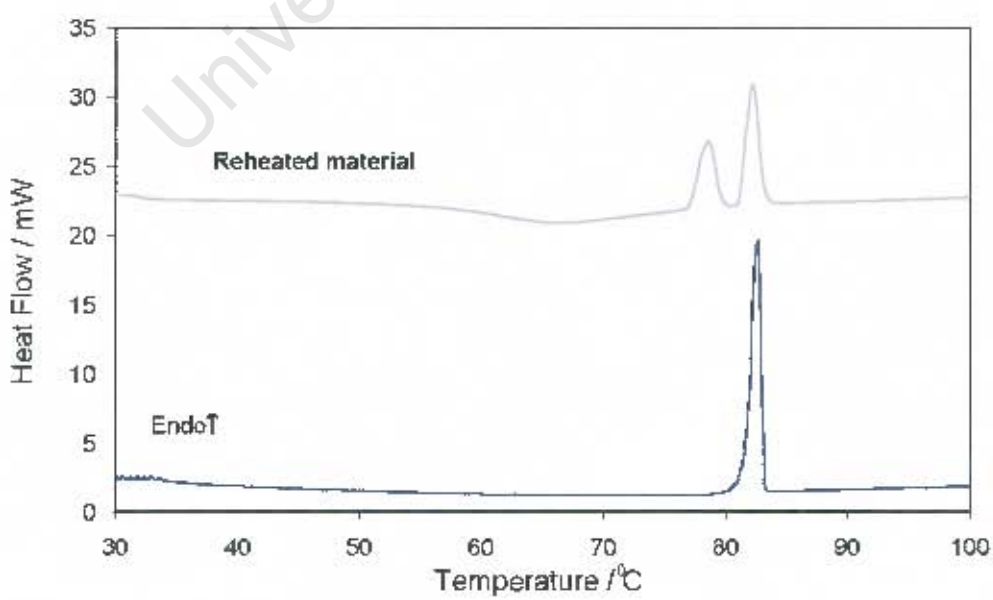

Figure 3.5 Heating and reheating DSC traces for **Form 2**

If a few minutes are allowed before reheating the initial melt and the heating rate is reduced to 1 K/minute the previously described broad exotherm becomes a clear, well defined exotherm at ~50°C. The two overlapping peaks also become resolved with a small exotherm evident between them. The position of the initial exotherm is obviously dependent on the heating rate, as a slower heating rate will lower the recrystallisation temperature. If the sample was left long enough to completely recrystallise before reheating, the above result could not be achieved, i.e. either a **Form 1** or **Form 2** peak, or both appeared. Reheating the melt before it recrystallises at room temperature thus seems to be necessary for recrystallisation into **Form 3**. Unfortunately, as stated earlier, attempts to obtain a PXRD trace to unequivocally identify this form as a new polymorph were unsuccessful. This could possibly be ascribed to practical considerations, such as the necessary sample grinding before PXRD analysis, which could induce transformation of **Form 3**. Variable temperature PXRD was used to try and eliminate the need for grinding material from DSC but this was also unsuccessful in obtaining **Form 3**, as shown when the top trace in Figure 3.5 could not be reproduced when using variable temperature PXRD to obtain the recrystallised material from the initial melt. This failure could be a result of the PXRD conditions, e.g. heating rates and material onto which the melt recrystallises, being different from those of DSC.

Stability relationship between polymorphs

The stability relationship between the polymorphs is discussed in this section as DSC analysis was the main tool used for this investigation. The accurate heats of fusion, ΔH_f, and extrapolated onset temperatures, T_f, for **Form 1** and **Form 2** are presented in Table 3.3. The reader is referred to **Chapter 1 – Introduction** [pages 4 – 7] for the theoretical background on which the following discussion is based.

Table 3.3 Thermal data for **Form 1** and **Form 2** [n = 4]

Polymorph	T_f (°C)	T_f (K)	ΔH_f (J g^{-1})	ΔH_f (kJ mol^{-1})
Form 1	90.9(0.2)	364.0(0.2)	119(1.3)	27.1(0.3)
Form 2	80.8(0.1)	354.0(0.1)	111.5(0.6)	25.4(0.1)

Table 3.3 shows that **Form 1**, the higher melting polymorph, also has the higher heat of fusion and thus, on the basis of Burger and Ramberger's Heat of Fusion rule,[20] this would establish the stability relationship as monotropic. In addition, Yu's treatment[23] of this issue was employed in order to confirm the stability relationship, as well as obtain an estimate of the transition temperature, T_{tr}, which for a monotropic relationship is virtual as it lies either above the melting temperatures of the polymorphs or below absolute zero. The values obtained for the various thermodynamic properties, to be used in Yu's derived equations for the calculation of T_{tr}, were: ΔH_0 = -887 $Jmol^{-1}$, ΔS_0 = -0.434 $JK^{-1}mol^{-1}$, and ΔG_0 = -733 $Jmol^{-1}$. Using these values T_{tr} was estimated to be ~2040K. This value is, however, very sensitive to the errors in the melting points and enthalpies of fusion, and should be considered a nominal value. If the reported standard deviations for the T_f values are taken into account, the error for T_{tr} is as high as ±500 K, being even higher if the ΔH_f standard deviations are considered as well. The small entropy difference implies a small difference in the slopes of the G vs T curves for **Form 1** and **Form 2** and is thus consistent with the high value of T_{tr}. Values higher than these have been reported for monotropically related polymorphs.[23] A semi-empirical G vs T diagram of the above results is presented in Figure 3.6. The transformation behaviour of several batches of **Form 2** to **Form 1** [**Form 2(Tr)** thermal behaviour] is consistent with this monotropic relationship as Figure 3.6 shows that this transformation is thermodynamically favoured.

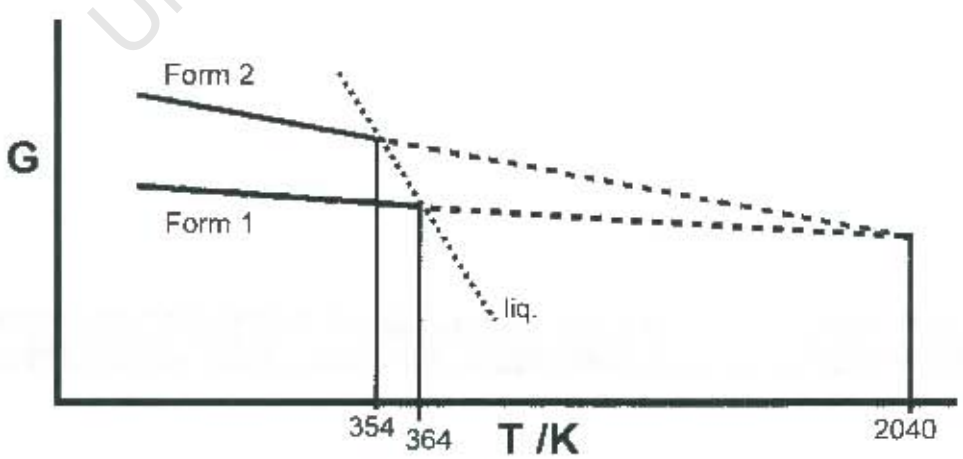

Figure 3.6 G vs T diagram for **Form 1** and **Form 2** [not to scale]

The experimental densities for **Form 1** and **Form 2** were determined to be 1.11(2) g cm^{-3} and 1.13(2) g cm^{-3} respectively by floatation of the crystals in an aqueous KI solution at 25°C. These densities are not significantly different but their nominal values agree with those for the computed densities of the room temperature polymorphic structures presented in the next section [Table 3.4]. The lower nominal density of **Form 1** is in contrast to what would be expected from the density rule of Burger and Ramberger[20] [**Chapter 1** - Table 1.1] which states that the stable form should have the higher density. However, these authors have noted that there are exceptions to this rule and Bernstein[122] has suggested that a *caveat* be associated with the use of it.

X-ray Crystallographic Analysis of Form 1 and Form 2

Single Crystal X-ray Diffraction

X-ray photography

X-ray photographic techniques were used to establish the preliminary unit cell parameters and Laue symmetries of **Form 1** and **Form 2**. The Laue symmetries were used to infer the crystal systems for the respective polymorphs. An oscillation photograph of **Form 1** indicated no intensity symmetry but *mm* symmetry was revealed by a 0-level Weissenberg photograph. This combined information indicated Laue *2/m* symmetry and therefore the monoclinic crystal system was assigned. An oscillation photograph for **Form 2** revealed no intensity symmetry whilst a 0-level Weissenberg photograph had only the inherently present Laue $\bar{1}$ symmetry. On this basis, the triclinic crystal system was assigned.

Data-collection and space group determination

Diffraction intensities were collected on a Nonius Kappa CCD diffractometer at room temperature [RT, 295K] and low temperature [LT, 173K]. RT data collections were performed to ensure that no phase changes were effected on cooling of the crystals. The program XPREP[109] was used to determine the space groups of **Form 1** and **Form 2** respectively. It indicated the monoclinic space group $P2_1/n$ (standard setting $P2_1/c$, space group No. 14) based on the reflection conditions h0l : h + l = 2n; 0k0 : k = 2n. Inspection of the reciprocal lattice layers with LAYER[117] confirmed these reflection conditions. The crystal system of **Form 2** was determined to be triclinic from the preliminary photographic data. Laue symmetry $\bar{1}$ was confirmed for the collected intensity data, thus indicating the space group P1 or $P\bar{1}$. Intensity statistics provided by XPREP[109] showed $|E^2-1| = 0.966$, indicating a centrosymmetric space group and therefore $P\bar{1}$ was chosen. This choice was justified by the successful refinement of the structure in this space group. In both cases, centrosymmetric space groups were expected since the free base had been prepared from the racemic hydrochloride salt.

Structure solution and refinement

SHELXS-97[110] was used for the structure solution of **Form 1** and **Form 2**, which revealed the positions of all the non-hydrogen atoms and allowed their placement. All non-hydrogen atoms were then refined isotropically on F^2 with SHELXL-97.[112] Conditional on satisfactory isotropic thermal parameters, this was followed by anisotropic refinement. Hydrogen atoms were placed in fixed geometric positions using a riding model except for the hydroxyl and amino hydrogens which were located in subsequent difference Fourier maps and allowed to refine freely with restrained O-H and N-H distances of 1.000(5) Å. The latter were refined isotropically with temperature factors 1.5 times those of their parent atoms. The rest of the hydrogen atoms were refined isotropically with thermal parameters equal to 1.2 times those of their parent atoms. Least-squares weights were employed in the final cycles of the refinement. The crystal and refinement data for both LT and RT determinations are presented in Table 3.4.

Description of the structures

The unit cell data of the respective LT and RT structures of **Form 1** are in close agreement and indicate that no phase changes occurred on cooling the crystals. The same applies to **Form 2** LT and RT structure determinations. **Form 1** crystallises in the monoclinic space group $P2_1/n$ with $Z = 12$ molecules per unit cell. This indicates three molecules per asymmetric unit since $P2_1/n$ has four general equivalent positions. **Form 2** crystallises in the triclinic space group $P\bar{1}$ with $Z = 6$ molecules per unit cell, which also indicates three molecules per asymmetric unit since this space group has two general equivalent positions. The ADDSYM function in PLATON[121] indicated no extra crystallographic symmetry for **Form 1** and **Form 2**, reaffirming the correct choice of space groups for these structures.

ORTEP[120] diagrams of both the LT and RT asymmetric units of **Form 1** and **Form 2** are presented in Figure 3.7. The smaller thermal ellipsoids of the LT structures indicate their reduced atomic thermal motion, which led to a higher precision of their structural determinations. These were therefore chosen for detailed structural analysis of molecular and crystal packing features.

Table 3.4 LT and RT crystal and refinement data of **Form 1** and **Form 2**

Parameter	Form 1 RT	Form 1 LT	Form 2 RT	Form 2 LT
Formula unit	$C_{12}H_{18}ClNO$	$C_{12}H_{18}ClNO$	$C_{12}H_{18}ClNO$	$C_{12}H_{18}ClNO$
Formula weight / g mol^{-1}	227.7	227.7	227.7	227.7
Crystal system	Monoclinic	Monoclinic	Triclinic	Triclinic
Space group	$P2_1/n$	$P2_1/n$	$P\bar{1}$	$P1$
a / Å	10.904(2)	10.802(1)	11.0506(2)	11.004(2)
b / Å	18.990(4)	18.949(2)	11.8859(3)	11.896(2)
c / Å	19.767(4)	19.649(1)	16.9846(5)	16.844(3)
α / °	90	90	91.558(1)	91.28(3)
β / °	95.31(1)	94.84(1)	97.296(1)	97.46(3)
γ / °	90	90	115.168(1)	115.32(3)
Volume / Å^3	4076(1)	4007.6(6)	1994.5(1)	1968.7(7)
Z	12	12	6	6
Density$_{calc}$ / g cm^{-3}	1.113	1.132	1.138	1.152
μ (MoK$_\alpha$) / mm^{-1}	0.26	0.26	0.27	0.27
F(000)	1464	1464	732	732
Crystal size / mm^3	0.20x0.25x0.30	0.20x0.30x0.40	0.30x0.30x0.35	0.38x0.46x0.55
Temperature / K	295(2)	173(2)	295(2)	173(2)
Range scanned θ / °	2≤θ≤28	2≤θ≤26	2≤θ≤27	2≤θ≤25
Index ranges	h: 0, 14 k: 0, 15 l: -26, 26	h: 0, 11 k: -23, 23 l: -23, 23	h: -14, 14 k: -12, 15 l: -21, 21	h: -13, 12 k: -14, 14 l: -20,20
φ scan angle / °	1.0	1.0	1.0	1.0
φ scan range / °, frames	360, 360	103, 103	183, 183	182, 182
ω scan angle / °	1.0	1.0	1.0	1.0
ω scan ranges / °, frames	163, 163	150, 150	67, 67	63, 63
Dx / mm	45	40	34	40
No. of measured reflections	40809	17746	22610	15988
No. of unique reflections	10087	6785	8463	7041
No. of reflections with I > 2σ(I)	5434	5029	5906	5531
No. of L.S. parameters	431	434	436	439
R_{int}, R_σ	0.041, 0.0423	0.0269, 0.0435	0.0285, 0.0498	0.0143, 0.0346
S	1.045	1.015	1.145	1.029
R_1 ($F_o > 4\sigma(F_o)$)	0.0634	0.0464	0.0976	0.0398
No. of reflections omitted	51	8	39	0
wR_2 (all reflections)	0.1982	0.1106	0.2998	0.1010
Weighting scheme	a = 0.0896 b = 0.81	a = 0.0396 b = 1.98	a = 0.1602 b = 0.75	a = 0.0396 b = 0.78
$(\Delta / \sigma)_{mean}$	< 0.001	< 0.001	< 0.001	< 0.001
Δρ excursions / e Å^{-3}	0.39, -0.45	0.30, -0.38	0.89, -0.80	0.40, -0.52

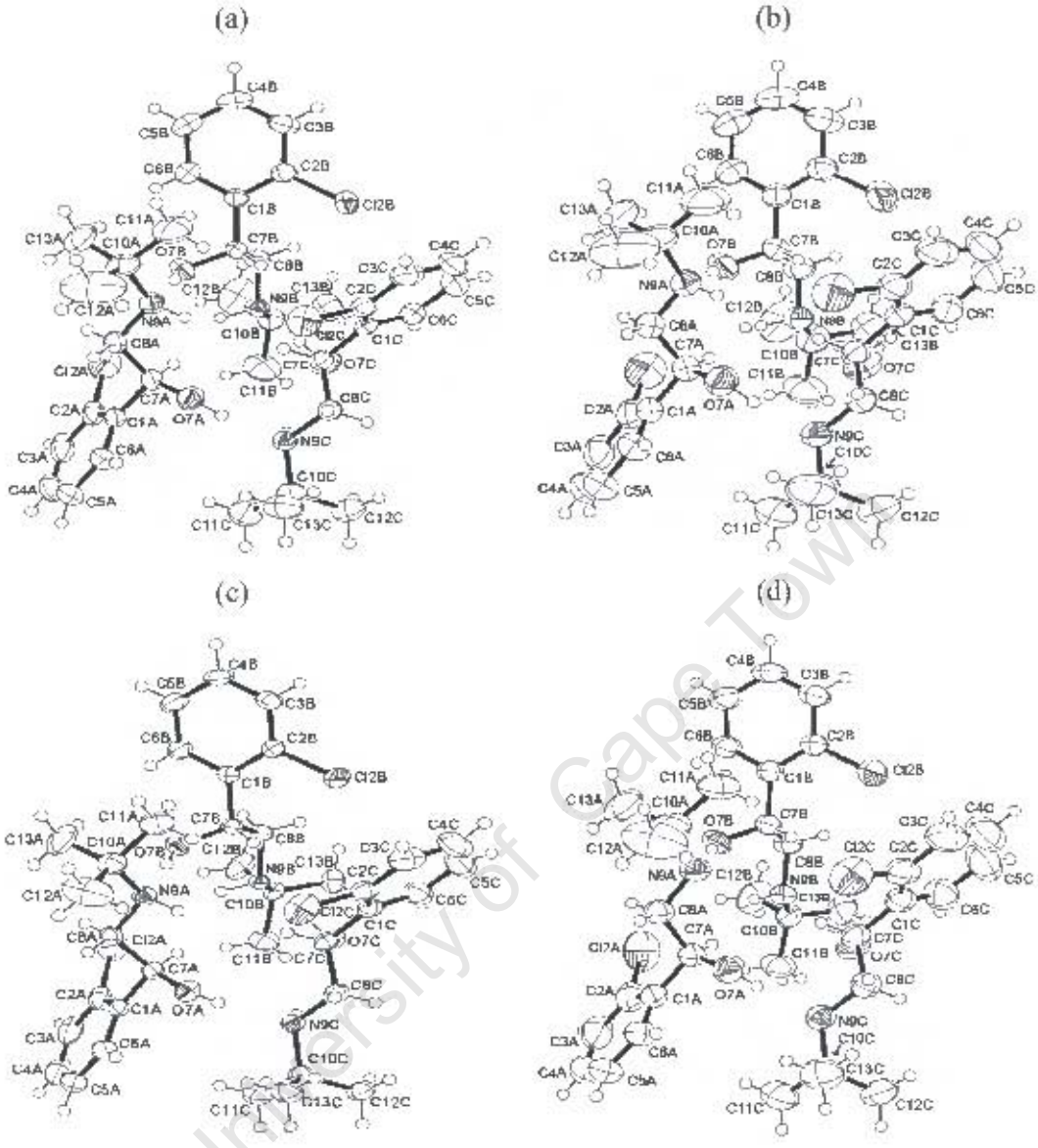

Figure 3.7 ORTEP diagrams of (a) **Form 1** LT, (b) **Form 1** RT, (c) **Form 2** LT and (d) **Form 2** RT. Thermal ellipsoids are drawn at the 50% probability level.

Figure 3.7 illustrates that there is a remarkable similarity between the asymmetric units of **Form 1** and **Form 2**; in fact they are practically identical. In both cases, the asymmetric unit is a cyclic trimer held together by three intermolecular O-H···N hydrogen bonds. The presence of strong hydrogen bond donor and acceptor groups in the tulobuterol molecule did suggest that the three molecules of the asymmetric unit in both polymorphs would be associated by hydrogen bonding, but that they do so in identical fashion was unexpected. A graphical overlay of the trimers showing the hydrogen bonding in each is presented in Figure 3.8.

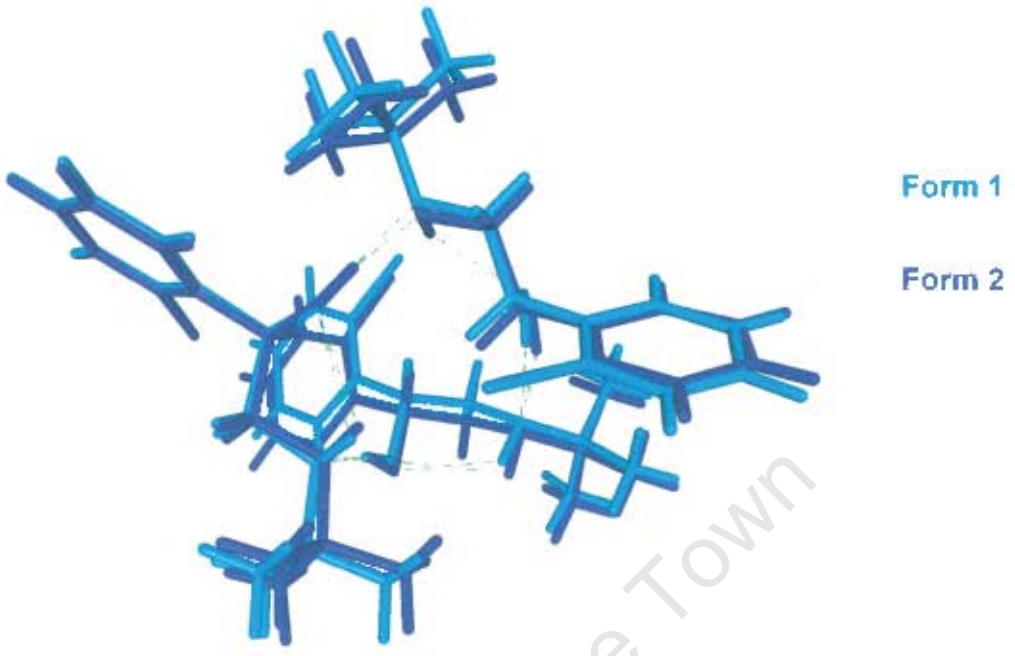

Figure 3.8 Overlay of the asymmetric units of **Form 1** and **Form 2**. Green dashed lines represent the intermolecular O-H···N hydrogen bonds

The overlay illustrates that the two trimers are nearly perfectly superimposable and that, from visual inspection, minimal conformational differences exist between them. A detailed geometrical analysis of the respective polymorph trimers follows to present a more detailed comparison of their structures.

Geometrical comparison of the trimers in Form 1 and Form 2

Table 3.5 presents randomly selected, representative bond distances and torsion angles of the **Form 1** and **Form 2** trimers for comparison as well as the distances and angles for all the strong intermolecular hydrogen bonds of the trimer in both polymorphs. The differences between corresponding parameters of the trimers in the respective polymorphs were calculated and the mean of these differences, as calculated over the whole trimer, are presented in the last column of Table 3.5. Corresponding bond distances and torsion angles have a mean difference of 0.005(1) Å and 2(2)° respectively, whilst mean differences for the donor···acceptor distances and donor-H···acceptor angles

are 0.02(1) Å and 3(1)° respectively. The torsion angles define the conformations of the trimer molecules and their close agreement confirms that the trimer conformations are essentially the same. In turn, the hydrogen bond distances and angles define the dimensions of the trimer hydrogen bonding framework and their close agreement is further evidence for the close similarity of the polymorph trimers. A full set of molecular parameters is available in Appendix A on the CD-ROM provided.

Table 3.5 Randomly selected geometrical parameters for the **Form 1** and **Form 2** trimers

Parameter	Form 1	Form 2	Δ_{mean} (trimer)
Selected bond distances / Å			
C1A-C6A	1.395(3)	1.395(3)	**0.005(1)**
C7B-O7B	1.413(2)	1.425(2)	
C2C-Cl2C	1.749(2)	1.758(2)	
Selected torsion angles / °			
C8A-N9A-C10A-C13A	-67.8(3)	-61.1(2)	**2(2)**
C1-C7B-C8B-N9B	-179.6(2)	-175.2(1)	
C6C-C1C-C7C-C8C	101.5(2)	98.0(2)	
D-H···A / Å			
O7A-H7A···N9C	2.821(2)	2.839(2)	**0.02(1)**
O7C-H7C···N9B	2.750(2)	2.765(2)	
O7B-H7B···N9A	2.778(2)	2.747(2)	
D-H···A / °			
O7A-H7A1-N9C	171(2)	173(2)	**3(1)**
O7C-H7C1-N9B	172(3)	169(2)	
O7B-H7B1-N9A	173(2)	177(2)	

This geometrical comparison confirms what is illustrated in Figure 3.8, namely that the trimers of the respective polymorphs are practically identical. From this point of view the discussion of the trimer will henceforth pertain to both polymorphs, unless stated otherwise. The remarkable consistency of the trimer is indicative of the stability of this arrangement and therefore closer, detailed investigation of its assembly is warranted, which follows next.

Trimer assembly

Figure 3.9 presents an oblique stereo view of a **Form 1** trimer taken as representative for both polymorphs. The immediate and most obvious feature of the trimer is the way the individual molecules assemble to form the hydrogen bonding framework that defines the asymmetric unit as a trimer. The O7 atom of each tulobuterol molecule acts as the donor in the hydrogen bond to the N9 atom of its neighbour, resulting in the formation of a cyclic trimer. The O7A-H···N9C, O7C-H···N9B and O7B-H···N9A hydrogen bonding sequence illustrates a homodromic arrangement of the hydrogen bonds that connect the molecules. The chirality combination of molecules **A**, **B** and **C** of the trimer chosen as the asymmetric unit is (S-), (R-), (R-) respectively. However, for each such trimer there is a counterpart in the crystal with the opposite combination of chiralities [(R-), (S-), (S-)], a requirement of the centrosymmetric space group.

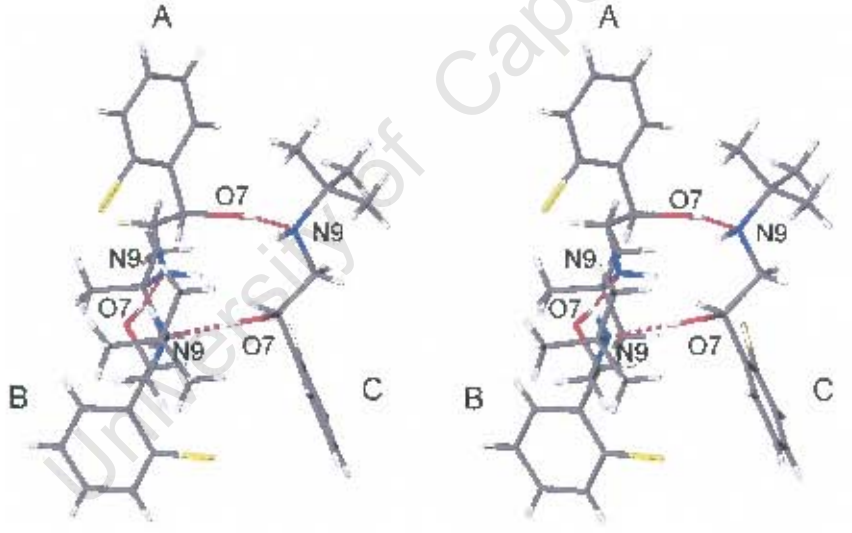

Figure 3.9 Stereo diagram of the **Form 1** trimer taken as a representative for both polymorphs

The termini of the tulobuterol molecules are on opposite sides of the mean plane of the hydrogen bond donor and acceptor atoms, with molecule **A** oriented in the opposite direction to molecules **B** and **C**. The latter feature coupled with the opposite chirality of molecule **A** enables cyclic completion of the hydrogen bonding framework of the trimer. From Figure 3.9 it is clear that if molecule **A** were oriented in the same direction or had

the same chirality as molecules **B** and **C**, the O7A atom would be incorrectly positioned to form its hydrogen bond with the N9C atom. For the O7A atom to be in position for an (R-) **A** molecule, it would have to twist around its C7-C8 bond or rotate around its long axis. These scenarios are sterically unfavourable since they bring the aromatic ring of the **A** molecule into contact with the *t*-butyl groups of the other two molecules. If the **A** molecule were oriented in the same direction as molecules **B** and **C**, the N9A atom would be out of position for its hydrogen bond to the O7B atom, irrespective of its chirality. Thus, the first condition for completion of the cyclic trimer is thus that molecule **A** should be oriented in the opposite direction to that of molecules **B** and **C**, followed by its having an opposite chirality to that of molecules **B** and **C**.

An interesting feature of the trimer is that for all three molecules the O7 and Cl2 atoms are *trans* to each other. The possible strong intramolecular hydrogen bond that could have formed between these two atoms is precluded by this *trans* relationship which could be due to the make-up of the trimer, as observed, possibly disallowing the O7 and Cl2 atoms to be *cis* for steric reasons. The preference of the observed arrangement to one in which an O-H···Cl hydrogen bond is present is further evidence of the stability of the former. The hydrogen bonding of the trimer also affects the geometry around the N9 atom. It is closer to tetrahedral than trigonal planar which is expected since the incoming hydrogen bond will 'force' the H9 atom out of the C8-N9-C10 plane. The non-bonded interactions of both polymorphs will be discussed in more depth in the section titled **Hydrogen bonding and C-H···π-ring interactions**.

Conformational aspects of the tulobuterol molecule

Since the tulobuterol molecule is central to all the structural investigations in this thesis the conformation of this molecule also warrants in-depth discussion. The reader will be referred to this section at relevant places later in the thesis. Five principal torsion angles of the tulobuterol backbone were identified that define the conformation of the molecule and these are shown in Figure 3.10(a) and (b). The five torsion angles are η_1 [C2-C1-C7-C8], η_2 [C2-C1-C7-O7], η_3 [C1-C7-C8-N9], η_4 [O7-C7-C8-N9] and η_5 [C7-C8-N9-C10]. The η_1 and η_2 torsion angles both describe rotation around the C1-C7 bond, η_1

describing the rotation of the aromatic ring plane relative to the tulobuterol backbone and η_2 describing the disposition of the Cl2 and O7 atoms. [The Cl2-C2 bond lies in the same plane as C2-C1 and therefore makes the same angle with C7-O7 thus justifying the use of the η_2 torsion angle for the description of the disposition of the Cl2 and O7 atoms]. The η_3 and η_4 torsion angles describe rotation around the C7-C8 bond, which is central in the tulobuterol backbone. The η_3 torsion angle describes the disposition of the aromatic ring relative to the N9 atom and thus the degree of 'extension' of the backbone, whilst the η_4 torsion angle describes the disposition of the O7 and N9 atoms. The η_5 torsion angle describes rotation around the C8-N9 bond in terms of the dispositions of the C7 and C10 [thus the tertiary butyl group] atoms and thus the degree of 'extension' of the tail of the tulobuterol molecule.

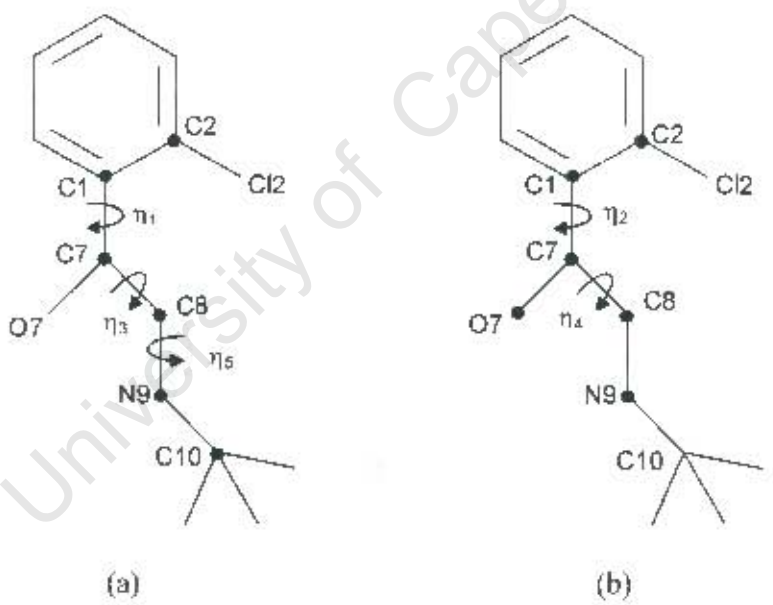

Figure 3.10 Schematic diagram of the principal torsion angles (a) η_1, η_3, η_5 (b) η_2 and η_4 for the tulobuterol backbone.

Table 3.6 lists the principal torsion angles for the molecules of the **Form 1** and **Form 2** trimers, as calculated by PLATON.[121] The signs of the torsion angles are those for the chosen asymmetric unit trimer in the respective polymorphs and are reversed for the centrosymmetrically related counterpart. The close agreement of the corresponding

torsion angles in the **Form 1** and **Form 2** trimers is evident and was demonstrated earlier in the chapter. However, Table 3.6 also highlights the close agreement of the torsion angle magnitudes of the molecules within the same trimer. The discussion of the principal torsion angles from this point on thus pertains to all the trimer molecules of both polymorphs. Figure 3.11 presents Newman projections of the torsion angles for the **A** molecule of **Form 1**, arbitrarily chosen as a representative molecule for both polymorphs.

Table 3.6 Principal torsion angles [°] for **Form 1** and **Form 2**

Polymorph	η_1	η_2	η_3	η_4	η_5
Form 1					
Molecule A [(S-)]	87.0(2)	-153.8(2)	-175.7(2)	62.2(2)	-170.5(2)
Molecule B [(R-)]	-81.4(2)	160.2(2)	-179.6(2)	-58.2(2)	173.7(2)
Molecule C [(R-)]	-77.8(2)	163.2(2)	178.1(2)	-60.1(2)	169.4(2)
Form 2					
Molecule A [(S-)]	84.0(2)	-157.2(2)	-174.0(2)	64.3(2)	-166.0(2)
Molecule B [(R-)]	-83.9(2)	157.1(2)	-175.2(2)	-54.1(2)	167.2(2)
Molecule C [(R-)]	-81.5(2)	159.9(2)	178.9(1)	-59.7(2)	172.6(2)

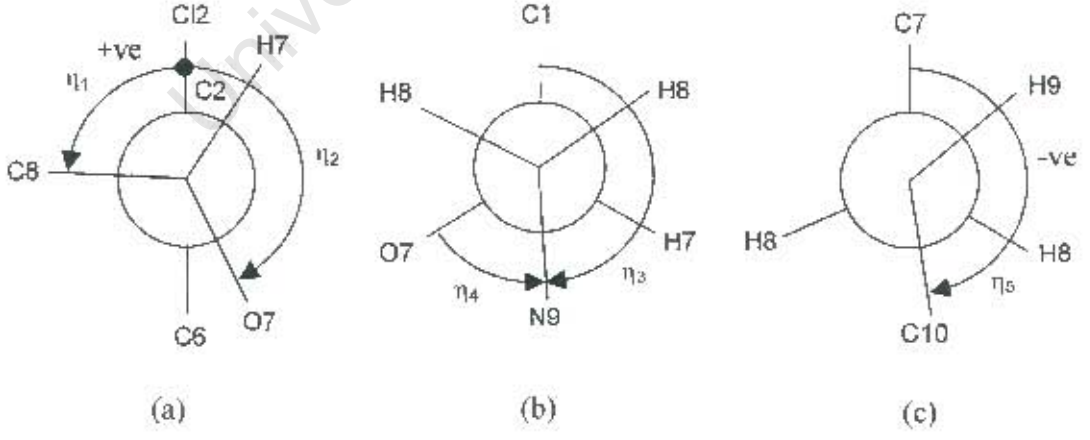

Figure 3.11 Newman projections illustrating the principal torsion angles (a) η_1, η_2 (b) η_3, η_4 and (c) η_5 for the **A** molecule of **Form 1**. The definition of the torsion angle signs is illustrated for η_1 and η_5

The η_1 torsion angle is close to 90° showing that the aromatic ring plane is nearly orthogonal to the tulobuterol backbone, whilst the η_2 torsion angle indicates that the Cl2 and O7 atoms are *trans* to one another. The η_3 torsion angle is close to 180° indicating that the tulobuterol molecule is in an 'extended' conformation with the aromatic ring being *trans* to the N9 atom. The η_4 torsion angle indicates that the O7 atom is *gauche* to the N9 atom. Finally, the η_5 torsion angle indicates that the tail of the backbone is also in an 'extended' conformation.

Hydrogen bonding and C-H···π-ring interactions

Table 3.7 lists all the hydrogen bonds for both polymorphs as calculated by PLATON.[121] The O-H···N hydrogen bonds that are responsible for the formation of the trimer are the only intermolecular hydrogen bonds, i.e there are no hydrogen bonds between symmetry related trimers in the crystal. The N-H···O, C-H···O and C-H···Cl intramolecular hydrogen bonds help stabilise the conformations of the tulobuterol molecules. The *gauche* relationship between atoms N9 and O7 is explained by the formation of the strong N-H···O intramolecular hydrogen bonds. Noticeably, **Form 2** has two additional intramolecular hydrogen bonds in the trimer, namely C6-H6A···O7A and C7C-H7C···Cl2C. Rotation around the C6-C7 bond, described by the η_1 and η_2 torsion angles, affects the donor···acceptor distances for the latter interactions. The torsion angles for the **A** and **C** molecules of **Form 1** [Table 3.6] are either at an absolute minimum or maximum relative to all their counterparts in both polymorphs. The absence of the C6-H6A···O7A and C7C-H7C···Cl2C intramolecular hydrogen bonds for **Form 1**, are thus due to these torsion angles being outside the range for their formation.

PLATON[121] revealed that the C-H···π-ring interactions for **Form 1** and **Form 2** all have symmetry operations other than x, y, z indicating that all the interactions are between molecules of different asymmetric units and thus different trimers. For this reason these interactions are discussed in more detail in the **Crystal packing** section. Distances for π···π-ring interactions were too long [~5Å] to be regarded as significant interactions of this type.

Table 3.7 Hydrogen bonding interactions for **Form 1** and **Form 2**

Hydrogen bond	H···A / Å	D···A / Å	D-H···A / °
Form 1			
O7A-H7A1···N9C	1.83(2)	2.821(2)	171(2)
O7B-H7B1···N9A	1.79(2)	2.778(2)	173(2)
O7C-H7C1···N9A	1.76(1)	2.750(2)	172(3)
N9A-H9A···O7A (intramolecular)	2.36(2)	2.807(2)	107(1)*
N9B-H9B···O7B (intramolecular)	2.32(2)	2.780(2)	107(1)
N9C-H9C···O7C (intramolecular)	2.26(2)	2.771(2)	111(1)
C6B-H6B···O7B (intramolecular)	2.45(2)	2.793(3)	102(2)
C6C-H6C···O7C (intramolecular)	2.41(2)	2.766(3)	102(2)
C7A-H7A···Cl2A (intramolecular)	2.70(2)	3.088(2)	104(2)
C7B-H7B···Cl2B (intramolecular)	2.71(2)	3.071(2)	102(2)
Form 2			
O7A-H7A1···N9C	1.99(2)	2.839(2)	173(2)
O7B-H7B1···N9A	1.75(2)	2.747(2)	177(2)
O7C-H7C1···N9A	1.78(2)	2.765(2)	169(2)
N9A-H9A···O7A (intramolecular)	2.36(2)	2.840(2)	109(1)
N9B-H9B···O7B (intramolecular)	2.21(1)	2.729(2)	111(1)
N9C-H9C···O7C (intramolecular)	2.31(2)	2.774(2)	108(1)
C6A-H6A···O7A (intramolecular	2.50(2)	2.820(2)	100(2)
C6B-H6B···O7B (intramolecular)	2.44(2)	2.777(2)	102(2)
C6C-H6C···O7C (intramolecular)	2.44(2)	2.787(3)	102(2)
C7A-H7A···Cl2A (intramolecular)	2.72(2)	3.089(2)	103(2)
C7B-H7B···Cl2B (intramolecular)	2.74(2)	3.107(2)	103(2)
C7C-H7C···Cl2C (intramolecular)	2.76(2)	3.099(2)	101(2)

* Interactions with D-H···A in the range 100-111° are included for completeness, but they may have low significance as 'hydrogen bonds'

Crystal packing

It was previously concluded that the trimers of the respective polymorphs are nearly identical so differences in crystal packing must exist between the two structures in order for the latter to qualify as polymorphs. The different space groups in which the polymorphs crystallise imply that these differences exist since the symmetry elements of the two space groups are different. Figure 3.12(a) and (b) present crystal packing

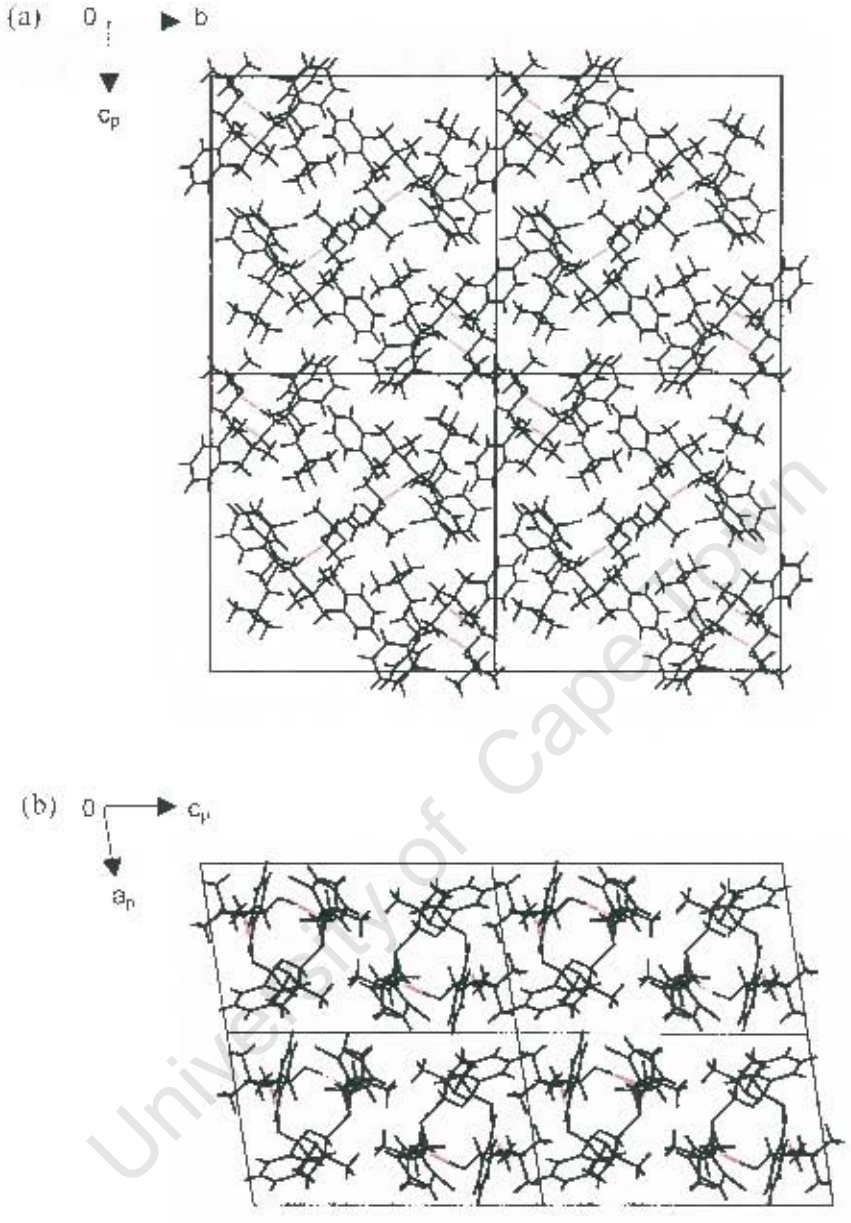

Figure 3.12 Crystal packing diagrams for (a) **Form 1** and (b) **Form 2.** Hydrogen bonds of the trimers are shown in red. Four unit cells are drawn in each case.

diagrams of **Form 1** and **Form 2** respectively. There are four trimers in the monoclinic **Form 1** unit cell, whilst the triclinic **Form 2** unit cell contains two trimers. **Form 2** trimers stack in columns parallel to the *b*-axis with planes defined by the intermolecular

O-H···N hydrogen bonds normal to this direction. No such view could be obtained for **Form 1**, and a 'common direction' could not be established in order to propose a possible transformation mechanism between the two polymorphs. The near uniformity of the polymorph trimers and lack of inter-trimer hydrogen-bonding also means that the graph set analysis descriptor [see **Chapter 1 – Introduction**, pages 10-11] is the same for both polymorphs, namely $R_3^3(15)$.

Although there are no inter-trimer hydrogen bonds for either polymorph, C-H···π-ring interactions exist between the trimers, and are listed in Table 3.8.

Table 3.8 C-H···π-ring interactions for **Form 1** and **Form 2**

Interaction	H···Cg / Å	C···Cg / Å	C-H···Cg / °	Symmetry code[b]
Form 1				
C4A-H4A···CgB[a]	2.70(2)	3.524(4)	149(2)	1/2-x, 1/2+y, 1/2-z
C5B-H5B···CgC	3.13(2)	3.724(2)	123(2)	-1+x, y, z
C12B-H14B···CgA	3.28(2)	4.223(3)	168(2)	1/2-x, -1/2+y, 1/2-z
Form 2				
C5B-H5B···CgC	3.17(2)	3.781(3)	125(2)	1+x, y, z
C5C-H5C···CgB	3.06(2)	3.859(3)	146(2)	1-x, -y, -z

[a] CgX = centre of gravity of the aromatic ring of molecule X
[b] Symmetry code applies to the second unit of the interaction

Table 3.8 lists three unique interactions for **Form 1** and two for **Form 2**. However, since all the interactions are inter-trimeric, the total number of interactions per trimer doubles to six and four for **Form 1** and **Form 2** respectively. Figure 3.13(a) and (b) illustrate the C-H···π-ring interactions for trimers in the **Form 1** and **Form 2** unit cells respectively.

In **Form 1** the C5B-H5B···CgC interaction has the symmetry code –1+x, y, z indicating that this interaction connects trimers of adjacent unit cells translated along the *a*-axis. Since only one trimer per unit cell is accommodated along this direction, each trimer is linked into a chain with its translated counterparts. The C4A-H4A···CgB and C12B-14B···CgA interactions connect trimers in the upper half of the unit cell, with an identical

network of C-H···Cg interactions occurring in the lower half of the unit cell due to centrosymmetry. There are no C-H···π-ring interactions along the *c*-axis. Thus in the **Form 1** crystal all trimers are connected to their neighbours in the *xy*-plane only which results in sheets of C-H···π-ring connected trimers that are stacked along the *c*-axis.

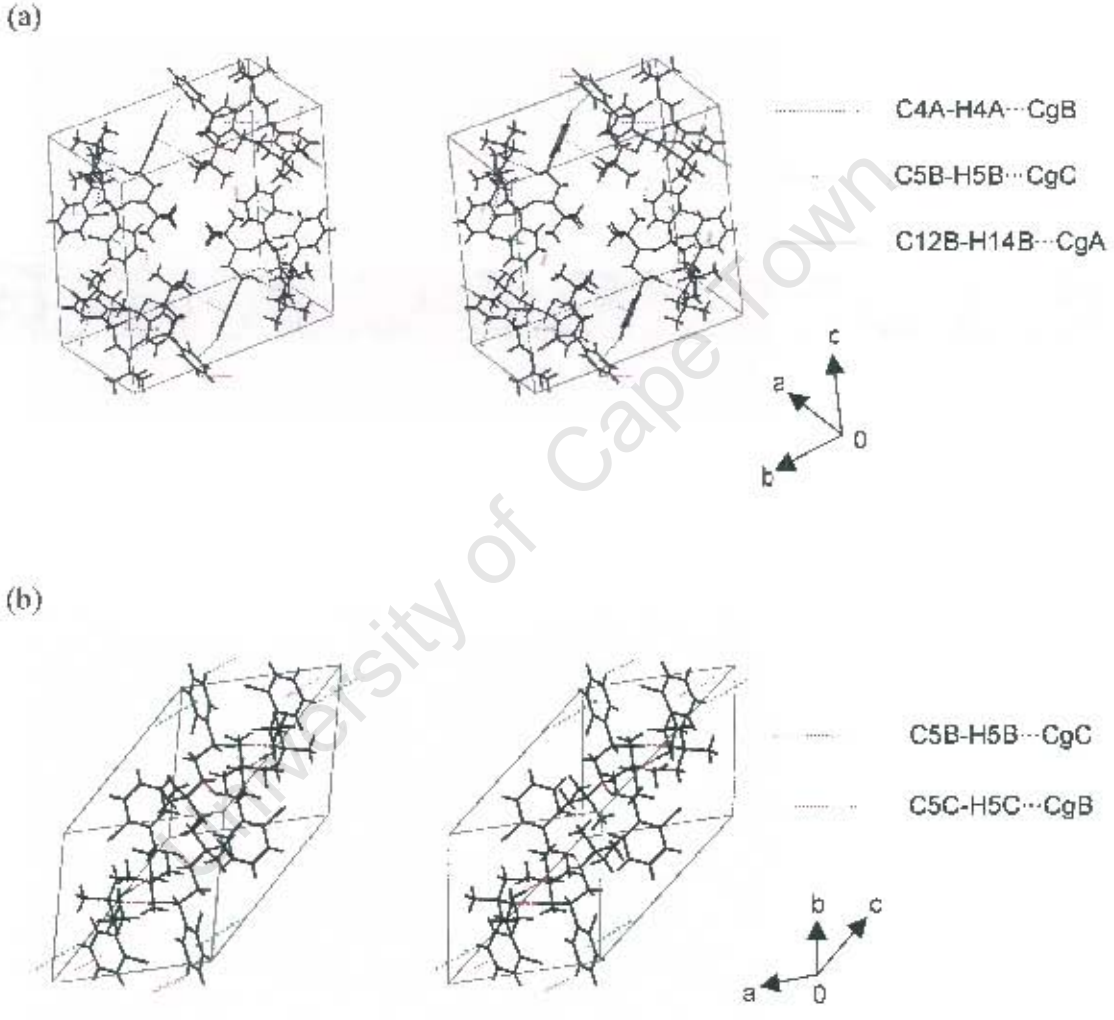

Figure 3.13 Stereo diagrams illustrating the C-H···π-ring interactions for (a) **Form 1** and (b) **Form 2**

In the **Form 2** unit cell, the C5B-H5B···CgC symmetry code of 1+x, y, z indicates that this interaction links trimers along the *a*-axis. As in the case of **Form 1**, only one trimer per unit cell is accommodated along this direction thus resulting in chains of translated trimers. The C5C-H5C···CgB interaction connects trimers diagonally along the *yz*-plane. However, trimers within a particular unit cell are not linked in this manner, but only trimers between adjacent unit cells, which thus results in a discontinuous connection of trimers diagonally along the *yz*-plane. This means that the chains down the *a*-axis are connected into sets of two. As in the case of **Form 1**, C-H···π-ring interactions are absent in a third dimension.

Form 2(NTr) and Form 2(Tr) crystal structure determinations

Structure determinations were performed on **Form 2(NTr)** [which were taken as representative data for the **Form 2** RT determination in Table 3.4] and **Form 2(Tr)** crystals to determine whether they are the same polymorph. One half of each crystal type was subjected to thermal analysis to confirm its thermal behaviour, RT X-ray structure determinations were performed using the remaining crystal portions since comparing these would be essential for making possible correlations with the different thermal behaviours. The unit cell data for **Form 2(NTr)** and **Form 2(Tr)** presented in Table 3.9 are in very close agreement. The small differences that exist are probably due to small variations in crystal characteristics such as size and mosaicity. Their structural refinements were taken to completion and diagrams of their asymmetric units and crystal packing were compared [not shown]. These were found to be superimposable leading to the conclusion that there are no structural differences between **Form 2(NTr)** and **Form 2(Tr)**, i.e. that they are the same polymorph. The different thermal behaviours can thus only be due to contamination effects and/or the presence of defects, as discussed in the **Thermal Analysis** section.

Table 3.9 Crystal and refinement parameters for **Form 2(NTr)** and **Form 2(Tr)**

Parameter	Form 2(NTr)	Form 2(Tr)
Formula unit	$C_{12}H_{18}ClNO$	$C_{12}H_{18}ClNO$
Formula weight / g mol^{-1}	227.7	227.7
Crystal system	Triclinic	Triclinic
Space group	$P\bar{1}$	$P\bar{1}$
a / Å	11.0506(2)	11.051(2)
b / Å	11.8859(3)	11.891(2)
c / Å	16.9846(5)	16.994(3)
α / °	91.558(1)	91.59(3)
β / °	97.296(1)	97.28(3)
γ / °	115.168(1)	115.16(3)
Volume / Å^3	1994.5(1)	1996.6(3)
Z	6	6
Density$_{calc}$ / g cm^{-3}	1.138	1.136
μ (MoK$_\alpha$) / mm^{-1}	0.27	0.264
F(000)	732	732
Crystal size / mm^3	0.30x0.30x0.35	0.35x0.40x0.45
Temperature / K	295(2)	295(2)
Range scanned θ / °	$2 \leq \theta \leq 27$	$3 \leq \theta \leq 27$
Index ranges	h: -14, 14 k: -12, 15 l: -21, 21	h: -14, 12 k: -15, 12 l: -22, 22
φ scan angle / °	1.0	1.0
φ scan range / °, no. of frames	183, 183	183, 183
ω scan angle / °	1.0	1.0
ω scan ranges / °, no. of frames	67, 67	44, 44; 43, 43; 36, 36; 78, 78
Dx / mm	34	32
No. of measured reflections	13165	13985
No. of unique reflections	8463	9052
No. of reflections with $I > 2\sigma(I)$	5906	4820
No. of least-squares parameters	436	430
R_{int}, R_σ	0.0285, 0.0498	0.0237, 0.0574
S	1.145	1.017
R_1 ($F_o > 4\sigma(F_o)$)	0.0976	0.0563
wR_2	0.2998	0.1575
No. of reflections omitted	39	15
Weighting scheme	a = 0.1602 b = 0.75	a = 0.628 b = 0.47
$(\Delta / \sigma)_{mean}$	< 0.001	< 0.001
Δρ excursions / e Å^{-3}	0.89, -0.80	-0.45, 0.43

Powder X-ray Diffraction

Experimental and computed PXRD patterns of **Form 1** and **Form 2** are presented in Figure 3.14. The peaks of the computed and experimental patterns match in their number and 2θ positions. The relative intensity distribution of the peaks of the experimental pattern is also similar to that of the computed pattern indicating the lack of preferred orientation in the analysed sample. The close agreement of experimental and computed patterns is also an indication of the correctness of the single crystal structural models. The slight shifts of the experimental pattern with respect to the computed pattern to lower 2θ are attributed to the temperature differences at which the respective traces were obtained. The powder patterns of the polymorphs also differ significantly showing that these can serve as references for their identification. Table 3.10 lists the three most intense peaks for the computed patterns of both polymorphs. The peaks of the computed patterns were chosen since experimental pattern peaks with close intensities might be reversed due to slight preferred orientation effects. However, from visual inspection, an easy, recognisable distinction is that the **Form 1** trace has four peaks around 10° 2θ, whilst **Form 2** has six in that region.

Table 3.10 The three most intense PXRD peaks for **Form 1** and **Form 2**

Polymorphs	Peak 1 (2θ, I_{rel})	Peak 2 (2θ, I_{rel})	Peak 3 (2θ, I_{rel})
Form 1	10.2, 100	18.7, 54	20.5, 44
Form 2	18.1, 100	9.5, 81	19.6, 73

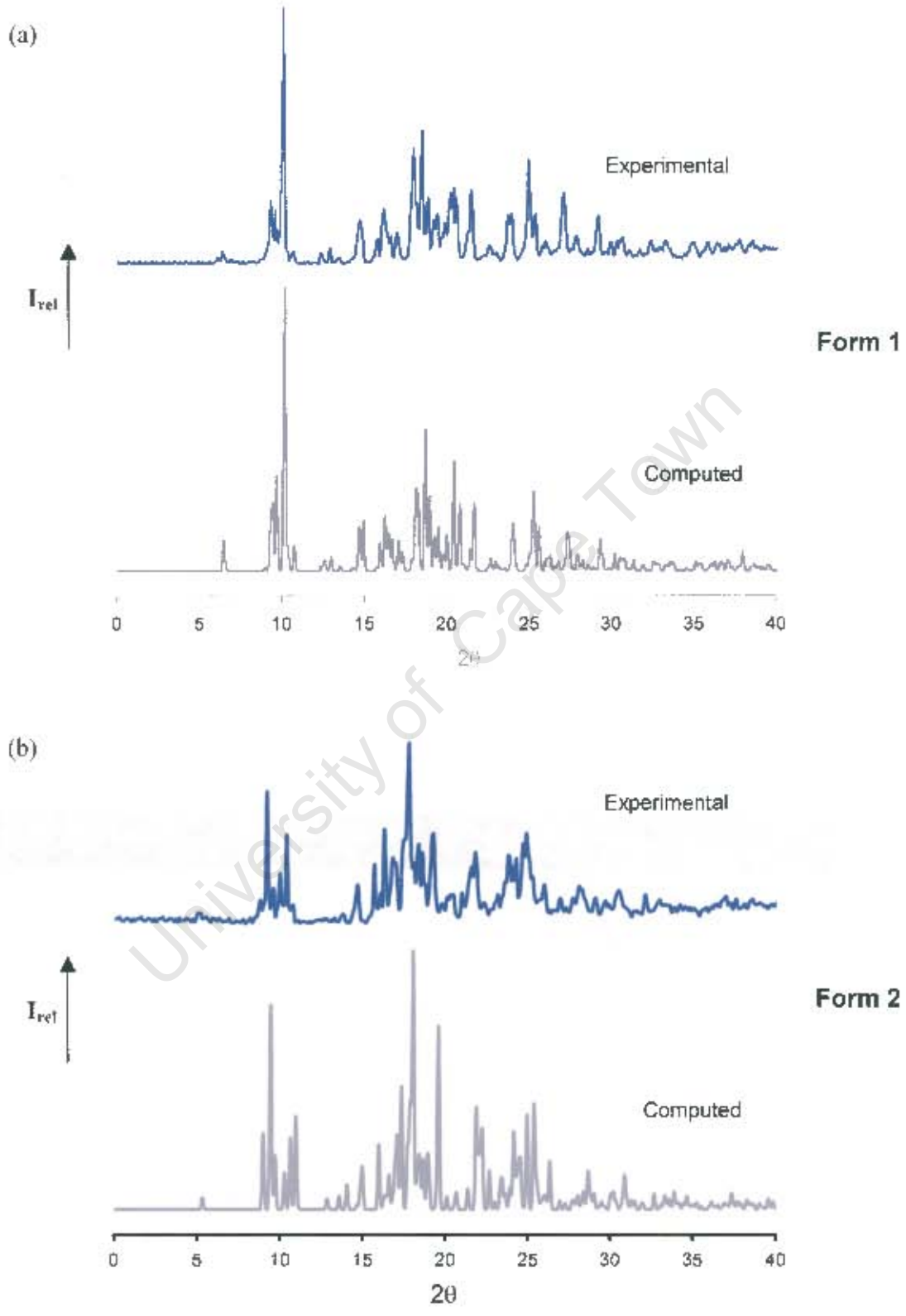

Figure 3.14 Experimental [295 K] and computed patterns [173 K] of (a) **Form 1** and (b) **Form 2**

Fourier-transform Infrared Spectroscopy

FTIR traces for **Form 1** and **Form 2** as Nujol mulls are presented in Figure 3.15. The traces are identical across the scanned frequency range, especially in the range 3000-3600 cm^{-1}. This region is often diagnostic for polymorphs containing O-H and N-H functional groups. Only one peak of equal intensity appears in both traces at 3288 cm^{-1} which is consistent with the uniform environment of the –OH and –NH groups in the trimers. This technique can thus not be used to distinguish the polymorphs but does further attest to the structural similarity of the polymorph trimers revealed by single crystal X-ray diffraction.

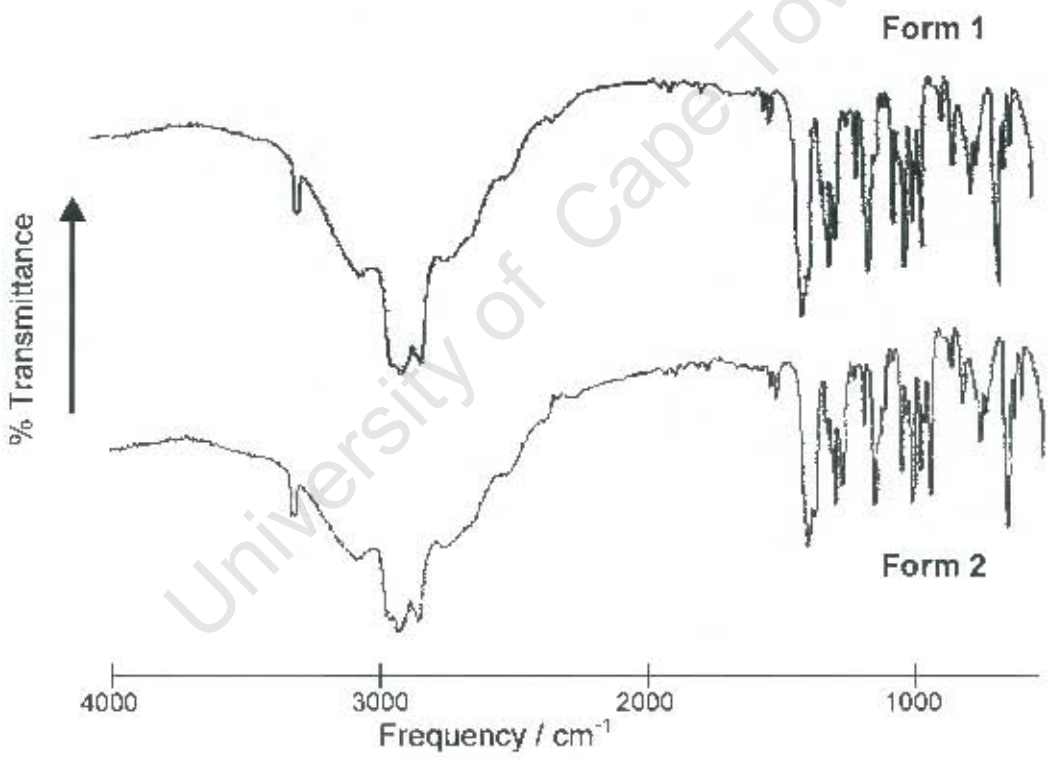

Figure 3.15 FTIR spectra of **Form 1** and **Form 2**

Solid-state Nuclear Magnetic Resonance Spectroscopy

SSNMR assignments were based on solution NMR peak assignments, which showed these peaks to be close in frequency to those of the SSNMR traces. These are tabulated together with those of the SSNMR peaks of **Form 1** and **Form 2** in Table 3.11.

Table 3.11 Peak assignments for the solution and solid-state ^{13}C NMR

Atom	Solution NMR / ppm	Form 1 SSNMR / ppm	Form 2 SSNMR / ppm
C1	131.77	136.19	135.24
C2	140.39	144.08	143.31
C3-C6	126.95-129.21	127.15-129.71	127.72
C7	68.9	67.92	67.66
C8	50.4	50.78	50.21
C10	47.9	49.04	48.24
C11-C13	29.2	29.36	30.46, 28.78

The ^{13}C SSNMR spectra for **Form 1** and **Form 2** are presented in Figure 3.16. Generally, SSNMR spectral peaks are broader than those of solution NMR due to factors such as different decoupling efficiencies, dipolar coupling to quadropolar atoms and overlapping peaks of chemically equivalent but crystallographically independent carbons. From Figure 3.16 it is clear that the broadening of peaks is extensive which is probably due to the overlap of the chemically equivalent but crystallographically independent carbons. For **Form 1**, the peak representing atoms C3-C6 displays fine structure that is not observed in the case of **Form 2**. PLATON[121] was used to determine the short intermolecular contacts present in the polymorphic structures. For **Form 1** more short intermolecular contacts were observed for atoms C3-C6 than for **Form 2** which could explain the fine structure of the peak representing these atoms in the **Form 1** spectrum. The only other difference between the spectra is that two methyl peaks are observed for **Form 2**, but only one for **Form 1**. Again, more short intermolecular contacts are observed for these carbons in the **Form 2** crystal than exist in **Form 1**. The atoms for which differences were observed in the SSNMR spectra can be explained structurally in

that they are located on the periphery of the trimer [see Figure 3.9, pg. 53] and are therefore in contact with neighbouring trimers. This also explains why atoms that are located on the inside of the trimer, such as C7 and C8, exhibit no spectroscopic differences as these environments for both polymorphs were determined to be uniform by X-ray diffraction. There is a general trend of an upfield shift of up to 0.9 ppm from **Form 1** to **Form 2**.

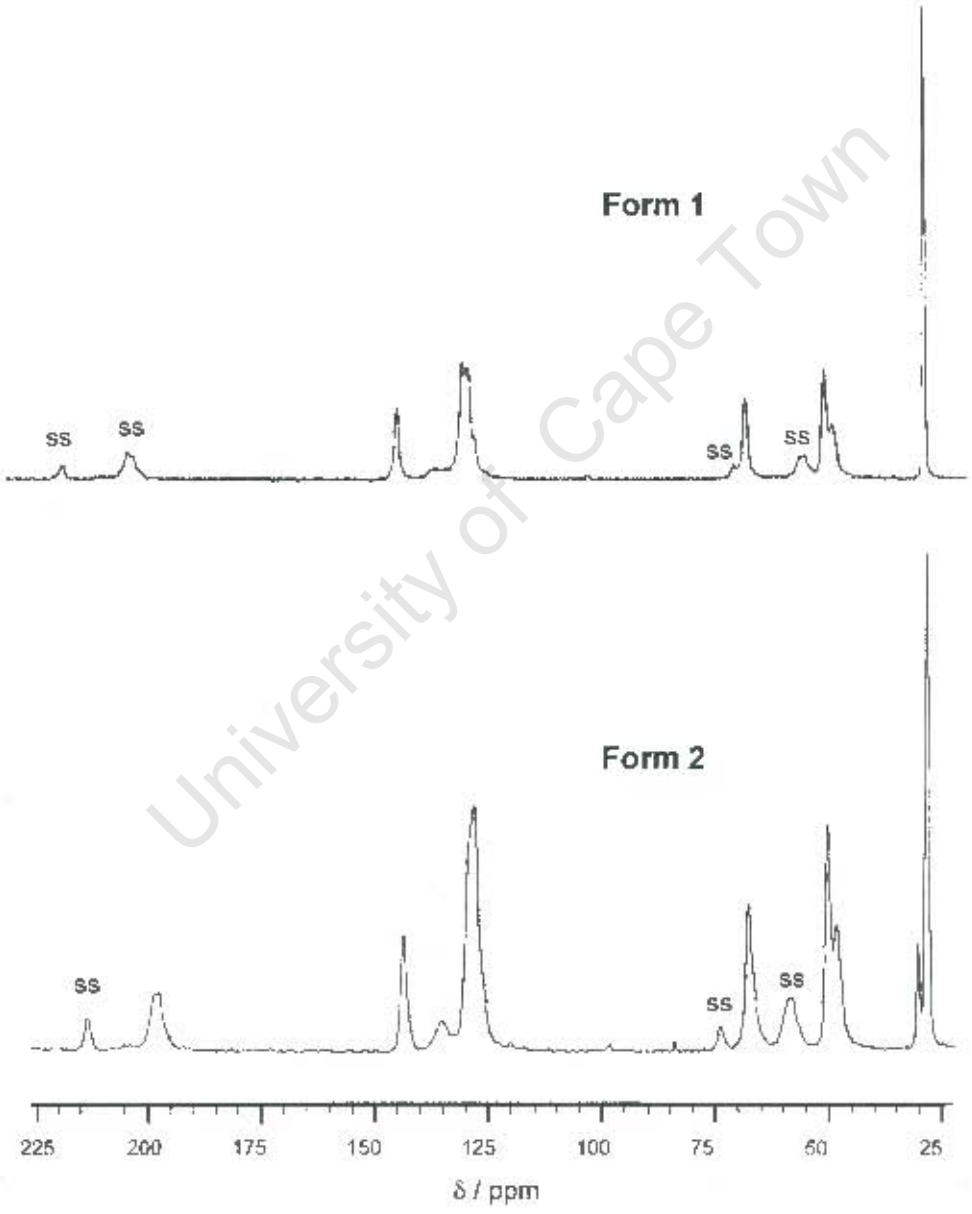

Figure 3.16 SSNMR spectra of **Form 1** and **Form 2**. Peaks marked 'ss' refer to spinning side bands.

Conclusion

Two polymorphs, **Form 1** and **Form 2**, of the free base of tulobuterol were isolated and characterised by thermal, spectroscopic and diffraction methods. A third form, **Form 3**, was prepared by thermal methods. This form proved difficult to isolate which left DSC analysis as its only form of characterisation.

The melting point of **Form 1**, 91°C, was found to correspond to the previously reported melting point [89-91°C] for tulobuterol.[98] It is the higher melting form of the dimorphic pair with **Form 2** having a melting point of 81°C. Accurate measurements of fusion enthalpies established the stability relationship of the polymorphs as monotropic with the higher-melting **Form 1** thus being the stable form at all temperatures. The transforming behaviour of **Form 2** upon melting to **Form 1** has been attributed to low-level contamination [by grains of **Form 1**] that is not detectable by PXRD.

Form 1 crystallises in the monoclinic space group $P2_1/n$ with a = 10.802(1), b = 18.949(2), c = 19.649(1) Å, β = 94.84° and 12 molecules per unit cell. **Form 2** crystallises in the triclinic space group $P\bar{1}$ with a = 11.004(2), b = 11.896(2), c = 16.844(3) Å, α = 91.283(3), 97.464(3), 115.324(3)° and 6 molecules per unit cell. In both crystal structures the asymmetric unit consists of three tulobuterol molecules hydrogen bonded to each other to form a cyclic trimer. The structural uniformity of these trimers has been demonstrated and attests to the stability of the hydrogen bonding arrangement. The trimeric asymmetric unit also results in the number of molecules per unit cell for each polymorph being unusually high from a crystallographic point of view. The polymorphs differ in the way these trimers pack in their respective unit cells. No inter-trimer hydrogen bonds were located but C-H···π-ring interactions were found to connect the trimers in both polymorphs. Thus only van der Waals and C-H···π-ring interactions are involved in crystal assembly, which is consistent with the low melting points of these polymorphs. Furthermore, **Form 2** was found to have fewer of these C-H···π-ring interactions per trimer as well as a less extensive network of C-H···π-ring connected trimers, which is consistent with its lower melting point relative to that of **Form 1**.

Experimental PXRD traces were found to be consistent with computed patterns allowing these to serve as reliable references for polymorphic identification.

Solid-state NMR highlighted differences between the polymorphs that allow this technique to be used for diagnostic purposes. The observed similarities and differences could be correlated with the crystal structures. FTIR spectra for the polymorphs are practically indistinguishable, especially in the –OH, –NH stretching frequency region. This is consistent with the uniformity of the intermolecular hydrogen bonding of the trimers in the polymorphs as established by X-ray diffraction.

Chapter 4 - β-CD and γ-CD Inclusion Complexes

Complex Preparation

Complexes of β-CD and γ-CD with tulobuterol free base [respectively referred to as **BCDTUL** and **GCDTUL** hereinafter] were prepared by kneading the CD and the drug in a 1:1 molar ratio with a mortar and pestle. This was done over a period of one hour, during which an appropriate amount of water was added to maintain a pasty consistency.

BCDTUL single crystals were obtained by dissolving and stirring 100 mg of the kneaded complex in 10 ml water at 60°C for two hours. The solution was then filtered and allowed to cool spontaneously and evaporate to produce single crystals. **GCDTUL** single crystals were obtained in an analogous manner to those of **BCDTUL**, except that 100 mg of CD was dissolved in 4 ml water.

Microanalysis

The host:guest ratios were determined by C, H, N microanalysis. The **BCDTUL** and **GCDTUL** complexes proved to be hygroscopic and therefore TGA was performed concurrently in order to ascertain the water content of the samples analysed by microanalysis. Prior to these analyses, the samples were removed from their mother liquor, dried on a filter paper and left in the open air for three days in order for their water content to equilibrate. The microanalysis results are presented in Table 4.1 and they indicate that the **BCDTUL** and **GCDTUL** complexes crystallise in a 2:1 and 3:2 host:guest ratio respectively.

Table 4.1 C, H, N microanalysis results [n −2] for **BCDTUL** and **GCDTUL**

Complex	Experimental			Calculated		
	%C	%H	%N	%C	%H	%N
BCDTUL $2(C_{42}H_{70}O_{35})\cdot C_{12}H_{18}ClNO\cdot 12.3(H_2O)$	42.68	6.53	0.67	42.46	6.81	0.52
GCDTUL $3(C_{48}H_{80}O_{40})\cdot 2(C_{12}H_{18}ClNO)\cdot 33.3(H_2O)$	40.97	6.50	0.38	40.85	6.72	0.57

Thermal analyses

Hot Stage Microscopy

HSM photographs of the complexes of **BCDTUL** and **GCDTUL** are presented in Figure 4.1. The analyses were done under silicone oil to assess the presence of included water as would be indicated by bubble formation. Photographs of the **BCDTUL** and **GCDTUL** were recorded at (a) the start of the analysis, (b) the first signs of bubbling, (c) the time by which extensive crystal cracking had taken place, (d) the onset of decomposition [indicated by a colour change of the crystals to brown] and (e) the subsequent appearance of bubbling as a result of decomposition. Figure 4.1 shows that the first signs of release of water from the crystals appear at 90°C and 53°C for the **BCDTUL** and **GCDTUL** respectively. By 120°C extensive cracking, a further consequence of dehydration of the crystals, had taken place for both complexes. The first signs of decomposition and its associated bubbling appear at 240 and 300°C respectively for **BCDTUL**, whilst these events respectively appear at 250 and 295°C for **GCDTUL**.

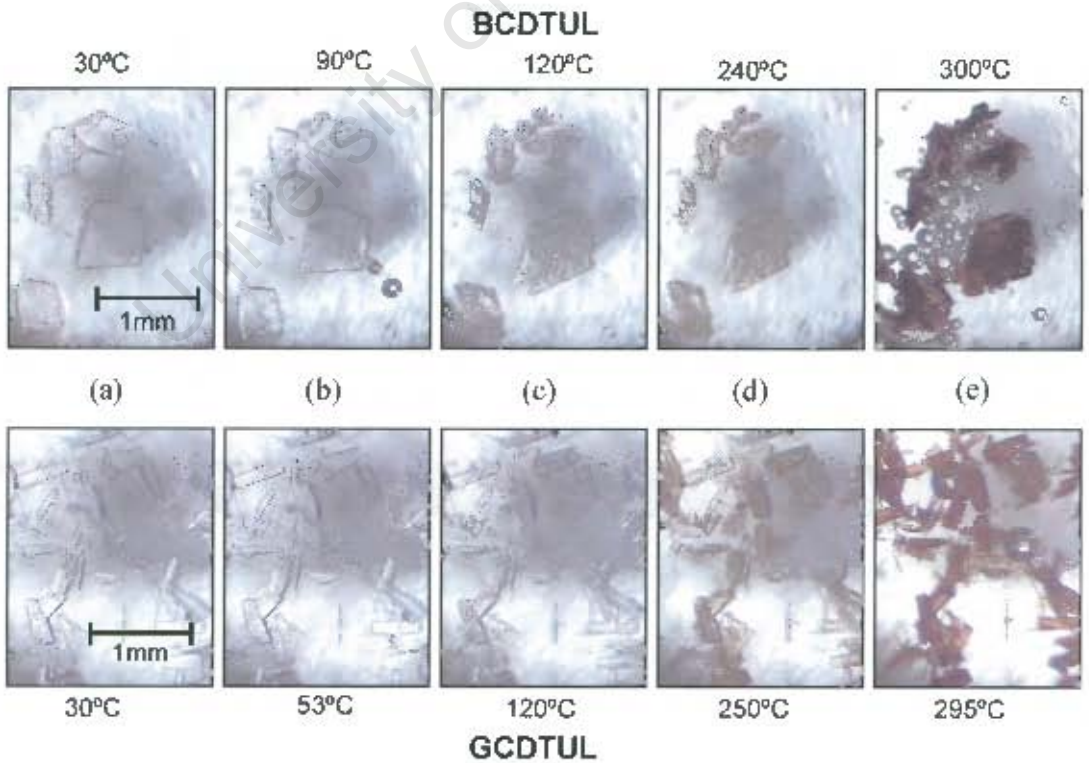

Figure 4.1 HSM photographs of **BCDTUL** and **GCDTUL** at various temperatures

Differential Scanning Calorimetry and Thermogravimetric Analysis

DSC and TGA traces for **BCDTUL** and **GCDTUL** are presented in Figure 4.2. TGA was used to determine the water content of the **BCDTUL** and **GCDTUL** complexes, which is indicated by the initial mass loss [mass loss A] in Figure 4.2. The TGA trace for **BCDTUL** shows a mass loss of 11.9% in the temperature range 30-150°C, which establishes its β-CD:tulobuterol:H_2O ratio as 2:1:18.7, whilst that of **GCDTUL** indicates a mass loss of 12.1% in the temperature range 30-150°C, in turn establishing its γ-CD:tulobuterol:H_2O ratio as 3:2:33.3. The TGA results over the whole range of the analyses are summarised in Table 4.2.

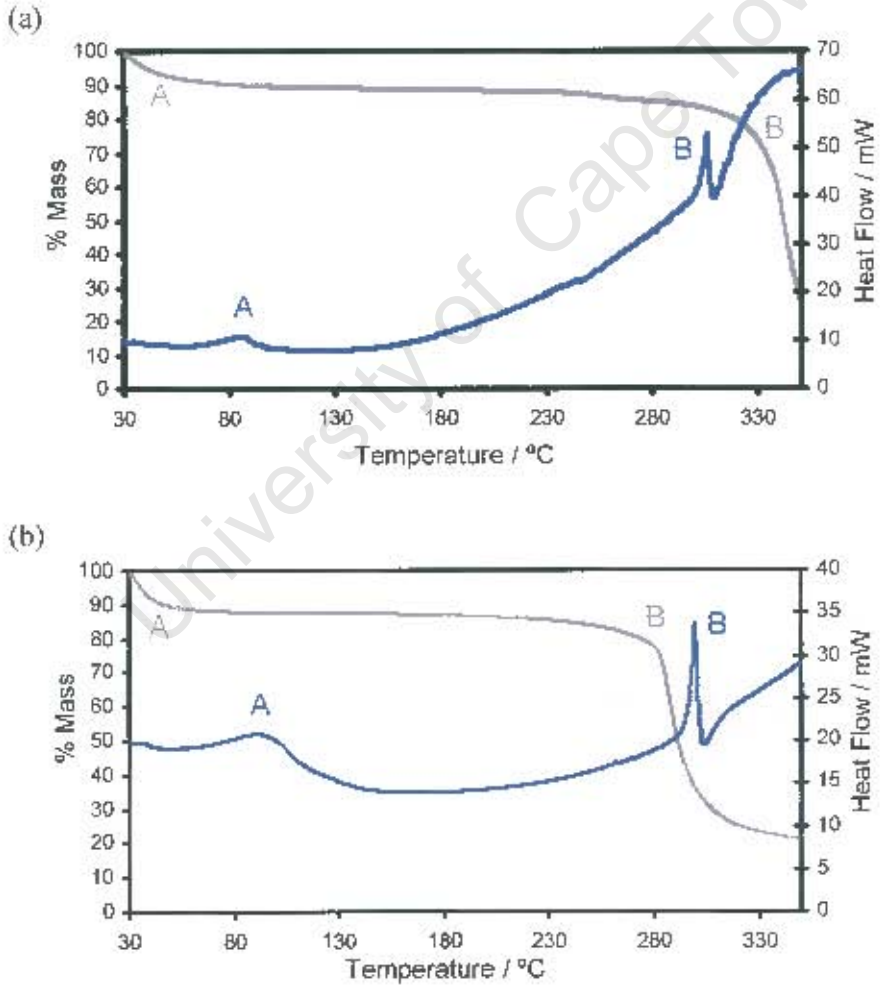

Figure 4.2 DSC [blue] and TGA [grey] traces of (a) **BCDTUL** and (b) **GCDTUL**

Table 4.2 TGA results [n =3] summarised for **BCDTUL** and **GCDTUL**

Temperature / °C	BCDTUL		GCDTUL	
	%Mass	% Mass Loss	%Mass	% Mass Loss
30	100	0	100	0
50	92.8	7.2	90.4	9.6
100	88.6	11.4	88.0	12.0
150	88.1	11.9	87.9	12.1
200	88.0	12.0	87.0	13.0
250	87.0	13.0	84.5	15.5
300	83.6	16.4	36.7	63.3
350	26.1	73.9	20.8	79.2

As is characteristic of hydrated complexes, the DSC traces for both **BCDTUL** and **GCDTUL** show an initial endotherm [endotherms A in Figure 4.2] indicative of dehydration, which revealed itself in the TGA traces as an initial mass loss [Mass loss A] for both complexes. The features of the final section of the DSC curves [endotherms B, which in each case is followed by an immediate exotherm] for both complexes correspond to decomposition. The HSM analysis confirmed this visually when the crystals turned brown at these temperatures. The onset of decomposition occurs at 305°C for **BCDTUL** and 298°C for **GCDTUL**. The very high and rapid mass losses occurring at these temperatures, as indicated by the TGA traces are a further confirmation of decomposition. The asymmetric shapes of the endotherms of dehydration and decomposition for both complexes indicate that these are multi-step processes. Generally the DSC and TGA results correlate well with the HSM results. The DSC results are summarised in Table 4.3.

Table 4.3 Summary of the DSC thermal events for **BCDTUL** and **GCDTUL**

Endotherm	Parameter	BCDTUL	GCDTUL
A	Temperature range (°C)	55-105	55-145
	T_{on} (°C)	62	62
	Peak (°C)	82	94
B	Temperature range (°C)	294-308	295-305
	T_{on} (°C)	305	298
	Peak (°C)	303	300

X-ray Crystallographic Analysis of BCDTUL

Single Crystal X-ray Diffraction

X-ray photography

Photographic techniques were used to establish the preliminary unit cell parameters for the **BCDTUL** complex. A suitable crystal was mounted on a glass fibre and covered with glue in order to prevent dehydration of the crystal. An oscillation photograph revealed no symmetry whilst a 0-level Weissenberg photograph indicated only the inherent Laue 1 symmetry. This led to the assignment of the triclinic crystal system for which the only two space group possibilities are P1 and $P\bar{1}$. Since the host molecule β-CD is chiral, the former space group was chosen.

Data-collection and space group determination

Intensity data were collected on a Nonius Kappa CCD diffractometer at 113K using graphite-monochromated MoKα radiation. XPREP[109] indicated the space group P1 on the basis of intensity statistics, which indicated $|E^2-1| = 0.733$. This is close to the value of 0.736 expected for non-centrosymmetric structures. The author is aware of the space group ambiguity that often surrounds β-CD complexes that crystallise in the space group P1 with unit cell parameters a ~ 15, b ~ 15, c ~ 15 Å, α ~ 100, β ~ 101, γ ~103°. The triclinic unit cell can be transformed to the monoclinic unit cell [a ~ 18, b ~ 24, c ~ 15 Å, β ~ 110°], space group C2, via a simple matrix. The latter space group has been shown to indicate the true symmetry for a number of β-CD complexes initially reported with the indicated P1 lattice.[123,124] In both space groups the β-CD host molecules form dimers, their constituent host molecules being related by a pseudo- [P1 lattice] or a crystallographic two-fold rotation axis [C2 lattice] that runs through the secondary interface of the β-CD molecules. To investigate whether the assigned space group of P1 for **BCDTUL** was correct, the appropriate transformation matrix was applied in order to generate the higher symmetry space group C2. The latter space group was subsequently rejected for two reasons. Firstly, the structure solution and refinement in the space group

C2 yielded too many inconsistent equivalents [3003 out of 10594 unique reflections, ~28%], thus indicating that the required Laue symmetry for a monoclinic space group was not met. Secondly, the α- and γ-angles of the transformed unit cell were not sufficiently close to 90° [α – 91.8°, γ – 89.5°] as required for a monoclinic unit cell. Post-refinement analysis of the **BCDTUL** structure using the ADDSYM routine in PLATON[121] indicated no obvious extra crystallographic symmetry, thus reaffirming the correct choice of space group.

Structure solution and refinement

Microanalysis indicated a 2:1 β-CD:tulobuterol ratio and from the unit cell volume it was deduced that the asymmetric unit comprises two β-CD host molecules and one tulobuterol guest molecule. SHELXD[113] was used to solve the structure by *ab initio* methods, which revealed the positions of all the non-hydrogen atoms of the two host molecules. For the first refinement in SHELXL,[112] only the host atoms [excluding the 'freely' rotating O6 atoms] were retained and refined isotropically. This was done so that any disorder of the O6 atoms could be modelled based on peak heights of their associated electron densities in the difference Fourier map. The glucopyranose units of the two host molecules of the asymmetric unit were labelled **A1**-**A7** and **B1**-**B7** respectively. The O6 atoms were located in the initial and subsequent difference Fourier maps with one O6 atom per host molecule being disordered [those of **A4** and **B6**] over two positions. These disordered O6 atoms [second disordered component labelled O7] were refined with s.o.f's of x and 1-x, the initial fraction x weighted according to the initial electron density peak heights of the disordered components. The initial values of x were 0.56 and 0.67 for O6A4 and O6B6 respectively, which refined to final values of 0.66 and 0.82. The host atoms were not refined anisotropically since several of these had thermal parameters that became 'non-positive definite' when this was attempted. This occurred despite isotropic thermal parameters behaving well. The host hydrogen atoms were placed using a riding model, except for the hydroxyl hydrogen atoms, which were refined using a hydrogen bond searching model [AFIX 83]. All the hydrogen atoms were refined isotropically with temperature factors 1.2 times those of their parent atoms.

Thirty-five sites were identified as water molecule locations. The oxygen atoms of these water molecules were placed with fixed temperature factors [0.05 $Å^2$ was chosen since the host oxygen atoms were well below this value] and refined with varying s.o.f.'s. The total site occupancy summed to 18.5, which is close to the value of 18.7 obtained from TGA analysis. The s.o.f.'s of the water molecules are presented in Table 4.4. Hydrogen atoms of water molecules were not placed.

The diffuse electron density in the cavity of the host molecules did not allow for placement of the guest atoms due to the unacceptable distances and angles between electron density peaks. Thus there were several, relatively high-density peaks [1.00-1.78 e $Å^{-3}$] remaining in the host cavity after the final refinement. This, together with the forced non-anisotropic refinement of the host atoms, impacted negatively on the precision of the refinement as the R_1-factor was relatively high at 0.18. The case presented here is the best of a number of data collections that were performed for several different **BCDTUL** crystals, in which the indicated negative factors were consistently present. These problems could be attributed to the relatively high mosaicity [~2°] of the crystals. The lack of guest modelling in β-CD inclusion complexes due to their disorder has been reported for other β-CD dimeric structures that crystallise with channel packing arrangement.[84] Crystal and refinement parameters for **BCDTUL** are presented in Table 4.5.

Table 4.4 Site occupancy factors for the water molecules of the **BCDTUL** structure

Molecule	s.o.f.	Molecule	s.o.f.	Molecule	s.o.f.	Molecule	s.o.f.
OW1	1.00	OW10	0.12	OW19	0.34	OW28	0.32
OW2	0.18	OW11	0.68	OW20	0.23	OW29	0.29
OW3	1.00	OW12	0.82	OW21	0.46	OW30	0.34
OW4	0.89	OW13	0.21	OW22	0.30	OW31	0.71
OW5	1.00	OW14	0.59	OW23	0.27	OW32	0.19
OW6	0.72	OW15	0.75	OW24	0.73	OW33	0.42
OW7	0.89	OW16	0.46	OW25	0.19	OW34	1.00
OW8	0.95	OW17	0.30	OW26	0.36	OW35	0.24
OW9	1.00	OW18	0.34	OW27	0.16		

Table 4.5 Crystal and refinement parameters for the **BCDTUL** structure

Parameter	
Formula unit	$2(C_{42}H_{70}O_{35})\cdot C_{17}H_{18}ClNO\cdot 18.7(H_2O)$
Formula weight / g mol^{-1}	2834.6
Crystal system	Triclinic
Space group	P1
a / Å	15.320(3)
b / Å	15.462(3)
c / Å	15.579(3)
α / °	104.10(3)
β / °	101.31(3)
γ / °	104.15(3)
Volume / Å^3	3340(1)
Z	1
Density$_{calc}$ / g cm^{-3}	1.409
μ(MoKα) / mm^{-1}	0.145
F(000)	1513
Crystal size / mm^3	0.35x0.40x0.40
Temperature / K	113
Range scanned θ / °	$1 \leq \theta \leq 26$
Index ranges	h: -17, 17; k: -17, 17; l: -17, 17
ϕ scan angle per frame / °	1.0
ϕ scan range / °, no. of frames	10, 10; 10, 10; 10, 10; 363, 363
ω scan angle / °	1.0
ω scan ranges / °, no. of frames	124, 124; 152, 152; 121, 121; 52, 52; 119, 119; 28, 28; 69, 69; 44, 44; 113, 113; 49, 49
Dx / mm	40
No. of measured reflections	85758
No. of unique reflections	20551
No. of reflections with $I > 2\sigma(I)$	16600
No. of least-squares parameters	763
R_{int}, R_{σ}	0.091, 0.056
S	2.245
R_1 ($F_o > 4\sigma(F_o)$)	0.1806
wR_2 (all reflections)	0.5025
No. of reflections omitted	7
Weighting scheme parameters	a = 0.200, b = 0
$(\Delta/\sigma)_{mean}$	0.033
Δρ excursions / e Å^{-3}	-1.61, 1.78

Description of the structure

BCDTUL crystallises in the space group P1 in a 2:1 β-CD:tulobuterol molar ratio with Z = 1 formula unit [formula unit defined in Table 4.5] per unit cell. A diagram of the asymmetric unit of the **BCDTUL** complex is presented in Figure 4.3. The glucopyranose units of the **A** and **B** host molecules are denoted **A1-A7** and **B1-B7** respectively, with the glucopyranose atom labelling shown for residue **B6**.

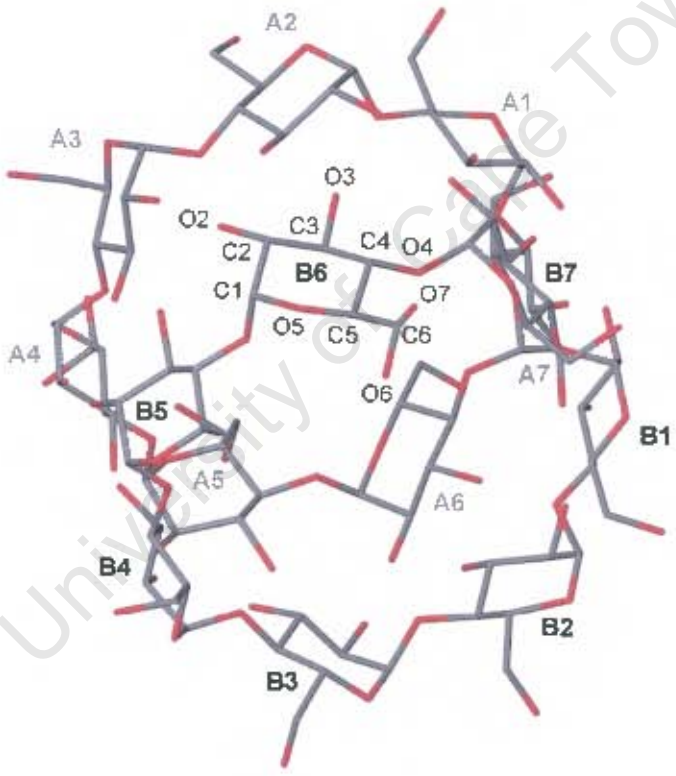

Figure 4.3 Oblique view of the asymmetric unit of the **BCDTUL** complex. The labelling for the **B6** residue is shown. The glucopyranose units of the front and rear host molecules are labelled in black and grey respectively. Hydrogen atoms as well as the unplaced cavity electron density are omitted for clarity.

The geometrical parameters that describe the conformations of cyclodextrin molecules, as discussed in **Chapter 1 – Introduction** [pages 14-16], are listed for the **BCDTUL** structure in Tables 4.6–4.8. Table 4.6 lists the principal torsion angles for the **BCDTUL** host molecule.

Table 4.6 Principal torsion angles [°] for **BCDTUL**

Glucopyranose unit	ω / °	Φ / °	Ψ / °	Θ_1 / °	Θ_2 / °
A1	-60(2)	114(1)	129(1)	54(2)	-53(1)
A2	71(2)	115(1)	127(1)	54(2)	-58(2)
A3	-63(2)	112(1)	121(1)	54(2)	-51(2)
A4 (O6, O7)*	-66(2), 52(2)	122(1)	128(1)	60(2)	-62(1)
A5	-58(2)	110(1)	134(1)	53(2)	-54(2)
A6	-63(2)	109(1)	130(1)	60(1)	-55(1)
A7	-70(2)	119(1)	133(1)	58(1)	-52(1)
Mean magnitude	**63**	**114**	**129**	**56**	**55**
B1	-68(2)	112(1)	131(1)	53(2)	-53(2)
B2	-58(2)	111(1)	126(1)	59(2)	-52(2)
B3	-49(2)	114(1)	126(1)	59(2)	-52(2)
B4	-68(2)	118(1)	126(1)	54(2)	-56(2)
B5	-66(2)	123(1)	125(1)	56(2)	-54(2)
B6 (O6, O7)*	66(2), -30(2)	117(1)	125(1)	59(2)	-55(2)
B7	-66(2)	113(1)	131(1)	57(2)	-53(2)
Mean magnitude	**59**	**115**	**127**	**57**	**54**

* Two values for the ω parameter as a result of the disorder of the O6 atom

The ω parameter indicates whether the direction of the C6-O6 bond is towards [positive] or away from [negative] the host cavity. In the **BCDTUL** structure, all the C6-O6 bonds are in the (-)-*gauche* conformation, except that for glucopyranose unit **A2** which is in the (+)-*gauche* conformation. The C6-O6 bonds for glucopyranose units **A4** and **B6** are both in the (-)- and (+)-*gauche* conformations, as a result of the disorder of their O6 atoms. The (+)-*gauche* conformations describe the conformations of the minor and major components of the disorder for the **A4** and **B6** glucopyranose units respectively. The Φ,

Ψ, Θ_1 and Θ_2 torsion angles agree closely with those observed for the parent β-CD.[66] All the glucopyranose units are in the $^4C_1$ chair conformation.

The parameters of the O4-heptagon for each host molecule are listed in Table 4.7. The **r**, **a** and **l** parameters, which respectively describe the distance of the O4-heptagon centroid to each O4 atom, the distance between adjacent O4 atoms and the angle between three adjacent O4 atoms, do not vary substantially within each β-CD molecule, thus reflecting the near ideal seven-fold symmetry of the O4-heptagons. This symmetry is also indicated by the low values of the **d** and **t** parameters, which respectively describe the deviation of each O4 atom from the mean O4 plane and the torsion angle defined by four adjacent O4 atoms. On the other hand, the close correspondence of the values in Table 4.7 between the two host molecules is indicative of the pseudo- two-fold rotation axis that relates them. The O4 mean planes of the **A** and **B** host molecules are also nearly parallel, as indicated by the angle of 1.14(6)° that these make with each other.

Table 4.8 lists the intersaccharradic angle, φ, and tilt angles [τ_1 and τ_2] for the **BCDTUL** structure. The φ angles for both host molecules are close to the average values for other β-CD molecules.[67] All the tilt angles for host molecule **A** are positive, except that for glucopyranose unit **A3** which is negative. Host molecule **B** has positive tilt angles for five glucopyranose units, with the tilt angles for glucopyranose units **B3** and **B4** being negative. Even though the tilt angles for the two host molecules are both positive and negative, their values are fairly small and within a fairly narrow range [-1.2 to 12.7° and 3.1 to 10.0° for host molecules **A** and **B** respectively]. This is consistent with other dimeric β-CD structures and is due to the intra- and intermolecular hydrogen bonding present within the dimers in these structures.[125]

Table 4.7 O4-heptagon parameters for the **BCDTUL** structure

Glucopyranose unit	r / Å	l / Å	a / °	d / Å	t / °
A1	5.13	4.32	126	-0.008(6)	6
A2	5.12	4.31	134	-0.079(6)	-3
A3	4.84	4.53	127	0.077(6)	-2
A4	5.10	4.30	125	0.018(6)	2
A5	5.23	4.41	132	-0.068(6)	1
A6	4.92	4.40	129	0.012(6)	-1
A7	4.97	4.38	127	0.048(6)	-3
Mean magnitude	**5.04**	**4.38**	**129**	**0.053***	**3**
B1	4.93	4.35	128	-0.059(6)	-2
B2	5.05	4.39	126	-0.023(6)	1
B3	5.14	4.33	131	0.063(7)	3
B4	4.95	4.40	130	0.009(6)	-4
B5	4.96	4.38	125	-0.082(6)	0
B6	5.16	4.35	129	0.039(6)	-1
B7	5.03	4.38	131	0.057(6)	-2
Mean magnitude	**5.03**	**4.37**	**129**	**0.053***	**2**

* Root-mean-square deviation

Table 4.8 φ and τ parameters for the **BCDTUL** structure

Glucopyranose unit	φ / °	τ_1 / °	τ_2 / °
A1	116(1)	6.9(3)	9.6(5)
A2	117(1)	6.0(4)	7.6(4)
A3	118(1)	-1.5(4)	-2.0(2)
A4	119(1)	9.3(4)	10.4(2)
A5	119(1)	12.7(4)	13.8(2)
A6	116(1)	6.9(4)	9.3(2)
A7	116(1)	9.3(4)	10.3(3)
Mean	**117**	**7.1**	**8.4**
B1	117(1)	9.7(4)	9.6(2)
B2	118(1)	7.6(4)	10.2(4)
B3	117(1)	-3.3(4)	-3.7(4)
B4	115(1)	-1.5(4)	-2.3(3)
B5	119(1)	6.4(3)	6.4(2)
B6	117(1)	8.9(4)	9.5(2)
B7	116(1)	6.0(3)	8.2(2)
Mean	**117**	**4.8**	**5.4**

Guest inclusion

As stated earlier in the chapter, the guest could not be modelled due to the high degree of disorder that prevailed in the difference Fourier map as indicated by the unacceptable distances and angles between electron density peaks. The only information about the guest molecule was obtained from microanalysis, which indicated that the **BCDTUL** crystallised with one guest molecule per two β-CD molecules. The highest electron density peaks in the host cavities [1.00-1.73 e $Å^{-3}$] are illustrated in stereo in Figure 4.4. It shows that the difference Fourier map did not reveal any recognisable fragment of the tulobuterol molecule that could be used as a starting model for further refinements. This situation prevailed even when investigating difference Fourier maps with more than two hundred residual electron density peaks.

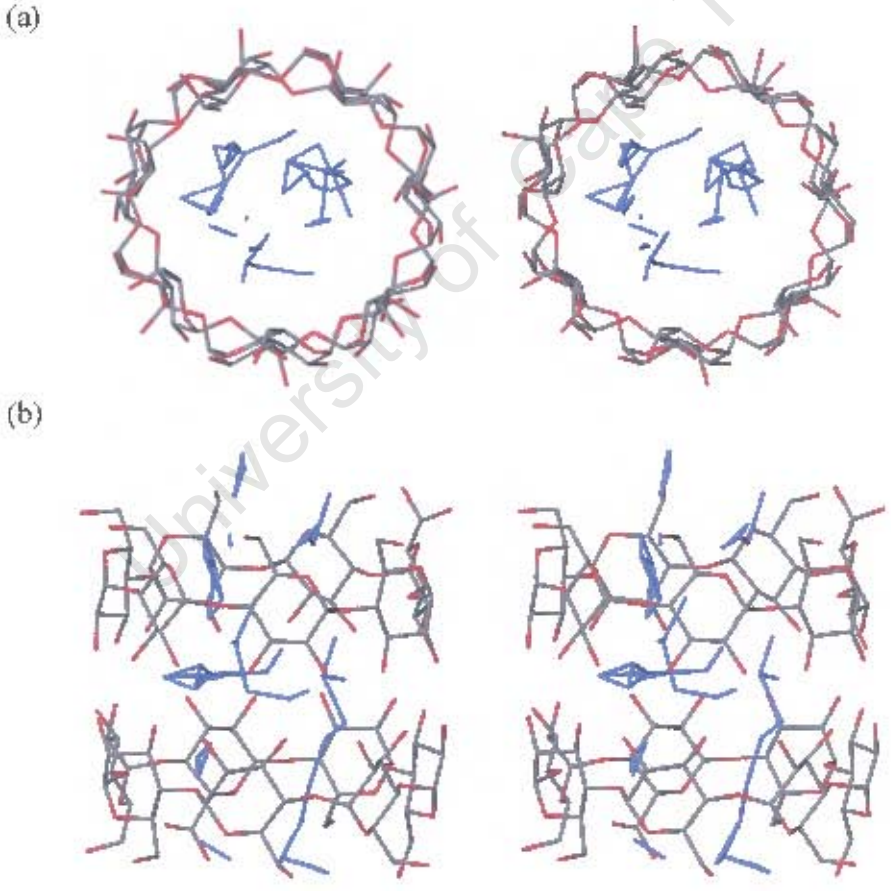

Figure 4.4 Stereo views of the (a) top and (b) side faces of the β-CD dimer in **BCDTUL** illustrating the highest electron density in the dimer cavity

Host hydrogen bonding interactions

PLATON[121] was used to calculate several hydrogen bonding interactions for the **BCDTUL** structure exclusively involving host atoms. These host hydrogen bonding interactions are categorised with respect to whether they occur within or between dimers, respectively referred to as intra- and inter-dimer host hydrogen bonding interactions.

Intra-dimer hydrogen bonds

Table 4.9 presents the intra-dimer host hydrogen bonding interactions. The intramolecular O-H···O hydrogen bonds [four for each host molecule] are between the O2 and O3 atoms of neighbouring glucopyranose units. These hydrogen bonds are responsible for the small tilt angles and thus relatively 'round' shapes of the β-CD molecules.[125] In addition to the O-H···O intramolecular hydrogen bonds, three and two C6-H···O5' intramolecular hydrogen bonds respectively stabilise the conformations of the **A** and **B** host molecules.

There are fifteen intermolecular, intra-dimer O-H···O hydrogen bonds that connect the two host molecules into a head-to-head dimer, and these involve the O2 and O3 atoms on the secondary sides of the β-CD molecules. Figure 4.5 presents a stereo diagram of all the intra- and intermolecular intra-dimer O-H···O hydrogen bonds. It shows that the O2 and O3 atoms that are not involved in O2···O3' intramolecular hydrogen bonds, instead engage in hydrogen bonds to the other host molecule of the dimer. The 'flip-flop' nature of the intramolecular hydrogen bonds involving the O2 and O3 atoms, i.e. the dynamic switching between O2···O3' and O3···O2' hydrogen bonds, has been highlighted in previous neutron diffraction studies,[62,63] indicating the mobility of the O2 and O3 hydrogen atoms. It has recently been shown for the first time with the aid of synchrotron data that the O3···O3' hydrogen bonds bind the dimer in the 2(β-CD)·(1,12)-dodecanedioic acid structure.[126] That these interactions bind β-CD dimers was previously concluded on the basis of the more favourable geometries of the O3···O3' hydrogen bonds. From Table 4.9 it can be seen that the O3···O3' hydrogen bonds for the **BCDTUL**

structure also have more favourable geometries than the other inter-host intra-dimer hydrogen bonds.

Table 4.9 Intra-dimer hydrogen bonds

Interaction	H···A / Å	D···A / Å	D-H···A / °
Intramolecular			
O3A1-H3A1···O2A2	2.05(4)	2.78(2)	148(4)
O2A2-H2A2···O3A1	2.07(5)	2.78(2)	146(3)
O2A5-H2A5···O3A4	2.22(5)	2.89(2)	138(3)
O3A6-H3A6···O2A7	2.10(4)	2.72(1)	132(5)
O2B1-H2B1···O3B7	2.12(4)	2.84(2)	146(3)
O3B2-H3B2···O2B3	2.05(5)	2.76(2)	144(5)
O3B4-H3B4···O2B5	2.10(4)	2.76(2)	138(5)
O3B7-H3B7···O2B1	2.14(6)	2.84(2)	143(5)
C6A2-H30···O5A3	2.55(5)	3.43(2)	150(5)
C6A4-H6A8···O5A5	2.56(5)	3.29(2)	132(3)
C6A6-H6AX···O5A7	2.60(4)	3.39(2)	139(5)
C6B6-H6BZ···O5B7	2.48(5)	3.37(2)	151(5)
C6B7-H43···O5B1	2.54(5)	3.35(2)	140(3)
Host···Host			
O2A1-H2A1···O3B7	2.30(5)	2.98(1)	140(4)
O2A3-H2A3···O3B5	2.33(5)	2.95(1)	133(3)
O2A4-H2A4···O3B4	2.34(5)	3.07(2)	149(5)
O2A7-H2A7···O3B1	2.41(4)	3.04(1)	134(3)
O2B3-H2B3···O3A5	2.28(4)	3.07(2)	160(5)
O2B4-H2B4···O3A4	2.43(6)	3.01(1)	129(5)
O2B6-H2B6···O2A3	2.51(4)	2.97(1)	117(5)
O3A2-H3A2···O3B6	2.00(4)	2.80(2)	164(5)
O3A3-H3A3···O3B5	2.00(4)	2.79(1)	162(5)
O3A4-H3A4···O3B4	1.97(4)	2.77(1)	166(5)
O3A5-H3A5···O3B3	1.98(6)	2.79(2)	168(5)
O3A7-H3A7···O3B1	2.04(4)	2.85(1)	171(5)
O3B1-H3B1···O3A7	2.04(6)	2.85(1)	172(5)
O3B3-H3B3···O3A5	2.01(4)	2.79(2)	158(5)
O3B6-H3B6···O3A2	2.00(6)	2.80(1)	162(5)

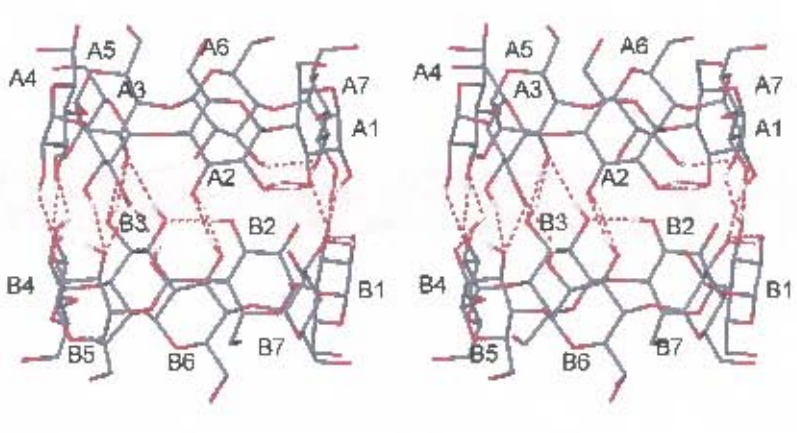

Figure 4.5 Stereo diagram of the intra-dimer hydrogen bonding for the **BCDTUL** structure. Only O-H···O hydrogen bonding hydrogen atoms are shown.

Inter-dimer hydrogen bonds

The inter-dimer hydrogen bonds are listed in Table 4.10. As will be elaborated on in the section titled **Crystal packing**, the dimers are arranged in layers that are stacked on top of one another. Thus, the hydrogen bonding between dimers is discussed in terms of whether they are within the same layer [intra-layer] or between adjacent layers [inter-layer] and are categorised as such in Table 4.10.

There are nine unique intra-layer hydrogen bonds of which only one is an O-H···O hydrogen bond, the rest being C-H···O hydrogen bonds. The former is an O2-H···O2' hydrogen bond, the latter being C1-H···O2', C1-H···O5', C2-H···O3' hydrogen bonds. The C1 and C2 hydrogen atoms are located on the outside of the cyclodextrin molecules, thus allowing them to interact with the atoms of neigbouring β-CD molecules.

On the other hand there are nine unique inter-layer O-H···O hydrogen bonds, all being O6-H···O6' and O6-H···O5' hydrogen bonds. The greater number of strong O-H···O hydrogen bonds for the inter-layer dimeric interactions indicates that dimers are more strongly associated between the dimeric layers than within.

Table 4.10 Inter-dimer hydrogen bonds for the **BCDTUL** structure

Interaction	H···A / Å	D···A / Å	D-H···A / °	Symmetry code*
Intra-layer				
O2B2-H2B2···O2A3	2.25(5)	2.70(2)	115(4)	1+x, y, z
C2A1-H1···O3A4	2.48(4)	3.31(2)	143(3)	x, -1−y, z
C2A3-H5···O3A6	2.41(4)	3.34(2)	157(3)	-1+x, y, z
C1A3-H1A3···O2A7	2.44(6)	3.28(2)	143(5)	-1+x, y, z
C2B2-H17···O3B5	2.42(4)	3.33(2)	154(4)	1+x, y, z
C2B4-H21···O3B7	2.43(5)	3.40(2)	169(3)	x, 1+y, z
C1B1-H1B1···O5B4	2.59(5)	3.52(2)	159(3)	x, -1+y, z
C1B2-H1B2···O2B6	2.46(6)	3.30(2)	144(4)	1+x, y, z
C1B4-H1B4···O2B1	2.51(5)	3.25(2)	132(4)	x, 1+y, z
Inter-layer				
O6A2-H6A3···O6B6	2.33(6)	2.86(2)	123(3)	x, y, 1+z
O6B7-H41···O6A4	2.54(4)	3.07(2)	123(4)	x, y, -1+z
C6B7-H39···O6A1	2.49(5)	3.24(2)	134(3)	x, y, -1+z
O6B5-H6B9···O5A7	2.34(6)	3.07(1)	149(4)	-1+x, y, -1+z
O6A6-H6A6···O5B5	2.44(6)	3.19(1)	152(4)	1+x, y, 1+z
O6A6-H6A6···O6B5	2.27(5)	2.86(2)	129(3)	1+x, y, 1+z
O6A4-H50···O5B1	2.05(4)	2.79(2)	149(3)	x, 1−y, 1−z
O6B7-H41···O5A4	2.01(5)	2.80(1)	162(4)	x, -1−y, -1+z
O6B1-H6B1···O6A7	2.00(6)	2.81(1)	167(3)	x, -1+y, -1+z

* Symmetry code applied to the second unit of the interaction

Water interactions

The **BCDTUL** structure from TGA analysis was found to have 18.7 water molecules, of which 18.5 were modelled over thirty-five sites as a result of the vast majority having only partial s.o.f.'s. The water molecules were located around the periphery of the host molecules. The possible presence of water molecules within the host cavities was difficult to ascertain due to the lack of modelling of the guest molecule and no attempts were thus made to do so. The close contacts involving water molecules, together with their averages and ranges, for the **BCDTUL** structure are summarised in Table 4.11.

The water molecules are involved in two networks of close contacts *viz.* those involving the primary and secondary sides of the β-CD molecule. These networks are almost entirely separated from each other, i.e the water molecules make contacts to atoms either on the primary or secondary sides of the β-CD molecules. The exception is the OW7 molecule, which is part of the primary water network but which also makes a weak C-H···O hydrogen bond to the C2B6 atom on the secondary side of host molecule **B**. Two water molecules [OW21 and OW34] are in close contact only with each other and with no other host atoms. The water molecules in the crystal structure are illustrated in the crystal packing diagram [Figure 4.6] in the next section.

Table 4.11 Summary of water close contacts for the **BCDTUL** structure

Contact atom	Number of interactions	Range / Å	Mean Distance / Å
O2A	8	2.43-3.12	2.75
O3A	11	2.62-3.14	2.88
O5A	6	3.02-3.24	3.10
O6A	10	2.71-3.15	2.91
C1A	3	3.22-3.36	3.29
C2A	4	3.02-3.55	3.32
C4A	1	-	3.26
C6A	4	3.13-3.39	3.32
Total Host(A)···Water	**47**		
O2B	14	2.60-3.25	2.87
O3B	8	2.73-3.17	2.99
O5B	5	2.78-3.20	3.01
O6B	11	2.73-3.16	2.91
C1B	6	3.15-3.32	3.21
C2B	5	3.12-3.56	3.26
C4B	2	3.09-3.33	3.21
C5B	2	3.29-3.42	3.36
C6B	5	3.16-3.40	3.32
Total Host(B)···Water	**58**		
Water···Water	**20**	2.67-3.24	2.84

Crystal packing

A stereo view of the crystal packing down the *c*-axis for the **BCDTUL** structure is presented in Figure 4.6. It displays the channel-type packing motif, a common packing motif for β-CD dimeric structures,[125] where head-to-head dimers stack on top of one another forming 'endless' channels. The diagram also illustrates the location of the water molecules for one interstice where they act as the 'glue' that maintains the crystal structure.

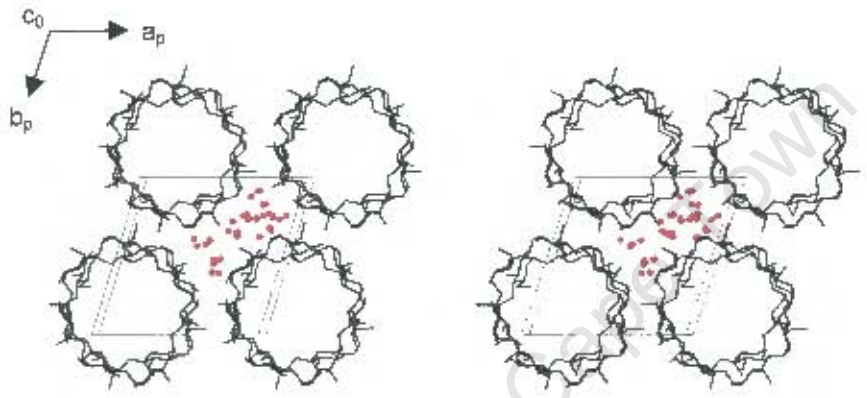

Figure 4.6 Stereo view of the crystal packing down the *c*-axis for the **BCDTUL** structure. The water molecules for one interstice are shown in red

Powder X-ray Diffraction

The computed and experimental PXRD patterns for **BCDTUL** are presented in Figure 4.7. These show a high degree of correlation despite the guest not being modelled in the single crystal structure due to its disorder. The slight shift of the experimental trace to lower 2θ when compared to the computed trace is a result of the lower temperature at which the information for the latter was obtained. This shift is responsible for the peak corresponding to the first peak in the computed trace being below the minimum 2θ at which the analysis was performed. The differences in relative intensities of the experimental trace compared to the computed trace are due to orientation effects in the sample prepared for experimental analysis. Nevertheless, the close match between the patterns shows that the computed trace can serve as a reference for **BCDTUL** identification.

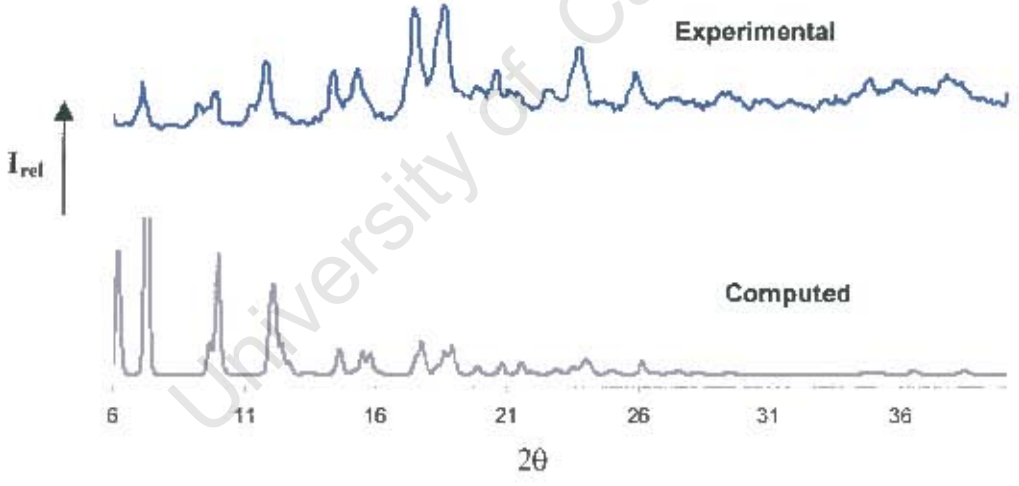

Figure 4.7 Computed [113K] and experimental [295K] PXRD traces for **BCDTUL**

Discussion

In this section, the conformations of the host molecules, host hydrogen bonding interactions and crystal packing of the **BCDTUL** structure will be discussed relative to other dimeric β-CD structures.

Firstly, the average unit cell parameters for various β-CD dimeric structures, as obtained from the CSD,[84] are presented in Table 4.12. It shows that there are only four β-CD structures with unit cell parameters similar to those of **BCDTUL**, and that β-CD dimeric structures to date generally prefer to crystallise in space groups P1 [IM packing type] and C2 [CH packing type].

Table 4.12 Average unit cell parameters for dimeric β-CD structures from the CSD[84]

Space group, Packing type	Number	a / Å	b / Å	c / Å	α / °	β / °	γ / °
P1, CH [a]	4	15.411	15.596	15.894	100.05	101.12	102.80
P1, CH [BCDTUL]	This work	15.320	15.462	15.579	104.10	101.31	104.15
P1, IM [b]	29	18.260	15.438	15.419	103.10	113.62	99.91
C2, CH [c]	26	19.284	24.547	15.874	90	109.15	90
$P2_1$, SC [d]	11	15.369	32.561	15.415	90	102.72	90
$C222_1$, CB [e]	7	19.327	24.113	33.230	90	90	90

[a] CCD refcodes used: BCYDPR, FERCOU, OKUFOP, XUBXUN
[b] CSD refcodes used: AGAZIR, AGAZOX, AGAZUD, AJUVAC, BCDIPH10, BCDMPH, BCDNPR10, BIDMOQ, BULFIX, CACPOM, CDEXPR, CEDMUT, CIGXDF10, DEVVAB, DIFHOP, DOCVUM04, GESVUV10, HEGXUM, LONGIE, MASBIR, MASBOX, QABHOR, TEJHAR, VOQDOU, VOQDUA, WISREV, WISRIZ, TAFZIK, UKAGOC
[c] CSD refcodes used: AJUVEG, BEFDOG, BEZLAT, COCMIQ, CYDXTF, DEVTED, DEVTIH, DOQPOO, DOQPUU, GOSQOU, HUTKOW, IJOLUO, KOGLIB, KUTJUE01, MASBAJ, ODEJOW, PUKPIU, PUKPOA, SOBHUM02, SOBJEY02, TEMCIX, TUXKUS, VIJXAN10, XERTET, YOVVIO01, ZUZXOH
[d] CSD refcodes used: BEGWEQ, CDETAN, CIVBUE, DUTLIN10, GETPAW, GETPEA, KIFPAQ, MACDAW, NIZGUY, QACXEX, SAJPIC
[e] CSD refcodes used: DEVTON, DEVTUT, FASXUS, GIPFEQ, KOFJEU, MEGQUK, TECYIJ

Conformations of the host molecules

The **BCDTUL** host molecules are fairly round, as is the case for other β-CD structures. This has been attributed to the intramolecular O2···O3' and O3···O2' hydrogen bonds that restrict the glucopyranose tilt angles to relatively small values.[125] Selected conformational parameters for several dimeric β-CD complex structures obtained from the CSD,[84] together with those of **BCDTUL**, are listed in Table 4.13.

Table 4.13 Selected averaged conformational parameters for the host molecules of a number of dimeric β-CD structures[127] and those for **BCDTUL** host molecule

Parameter	Dimeric B-CD complexes from CSD	BCDTUL
r / Å	5.04	5.04
l / Å	4.38	4.38
a / °	129	129
d / °	0.11	0.06
|t| / °	5.9	3
τ_2 / °	7.9	8

The conformational parameters for the **BCDTUL** host molecules are in close agreement with those for the dimeric β-CD complexes. This shows that, despite the inclusion of a variety of guests within the β-CD dimers, the symmetrical shapes of the host molecules of β-CD dimeric structures are maintained. This is probably due to the intra- and intermolecular hydrogen bonding within the β-CD dimers that restrains the geometry of the β-CD molecules. It has also been noted that the conformations of dimeric β-CD molecules deviate less from ideal seven-fold symmetry than their monomeric counterparts.[125]

Host hydrogen bonding interactions

Different packing types of β-CD molecules display similar hydrogen bonding networks within specific layers.[128] The host hydrogen bonding network can be divided into those involving the primary and the secondary hydroxyl groups of the β-CD molecule. It has

been found for dimeric β-CD structures that the secondary hydroxyl groups form part of an invariant hydrogen bonding network that is not influenced by the included guest molecules, but that the hydrogen bonding network of the primary hydroxyl groups is influenced to a greater extent by guest molecules that protrude from the host cavities.[129] In the majority of the complexes, primary hydroxyl groups of adjacent dimers within a layer form direct hydrogen bonds with each other, this type of hydrogen bonding between dimers of adjacent layers being rare. In contrast, the hydrogen bonding involving the primary hydroxyl groups of the **BCDTUL** structure is observed exclusively between dimers of adjacent layers.

Water interactions

The water molecules in **BCDTUL**, as for most other β-CD dimeric complexes have low occupancy factors indicating a high degree of disorder. Despite this, these water molecules have been shown to form a quasi-invariant water network that is organised in layers.[130,131] The layers are separated and their constituent water molecules interact with the same side of the CD molecules, i.e either with the secondary or primary hydroxyl groups, as is the case in the **BCDTUL** structure.

Crystal packing

The general packing motifs of β-CD dimeric structures have been described in **Chapter 1 – Introduction**. Despite the differences in the unit cell parameters and space groups of the different dimeric β-CD structures they all consist of dimers that pack so that they form centred or pseudo-centred dimeric layers. The different packing motifs come about in the way these layers are stacked on top of one another. There are four packing arrangements known thus far for dimeric β-CD structures, which result from different relative settings of these dimeric layers. As stated earlier, these are the channel **[CH]**, intermediate **[IM]**, chessboard **[CB]** and screw-channel **[SC]** packing arrangements. The **CH** and **IM** dimers are stacked on top of one another parallel either to the *a*- or *c*-axes. The relative shifts of consecutive dimers are 2.7 Å for the former and 6.0 Å for the latter. The **CB** and **SC** dimeric layers are related by 2_1 axes. The **CB** dimers of adjacent layers are located in each other's inter-dimer spaces so that a chessboard pattern is formed. The

SC dimers of consecutive layers are also stacked on top of one another, as in the case of the **CH** mode, but the O4 mean planes of consecutive **SC** dimers are inclined to one another so that a screw-channel is formed. The relative displacement of consecutive dimers of **CB** and **SC** are 2.6 and 8.7 Å respectively.

BCDTUL has the **CH** type packing arrangement and its computed PXRD trace corresponds with isostructural series **10** and **11** computed for this packing arrangement.[80] The former and the latter correspond to the space groups P1 and C2 respectively. Due to their similar packing arrangements, and subtle structural differences alluded to at the beginning of this chapter, the computed PXRD traces for β-CD complexes crystallising in these two space groups are virtually indistinguishable. However, Figure 4.8 presents the computed PXRD traces for **BCDTUL** and isostructural series **10**, as the space group P1 was chosen as the correct space group for **BCDTUL**, based on the reasons mentioned earlier in the chapter. The **BCDTUL** trace closely matches the trace for isostructural series **10** as is expected from the single crystal X-ray analysis.

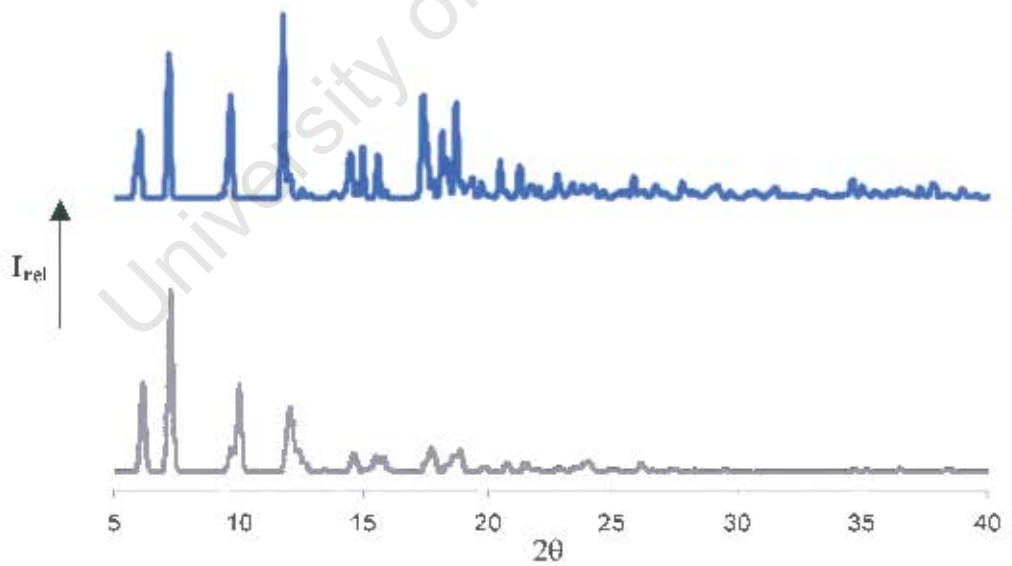

Figure 4.8 The computed trace for **BCDTUL** [bottom] and the trace for isostructural series **10** [β-CD complexes with similar unit cell parameters and the same space group as **BCDTUL**]

X-ray Crystallographic Analysis of GCDTUL

Single Crystal X-ray Diffraction

X-ray photography

Preliminary unit cell parameters for the **GCDTUL** complex were established using photographic techniques. The crystal was mounted on a glass fibre and covered with protective glue in order to prevent dehydration of the crystal. Oscillation and Weissenberg photographs collectively revealed Laue *4/mmm* symmetry and h00: h = 2n. These indicated the two space groups $P42_12$ or $P42_1m$ but since the host is chiral the former space group was chosen.

Data-collection and space group determination

The mosaicity of the **GCDTUL** crystal increased on cooling in a stream of N_2 vapour and therefore intensity data were collected on a Nonius Kappa CCD diffractometer at room temperature [298K] using graphite-monochromated MoKα radiation. The unit cell parameters confirmed those obtained by photography and XPREP[109] indicated the space group $P42_12$. Inspection of the reciprocal lattice layers with LAYER[117] showed this to be consistent with X-ray photography.

Structure solution and refinement

To date, all γ-CD complexes crystallise in the space group $P42_12$ and contain three crystallographically independent host molecules that are stacked on top of one another.[132] These host molecules are located on a four-fold rotation axis that is orthogonal to their O4 mean planes running down their cavities parallel to the *c*-axis. The four-fold rotation axis reduces the asymmetric unit to six glucopyranose units, i.e. two per crystallographically independent γ-CD molecule. The space group and unit cell volume of **GCDTUL** are consistent with those for other γ-CD complexes and therefore the isomorphous replacement method was employed to solve the **GCDTUL** structure using the coordinates of one of these known complexes. The coordinates of the host atoms of 3(γ-CD)·cyclizine·49.2(H_2O)[83] [excluding the 'freely rotating' O6 atoms] were used as an

initial phasing model in the structure solution of **GCDTUL**. The O6 atoms were excluded in order to model their possible disorder using the electron density peak heights of their disordered components. The host atom labelling of the 3(γ-CD)·cyclizine·49.2(H_2O) structure was retained, the glucopyranose units of the **A**, **B** and **C** asymmetric unit host molecules being labelled **A1-A2**, **B1-B2** and **C1-C2** respectively. SHELXL-97[112] was used to refine this initial model and to locate the remaining asymmetric unit atoms. The O6 atoms were located in the initial and subsequent difference Fourier maps with those for the **A1**, **A2** and **C1** glucopyranose units being disordered over two positions [the minor disordered component was labelled O7]. The disordered O6 atoms were placed with s.o.f. s based on their initial peak heights and allowed to refine freely with s.o.f. s of x and 1-x for the major and minor disordered components respectively. Their temperature factors were fixed at 0.09 $Å^2$, the average value of the isotropic temperature factors of the ordered O6 atoms. The initial x values of 0.75, 0.68 and 0.67 for **A1**, **A2** and **C1** respectively, refined to 0.77, 0.80 and 0.75. The isotropic thermal parameters for all host atoms refined satisfactorily and these atoms were thus subsequently refined anisotropically, except for the disordered O6 atoms. The hydroxyl hydrogen atoms were placed using a hydrogen-bond searching model [AFIX 83], whilst the rest of the host hydrogen atoms were placed using a riding model. All the hydrogen atoms were refined isotropically with temperature factors 1.2 times those of their parent atoms.

The four-fold rotation axis that exists down the cavity of the cyclodextrin molecules requires any asymmetrical guest molecule to be at least four-fold disordered. This requirement made the interpretation of the difference Fourier map very difficult. In fact, no guest atoms could be placed due to the unacceptable geometries and distances between the electron density peaks in the host cavities, as well as their extremely low electron densities [highest peak in cavity 0.48 e $Å^{-3}$]. After all the host and water atoms were placed, four of the highest peaks in the map did consistently appear on this four-fold rotation axis but the distances between them could not be reconciled with expected distances between non-bonded atoms of the tulobuterol guest molecule. The reconciliation of distances between peaks that appeared on this four-fold axis with

distances between non-bonded atoms of the guest molecule in the 3(γ-CD)·cyclizine·49.2(H_2O) structure was a departure point for successful guest molecule modelling.[83]

Nineteen sites were identified as water molecules. These were placed with fixed isotropic temperature factors [0.09 $Å^2$ which was the fixed value for the disordered O6 host oxygen atoms] and site occupancy factors were allowed to vary. Effectively all the water molecules were disordered as indicated by their close proximity to a neighbouring water molecule of less than the usual hydrogen-bonding distance, as well as their partial s.o.f.'s. At the end of the refinement the total site occupancy for the unique water molecules was 5.7 which translated to 22.8 water molecules for the three independent host molecules. This is considerably less than the 33.3 water molecules as calculated from the TGA analysis, which emphasises that this information is best obtained from thermal analysis rather than X-ray diffraction. The s.o.f.'s of the water molecules are presented in Table 4.15, whilst the crystal and refinement parameters are presented in Table 4.16.

Table 4.15 Site occupancy factors for the water molecules of the **GCDTUL** structure

Molecule	s.o.f.	Molecule	s.o.f.
OW1	0.94	OW7A	0.21
OW2	0.57	OW7B	0.14
OW3A	0.37	OW8A	0.37
OW3B	0.49	OW8B	0.23
OW4A	0.31	OW9	0.45
OW4B	0.30	OW10	0.01
OW5	0.37	OW11	0.04
OW6A	0.25	OW12	0.13
OW6B	0.28	OW13	0.03
OW6C	0.18		

Table 4.16 Crystal and refinement parameters for the **GCDTUL** structure

Parameter	
Formula unit	$3(C_{48}H_{80}O_{40})\cdot2(C_{12}H_{18}ClNO)\cdot33.3(H_2O)$
Formula weight / g mol^{-1}	4946.7
Crystal system	Tetragonal
Space group	$P42_12$
a / Å	23.731(3)
c / Å	23.069(5)
α / °	90
β / °	90
γ / °	90
Z	2
Volume / Å^3	12992(4)
Density$_{calc}$ / g cm^{-3}	1.265
μ(MoKα) / mm^{-1}	0.132
F(000)	5282
Crystal size / mm^3	0.22x0.27x0.30
Temperature / K	295(2)
Range scanned θ / °	$2\leq\theta\leq24$
Index ranges	h : -11, 26 k : -24, 26 l : -21, 23
φ scan angle per frame / °	0.4
φ scan range / °, no. of frames	170, 425
ω scan angle / °	1.0
ω scan ranges / °, no. of frames	160, 160
Dx / mm	65
No. of measured reflections	22976
No. of unique reflections	8604
No. of reflections with $I > 2\sigma(I)$	6604
No. of least-squares parameters	651
R_{int}, R_σ	0.071, 0.071
S	1.048
R_1 ($F_o > 4\sigma(F_o)$)	0.0969
wR_2 (all reflections)	0.2874
No. of reflections omitted	11
Weighting scheme parameters	a = 0.1966, b = 9.9417
$(\Delta/\sigma)_{mean}$	0.046
Δρ excursions / e Å^{-3}	-0.54, 0.69

Description of the structure

GCDTUL crystallises in the tetragonal space group $P42_12$ in a 3:2 γ-CD:tulobuterol ratio with $Z = 2$ formula units per unit cell [formula unit in Table 4.16]. Three crystallographically independent host molecules are located on a four-fold rotation axis and thus the asymmetric unit consists of only six glucopyranose units, two from each host molecule. A side view of the three crystallographically independent molecules, as well as the asymmetric unit with its atom labelling scheme are presented in Figure 4.9.

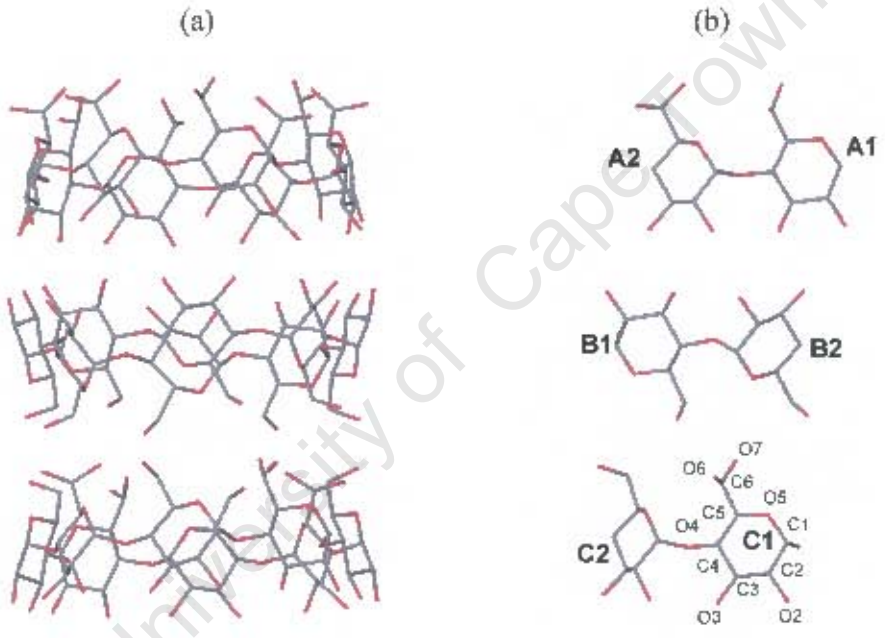

Figure 4.9 (a) Side view of the three independent crystallographic γ-CD host molecules in the **GCDTUL** structure

(b) Asymmetric unit of the **GCDTUL** structure with the atom labelling of glucopyranose unit **C1** shown as representative of the host atom labelling for the other glucopyranose units.

The parameters that describe the conformations of the **GCDTUL** host molecules are presented in Tables 4.17-4.19. The principal torsion angles are presented in Table 4.17.

Table 4.17 Principal torsion angles [°] for the **GCDTUL** structure

Glucopyranose unit	ω / °	Φ / °	Ψ / °	Θ_1 / °	Θ_2 / °
A1 (O6, O7)*	-71.8(8), 66.3(8)	110.7(6)	128.0(6)	55.9(7)	-57.8(7)
A2 (O6, O7)*	-70.3(8), 75.5(8)	110.7(6)	126.7(6)	55.3(8)	-56.6(7)
Mean magnitude	**71.0**	**110.7**	**127.4**	**55.6**	**57.2**
B1	-60.9(8)	108.9(6)	129.9(6)	56.7(7)	-58.5(7)
B2	-59.4(9)	106.3(6)	129.7(6)	57.7(8)	-56.9(7)
Mean magnitude	**60.2**	**107.6**	**129.8**	**57.2**	**57.7**
C1 (O6, O7)*	-61.7(9), 81.6(9)	105.3(6)	129.6(6)	55.5(8)	-57.9(8)
C2	-59.3(8)	106.8(6)	128.3(6)	58.1(7)	-58.1(7)
Mean magnitude	**67.5**	**106.1**	**129.0**	**57.0**	**58.0**

* Two values for the ω parameter due to the disorder of the O6 atom

The ω torsion angle describes the rotation around the C5-C6 bond and thus the direction of the freely rotating C6-O6 bond. It is both positive and negative for the **A1**, **A2** and **C1** glucopyranose units corresponding to the disordered positions of the O6 atom for these residues. In each case the positive sign of ω [indicating that the C6-O6 bond points towards the host cavity] represents the conformation of the minor disordered component. The ω parameter for the **B1**, **B2** and **C2** glucopyranose units is negative, indicating that the C6-O6 bonds are directed away from the host cavity. The four-fold symmetry of the γ-CD molecules requires the direction of the C6-O6 bonds for each of the γ-CD molecules to be as follows. For host molecule **A** the C6-O6 bonds point both towards and away from the host cavity due to the disorder of both unique O6 atoms, whilst all those for host molecule **B** point away from the host cavity, and lastly that half of those for the residues in host molecule **C** point both towards and away from the host cavity with the other half having their C6-O6 bonds pointing exclusively away from the host cavity. The glucopyranose units are all in the $^4C_1$ chair conformation with the Φ, Ψ, Θ_1 and Θ_2 torsion angles agreeing well with those for the parent γ-CD.

Table 4.18 presents the parameters for the O4-octagons in the **GCDTUL** structure. The parameters listed are the O4-octagon centroid to O4 atom distance, **r**, the O4···O4' distance, **l**, the O4···O4'···O4" angle, **a**, the deviation of the O4 atom from the mean O4 plane, **d**, and the O4···O4'···O4"···O4"' torsion angle, **t**. The values for the **r**, **l** and **a** parameters show that, in addition to the four-fold symmetry of each host molecule required by the space group $P42_12$, the unique residues also have very close values both within and between host molecules. This indicates that the O4-octagons are very close to regular octagons. This is also substantiated by the **d** and **t** parameters, whose values are close to zero.

Table 4.18 The geometrical parameters of the O4-octagons of the **GCDTUL** structure

Glucopyranose unit	r / Å	l / Å	a / °	d / Å	t / °
A1	5.89	4.50	135	-0.006(3)	-1
A2	5.89	4.52	135	0.006(3)	1
Mean magnitude	**5.89**	**4.51**	**135**	**0.006***	**1**
B1	5.89	4.51	136	0.009(3)	-1
B2	5.84	4.48	134	-0.009(3)	1
Mean magnitude	**5.87**	**4.50**	**135**	**0.009***	**1**
C1	5.91	4.48	137	0.016(3)	2
C2	5.84	4.51	133	-0.016(3)	-2
Mean magnitude	**5.88**	**4.50**	**135**	**0.016***	**2**

* Root-mean-square deviation

Table 4.19 presents the tilt and intersaccharradic angles for the **GCDTUL** structure. The tilt angles are all positive, small and span a fairly narrow range [12.3 to 16.7°]. This is in keeping with the high degree of symmetry indicated by the parameters in Table 4.18. The relatively small positive angles indicate that the secondary side of the CD is only slightly more open than the primary side of the CD molecules giving them the shape of a truncated cone.

Table 4.19 φ and τ parameters for **GCDTUL**

Glucopyranose unit	φ / °	τ_1 / °	τ_2 / °
A1	117.5(5)	12.5(2)	13.1(2)
A2	117.7(5)	12.0(2)	12.5(1)
Mean	**117.6**	**12.3**	**12.8**
B1	117.0(5)	14.8(2)	16.0(2)
B2	116.4(5)	13.8(2)	15.5(2)
Mean	**116.7**	**14.3**	**15.8**
C1	118.2(5)	14.8(4)	16.6(2)
C2	116.3(5)	12.8(4)	16.7(2)
Mean	**117.3**	**13.8**	**16.7**

Guest inclusion

As stated, earlier the guest could not be modelled due to the inherent disorder resulting from the host molecules being located on a four-fold axis. Figure 4.10 is a stereo diagram of the highest electron density peaks [0.48-0.23 e $Å^{-3}$] in the host cavities.

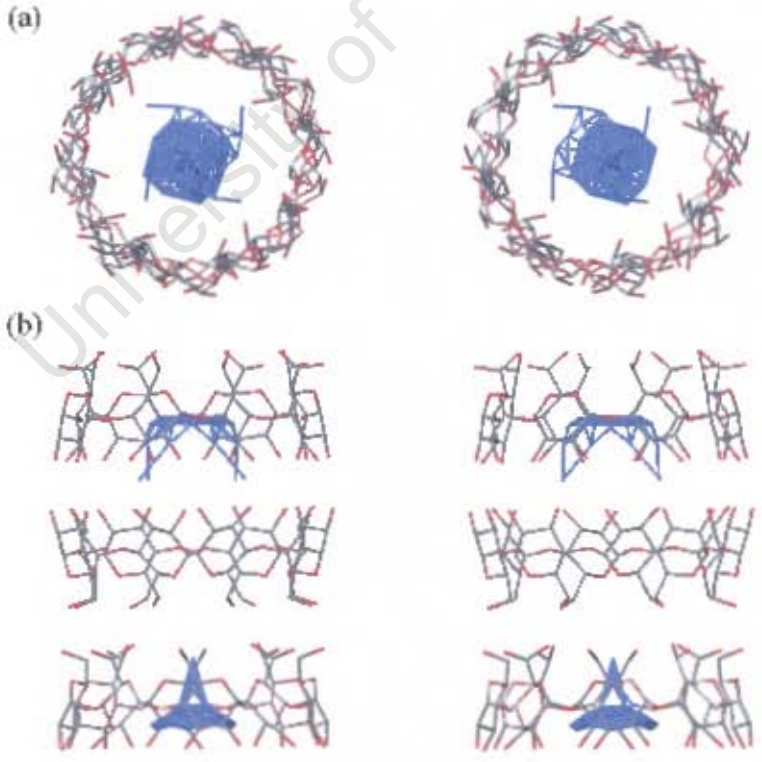

Figure 4.10 (a) Top and (b) side stereo views of the electron density in the **GCDTUL** host cavities.

Host hydrogen bonding interactions

PLATON[121] was used to calculate several hydrogen bonding interactions exclusively involving host atoms of the **GCDTUL** structure. These are discussed next in terms of the intra- and intermolecular hydrogen bonding interactions.

Intramolecular hydrogen bonding

Table 4.20 lists four unique O-H···O and three unique C-H···O intramolecular hydrogen bonds. The O-H···O hydrogen bonds are the characteristic O3-H···O2' and O2-H···O3' hydrogen bonds that are present in β-CD and γ-CD complexes.[125,132] Figure 4.11(a) is a diagram of these unique O-H···O hydrogen bonds. The **A** and **C** host molecules each have one unique O3-H···O2' hydrogen bond present with the four-fold symmetry of these molecules requiring three other identical hydrogen bonds. In the **B** host molecule there is a unique O2-H···O3' and O2···H-O3' hydrogen bond present that connects the **B2** glucopyranose unit to each neighbouring residue on both sides. The four-fold symmetry of the molecule, results in each glucopyranose unit of the **B2** host molecule being connected to its neighbouring residue on either side, thus yielding a total of eight of these interactions. The O2-H···O3' and O2···H-O3' hydrogen bonds are responsible for the rigidity and small tilt angles of the host molecules. As in the case of the **BCDTUL** structure, C6-H···O5' intramolecular hydrogen bonds were also present in the **GCDTUL** structure, contributing to the stabilisation of the host molecules.

Table 4.20 Intramolecular hydrogen bonding interactions for the **GCDTUL** structure

Hydrogen bond	H···A / Å	D···A / Å	D-H···A / °	Symmetry Code*
O3A2-HA23···O2A1	2.06(2)	2.793(7)	149(3)	½-x, ½+y, z
O2B2-HB22···O3B1	2.11(2)	2.879(7)	155(3)	x, y, z
O3B2-HB23···O2B1	2.22(2)	2.842(7)	133(3)	-½-x, ½-y, z
O3C2-HC23···O2C1	2.19(3)	2.899(7)	144(2)	½-x, ½+y, z
C6B1-H7B1···O5B2	2.53(2)	3.29(1)	135(4)	x, y, z
C6B2-H7B2···O5B1	2.54(2)	3.30(1)	134(4)	-½+x, ½-y, z
C6C2-H7C2···O5C1	2.58(2)	3.31(1)	132(4)	½-x, ½+y, z

* Symmetry code applies to the second unit of the interaction

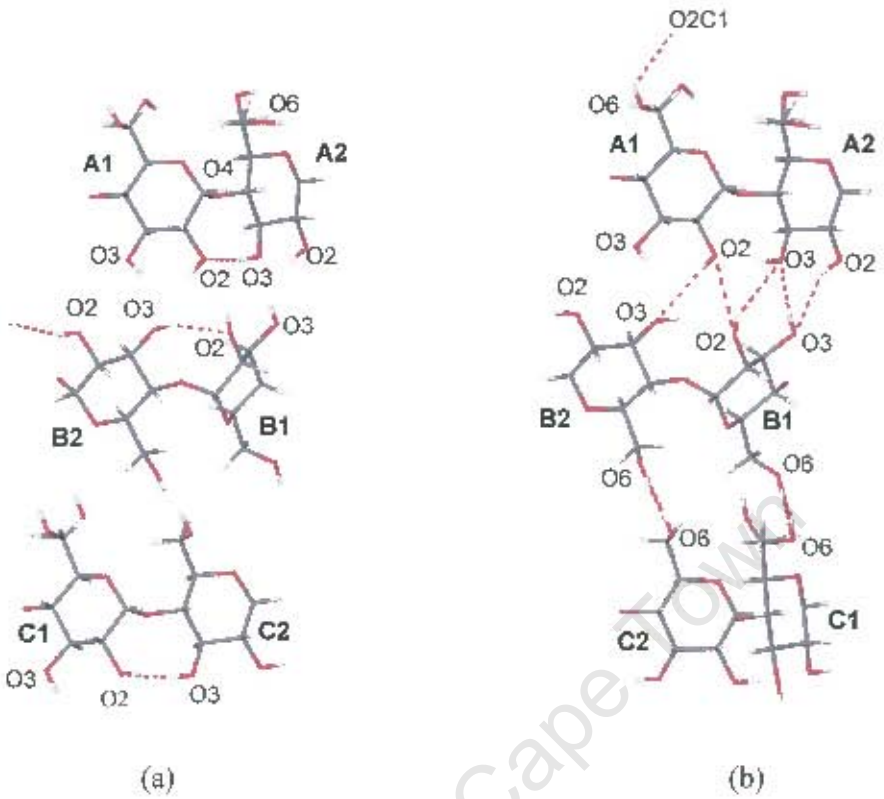

(a) (b)

Figure 4.11 Diagram of the **GCDTUL** asymmetric unit showing the (a) intramolecular and (b) the intermolecular, intra-channel O-H···O hydrogen bonding

Intermolecular hydrogen bonding

As stated earlier, the **GCDTUL** host molecules stack on top of one another and thus form 'endless' channels down the *c*-axis. The intermolecular hydrogen bonding is thus discussed in terms of whether it occurs within these channels [intra-channel] or between them [inter-channel]. The intermolecular, intra-channel hydrogen bonds for the **GCDTUL** structure are presented in Table 4.21. There are ten unique O-H···O hydrogen bonds and these are shown in Figure 4.11(b). The **A** and **B** host molecules are arranged head-to-head and are hydrogen bonded to each other via their O2 and O3 atoms. All the O2 and O3 atoms that were not hydrogen bond donors for intramolecular hydrogen bonding interactions, are instead donors for the intermolecular, intra-channel hydrogen bonding, the exception being the O3A1 atom, which is a hydrogen bond donor to a host atom of a neighbouring channel. The **B** and **C** host molecules are arranged tail-to-tail and are linked to each other via four O6-H···O6 hydrogen bonds. Lastly, the O6-H···O2'

hydrogen bond links the **C** and **A** molecules [arranged head-to-tail] of adjacent sets of three crystallographically independent γ-CD molecules within a channel to each other. Thus in the **GCDTUL** structure, all the γ-CD molecules within a particular channel are linked to each via O-H···O hydrogen bonding.

Table 4.21 Intra-channel hydrogen bonding interactions for the **GCDTUL** structure

Hydrogen bond	H···A / Å	D···A / Å	D-H···A / °	Symmetry Code*
O2A1-HA12···O3B2	2.52	3.195(6)	140(3)	½-x, ½+y, z
O2A2-HA22···O3B1	2.54	3.196(7)	138(3)	½-x, ½+y, z
O2B1-HB12···O2A1	2.51	2.993(6)	118(3)	x, y, z
O2B1-HB12···O3A2	2.56	3.264(7)	145(3)	-1/2-x, 1/2-y, z
O3B1-HB13···O3A2	2.01	2.816(7)	170(3)	-1/2-x, 1/2-y, z
O6B1-HB16···O6C1	2.05	2.85(1)	169(4)	-1/2-x, 1/2-y, z
O6C2-HC26···O6B2	2.02	2.841(9)	175(4)	1-x, -y, z
O6B2-HB26···O6C2	2.02	2.841(9)	174(4)	1-x, -y, z
O6A1-HA16···O2C1	2.30	2.830(8)	123(4)	x, y, 1+z
O6C1-HC16···O6B1	2.04	2.85(1)	169(4)	½-x, ½+y, z

* Symmetry code applies to the second unit of the interaction

Table 4.22 lists the inter-channel hydrogen bonding interactions that were observed for the **GCDTUL** structure. There are six unique hydrogen bonds of which two are O-H···O hydrogen bonds, the other four being C-H···O hydrogen bonds. Figure 4.12 is a stereo diagram of two neighbouring channels, showing three crystallographically independent host molecules and inter-channel hydrogen bonding for one asymmetric unit. Each asymmetric unit is involved in twelve hydrogen bonds, because it is at the receiving end of the interaction as well. However, the four-fold rotation axis requires that each set of three crystallographically independent CDs be involved in a total of forty-eight hydrogen bonds with its neighbouring sets.

Table 4.22 Inter-channel hydrogen bonds in the **GCDTUL** structure

Hydrogen bond	H···A / Å	D···A / Å	D-H···A / °	Symmetry Code*
O3A1-HA13···O2C1	2.10(2)	2.843(7)	149(3)	1-x, 1-y, 1-z
O2C1-HC12···O3A1	2.28(3)	2.843(7)	126(4)	1-x, 1-y, 1-z
C1B1-H1B1···O6C2	2.49(3)	3.469(9)	173(4)	3/2-x, ½+y, 1+z
C1C1-H1C1···O3B2	2.41(3)	3.289(1)	149(4)	½+x, ½-y, 1-z
C2C1-H2C1···O2B2	2.60(2)	3.504(9)	154(4)	½+x, ½-y, 1-z
C2C2-H2C2···O2B1	2.49(3)	3.397(9)	154(4)	3/2-x, -1/2+y, 1-z

* Symmetry code applies to the second unit of the interaction

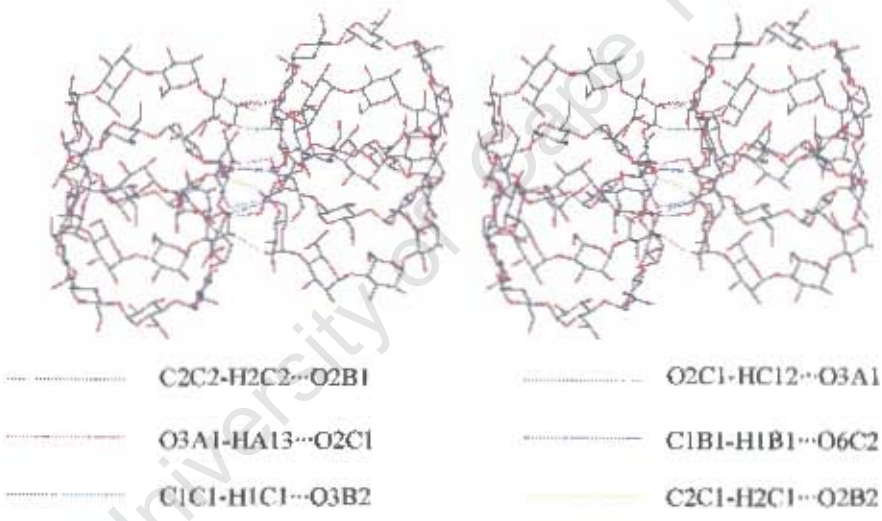

Figure 4.12 Stereo diagram of the inter-channel O-H···O and C-H···O hydrogen bonding in the **GCDTUL** complex.

Water interactions

Table 4.23 lists all the unique water interactions for the **GCDTUL** structure. The host···water interactions are more predominant than the water···water interactions [seventeen host···host vs. three water···water interactions]. Only water molecules on the periphery of the γ-CD molecules were located as the lack of guest modelling made it difficult to assign water molecules that are possibly located within the host cavities.

Table 4.23 Water contacts for the **GCDTUL** structure

Hydrogen bond	D···A / Å	Symmetry Code*
O2A2···OW3A	2.73(2)	x, y, z
O2A2···OW3B	2.76(2)	x, y, z
O3A2···OW2	2.91(1)	1+y, -1+x, 1-z
O5A2···OW6B	3.08(2)	1-y, 1-x, 2-z
O5A2···OW6C	2.87(3)	1-y, 1-x, 2-z
OW3A···O3C1	2.72(2)	1-y, 1-x, 1-z
O2C2···OW2	2.71(1)	x, y, z
O5B2···OW9	3.05(2)	x, y, z
OW1···O5C2	3.23(1)	½+y, ½-x, z
O6B1···OW1	2.78(1)	x, y, z
OW3B···O3C1	3.06(2)	1-y, 1-x, 1-z
O6C2···OW1	2.86(1)	3/2-x, -1/2+y, 1-z
O6B2···OW9	2.68(2)	x, y, z
OW2···C2C2	3.40(1)	x, y, z
OW2···OW7A	2.92(4)	x, y, z
OW9···C6B2	3.42(2)	x, y, z
OW6B···OW6B	3.04(3)	1-y, 1-x, 2-z
OW8B···O2B2	3.11(2)	½+x, ½-y, 1-z
OW3A···C2A2	3.36(2)	x, y, z
OW3B···OW6B	2.87(3)	x, y, z

* Symmetry code applies to the second unit of the interaction

Crystal packing

Figure 4.13 is a stereo view of the crystal packing of the **GCDTUL** structure projected down the *c*-axis. It illustrates the 'endless' channels that are formed down this axis and the location of the water molecules for one interstice is shown. The diameter of the interstice is fairly large [almost comparable to that of the host cavities] and is a result of the channels arranging in a square pattern, as opposed to a more closely-packed hexagonal arrangement. The wide interstices facilitate diffusion of the water molecules upon heating the crystals, as was suggested to be the case for γ-CD complexes in a study of the dehydration kinetics of γ-CD·clofibric acid·15.5(H_2O).[133]

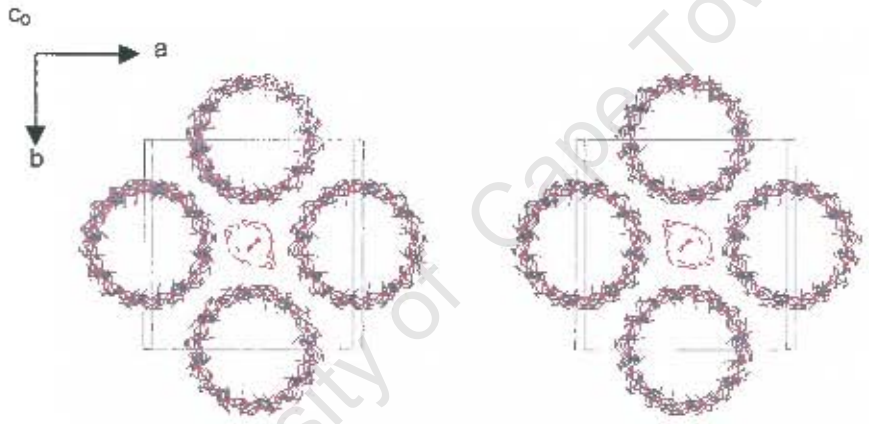

Figure 4.13 Stereo view of the crystal packing of the **GCDTUL** structure down the *c*-axis. The water molecules for one interstice are shown

Powder X-ray diffaction

The experimental and computed PXRD patterns for **GCDTUL** are presented in Figure 4.14. There is generally good agreement between the two traces despite the guest molecule not being modelled in the **GCDTUL** structure. Differences in relative intensities of the peaks in the experimental trace when compared to the computed pattern are due to preferred orientation effects in the former and incomplete modelling in the latter. The complex crystallises as fine columnar rods, which are conducive to preferred orientation despite the sample being finely ground. The close agreement of the traces shows that the computed trace can serve as identification for **GCDTUL**. The traces were obtained at similar temperatures and therefore the angular shift that was observed in the case of **BCDTUL** [Figure 4.7] was not present here.

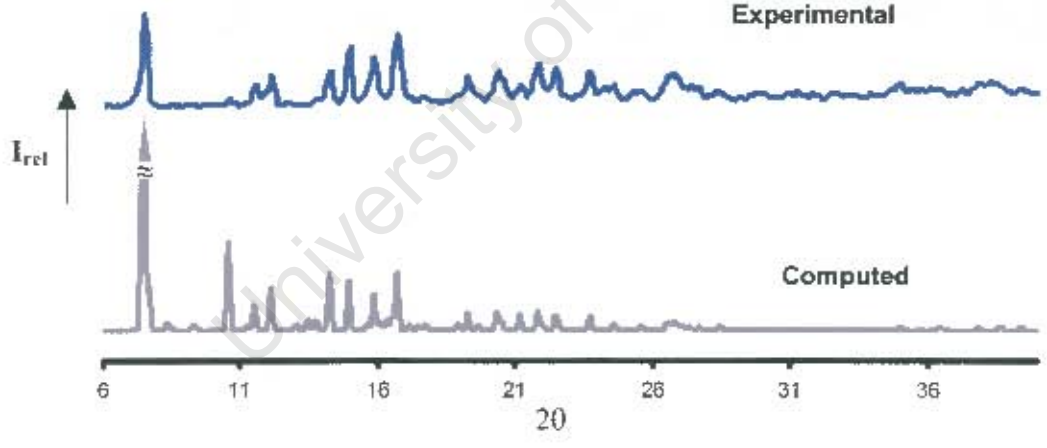

Figure 4.14 Computed [298K] and experimental [295K] PXRD traces for **GCDTUL**

Discussion

The structural features of the **GCDTUL** crystal will be discussed next in relation to the other known γ-CD complexes. This will be done in terms of the conformation of the host molecules, the host hydrogen bonding and water interactions and finally the crystal packing.

Firstly, Table 4.24 presents the unit cell parameters of the γ-CD structures of which the author is aware. Of the twelve structures presented, ten structures were obtained from the CSD,[84] whilst two were determined by members of the Supramolecular Chemistry Research Unit [SCRU] at the University of Cape Town [UCT]. All the γ-CD species crystallise with similar unit cell parameters in the space group $P42_12$, except those of the parent, which crystallises as two hydrated forms in the space group $P2_1$.

Table 4.24 Unit cell parameters of the known γ-CD structures

Guest	a / Å	b / Å	c / Å	α / °	β / °	γ / °	CSD Refcode
Space group $P2_1$							
$11H_2O$	20.287	22.079	16.858	90	105.07	90	CIMSAS
$14H_2O$	16.847	11.098	20.271	90	104.97	90	CIWMIE10(1)*
Space group $P42_12$							
12-Crown-4	23.808	23.808	23.175	90	90	90	DOCYID
12-Crown-4LiSCN	23.750	23.750	22.920	90	90	90	FEJFIJ
12-Crown-4KCl	23.842	23.842	23.132	90	90	90	FEJPOP
polyrotaxane	23.370	23.370	23.910	90	90	90	MOPBUO
methanol	23.808	23.808	23.140	90	90	90	NUNRIX
12-Crown-4-NaCl	23.816	23.816	23.072	90	90	90	SAJNAS
1-propanol (crystal 1)	23.840	23.840	23.227	90	90	90	SEBJAO
1-propanol (crystal 2)	23.809	23.809	23.207	90	90	90	SIBJES
UCT SCRU							
clofibric acid	23.650	23.650	23.640	90	90	90	UCT SCRU[138]
cyclizine	23.824	23.824	23.083	90	90	90	UCT SCRU[83]
Tulobuterol	23.731	23.731	23.069	90	90	90	This work

* Number of redeterminations in parentheses

Conformation of the host molecule

All γ-CD complexes known to date crystallise in the space group $P42_12$ and consist of three crystallographically independent host molecules that are located on a four-fold rotation axis.[132] This indicates that the host molecules have four-fold internal symmetry which contributes to the 'roundness' of the γ-CD molecules. The main contributions to the 'roundness' of the γ-CD molecules are the O2···O3' and O3···O2', as well as the intermolecular, intra-channel hydrogen bonding interactions which restrict the tilt angles [between 10 and 20°] of the glucopyranose units.

Host hydrogen bonding interactions

The hydrogen bonding interactions in the γ-CD·1-propanol·$17H_2O$ complex have been extensively described[134] and this complex is taken as a model for these interactions in isostructural γ-CD complexes.[132] The hydrogen bonding in the **GCDTUL** structure is in close agreement with this.

Water interactions

The water molecules are mainly found in the interstices which have fairly large diameters due to the arrangement of the γ-CD channels, as described in the next section. This allows for easy diffusion of the water molecules and explains the reason for γ-CD complexes desolvating so readily when exposed to open air or mild heating.

Crystal packing

The space group $P42_12$ is an extremely rare space group for compounds to crystallise in and these complexes are the only non-biological, organic compounds to do so.[132] The γ-CD molecules stack on top of one another forming channels down the tetragonal *c*-axis. These channels are not arranged in a hexagonal or quasi-hexagonal pattern and are thus not close packed. Instead the columns arrange in a square pattern, resulting in large channels between the columns [Figure 4.13]. The diameters of the interstitial channels are only slightly smaller than those of the host cavities [~7Å vs, ~8Å]. Neigbouring

channels run anti-parallel to each other as illustrated in Figure 4.15, which illustrates the orientation of the three crystallographically independent γ-CD molecules of the neighbouring channels relative to each other. The molecules are arranged head-to-head [A-B], tail-to-tail [B-C] and head-to-tail [C-A]. This stacking sequence is unusual for CD molecules within a channel, which normally have their neighbouring molecules exclusively parallel or anti-parallel.[132]

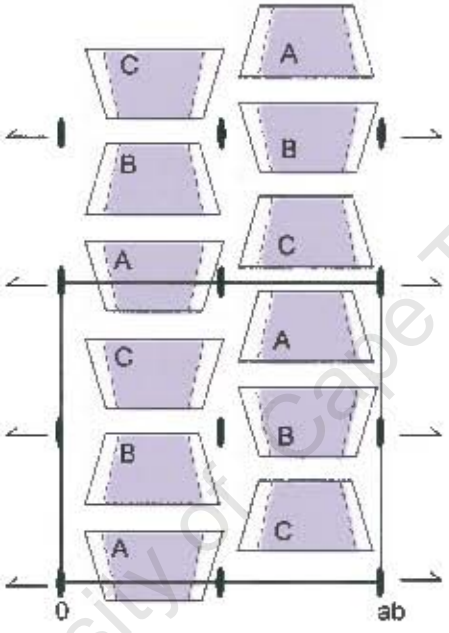

Figure 4.15 Schematic diagram of the stacking within a channel relative to its neighbouring channel in γ-CD complex structures

Figure 4.16 presents the computed trace for **GCDTUL** and that of the averaged trace for γ-CD complexes, published by Caira as isostructural series **17**.[80] The close agreement in the traces is expected as **GCDTUL** is isostructural with the other known γ-CD complexes.

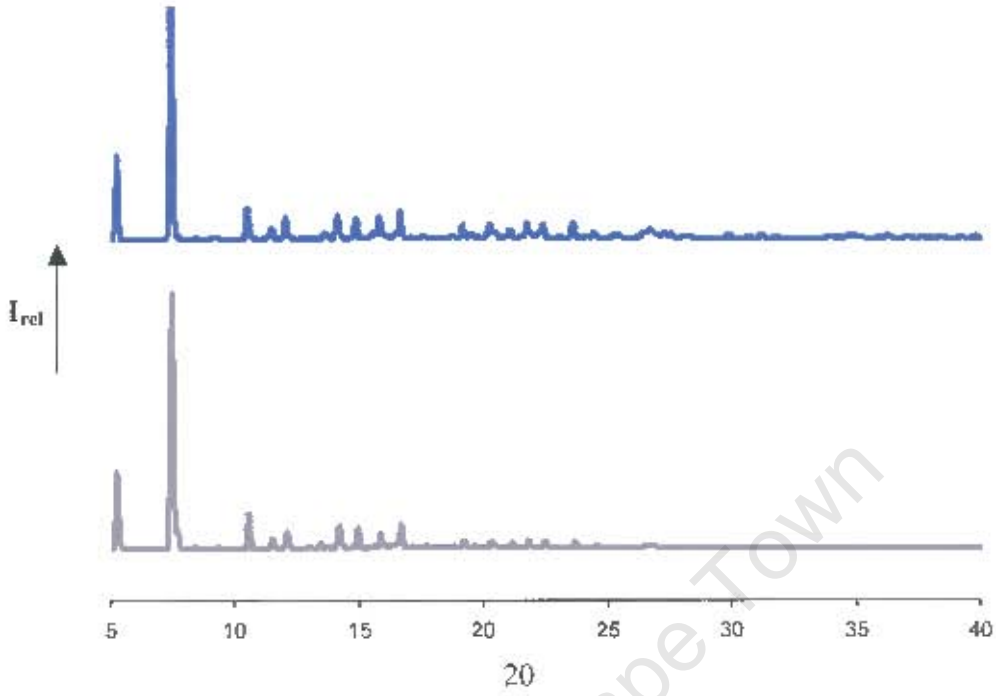

Figure 4.16 The computed trace for **GDDTUL** [bottom] and the trace for isostructural series **17** [γ-CD complexes with similar unit cell parameters and the same space group as **GCDTUL**]

Conclusion

Complexes of β-CD and γ-CD complexes with tulobuterol [named **BCDTUL** and **GCDTUL** respectively] have successfully been prepared. These complexes were characterised by elemental analysis, thermal and X-ray diffraction techniques.

The host:guest:H_2O ratio for **BCDTUL** was established from the combined information of microanalysis and TGA to be 2:1:18.7. Inclusion of tulobuterol within β-CD increased its thermal stability as the temperature at which the complex decomposes [T_{on} = 305°C] is higher than that at which the uncomplexed drug melts [**Form 1**, T_{on} = 91°C; **Form 2** – T_{on} = 81°C]. **BCDTUL** was found to crystallise in the space group P1 with a = 15.320(3), b = 15.462(3), 15.579(3) Å, α = 104.10(3), β = 101.31(3), γ = 104.15(3)°. The structure was solved but the guest molecule could not be located due to its high degree of

disorder. Nevertheless, the host and water molecules were modelled and their geometrical parameters and interactions characterised. Powder X-ray diffraction confirmed that **BCDTUL** is a member of an existing isostructural series of β-CD complexes.

The host:guest:H_2O ratio for **GCDTUL** was established as 3:2:33.3 from the combined information of microanalysis and TGA. As with **BCDTUL**, inclusion of tulobuterol in γ-CD increased its thermal stability as the temperature at which the complex decomposes [T_{on} – 298°C] is higher than the melting temperature [**Form 1**, T_{on} = 91°C; **Form 2** = T_{on} = 81°C] of the uncomplexed drug. **GCDTUL** crystallises with unit cell parameters a = b = 23.731(3) and c = 23.069(5) Å. It, together with all other known γ-CD complexes, crystallises in the space group $P42_12$ with its host molecules located on a four-fold rotation axis, thus requiring that any asymmetrical guest molecule be at least four-fold disordered. For this reason, it was not possible to model the guest molecules in the **GCDTUL** structure. However, the host and water molecules were modelled and their geometrical parameters and interactions elucidated. Powder X-ray diffraction of the **GCDTUL** complex confirmed that it is isostructural with the other known γ-CD complexes.

Chapter 5 - DIMEB and TRIMEB Inclusion Complexes

Complex Preparation

The methylated CDs have an inverse temperature-solubility relationship, i.e. their solubilities decrease with an increase in temperature. Complex crystals of these CDs are therefore prepared by dissolution of the CD at lower temperatures, the dissolved CD in turn solubilising the drug, and the formed complex allowed to crystallize at elevated temperature.

The DIMEB complex of tulobuterol [hereinafter referred to as **DMBTUL**] was first prepared by kneading the host and guest in a 1:1 molar ratio with a mortar and pestle for an hour. During this period a suitable amount of water was added to maintain a pasty consistency. Single crystal preparation followed by stirring the kneaded complex in water at a concentration of 20 mg/ml, and on ice in order to aid dissolution. The solution was then filtered and allowed to crystallise at 70°C over a period of a few days.

Single crystals of the TRIMEB complex of tulobuterol [hereinafter referred to as **TMBTUL**] were prepared by adding to a saturated, aqueous solution of TRIMEB an equivalent amount of tulobuterol. The solution was filtered and allowed to crystallize at 60°C. **TMBTUL** could also be prepared by kneading, the protocol being identical to that for the **DMBTUL** preparation.

Microanalysis

C, H, N microanalysis was used for establishing the host to guest ratios. These data are presented in Table 5.1 and indicated a 1:1 host:guest ratio for the **DMBTUL** and **TMBTUL** complexes.

Table 5.1 C, H, N microanalysis results [n=2] for **DMBTUL** and **TMBTUL**

Complex	Experimental			Calculated		
	%C	%H	%N	%C	%H	%N
TMBTUL [$C_{63}H_{112}O_{35}{\cdot}C_{12}H_{18}ClNO$]	54.57	7.83	1.10	54.35	7.91	0.85
DMBTUL [$C_{56}H_{98}O_{35}{\cdot}C_{12}H_{18}ClNO$]	52.61	7.65	0.72	52.38	7.50	0.90

Thermal Analyses

Hot Stage Microscopy

Figure 5.1 shows the visual characterization of the **DMBTUL** and **TMBTUL** crystals on heating. The analyses were performed under silicone oil to determine the presence of possible included solvent. The **DMBTUL** crystals are initially clear but from 190-260°C they completely opacify. This was evidenced on TGA as a mass loss equivalent to the dissociation of one guest per host molecule. At 260°C the crystals also show signs of decomposition, indicated by a brown tinge. The crystals gradually become darker up to 350°C at which point bubbling occurs as a result of the increased rate of decomposition. The **TMBTUL** crystals remain clear throughout the temperature range and the lack of bubbling or crystal cracking, is indicative of a lack of included water. The crystals show signs of melting at 149°C and are completely melted by 160°C.

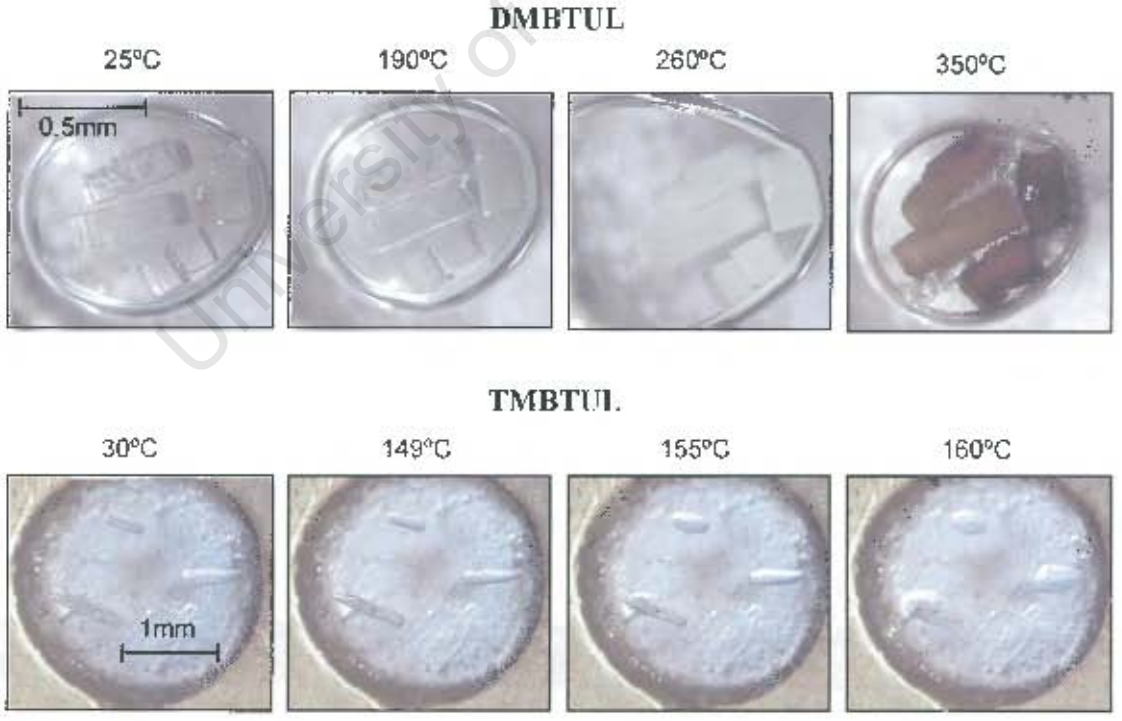

Figure 5.1 HSM photographs of **DMBTUL** and **TMBTUL**

Differential Scanning Calorimetry and Thermogravimetric Analysis

Figure 5.2(a) and (b) present the TGA and DSC analyses of the single crystals of the **DMBTUL** and **TMBTUL** complexes respectively. The **DMBTUL** DSC trace shows a complicated endothermic event in the range 205-269°C [endotherm B], which on the TGA [mass loss A in the range 150-250°C] corresponds to a mass loss equal to one guest molecule per host molecule. This indicates the dissociation of the complex, a phenomenon that has been observed for other DIMEB complexes. The peak at 353°C [endotherm A], together with the exotherm and endotherm that follow it [355-390°C], indicates decomposition of the DIMEB host. This is reflected in the TGA trace by a large and rapid mass loss in the range 350-390°C. The lack of an endothermic peak and negligible mass loss [the mass loss observed is attributed to surface water] before 150°C in the DSC and TGA traces respectively, indicate the absence of included water. **TMBTUL** shows a single thermal event at 156°C [endotherm A] representing the melt of the complex. The TGA trace shows negligible mass loss [observed mass loss attributed to surface water] indicating the lack of included solvent. The above results are consistent with the HSM analysis. Table 5.2 summarises the DSC thermal events.

Table 5.2 Summary of the DSC thermal events for **DMBTUL** and **TMBTUL**.

			DMBTUL	TMBTUL
Temperature range	A	(°C)	345-355	153-161
Endotherm A	T_{on}	(°C)	347	155
	Peak	(°C)	353	156
Temperature range	B	(°C)	205-269	
	T_{on}	(°C)	208	
	Peak	(°C)	238	

(a)

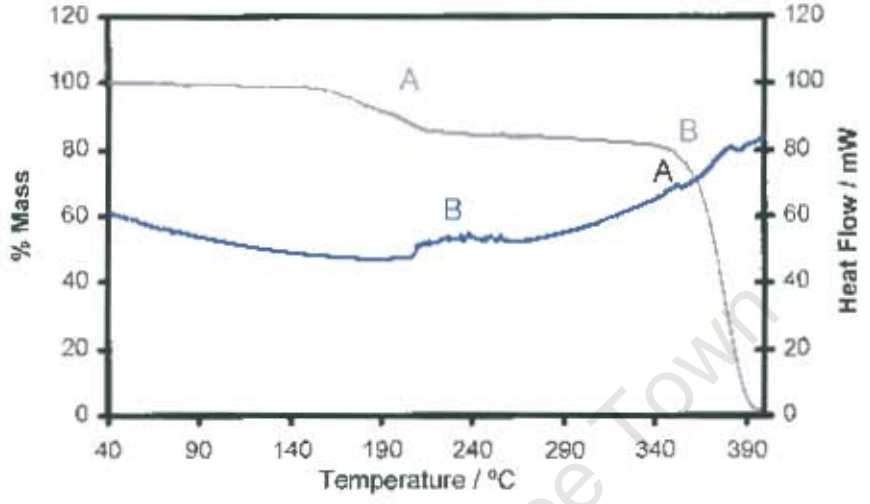

(b)

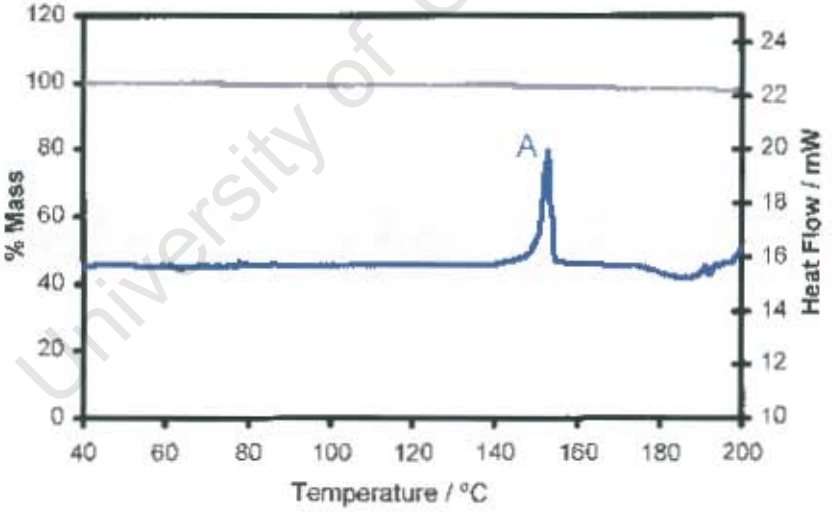

Figure 5.2 DSC [blue] and TGA [grey] traces of (a) **DMBTUL** and (b) **TMBTUL**

X-ray Crystallographic Analysis of DMBTUL

Single Crystal X-ray Diffraction

X-ray photography

Preliminary unit cell parameters were established by photographic techniques. The crystal was mounted on a glass fibre and oscillation and Weissenberg photographs were recorded which collectively revealed Laue *mmm* symmetry, indicating the orthorhombic crystal system.

Data-collection and space group determination

Intensity data were collected on a Nonius Kappa CCD diffractometer at 173K using graphite-monochromated MoKα radiation. XPREP[109] indicated the space group $P2_12_12$ and inspection of the zero levels of the reciprocal lattice with LAYER[117] showed the reflection conditions to be h00: h = 2n, 0k0: k = 2n, which uniquely identify this space group.

Structure solution and refinement

The structure of **DMBTUL** could not be solved by isomorphous replacement since there are no previously published DIMEB complexes with similar unit cell parameters to those of **DMBTUL**. Unfortunately, the structure of **DMBTUL** could not be solved by other methods either, despite many attempts to do so. Many strategies were employed which included *ab initio* structure solution [using SHELXD,[111] SIR2002,[135] SHAKE-AND-BAKE,[114] DIRDIF,[136] SHELXS-97[110]] and fragment phasing [using PATSEE,[137] DIRDIF,[136] SHELXD[111]]. A 'partial' answer was obtained from *ab initio* methods using SHELXD,[111] which revealed approximately half of the asymmetric unit host atoms, but these could not be refined to locate the rest of the atoms. This was probably due to the fragment being translated from its 'true' position, which then could not be successfully refined. This fragment was also used as an input model in SHELXD[111] and PATSEE[137] for rotational and translational searches which were also unsuccessful in providing a satisfactory solution. The crystals of **DMBTUL** were very weakly diffracting which could have hindered the *ab initio* structure solution of **DMBTUL** since observable

reflections at high θ were lacking. Twinning could not be discarded as a possibility, but strong evidence for this phenomenon in this case was lacking.

Table 5.3 Crystal and data-collection parameters for **DMBTUL**

Parameter	
Formula unit	$C_{56}H_{88}O_{35}{\cdot}C_{12}H_{18}ClNO$
Formula weight / g mol^{-1}	1559.1
Crystal system	Orthorhombic
Space group	$P2_12_12$
a / Å	26.7561(4)
b / Å	30.6918(5)
c / Å	19.7482(2)
α / °	90
β / °	90
γ / °	90
Volume / Å^3	16217.1(4)
Z	8
Density$_{calc}$ / g cm^{-3}	1.240
Crystal size / mm^3	0.27x0.22x0.17
Temperature / K	173
Range scanned θ / °	2≤θ≤21
Index ranges	h : -26, 26 k : -30, 30 l : -19, 19
ϕ scan angle per frame / °	1.0
ϕ scan range / °, no. of frames	183, 183
ω scan angle / °	1.0
ω scan ranges / °, no. of frames	58, 58; 55, 55
Dx / mm	46
No. of measured reflections	16440
No. of unique reflections	16421
No. of reflections with I > 2σ(I)	8979
R_{int}, R_σ	0.099, 0.076

X-ray Crystallographic Analysis of TMBTUL

Single Crystal X-ray Diffraction

X-ray photography

Preliminary unit cell parameters were established by photographic techniques. Laue *mmm* symmetry was revealed by the collective information from oscillation and Weissenberg photographs. This indicated the orthorhombic crystal system.

Data-collection and space group determination

Intensity data were collected on a Nonius Kappa CCD diffractometer at 162K using graphite-monochromated MoKα radiation. XPREP[109] indicated the space group $P2_12_12_1$ and inspection of the zero levels of the reciprocal lattice with LAYER[117] showed the reflection conditions to be h00: h = 2n, 0k0: k = 2n, 00l: l = 2n, thus uniquely identifying this space group.

Structure solution and refinement

The structure of **TMBTUL** was solved by isomorphous replacement with the coordinates of an isostructural TRIMEB complex, TRIMEB·clofibrate·H_2O.[138] The coordinates of the host non-hydrogen atoms of the TRIMEB·clofibrate·H_2O complex unit [excluding the 'freely' rotating O6, C7, C8 and C9 atoms] were used for the positions of the corresponding atoms in the **TMBTUL** structure. The refinement proceeded in SHELXL-97[112] and the difference Fourier map revealed the positions of the O6, C7, C8 and C9 atoms in the initial and subsequent refinement runs. All host atoms were initially refined isotropically. Peaks for the guest appeared concurrently, but these were not placed as atoms before complete placement of all host atoms in order to optimise the former's peak positions. Satisfactory isotropic thermal parameters for the host atoms allowed for anisotropic refinement. After it was assessed that these atoms refined satisfactorily with anisotropic temperature factors, hydrogen atoms were placed on the host in fixed geometric positions using a riding model and refined with isotropic temperature factors of 1.2 times those of their parent atoms. The methyl hydrogen atoms were placed using the

rotating group refinement strategy [AFIX 137] with isotropic temperature factors 1.5 times those of their parent atoms.

After all the cyclodextrin atoms had been placed all the guest atom peaks appeared in the difference Fourier map. The map revealed a substituent peak at both *ortho*-positions of the phenyl ring which clearly corresponded to the positions of a disordered chlorine atom. The disorder is effected through the rotation of the chlorophenyl ring around the C1-C7 bond, as illustrated in Figure 5.3.

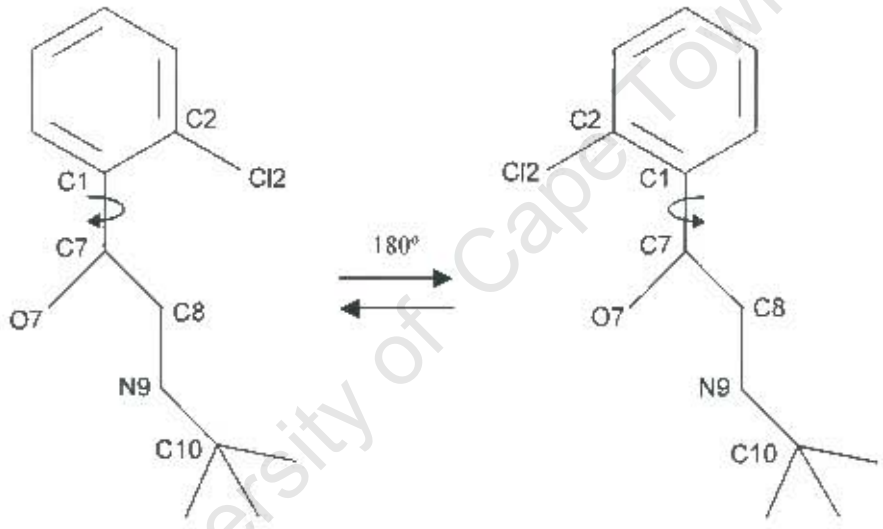

Figure 5.3 Schematic diagram illustrating the mode of guest disorder effected through rotation around the C1-C7 bond

Since there was only one peak position for each phenyl ring atom the disorder was modelled as the result of an exact 180° rotation around the C1-C7 bond. The two rotational conformations will respectively be referred to as the Cl2A and Cl2B rotamers hereinafter. The Cl2A and Cl2B atoms were refined with partial s.o.f. s of x and 1-x respectively. The initial value of 0.58 for x was based on the initial peak heights and allowed to freely refine in subsequent runs. This value converged to 0.56. The phenyl ring geometry was distorted and therefore a geometrical constraint [AFIX 66] was applied in order to fit the phenyl ring atoms to a regular hexagon. The guest atoms were not refined anisotropically due to their high temperature factors, final values ranging

from 0.10-0.29 $Å^2$. The disorder of the Cl2 atom did not allow for the placement of the phenyl H6A and H6B atoms using a riding model [AFIX 43] due to the connectivity conditions of the model described, but instead their fixed positions were calculated based on the distance and geometry for the other phenyl hydrogens. The s.o.f. s of the H6A and H6B atoms were refined with those of the Cl2A and Cl2B atoms respectively and their isotropic temperature factors assigned as 1.2 times those of their parent atoms. The O7 hydrogen atom [labelled H7] could not be located in the difference Fourier map and was thus placed using a hydrogen bond searching model [AFIX 83] and refined with an isotropic temperature factor 1.5 times that of its parent atom. The amino hydrogen atom [labelled H9] could also not be located in the difference Fourier map and was therefore placed at a calculated distance of 1.00(5) Å from the N9 atom in the C8-N9-C10 plane with the C8-N9-H9 and C10-N9-H9 angles being equal. Appropriate distance restraints relative to the C8 and C10 atoms were applied to ensure sensible geometry but with enough flexibility to allow the H9 atom to settle in either a trigonal planar or tetrahedral geometry around the N9 atom. It was refined with an isotropic temperature factor 1.5 times that of its parent atom. The rest of the guest hydrogens were placed and refined in the same manner as their counterparts on the host molecule. The highest electron density peaks at the end of the refinement [0.40-0.69 e $Å^{-3}$] were situated around the Cl2A and Cl2B atoms and are associated with the non-anisotropic refinement of these atoms. The peaks around the *t*-butyl methyl carbons were discarded as possible disordered methyl groups on the basis of their unacceptable geometry and very low peak density [0.30-0.39 e $Å^{-3}$]. Crystal and refinement parameters are presented in Table 5.4.

Table 5.4 Crystal and refinement parameters for **TMBTUL**

Parameter	
Formula unit	$C_{63}H_{112}O_{35}{\cdot}C_{12}H_{18}ClNO$
Formula weight / g mol^{-1}	1657.3
Crystal system	Orthorhombic
Space group	$P2_12_12_1$
a / Å	15.063(1)
b / Å	21.290(1)
c / Å	27.671(1)
α / °	90
β / °	90
γ / °	90
Volume / Å^3	8874(1)
Z	4
Density$_{calc}$ / g cm^{-3}	1.240
μ(MoKα) / mm^{-1}	0.127
F(000)	3568
Crystal size / mm^3	0.27x0.22x0.17
Temperature / K	162
Range scanned θ / °	$2 \leq \theta \leq 30$
Index ranges	h : 0, 19 k : -29, 30 l : -38, 38
φ scan angle per frame / °	1.0
φ scan range / °, no. of frames	161, 161
ω scan angle / °	1.0
ω scan ranges / °, no. of frames	38, 38; 37, 37
Dx / mm	50
No. of measured reflections	35636
No. of unique reflections	19882
No. of reflections with $I > 2\sigma(I)$	9900
No. of least-squares parameters	954
R_{int}, R_σ	0.0739, 0.1157
S	1.038
R_1 ($F_o > 4\sigma(F_o)$)	0.0858
wR_2	0.2714
No. of reflections omitted	17
Weighting scheme parameters	a = 0.1487, b = 0.14
$(\Delta/\sigma)_{max}$	< 0.001
Δρ excursions / e Å^{-3}	0.69, –0.68

Description of the structure

TMBTUL crystallizes in a 1:1 TRIMEB:tulobuterol ratio in the orthorhombic space group $P2_12_12_1$ with Z = 4 complex formula units per unit cell and thus one complex formula unit per asymmetric unit. A diagram of the **TMBTUL** structure is presented in Figure 5.4. The methylglucose units are denoted **G1** to **G7** and the numbering of the guest and one methylglucose unit is shown. The geometrical parameters used to describe the structural features of the CD host, as described in **Chapter 1** are listed in Tables 5.5-5.7.

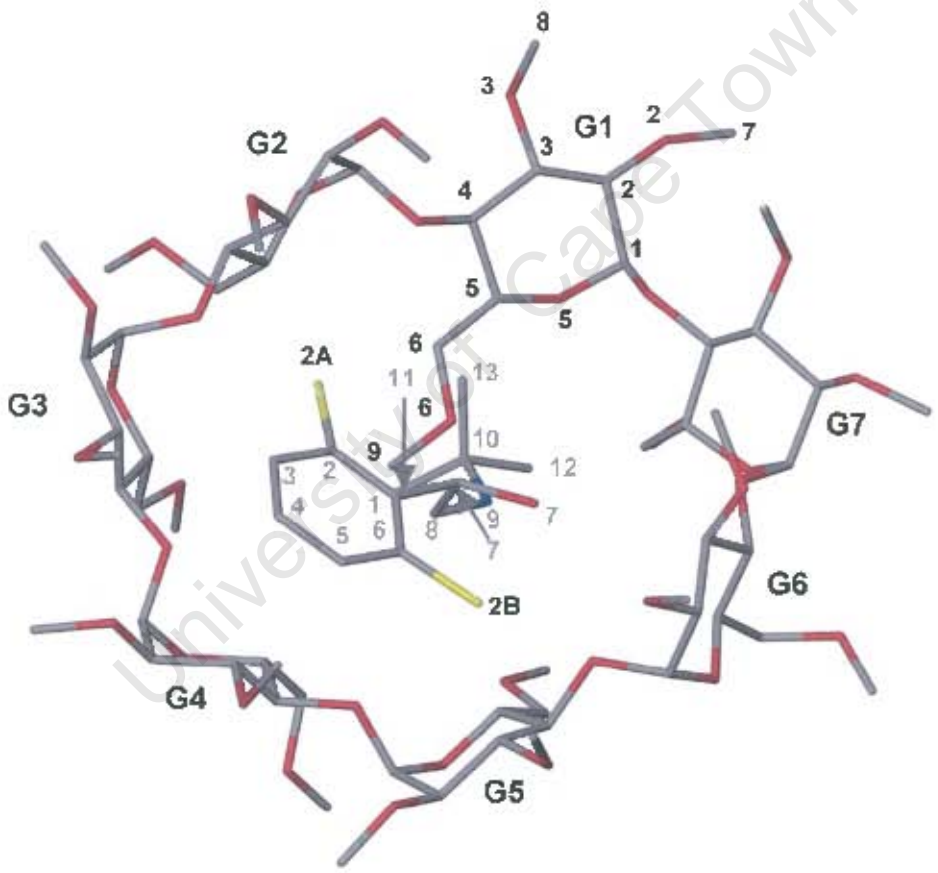

Figure 5.4 View of the **TMBTUL** complex from the host secondary face. Host and guest numbering schemes are in black and grey respectively. Hydrogens atoms are omitted for clarity.

Table 5.5 Torsion angles [°] for **TMBTUL**

Methylglucose unit	ω	Φ	Ψ	Θ_1	Θ_2
G1	82.1(7)	101.9(5)	144.5(4)	44.7(6)	-50.9(6)
G2	-70.0(5)	81.7(5)	93.5(5)	52.8(6)	-57.4(5)
G3	72.9(6)	105.8(5)	144.8(5)	45.9(6)	-49.0(5)
G4	-74.1(5)	110.0(4)	131.9(4)	56.4(5)	-58.0(5)
G5	73.0(6)	106.6(4)	136.7(4)	48.0(5)	-47.4(5)
G6	-81.9(5)	89.2(4)	101.0(4)	48.5(5)	-53.3(5)
G7	-73.5(5)	108.0(4)	162.8(4)	52.7(5)	-55.9(5)
Mean magnitude	**75.4**	**100.5**	**130.7**	**49.9**	**53.1**

Table 5.5 lists some of the principal torsion angles of the TRIMEB molecule. The ω parameter [describing the direction of the C6-O6 bonds with respect to the cavity] is positive for **G1**, **G3** and **G5** [pointing towards the cavity] and negative for **G2**, **G4**, **G6** and **G7** [pointing away from the cavity]. The C9 methyl carbon atoms of the methylglucose units for which ω is positive extend across the primary rim to effectively seal this side of the CD as is discussed later in the **Guest inclusion** section and illustrated in Figure 5.4. The O6-C9 bond is *trans* to C5-C6 for all residues, except for **G6** where it is *gauche*. On the secondary rim all the O2-C7 bonds point away from the cavity, except for that of **G2**, which together with all the O3-C8 bonds, points towards the cavity. For steric reasons the C7 and C8 methyl carbons also point away from each other in all the units. The methylglucose units are all in the $^4C_1$ chair conformation and the conformation around the C4 atoms, as described by the parameters Θ_1 and Θ_2, show minimal deviation from the ideal values for such a residue. Table 5.6 lists the parameters for the O4 heptagon.

Table 5.6 O4-heptagon parameters for **TMBTUL**

Methylglucose unit	r / Å	l / Å	a / °	d / Å	t / °
G1	4.64	4.49	123	-0.085(3)	18
G2	5.13	4.27	125	-0.496(3)	3
G3	5.21	4.49	128	0.261(2)	-22
G4	4.92	4.29	134	0.390(2)	1
G5	4.77	4.43	122	-0.379(2)	26
G6	5.23	4.40	121	-0.315(2)	-24
G7	5.15	4.33	138	0.625(3)	-7
Mean magnitude	**5.01**	**4.39**	**127**	**0.398***	**14**

* Root-mean-square deviation

The O4-heptagon of **TMBTUL** deviates significantly from a regular heptagon and is elliptical as is evident from Figure 5.4. This is indicated numerically by the increasing/decreasing patterns in the **r, l** and **a** parameters. The deviation of the individual O4 atoms from the O4 mean plane is also significant as indicated by the **d** and t parameters and is a result of the tilt angles described next. The tilt angles for the **TMBTUL** structure together with the intersaccharidic bond angles are listed in Table 5.7. Five of the methylglucose units have positive tilt angles, those for **G2** and **G6** being negative, indicating that the majority of the methylglucose units are tilted towards the inside of the cavity on the O6 side. The degree of tilt of the methylglucose units varies sequentially around the ring. There is an increase between neighbouring units in the tilt angle in a numerical order from **G1** to **G7**, except for **G2** and **G6** for which the tilt angles are negative. **G2** and **G6** are nearly on opposite sides of the CD and thus have the effect of squaring the CD off at these points and giving the CD a 'bent' appearance as illustrated in Figure 5.5. The intersaccharidic bond angles are close to what is observed for β-CD molecules.

Table 5.7 φ and τ parameters for **TMBTUL**

Methylglucose unit	φ / °	τ_1 / °	τ_2 / °
G1	116.5(4)	+44.5(1)	+50.6(2)
G2	118.8(4)	-8.5(1)	-9.1(1)
G3	119.6(4)	+16.3(1)	+17.0(1)
G4	117.8(3)	-27.1(1)	+27.2(2)
G5	115.2(3)	+28.7(1)	+33.6(2)
G6	118.3(3)	-12.4(1)	-13.0(1)
G7	116.9(4)	+37.6(1)	36.8(2)
Mean	**117.6**	**19.0**	**20.4**

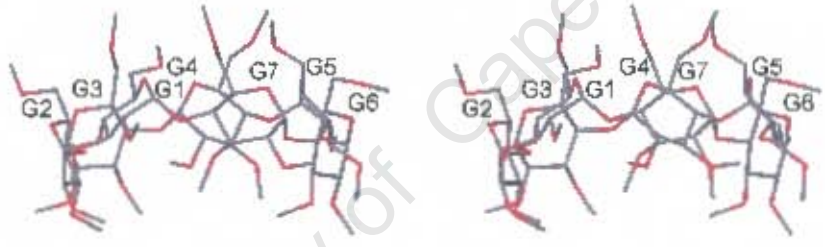

Figure 5.5 Stereo view from the side of the TRIMEB molecule in **TMBTUL** in order to illustrate its 'curvature'

Guest inclusion

The *t*-butyl group of the tulobuterol molecule inserts into the cyclodextrin cavity from the secondary face with the chlorophenyl group located on the outside of the cavity as illustrated in Figure 5.6. The *t*-butyl group is located very close to the centre of the **TRIMEB** cavity [the distance of the C10 atom to O4-heptagon centroid is only 0.41Å] whilst the chlorophenyl group is located on the outside of the cavity over the secondary side of the **G4** methylglucose unit. The tulobuterol backbone mean plane defined by the C1, C7, C8, N9 and C10 atoms [refer to Figure 5.3 for atom labelling of the tulobuterol

molecule] makes an angle of 29.2(7)° with the molecular axis of the host molecule, defined as being orthogonal to the O4 mean plane.

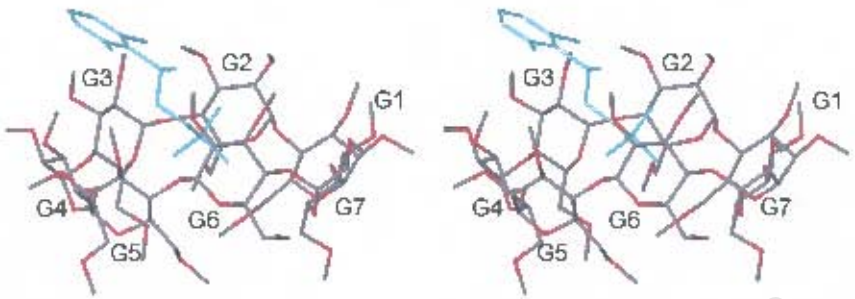

Figure 5.6 Stereo view illustrating the mode of guest inclusion in the **TMBTUL** complex

Figures 5.7(a)-(d) are space-filling diagrams presenting different views of the **TMBTUL** complex. Figure 5.7(a) is a view from the primary face illustrating the effect of the C9 methyl groups of the methylglucose units for which ω is positive and which thus extend over the TRIMEB cavity, effectively 'sealing off' this side of the CD. The view from the secondary face, presented in Figure 5.7(b), shows the 'open' side of the TRIMEB molecule and how the guest is 'buried' in the cavity. The degree of guest protrusion from the host cavity is illustrated in a side view of the **TMBTUL** complex in Figure 5.7(c), which shows that the chlorophenyl group is located above the secondary 'upper' rim of the TRIMEB molecule. Figure 5.7(d), with part of the host removed, presents a side view of the degree of insertion of the guest molecule into the host cavity.

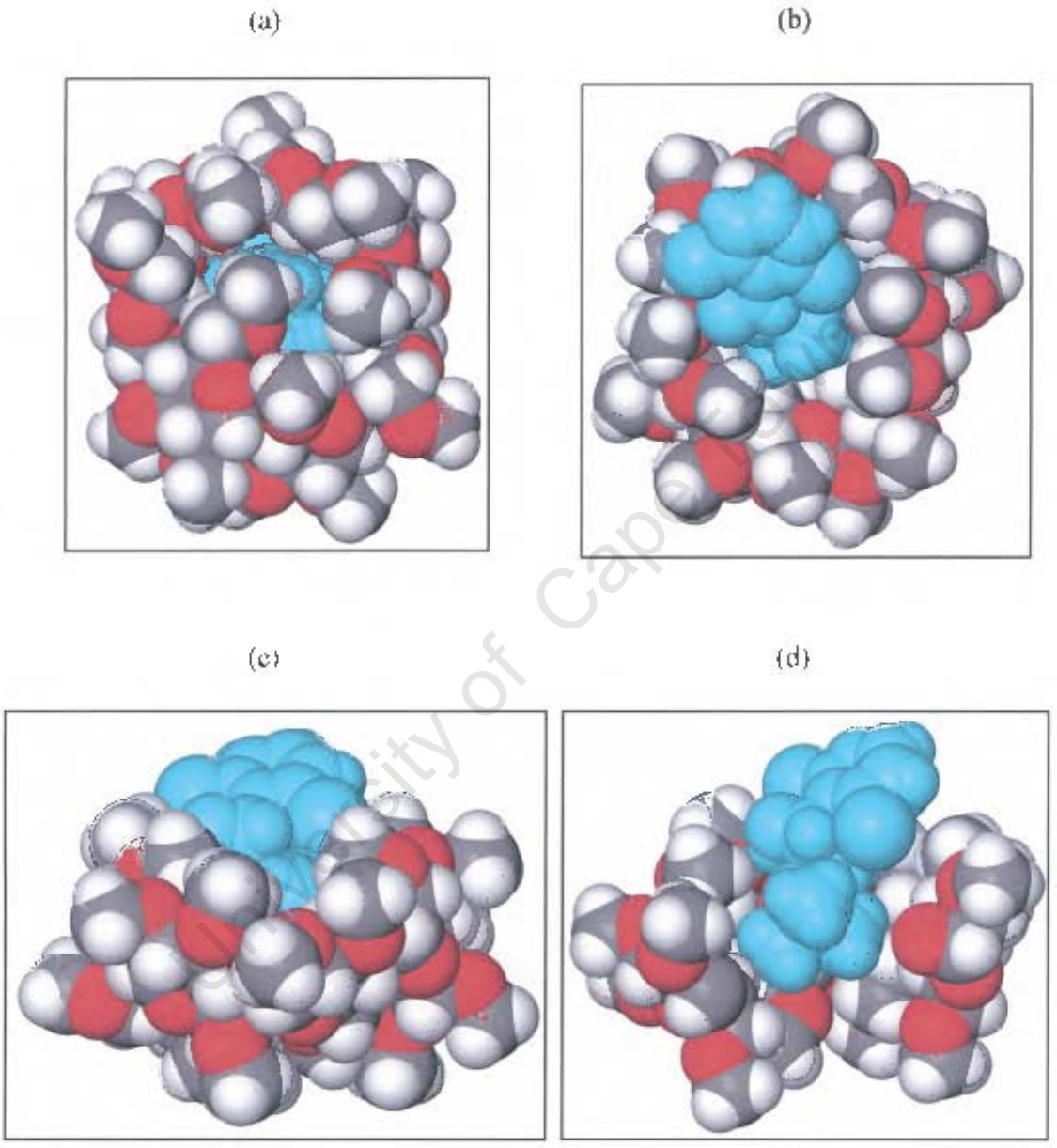

Figure 5.7 View of the (a) primary, (b) secondary and (c) side face of the **TMBTUL** complex, whilst (d) is a view of the side with part of the host molecule removed

Conformation and configuration of the guest molecule

The conformation of the tulobuterol molecule in **TMBTUL** is discussed next relative to its conformation in the **Form 1** and **Form 2** polymorphs of tulobuterol. The principal torsion angles for the tulobuterol molecule in **TMBTUL**, **Form 1** and **Form 2** are presented in Table 5.8, whilst Figure 5.8 is a repeat of Figure 3.10, illustrating the definitions of the torsion angles. For more background the reader is referred back to **Chapter 3**. The configuration at the chiral centre C7 of the included tulobuterol molecule is (R-), which will be elaborated on in the **Discussion** section of this chapter.

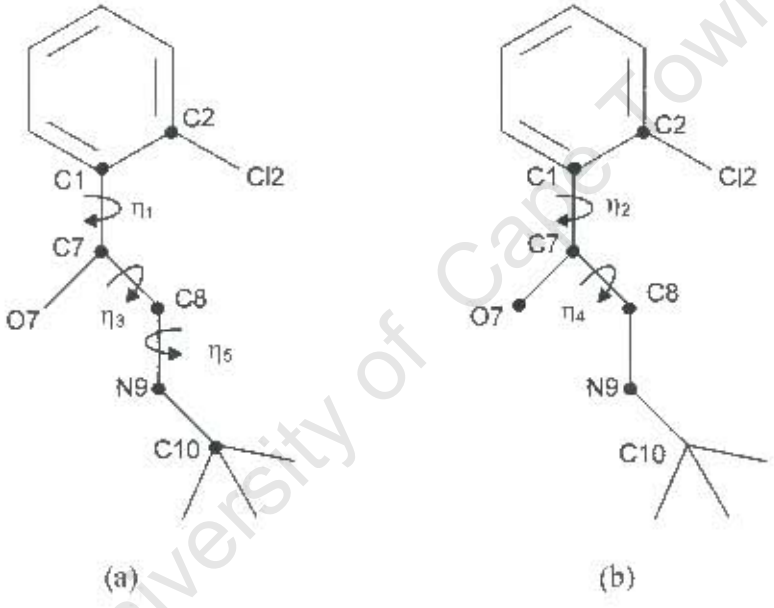

Figure 5.8 Schematic diagram of the principal torsion angles (a) η_1, η_2, η_5 (b) η_2 and η_4 for the tulobuterol backbone.

The two entries each for the η_1 and η_2 torsion angle for the tulobuterol molecule in **TMBTUL** correspond to the two rotational orientations of the chlorophenyl ring [refer to Figure 5.4]. The η_1 and η_2 torsion angles of the Cl2A conformer agree closely with those for **Form 1** and **Form 2**, respectively indicating that the aromatic ring plane is nearly orthogonal to the tulobuterol backbone and that the O7 and Cl2A atoms are *trans*. The η_1 angle for the Cl2B conformer is larger than in the uncomplexed state but the aromatic ring plane is still nearly orthogonal to the tulobuterol backbone. The η_2 torsion angle is markedly different though, indicating that the Cl2B and O7 atoms are *gauche*, which

contrasts with the exclusively *trans* relationship observed in the uncomplexed state. The Cl2A conformer is slightly favoured over the Cl2B conformer as indicated by its s.o.f. of 0.56.

Table 5.8 Principal torsion angles [°] of tulobuterol in **TMBTUL**, **Form 1** and **Form 2**

Compound	η_1	η_2	η_3	η_4	η_5
TMBTUL [(R-)]	-75.5(8)[a], 100.9(8)[b]	153.5(6)[a], -30.2(10)[b]	179.5(7)	-49.6(12)	-119.5(9)
Form 1					
Molecule **A** [(S-)]	87.0(2)	-153.8(2)	-175.7(2)	62.2(2)	-170.5(2)
Molecule **B** [(R-)]	-81.4(2)	160.2(2)	-179.6(2)	-58.2(2)	173.7(2)
Molecule **C** [(R-)]	-77.8(2)	163.2(2)	178.1(2)	-60.1(2)	169.4(2)
Form 2					
Molecule **A** [(S-)]	84.0(2)	-157.2(2)	-174.0(2)	64.3(2)	-166.0(2)
Molecule **B** [(R-)]	-83.9(2)	157.1(2)	-175.2(2)	-54.1(2)	167.2(2)
Molecule **C** [(R-)]	-81.5(2)	159.9(2)	178.9(1)	-59.7(2)	172.6(2)

[a] Cl2A rotamer
[b] Cl2B rotamer [C2 is replaced by C6 in the torsion angle definitions]

The η_3 torsion angle for the tulobuterol molecule in **TMBTUL** is close to 180° and in agreement with that observed in **Form 1** and **Form 2**, indicating that the backbone is in the 'extended' conformation with the aromatic ring *trans* to the N9 atom. The η_4 torsion angle indicates that the O7 and N9 atoms are *gauche* as is the case for the **Form 1** and **Form 2** tulobuterol molecules.

The η_5 torsion angle of –119.5(9)° in the **TMBTUL** complex constitutes a significant difference from the angles observed in the uncomplexed tulobuterol molecules as illustrated in Figure 5.9. This is probably necessary to allow for a better fit of the tulobuterol molecule in the TRIMEB cavity.

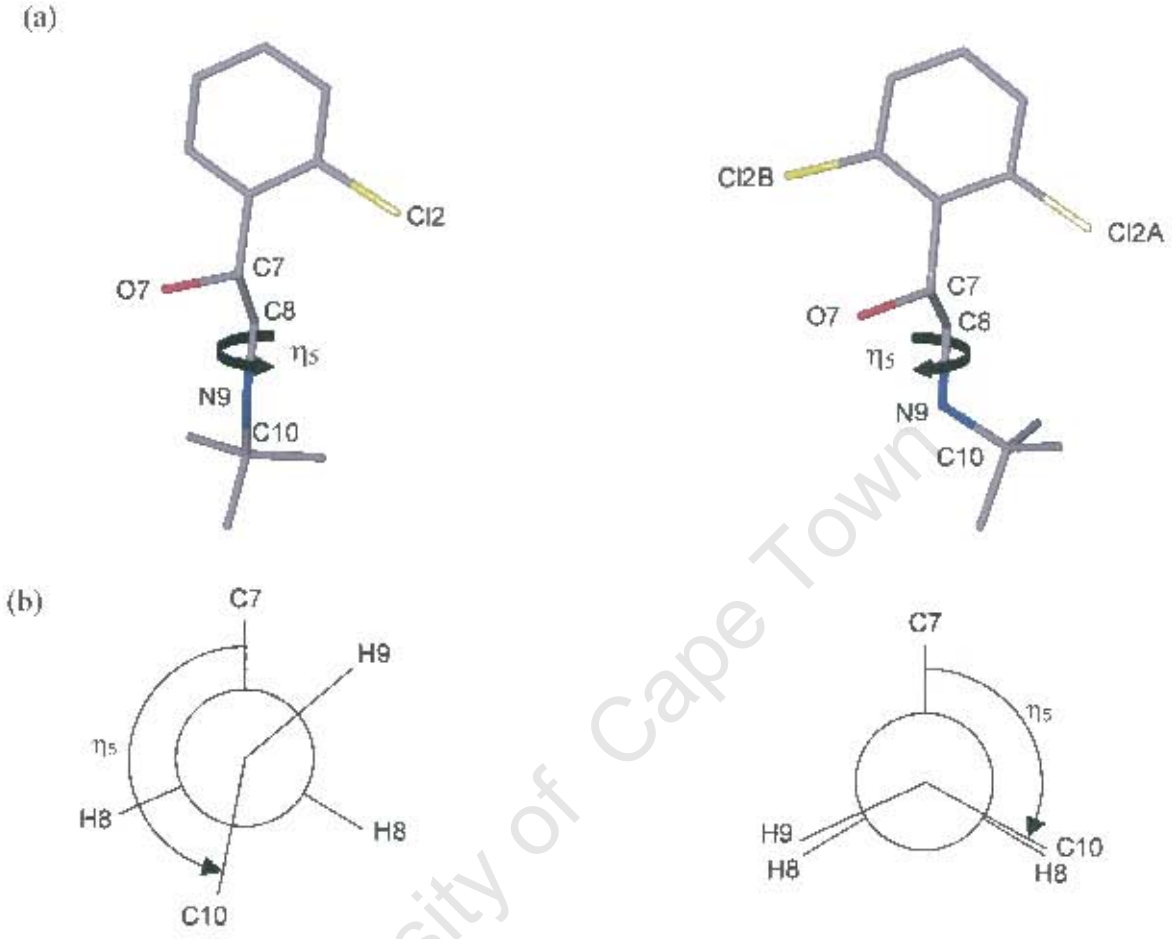

Figure 5.9 (a) Diagram illustrating the difference in the η_5 torsion angle for tulobuterol in **Form 1**, molecule C [left] and in **TMBTUL** [right]. Hydrogen atoms are omitted for clarity

(b) Newman projections illustrating the η_5 torsion angle of the corresponding molecules in (a)

Hydrogen bonding and C-H···π-ring interactions

Hydrogen bonding and C-H···π-ring interactions for **TMBTUL** are listed in Table 5.9, indicating that it is not only van der Waals and hydrophobic interactions that stabilise the **TMBTUL** structure.

Intramolecular host interactions

There are eleven host hydrogen bonds that stabilise the structure of the TRIMEB molecule in **TMBTUL**. They do so for different conformational aspects of the molecule. On the primary side of the TRIMEB molecule, C6-H···O5' hydrogen bonds have been implicated as factors for the high positive tilt angles observed for the methylglucose units in general,[139] and it has also been suggested that these hydrogen bonds are usually not present for methylglucose units with lower tilt angles. In the **TMBTUL** structure there are five methyl glucose units at the receiving end of such hydrogen bonds [Figure 5. 10] with **G2** and **G6**, the methylglucose units with the lowest tilt angles, being the exceptions.

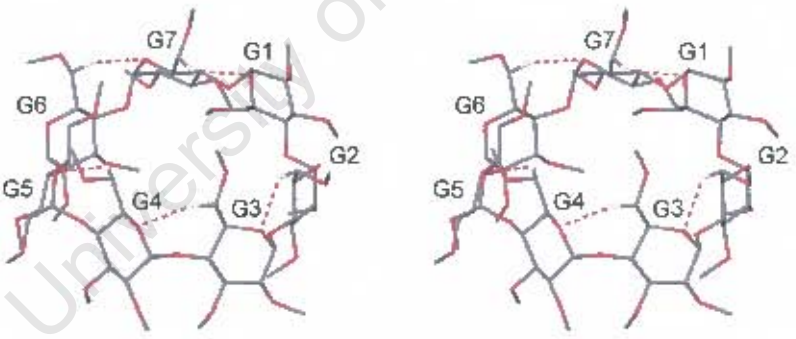

Figure 5.10 Stereo view of the C6-H···O5' hydrogen bonds in the **TMBTUL** structure. Only the hydrogen atoms involved in the relevant hydrogen bonding are shown.

Interestingly, **G2** on the secondary side is involved in a C1-H···O3' hydrogen bond [C1G2-H1G2···O3G1] which could be responsible for its low tilt angle. There are two other C-H···O hydrogen bonds on the primary side of the TRIMEB molecule, namely C6G7-H6B7···O6G1 and C1G7-H1G7···O6G6 [not shown], and these 'lock' the O6 atoms in their observed positions in their rotation around the C5-C6 bond [defined by

parameter ω in Table 5.5]. The other hydrogen bonds on the secondary side of the TRIMEB molecule are C8-H···O2 and C8-H···O3' hydrogen bonds, which 'lock' the C8 methyl groups in the positions that they are observed on their respective methylglucose units.

Table 5.9 Hydrogen-bonding and C-H···π-ring interactions for **TMBTUL**

Interaction	H···A / Å	D···A / Å	D-H···A / °	Symmetry code[a]
Host				
C1G2-H1G2···O3G1	2.43(4)	3.10(1)	125(4)	x, y, z
C1G7-H1G7···O6G6	2.46(4)	3.22(1)	134(4)	x, y, z
C6G2-H6B2···O5G3	2.43(4)	3.16(1)	132(4)	x, y, z
C6G3-H6A3···O5G4	2.48(4)	3.38(1)	154(4)	x, y, z
C6G4-H6B4···O5G5	2.53(4)	3.16(1)	123(4)	x, y, z
C6G6-H6B6···O5G7	2.41(4)	3.15(1)	133(4)	x, y, z
C6G7-H6B7···O5G1	2.40(4)	3.10(1)	128(4)	x, y, z
C6G7-H6B7···O6G1	2.56(4)	3.48(1)	158(4)	x, y, z
C8G1-H8C1···O2G1	2.55(4)	3.12(1)	118(4)	x, y, z
C8G2-H8A2···O2G3	2.37(4)	3.20(1)	145(4)	x, y, z
C8G5-H8C5···O2G5	2.53(4)	3.12(1)	120(4)	x, y, z
Guest				
C8-H8B···Cl2A	2.72(4)	3.35(1)	123(4)	x, y, z
Host-guest				
O7-H7···O2G6	2.16(4)	2.86(1)	143(4)	x, y, z
N9-H9···O4G5	2.51(4)	3.47(1)	160(4)	x, y, z
C8G4-H8C4···Cg*	3.30(4)	3.80(1)	114(4)	x, y, z
Host-host				
C4G2-H4G2···O3G5	2.51(4)	3.42(1)	154(4)	1+x, y, z
C2G5-H2G5···O6G2	2.55(4)	3.46(1)	154(4)	-1+x, y, z
C9G6-H9A6···O3G1	2.59(4)	3.07(1)	111(4)	-1+x, y, z
C2G4-H2G4···O5G7	2.58(4)	3.42(1)	143(4)	3/2-x, 1-y, 1/2+z
C2G4-H2G4···O6G7	2.56(4)	3.43(1)	149(4)	3/2-x, 1-y, 1/2+z
C2G7-H2G7···O6G4	2.41(4)	3.32(1)	155(4)	3/2-x, 1-y, -1/2+z
C9G7-H9B7···O3G4	2.50(4)	3.19(1)	128(4)	3/2-x, 1-y, -1/2+z

[a] Symmetry code applied to second unit of interaction

* Cg = Centre of gravity of the aromatic ring of the guest

Intramolecular guest interactions

Only one guest hydrogen bond, namely C8-H8···Cl2A, was found which could explain the slight preference of the Cl2A over the Cl2B rotamer, as indicated by the former's s.o.f. of 0.56.

Host-guest interactions

There are two host-guest hydrogen bonds and one C-H···π-ring interaction that are listed in Table 5.9, which strengthen the association of the host and guest molecules. These are the O7-H7···O2G6 and N9-H9···O4G5 hydrogen bonds and the C8G4-H8C4···Cg interaction which are illustrated in Figure 5.11. The presence of the host-guest hydrogen bonds involving the N9 and O7 atoms explains the absence of the intramolecular N-H···O hydrogen bond that is observed for the tulobuterol molecules in the uncomplexed state. The symmetry codes also indicate that these are within the same asymmetric unit, i.e. no contacts are made between guest and host molecules of neighbouring units.

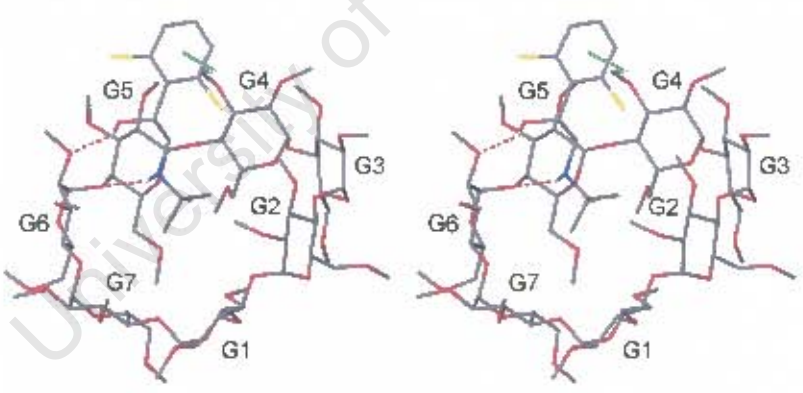

Figure 5.11 Stereo diagram illustrating the host-guest interactions. The O7-H7···O2G6 and N9-H9···O4G5 hydrogen bonds are shown in red, whilst the C8G4-H8C4···Cg interaction is shown in green. Only the hydrogen atoms involved in the interactions are shown for clarity

Host-host interactions

The seven host-host C-H···O hydrogen bonds that are present in the **TMBTUL** structure contribute to the stabilisation of the crystal structure in the absence of water molecules that fulfil this function in hydrated complexes. The symmetry codes for the C4G2-H4G2···O3G5 [1+x, y, z], C2G5-H2G5···O6G2 [-1+x, y, z] and C9G6-H9A6···O3G1 [-1+x, y, z] hydrogen bonds indicate that they link the host molecules along the *a*-axis. Likewise the symmetry codes for the C2G4-H2G4···O5G7 [3/2-x, 1-y, 1/2+z], C2G4-H2G4···O6G7 [3/2-x, 1-y, 1/2+z], C2G7-H2G7···O6G4 [3/2-x, 1-y, -1/2+z] and C9G7-H9B7···O3G4 [3/2-x, 1-y, -1/2+z] hydrogen bonds indicate that they link the screw-related host molecules along the *c*-axis. The number of these hydrogen bonds per host molecule doubles to fourteen as a result of it also being at the receiving end of the interaction. These are illustrated in Figure 5.12, which also shows that each host molecule is connected to four surrounding host molecules along the directions mentioned above.

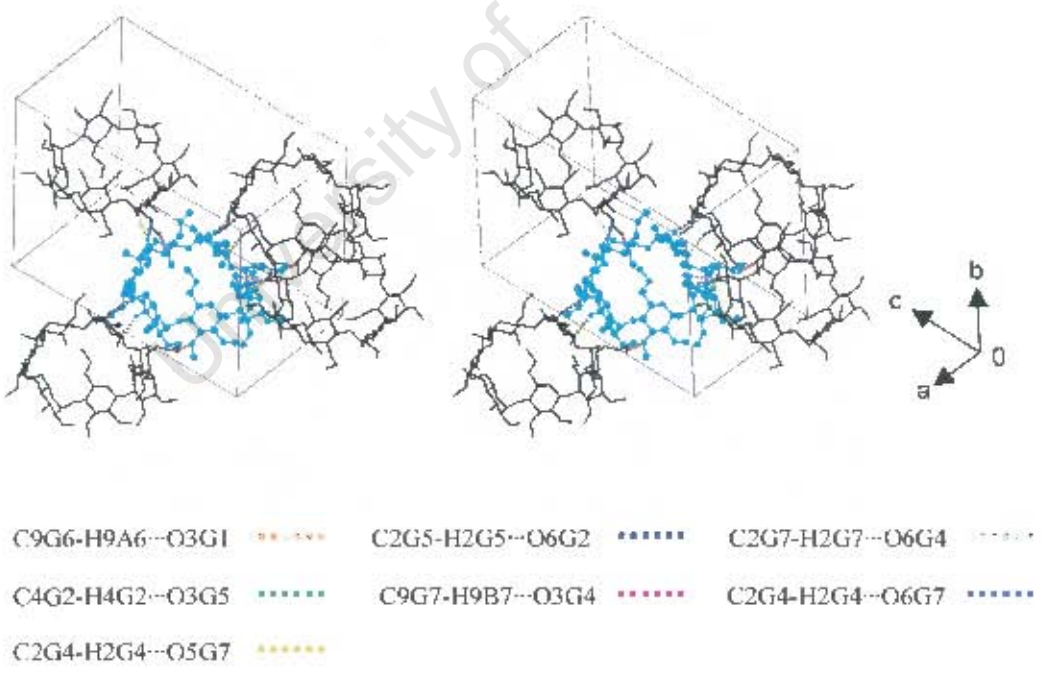

Figure 5.12 The intermolecular C-H···O hydrogen bonds that link TRIMEB molecules in the **TMBTUL** structure.

Crystal packing

Crystal packing diagrams of the **TMBTUL** structure are presented in Figure 5.13. The O4-heptagon mean plane is parallel to the *ac*-plane with the cavity axis of the CD parallel to the *b*-axis. The molecules are stacked head-to-tail down this direction with slight lateral offsets resulting in a screw-channel. The crystal packing diagrams also visually confirm that there are no inter-guest interactions and also show that the chlorophenyl ring does not protrude into the cavities of neighbouring host molecules.

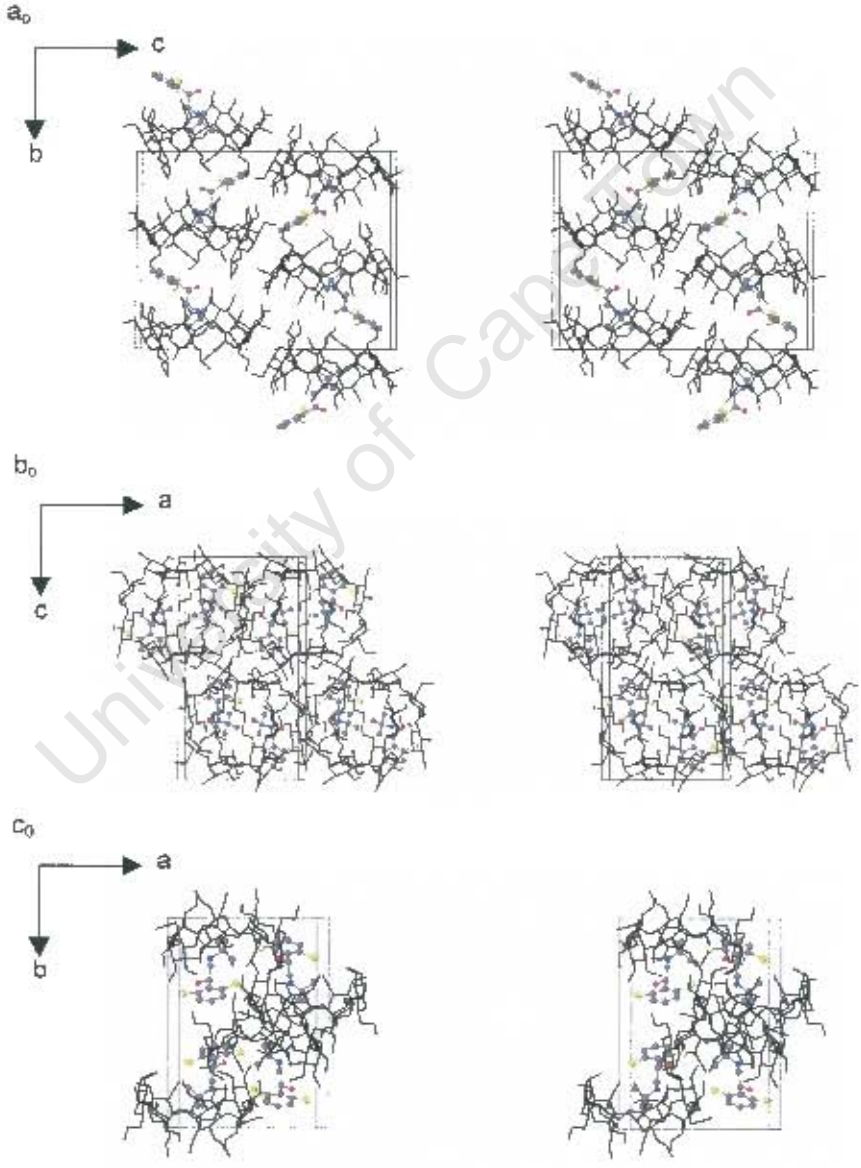

Figure 5.13 Stereo packing diagrams of **TMBTUL** down the (a) *a*- (b) *b*- and (c) *c*-axes respectively

Powder X-ray Diffraction

The computed and experimental PXRD patterns for **TMBTUL** are presented in Figure 5.14. The patterns match in their number of peaks as well as their profiles. The slight shift of the experimental trace to lower 2θ values is attributed to the difference in temperatures at which the information for the traces was obtained. The close agreement also indicates the lack of a phase change on grinding the complex, whilst the mismatch in relative peak intensities of the experimental trace with respect to the computed trace is due to preferred orientation effects.

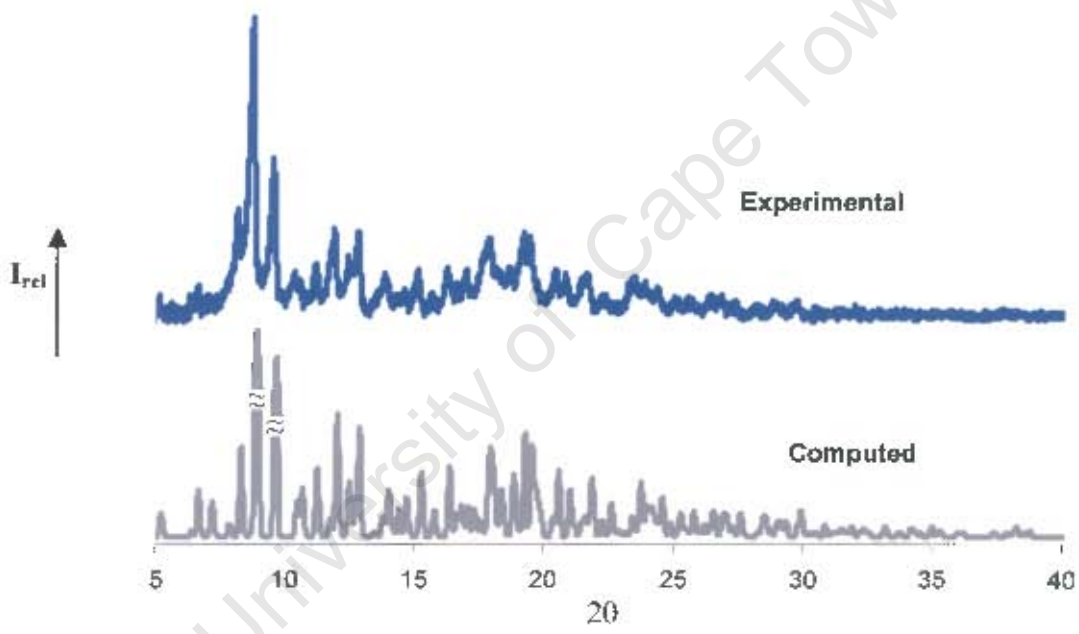

Figure 5.14 Computed [162K] and experimental [295K] PXRD traces of **TMBTUL**

Discussion

A search of the CSD[84] for TRIMEB structures yielded twenty entries, but seven of these are redeterminations, thus making a total of thirteen unique TRIMEB structures that the database contains. The unit cell parameters for these are listed in Table 5.10. However, in addition to the CSD[84] structures, members of the Supramolecular Chemistry Research Unit [SCRU] at the University of Cape Town [UCT] have determined several TRIMEB structures that have recently been published, or are 'in press', but which are not yet listed in the CSD.[84] The unit cell parameters for these structures, as well as those for **TMBTUL**, are listed at the bottom of Table 5.10. The CSD[84] structures all crystallise in the space group $P2_12_12_1$. Two **TRIMEB** complex structures, isolated by the SCRU at UCT, with butamben[85] and (E)-ajoene[86] as guests crystallise in the monoclinic space group $P2_1$, the former being the first reported TRIMEB structure to crystallise in the monoclinic crystal system. Two new crystalline forms of the host TRIMEB, an anhydrate and a trihydrate,[140] were also recently prepared by the UCT SCRU. As stated earlier, the initial phasing trial model used for the structure solution of **TMBTUL** was obtained from TRIMEB·clofibrate·H_2O,[138] whose unit cell parameters [Table 5.10] agree closely with those of **TMBTUL**, one of the two necessary conditions for successful structure solution using the isomorphous replacement method.

Conformation of the host molecule

Permethylation of the β-CD molecule has a marked effect on its conformation, as discovered with the first structural determination of a TRIMEB complex, namely TRIMEB·*p*-iodophenol.[141] It was found that the O4 heptagon is elliptically distorted with relatively large positive values for the methylglucose tilt angles when compared to those of β-CD. The reason for the distortion of the heptagon, and more specifically the relatively large tilt angles in TRIMEB structures is the lack of O2···O3' hydrogen bonds[141] that are responsible for the 'round structure' of β-CD molecules.[142,125] It was suggested that in addition to this, C6-H···O5' interactions are responsible for the stabilisation of the distortion of the TRIMEB molecules in general.[139]

Table 5.10 Unit cell parameters of the known TRIMEB structures

Guest	a / Å	b / Å	c / Å	α / °	β / °	γ / °	CSD Refcode
CSD structures							
Space group – $P2_12_12_1$							
H_2O	14.823	19.382	26.534	90	90	90	HEZWAK[143](1)*
methylcyclohexane	11.043	25.333	29.132	90	90	90	XAQJII[144] (1)
(S)-1,7-dioxaspiro(5,5)undecane	10.936	25.530	29.640	90	90	90	QOYLIZ[145]
(R)-5-ethyl-1,3,5-trimethylhydantoin	11.190	26.080	29.185	90	90	90	MODHUI[146]
(L)-menthol	11.060	26.138	29.669	90	90	90	NIZHAF[139]
p-iodophenol	14.997	21.368	28.205	90	90	90	CAMPIP[141](1)
(R)-flurbiprofen	15.092	21.714	28.269	90	90	90	COYXAP10[147](1)
(S)-flurbiprofen	15.271	21.451	27.895	90	90	90	COYXET20[147](2)
m-iodophenol	15.669	20.798	25.486	90	90	90	GELKEN10[148](1)
4-biphenylacetic acid	14.890	21.407	28.540	90	90	90	PAFSOE[148]
ethyl laurate	14.796	22.444	27.720	90	90	90	PINMAA[149]
(S)-ibuprofen	15.232	21.327	27.597	90	90	90	RONWOG[150]
(S)-naproxen	15.179	21.407	27.670	90	90	90	ZIFQOU[151]
UCT SCRU							**References**
Space group – $P2_1$							
Butamben	10.891	14.858	27.583	90	99.62	90	85
(E)-ajoene	11.553	27.715	14.605	90	109.39	90	86
Space group – $P2_12_12_1$							
$3H_2O$	16.205	16.287	30.099	90	90	90	140
none	15.951	16.577	28.941	90	90	90	140
clofibric acid	11.601	26.284	28.882	90	90	90	138,152
psoralen	10.945	25.652	29.939	90	90	90	153
(Z)-ajoene	15.102	21.520	27.313	90	90	90	86
clofibrate	15.010	21.490	27.700	90	90	90	138
tulobuterol	15.063	21.290	27.671	90	90	90	This work

* Number of re-determinations in brackets

In the parent TRIMEB, a monohydrate, the O4-heptagon is even more elliptically distorted from the native β-CD.[143] Deviation from the usual $^4C_1$ chair conformation of the methylglucose unit seemed to promote further distortion of that already inherent in TRIMEB structures, as one of the methylglucose units was found to exist in the high-energy, inverted $^1C_4$ chair conformation. This is the only example of deviation from the usual $^4C_1$ chair conformation found in cyclodextrins, except for one of the methylglucose units of TRIMEB·*m*-iodophenol[148] which exists in the $^0S_2$ twist conformation, a high energy intermediate of the two chair conformations.[154] The $^0S_2$ twist conformation also partly adds to the distortion of the TRIMEB molecule, supported by the fact that the TRIMEB·*m*-iodophenol complex host molecule is the most distorted to date of any other TRIMEB complex host molecule.

Table 5.11 presents the average values of selected conformational parameters for the TRIMEB molecules of the species in Table 5.10, presenting a comparison with those for the **TMBTUL** host molecule. Generally the average values for the various parameters agree closely amongst the various TRIMEB structures but differences exist in their respective ranges. The TRIMEB host of **TMBTUL** forms part of the group with smaller ranges for the various parameters and thus those with a 'rounder' host molecule which include, amongst others, the complexes of TRIMEB with (S)-naproxen,[151] (E)-ajoene[86] and (Z)-ajoene.[86] Its parameters are also, as expected, very close to those of the host of TRIMEB·clofibrate·H_2O.[138] An overlay of the hosts of the two structures is presented in Figure 5.15. The hosts are virtually superimposable with even the 'freely rotating' methyl groups of **TMBTUL**, which were not part of the initial phasing model, showing a high degree of overlap. **TMBTUL** forms part of the group of complexes for which five methylglucose tilt angles are positive and two are negative, the other complexes all having positive tilt angles. With the majority of the tilt angles for **TMBTUL** being positive, as well as the fact it has three C6-O6 bonds pointing towards the cyclodextrin cavity, the primary side of the host molecule is capped, thus preventing any inter-guest contacts. This 'capping' of the primary side of the TRIMEB molecule is consistent with most other TRIMEB complexes, an exception being the butamben-TRIMEB complex where all the C6-O6 bonds point away from the cavity allowing a significant portion of the guest to protrude from the primary side.[85]

Table 5.11 Average values of selected host conformational parameters [ranges in brackets] for the TRIMEB structures presented in Table 5.10

Guest[a]	r / Å	l / Å	a / °	d_{rms}[b] / Å	Tilt angle (τ_2)
H_2O	4.82(3.41-5.94)	4.38(4.09-4.68)	124(92-162)	0.60(-0.62, 1.09)	26(-25, 73)
methylcyclohexane	5.04(4.79-5.21)	4.39(4.24-4.50)	128(121-137)	0.23(-0.35, 0.32)	22(7, 52)
S-1,7-dioxaspiro(5,5)undecane	5.04(4.32-5.58)	4.42(4.26-4.61)	128(115-145)	0.37(-0.55, 0.42)	26(6, 57)
(L)-menthol	5.03(4.40-5.53)	4.41(4.26-4.55)	128(115-143)	0.36(-0.42, 0.51)	20(-9, 48)
p-iodophenol	4.99(4.63-5.35)	4.33(4.20-4.45)	127(118-139)	0.44(-0.57, 0.65)	20(-16, 43)
(R)-flurbiprofen	5.00(4.63-5.36)	4.39(4.27-4.53)	127(119-138)	0.46(-0.58, 0.66)	20(-13, 44)
(S)-flurbiprofen	5.01(4.70-5.23)	4.39(4.22-4.55)	127(119-138)	0.40(-0.50, 0.60)	19(-12, 43)
m-iodophenol	5.00(4.16-5.47)	4.41(4.15-4.79)	127(114-152)	0.42(-0.65, 0.59)	21(-14, 52)
4-biphenylacetic acid	4.97(4.60-5.37)	4.37(4.23-4.53)	127(118-139)	0.45(-0.56, 0.66)	20(-14, 44)
ethyl laurate	5.00(4.63-5.43)	4.38(4.16-4.60)	127(116-136)	0.42(-0.58, 0.54)	18(-14, 38)
(S)-ibuprofen	4.99(4.71-5.16)	4.38(4.22-4.51)	127(120-137)	0.39(-0.51, 0.57)	19(-14, 42)
(S)-naproxen	5.00(4.64-5.21)	4.38(4.25-4.51)	127(120-139)	0.39(-0.50, 0.58)	20(-14, 44)
butamben	4.98(4.40-5.31)	4.37(4.27-4.58)	127(119-141)	0.41(-0.50, 0.62)	18(-23, 41)
(E)-ajoene	4.98(4.67-5.20)	4.37(4.23-4.47)	128(119-138)	0.39(-0.65, 0.40)	25(10, 54)
$3H_2O$	4.99(4.67-5.49)	4.38(4.17-4.55)	127(112-136)	0.46(-0.80, 0.47)	26(-4, 67)
none	4.99(4.59-5.50)	4.38(4.12-4.61)	127(111-136)	0.41(-0.72, 0.35)	30(8, 72)
clofibric acid	5.02(4.49-5.45)	4.40(4.24-4.62)	128(116-141)	0.37(-0.54, 0.46)	18(-15, 47)
psoralen	5.01(4.30-5.60)	4.39(4.22-4.63)	128(113-144)	0.36(-0.41, 0.54)	24(7, 51)
(*Z*)-ajoene	5.00(4.73-5.17)	4.37(4.23-4.49)	128(121-137)	0.38(-0.51, 0.56)	24(12, 43)
clofibrate	5.01(4.71-5.20)	4.39(4.27-4.50)	128(121-138)	0.40(-0.52, 0.60)	19(-12, 45)
tulobuterol	5.01(4.64-5.23)	4.39(4.27-4.49)	127(121-138)	0.40(-0.38, 0.63)	21(-13, 51)

[a] Coordinates for *R*-5-ethyl-1,3,5-trimethylhydantoin-TRIMEB [MODHUI] do not appear in the CSD
[b] Ranges of the individual deviations from the mean O4 plane in brackets

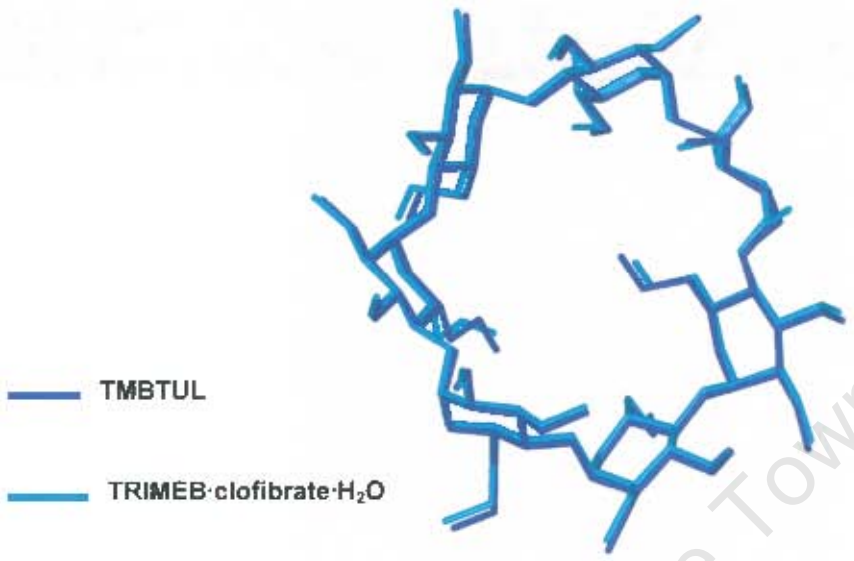

Figure 5.15 Overlay of the hosts of **TMBTUL** and TRIMEB·clofibrate·H_2O illustrating their close conformations.

Guest inclusion

Tulobuterol is one of the larger molecules that have been included within the TRIMEB cavity, other examples of comparably sized guests being (R)- and (S)-flurbiprofen, and (S)-ibuprofen. **TMBTUL** forms part of the group of TRIMEB complexes that crystallise with common unit cell parameters of a ~ 15, b ~ 21, c ~ 28Å, space group $P2_12_12_1$, whose members have a significant portion of the guest protruding from the secondary side, the exceptions being the guests *p*-iodophenol and *m*-iodophenol. These complexes, with the exception of *m*-iodophenol in which one of the methylglucose units deviates from the usual $^4C_1$ chair conformation, have a relatively small range for their O4-heptagon radii, when compared to host molecules with smaller guests such as (S)-1,7-dioxaspiro(5,5)undecane and psoralen that crystallise with unit cell parameters of a ~ 11, b ~ 26 and c ~ 29Å, space group $P2_12_12_1$, and have their respective guest molecules completely encapsulated in their host cavities. The exception is for the TRIMEB·methylcyclohexane complex, which also has a relatively small range for its O4-heptagon radii.

The chlorophenyl ring of the tulobuterol molecule in **TMBTUL** is located on the secondary face, as is found for other TRIMEB complex guests containing a chlorophenyl moiety, namely clofibric acid and clofibrate.[138]

Guest chirality

The chirality of the guest was found to be (R-) and the absence of any sign of disorder, e.g. as two superimposed enantiomers, indicates that there is a resolution of the drug, at least for the chosen crystal. The use of CDs for the resolution of racemic compounds has been reviewed.[154] Unlike the native CDs, the permethylated CDs have been found to be more suitable for chiral recognition due to the increased flexibility of the hosts, enabling them to change their conformation to accommodate a specific enantiomer. In the case of the **TMBTUL** complex the conformation of the host is thus probably more accommodating to the (R-)-enantiomer. Unfortunately, time constraints did not allow experiments to be carried out in order to ascertain whether this extended to the entire batch of crystals.

Crystal packing

The crystal packing of **TMBTUL** is consistent with what is found in TRIMEB complexes crystallising in the space group $P2_12_12_1$, i.e. head-to-tail packing of the host molecules down the *b*-axis. The partial inclusion results in the stacking not being as close as in complexes where the guest is almost completely encapsulated, e.g. TRIMEB·psoralen.[153] The computed PXRD trace corresponds, as expected, to the averaged calculated trace that was published by Caira for TRIMEB complexes with unit cell parameters a ~ 15, b ~ 21 and c ~ 28 Å, space group $P2_12_12_1$ [Figure 5.16] in a review of the phenomenon of isostructurality in cyclodextrins.[80]

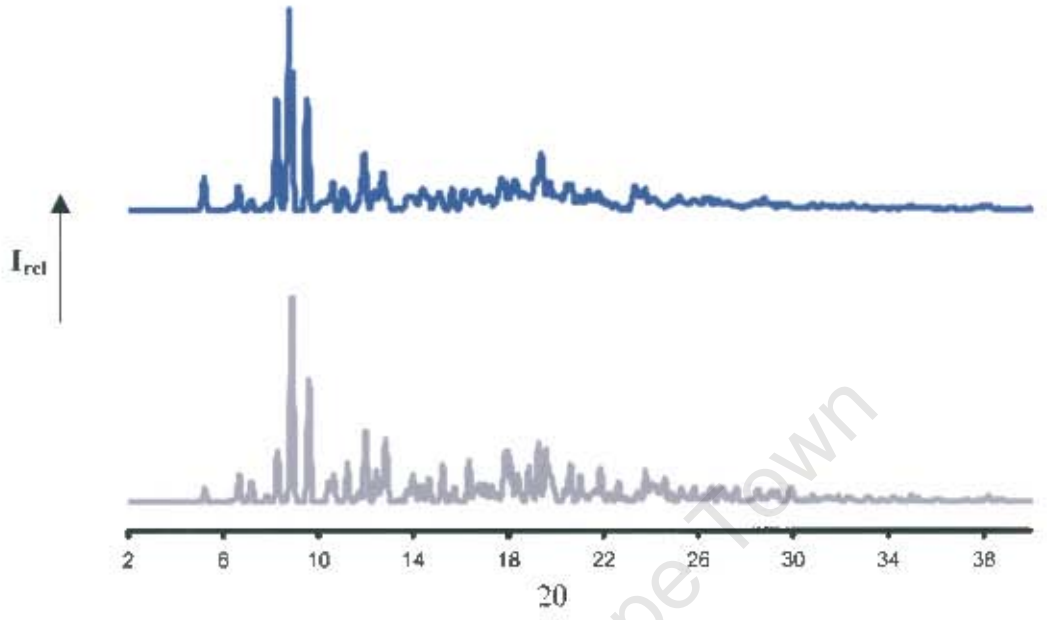

Figure 5.16 The computed trace for **TMBTUL** [bottom] and the trace for isostructural series 16 [TRIMEB complexes with similar unit cell parameters and the same space group as **TMBTUL**][80]

Conclusion

Tulobuterol has been successfully complexed with **DIMEB** and **TRIMEB**. These complexes have been characterised by thermal and X-ray diffraction techniques.

DMBTUL crystallises in a 1:1 host:guest ratio as established by microanalysis. TGA established that the complex is anhydrous and also confirmed the 1:1 host:guest ratio as evidenced by the dissociation of the guest at 150-250°C before the host decomposed at ~350°C. It crystallises in the orthorhombic space group $P2_12_12$ with a = 26.7561(4), b = 30.6918(5), c = 19.7482(2) Å, and Z = 4 molecules per unit cell. Attempts to solve the structure failed.

Microanalysis indicated that **TMBTUL** crystallises in 1:1 host:guest ratio, whilst TGA and DSC analyses respectively showed that it is anhydrous and melts at 155°C. Single crystal X-ray diffraction indicated the orthorhombic space group $P2_12_12_1$, with Z = 4

molecules per unit cell and a = 15.063(1), b = 21.290(1) and c = 27.671(1) Å. The tertiary butyl group of the tulobuterol guest molecule was found to insert into the TRIMEB cavity from the secondary side with the chlorophenyl group located on the outside. Host and guest are linked via one strong, classical (guest)O-H···O(host) hydrogen bond and a weaker (guest)N-H···O(host) hydrogen bond. The host distortion was not as pronounced as in some other TRIMEB complexes. **TMBTUL** was found to be isostructural with a known series of TRIMEB complexes.

Chapter 6 - Tulobuterol Salts

Salt Preparation

Three novel salts of tulobuterol were prepared. The salts formed with (R,R)-tartaric, succinic and benzoic acids will respectively be referred to as **TULTAR**, **TULSUC** and **TULBEN**.

(*R,R*)-tartaric acid and succinic acid have two ionisable functional groups. Therefore, **TULTAR** and **TULSUC** were prepared in a 2:1 tulobuterol:acid molar ratio. Saturated solutions of each mixture in pentanol were prepared at 60°C, with the resulting solutions being filtered and allowed to cool spontaneously to 25°C. Single crystals of good quality appeared over a period of a few days. Pentanol was the solvent of choice for producing such crystals of **TULTAR** and **TULSUC**, as these compounds proved to be too soluble in a wide variety of other organic solvents.

Benzoic acid has only one ionisable functional group and therefore **TULBEN** was prepared using a 1:1 tulobuterol:benzoic acid molar ratio. A saturated solution of the mixture in water was prepared at 25°C with the resulting solution being filtered and allowed to evaporate slowly to produce single crystals meeting the requirements for single crystal X-ray studies.

Microanalysis

The results of C, H, N microanalysis are presented in Table 6.1. The experimental results agree closely with the computed percentages. These confirm the purity of the salts and that they crystallised in the ratios in which were prepared.

Table 6.1 C, H, N microanalysis results [n=2] for **TULTAR**, **TULSUC** and **TULBEN**

Salt	Experimental			Calculated		
	%C	%H	%N	%C	%H	%N
TULTAR $[2(C_{12}H_{19}ClNO)^{+}\cdot(C_4H_4O_6)^{2-}]$	55.72	6.98	4.67	55.54	6.99	4.64
TULSUC $[(C_{12}H_{19}ClNO)^{+}\cdot 0.5(C_4H_4O_4)^{2-}]$	59.27	7.51	4.81	58.63	7.38	4.80
TULBEN $[(C_{12}H_{19}ClNO)^{+}\cdot(C_7H_5O_2)^{-}]$	65.50	6.85	4.02	65.27	6.91	4.00

Thermal Analyses

Hot Stage Microscopy

HSM of the salt crystals afforded a visual characterisation of their behaviour upon heating. Photographs of these analyses are presented in Figure 6.1. The analyses were done under silicone oil to detect the presence of possible included solvent as this would be indicated by bubble formation upon heating. The HSM analyses show that the salts are uniform in their thermal events. In each case, the absence of bubbling indicates the lack of included solvent. The analyses for all three salts also display a single thermal event, namely fusion, which occurs in the ranges 186-198, 157-160 and 155-157°C for **TULTAR**, **TULSUC** and **TULBEN** respectively.

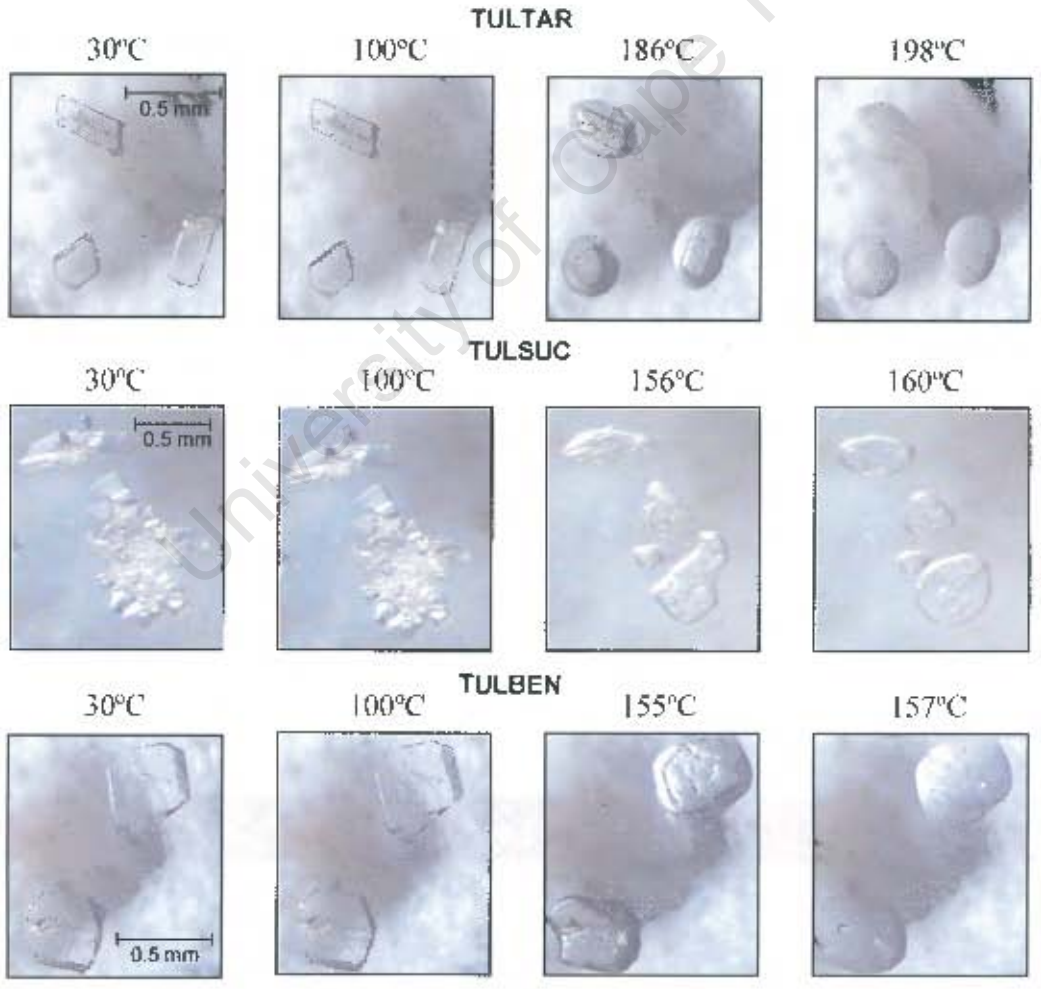

Figure 6.1 HSM photographs for **TULTAR**, **TULSUC** and **TULBEN**

Differential Scanning Calorimetry and Thermogravimetric Analysis

The DSC traces of the salts are presented in Figure 6.2. In all three cases the DSC traces show only fusion endotherms with extrapolated onset temperatures of 191, 163 and 147°C for **TULTAR**, **TULSUC** and **TULBEN** respectively. Grinding the crystals prior to DSC analysis did not affect the traces, thus showing that prior mechanical treatment did not induce phase transformations on heating. TGA traces [not shown] indicated negligible mass loss in all three cases, confirming the lack of included solvent. These results correlate well with the HSM findings and are summarised in Table 6.2.

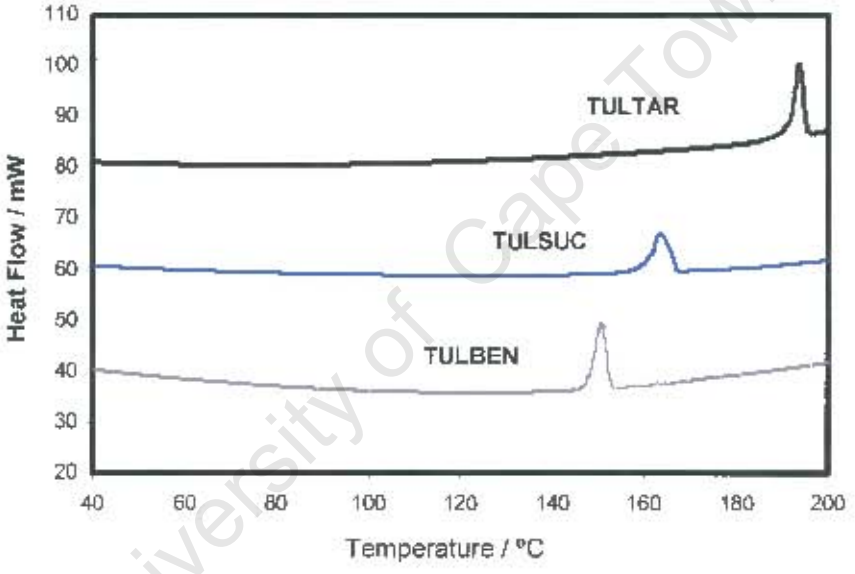

Figure 6.2 DSC traces for **TULTAR**, **TULSUC** and **TULBEN**

Table 6.2 Summary of the DSC events for **TULTAR**, **TULSUC** and **TULBEN**

Endotherm parameters		TULTAR	TULSUC	TULBEN
Temperature range investigated	(°C)	187-198	158-169	145-154
T_{on}	(°C)	191	163	147
Peak	(°C)	193	165	149

X-ray Crystallographic Analysis of TULTAR

Single Crystal X-ray Diffraction

Data-collection and space group determination

Diffraction intensity data for the salt formed between tulobuterol and (R,R)-tartaric acid were collected on a Nonius Kappa CCD diffractometer at 173K. A suitable crystal was mounted under paratone oil to glue the crystal to the fibre on freezing. The Laue symmetry [$\bar{1}$] of **TULTAR** indicated that it belongs to the triclinic crystal system for which the only two possible space groups are P1 and P$\bar{1}$. Since a chiral tartaric acid was used it followed that the chiral space group P1 was the only choice. Intensity statistics provided by XPREP[109] corroborated the choice of a chiral space group with $|E^2-1|$ = 0.777, which is close to the expected value of 0.736 for non-centrosymmetric structures.

Structure solution and refinement

SHELXS-97[110] was used to solve the structure of **TULTAR** by direct methods. From the unit cell volume it was deduced that the asymmetric unit comprises four tulobuterol cations and two tartrate anions. The E-map revealed the positions of all the non-hydrogen atoms and these were placed and refined in SHELXL-97[112] with isotropic temperature factors. Anisotropic refinement followed subject to satisfactory behaviour of isotropic thermal parameters. Only three amino hydrogen atoms of the eight in the asymmetric unit appeared in the difference Fourier map, but the equalisation of the terminal C-O bond lengths on both tartrate anions was proof that the carboxylic acid groups had lost their hydrogen atoms and thus that a salt had formed. Two amino hydrogen atoms per tulobuterol cation, with tetrahedral geometry, were thus placed. The hydrogen atoms of the freely rotating hydroxyl [only one hydroxyl hydrogen atom found in the difference Fourier map] and methyl groups of the tulobuterol cations were placed in fixed positions and refined using a rotating refinement strategy. The rest of the hydrogen atoms for the **TULTAR** structure were placed in fixed geometric positions using a riding model. All hydrogen atoms were refined with thermal parameters 1.2 times those of their parent atoms. For methyl hydrogen atoms the factor was 1.5. The crystal data and refinement parameters are presented in Table 6.3.

Table 6.3 Crystal and refinement parameters for **TULTAR**

Parameter	
Formula unit	$2(C_{12}H_{18}ClNO)^{+}\cdot C_4H_4O_6^{2-}$
Formula weight / g mol^{-1}	605.5
Crystal system	Triclinic
Space group	P1
a / Å	9.665(2)
b / Å	10.685(2)
c / Å	16.923(3)
α / °	94.06(3)
β / °	93.80(3)
γ / °	115.46(3)
Volume / Å^3	1564.9(5)
Z	2
Density$_{calc}$ / g cm^{-3}	1.285
μ(MoKα) / mm^{-1}	0.256
F(000)	644
Crystal size / mm^3	0.50x0.30x0.10
Temperature / K	203(2)
Range scanned θ / °	$4 \leq \theta \leq 28$
Index ranges	h : -12, 12 k : -14, 14 l : -22, 22
ϕ scan angle per frame / °	1.0
ϕ scan range / °, no. of frames	363, 363
ω scan angle / °	1.0
ω scan ranges / °, no. of frames	36, 36; 33, 33; 32, 32; 116, 116; 116, 116; 111, 111; 76, 76; 53, 53; 75, 75
Dx / mm	35
No. of measured reflections	46920
No. of unique reflections	14611
No. of reflections with $I > 2\sigma(I)$	12622
No. of least-squares parameters	741
R_{int}, R_σ	0.0504, 0.0439
S	1.056
R_1 ($F_o > 4\sigma(F_o)$)	0.0636
No. of reflections omitted	57
wR_2 (all data)	0.1965
Weighting scheme parameters	a = 0.1286, b = 0.61
$(\Delta/\sigma)_{mean}$	< 0.001
Δρ excursions / e Å^{-3}	0.63, -0.72

Description of the structure

TULTAR crystallises in the triclinic space group P1 in a 2:1 tulobuterol cation:tartrate anion ratio with Z = 2 formula units per unit cell. Thus the asymmetric unit, as illustrated by the ORTEP[120] diagram in Figure 6.3(a), consists of four tulobuterol cations and two tartrate anions.

(a)

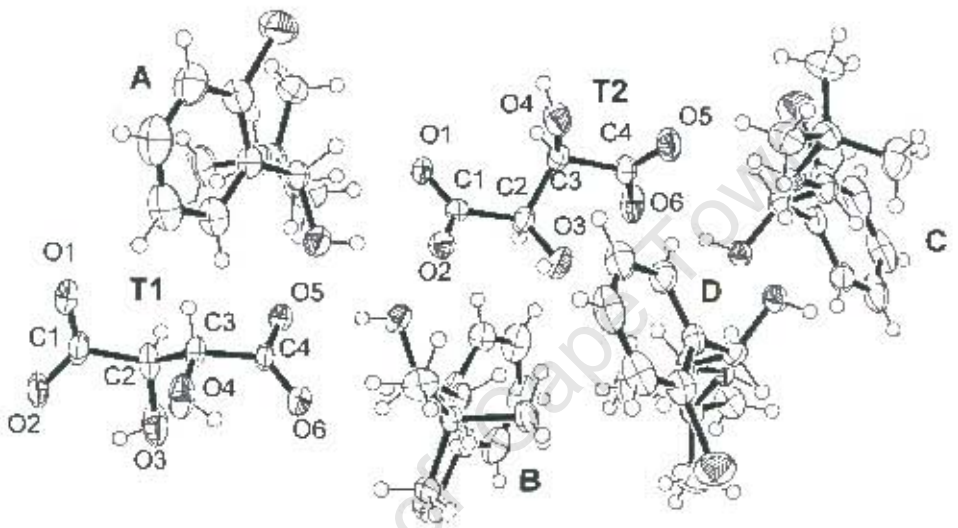

(b)

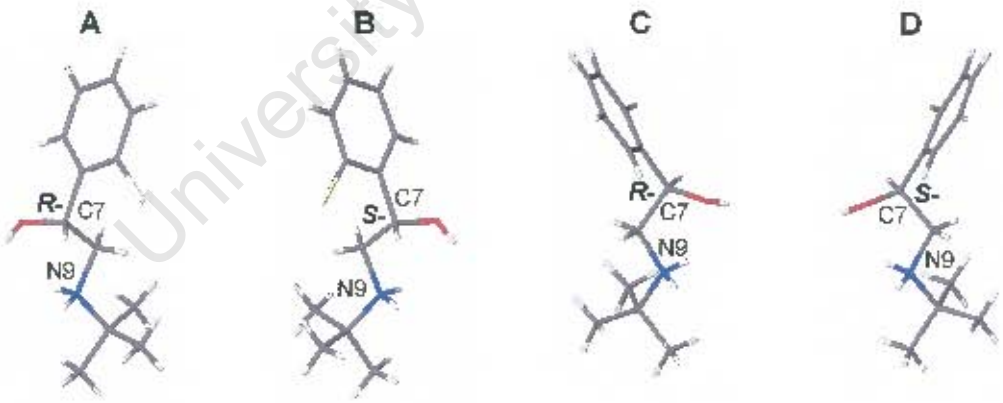

Figure 6.3 (a) ORTEP diagram of the asymmetric unit of **TULTAR**. Tulobuterol cations are labelled **A**, **B**, **C** and **D** but for clarity their individual atoms are not numbered. The tartrate anions are labelled **T1** and **T2** with their individual atom numbering shown. Thermal ellipsoids are drawn at the 50% probability level. Hydrogen atoms are drawn as spheres with arbitrary radii.

(b) The individual tulobuterol cations with the configuration at the C7 atoms and protonation of the N9 atoms shown.

Figure 6.3(b) presents the individual tulobuterol cations, with their chiralities, and shows that the nitrogen atoms are protonated when the salt between tulobuterol and (R,R)-tartaric acid is formed.

Hydrogen bonding and C-H···π-ring interactions

A PLATON[121] geometrical structure analysis revealed several N-H···O, O-H···O, C-H···O and C-H···Cl hydrogen bonds, which are presented in Table 6.4. Figure 6.4 illustrates the strongest of these, the N-H···O and the O-H···O hydrogen bonds. All the ions in the asymmetric unit are involved in this type of hydrogen bonding in an extensive and intricate manner, which will be described next.

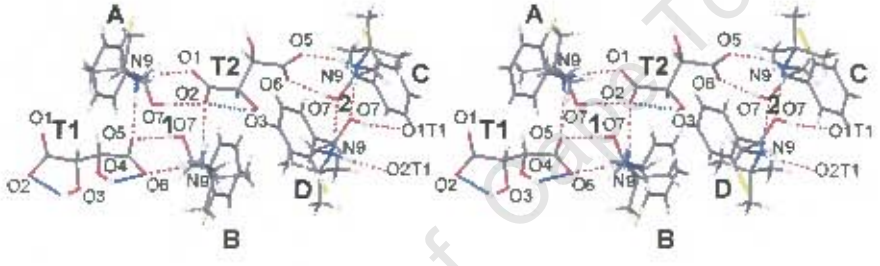

Figure 6.4 Stereo view of the intermolecular hydrogen bonds [O-H···O and N-H···O in red] and intramolecular bonds [O-H···O in blue] for **TULTAR**. Only the labelling of the donor and acceptor atoms is shown.

There are two hydrogen bonding motifs [**1** and **2** in Figure 6.4] that connect the ions in the asymmetric unit. In motif **1**, cation **A** is connected to anion **T1** by the N9A-H9A2···O5T1 hydrogen bond, whilst cation **B** is connected to anion **T1** by the O7B-H7B1···O5T1 and N9B-H9B1···O6T1 hydrogen bonds. Cation **A** is also connected to anion **T2** by the N9A-H9A1···O1T2 and O7A-H7A1···O2T2 hydrogen bonds, whilst cation **B** is connected to anion **T2** by the N9B-H9B2···O2T2 hydrogen bond. In motif **2**, cation **C** is linked to anion **T2** by the O7C-H7C1···O6T2 and N9C-H9C1···O5T2 hydrogen bonds, whilst cation **D** is linked to anion **T1** of the adjacent unit cell by the O7D-H7D1···O1T1 [x, y, 1+z] and N9D-H9D1···O2T1 [x, y, 1+z] hydrogen bonds. The cations of motif **2** are linked to each other via the N9C-H9C2···O7D and N9D-

H9D2···O7C hydrogen bonds, unlike the situation in motif 1 where the cations are not linked via any hydrogen bonds.

Table 6.4 Hydrogen bonds for **TULTAR**

Hydrogen bond	H···A / Å	D···A / Å	D-H···A / °	Symmetry Code
O-H···O, N-H···O				
N9A-H9A2···O5T1	1.93(4)	2.830(4)	177(4)	x, y, z
N9A-H9A1···O1T2	1.83(3)	2.711(3)	167(4)	x, y, z
O7A-H7A1···O2T2	1.90(3)	2.712(3)	168(2)	x, y, z
O7B-H7B1···O5T1	1.88(4)	2.701(4)	176(2)	x, y, z
N9B-H9B1···O6T1	1.83(3)	2.715(3)	168(2)	x, y, z
N9B-H9B2···O2T2	1.98(3)	2.881(4)	176(4)	x, y, z
O7C-H7C1···O6T2	1.76(3)	2.563(3)	168(2)	x, y, z
N9C-H9C1···O5T2	1.83(2)	2.701(4)	161(3)	x, y, z
N9C-H9C2···O7D	1.94(2)	2.838(4)	173(4)	x, y, z
O7D-H7D1···O1T1	1.76(4)	2.562(4)	167(4)	x, y, 1+z
N9D-H9D1···O2T1	1.79(3)	2.676(4)	167(3)	x, y, 1+z
N9D-H9D2···O7C	1.96(2)	2.861(4)	173(4)	x, y, z
O3T1-H4T1···O2T1 (intramolecular)	2.10(2)	2.587(4)	118(4)	x, y, z
O4T1-H5T1···O6T1 (intramolecular)	2.15(3)	2.638(4)	118(3)	x, y, z
O3T2-H4T2···O2T2 (intramolecular)	2.16(2)	2.606(4)	114(4)	x, y, z
C-H···O				
C4A-H4A···O3T1	2.37(4)	3.287(6)	170(2)	1-x, 1+y, z
C4B-H4B···O4T2	2.45(2)	3.372(5)	168(2)	-1+x, -1+y, z
C8C-H8C2···O1T1	2.57(2)	3.391(6)	142(4)	x, y, 1+z
C8D-H8D2···O3T2	2.49(4)	3.423(5)	163(3)	x, y, z
C6A-H6A···O7A (intramolecular)	2.39(3)	2.730(5)	102(3)	x, y, z
C6B-H6B···O7B (intramolecular)	2.40(2)	2.735(5)	101(4)	x, y, z
C2T1-H2T1···O5T1 (intramolecular)	2.59(4)	2.926(4)	100(3)	x, y, z
C-H···Cl				
C7A-H7A···Cl2A (intramolecular)	2.78(4)	3.123(4)	101(2)	x, y, z
C7B-H7B···Cl2B (intramolecular)	2.77(2)	3.110(4)	101(4)	x, y, z
C7C-H7C···Cl2C (intramolecular)	2.62(4)	3.124(4)	112(3)	x, y, z
C7D-H7D···Cl2D (intramolecular)	2.62(2)	3.114(3)	111(3)	x, y, z

Both motifs consist of six intermolecular hydrogen bonds that are related by a pseudo-centre of inversion [the motif labels **1,2** in Figure 6.4 are placed at these pseudo-centres of inversion]. The three O-H···O intramolecular hydrogen bonds that are listed in Table 6.4 and illustrated in Figure 6.4 [indicated in blue], occur only in the tartrate anions.

There are seven C-H···O hydrogen bonds listed in Table 6.4, of which four are intermolecular and three intramolecular. Three of the intermolecular C-H···O hydrogen bonds link asymmetric units of neighbouring unit cells, whilst one is within the same asymmetric unit. The C4A-H4A···O3T1 and C4B-H4B···O4T2 hydrogen bonds link asymmetric units diagonally along the *xy*-plane whilst the C8C-H8C2···O1T1 hydrogen bond links asymmetric units along the *c*-axis. The C8D-H8D2···O3T2 hydrogen bond links the **D** cation and the **T2** anion within the same asymmetric unit. The C-H···O and C-H···Cl hydrogen bonds contribute to stabilisation of the ions in which they occur.

PLATON[121] was used to calculate five unique C-H···π-ring interactions for the **TULTAR** structure and these are presented in Table 6.5. 'Cg' refers to the centre of gravity of the aromatic ring of the tulobuterol cation. The **A** and **C** cations of adjacent asymmetric units along the *c*-axis are connected by the C12A-H16A···CgC and C12C-H16C···CgA interactions, whilst the **B** and **D** cations are connected by the C12B-H15B···CgD, C12B-H16B···CgD and C12D-H16D···CgB interactions along this direction. Figure 6.5 illustrates the C-H···π-ring interactions for the **TULTAR** structure. The π···π-ring distances were not considered as representing significant interactions as they were all greater than 5Å.

Table 6.5 C-H···π-ring interactions for **TULTAR**

Interaction	H···Cg / Å	C···Cg / Å	C-H···Cg / °	Symmetry code applied to second unit
C12A-H16A···CgC	2.91(2)	3.563(4)	126(4)	x, y, -1+z
C12C-H16C···CgA	3.24(2)	3.832(5)	122(2)	x, y, 1+z
C12B-H15B···CgD	3.09(3)	3.620(4)	116(3)	x, y, z
C12B-H16B···CgD	3.26(4)	3.620(4)	105(3)	x, y, z
C12D-H16D···CgB	2.95(3)	3.614(4)	127(4)	x, y, z

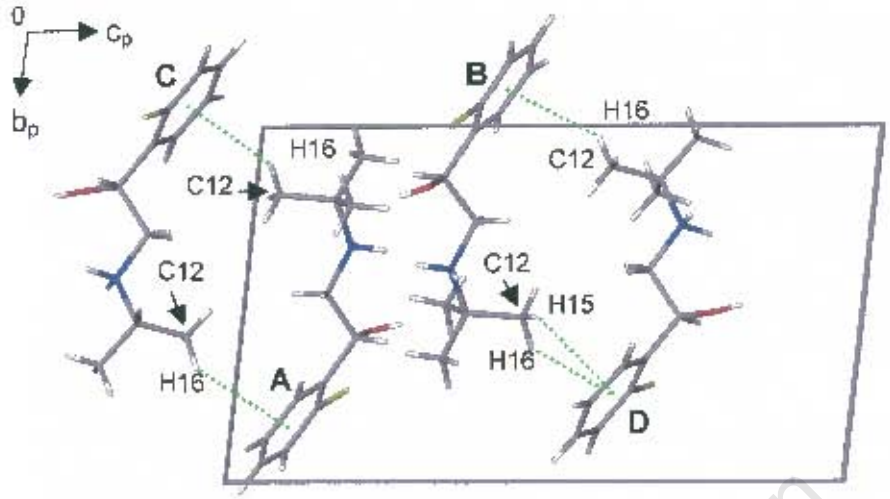

Figure 6.5 C-H···π-ring interactions for the **TULTAR** structure with the tartrate anions omitted for clarity. View is down the *a*-axis.

Conformations and configurations of the tulobuterol cations

Figure 6.6, a repeat of Figure 3.10 for the reader's convenience, illustrates the definition of the principal torsion angles for tulobuterol. For more background to these principal torsion angles the reader is referred to **Chapter 3**. Table 6.6 lists the principal torsion angles η_1, η_2, η_3, η_4 and η_5 for the **A**, **B**, **C** and **D** cations compared to the corresponding parameters for the **Form 1** and **Form 2** molecules.

The magnitudes of the η_1 and η_2 torsion angles for the **TULTAR** cations compare well with those for the **Form 1** and **Form 2** molecules, except those for the **C** and **D** cations which are respectively larger and smaller for the η_1 and η_2 torsion angles. Table 6.6 indicates that for both cations **C** and **D** the C7-O7 bond changes from antiperiplanar to anticlinal with respect to the C2-Cl2 bond, whilst the C2-C1 bond changes from synclinal to anticlinal with respect to the C7-C8 bond. The angles do, however, still generally show that the aromatic ring plane is nearly orthogonal to the tulobuterol backbone with the Cl2 and O7 atoms being *trans*.

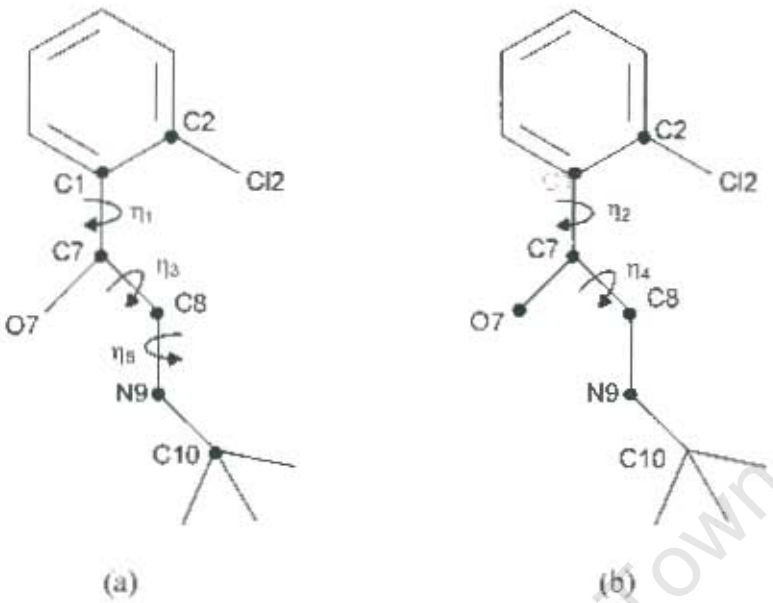

Figure 6.6 Schematic diagram of the principal torsion angles (a) η_1, η_3, η_5 (b) η_2 and η_4 for the tulobuterol backbone.

Table 6.6 Principal torsion angles for the **TULTAR** cations and polymorph molecules

Compound	η_1	η_2	η_3	η_4	η_5
TULTAR					
Cation **A** [(R-)]	-81.1(4)	158.3(3)	-168.8(3)	-48.8(4)	-162.6(3)
Cation **B** [(S-)]	81.3(4)	-159.6(3)	170.5(3)	50.6(4)	156.7(3)
Cation **B** [(R-)]	-100.2(4)	137.6(3)	-173.7(3)	-51.2(4)	-155.1(3)
Cation **D** [(S-)]	99.5(4)	-139.6(3)	174.4(3)	53.9(4)	154.9(3)
Form 1					
Molecule **A** [(S-)]	87.0(2)	-153.8(2)	-175.7(2)	62.2(2)	-170.5(2)
Molecule **B** [(R-)]	-81.4(2)	160.2(2)	-179.6(2)	-58.2(2)	173.7(2)
Molecule **C** [(R-)]	-77.8(2)	163.2(2)	178.1(2)	-60.1(2)	169.4(2)
Form 2					
Molecule **A** [(S-)]	84.0(2)	-157.2(2)	-174.0(2)	64.3(2)	-166.0(2)
Molecule **B** [(R-)]	-83.9(2)	157.1(2)	-175.2(2)	-54.1(2)	167.2(2)
Molecule **C** [(R-)]	-81.5(2)	159.9(2)	178.9(1)	-59.7(2)	172.6(2)

The magnitudes of the η_3 torsion angle for the **TULTAR** cations are only slightly smaller than those for the **Form 1** and **Form 2** molecules, indicating that the backbone remains in an 'extended' conformation in **TULTAR** with the aromatic ring *trans* to the N9 atom. The small difference in the η_3 torsion angle magnitudes means that there is a small difference in the magnitude for the η_4 torsion angle as well when compared to the corresponding parameters for the **Form 1** and **Form 2** molecules. It indicates that the O7 and N9 atoms are also *gauche* for the **TULTAR** cations.

The magnitudes of the η_5 torsion angle for the **TULTAR** cations are significantly smaller than those for the **Form 1** and **Form 2** molecules indicating that the backbone tail is more 'bent', with the tertiary butyl group 'swung' away from the O7 atom side of the backbone for all the cations.

The torsion angles of the cations show that the latter are generally close in conformation to those of the **Form 1** and **Form 2** molecules, except for the differences mentioned above. The signs of the torsion angles also reflect the pseudo centres of symmetry relating the **A** and **B**, and **C** and **D** cations respectively.

There is an equal number of cations with opposite configuration at the C7 atom [two (S-) and two (R-)] indicating that tulobuterol was not resolved on salt formation with (R,R)-tartaric acid.

Crystal packing

Figure 6.7 presents the crystal packing of the **TULTAR** structure down the *a*-axis. It shows that adjacent motifs share common anions and therefore infinite chains of N-H···O and O-H···O hydrogen bonded ions are formed along the *c*-axis. These chains are stacked parallel to the *b*-axis and connected diagonally along the *xy*-plane by the intermolecular C4-H4A···O3T1 and C4B-H4B···O4T2 hydrogen bonds [not shown].

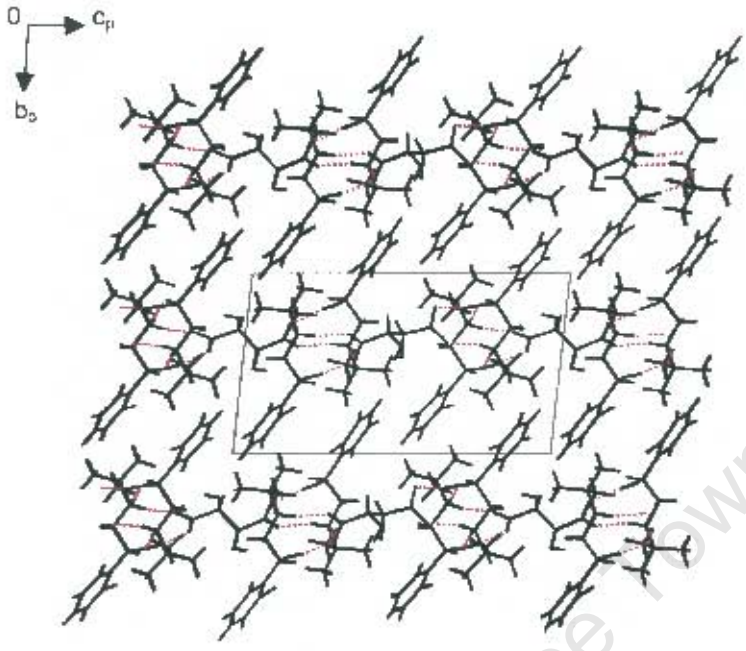

Figure 6.7 Crystal packing diagram of **TULTAR** down the *a*-axis. The intermolecular hydrogen bonding is shown in red.

Powder X-ray Diffraction

The computed and experimental PXRD patterns for **TULTAR** are presented in Figure 6.8. These patterns match closely, indicating that no phase transformation took place on grinding of **TULTAR**. The slight shift of the experimental trace to lower 2θ values when compared to the computed trace is attributed to the difference in temperature at which the information for the respective traces was obtained. The close match of the experimental and computed patterns indicates that the latter can serve as a reference for **TULTAR** identification.

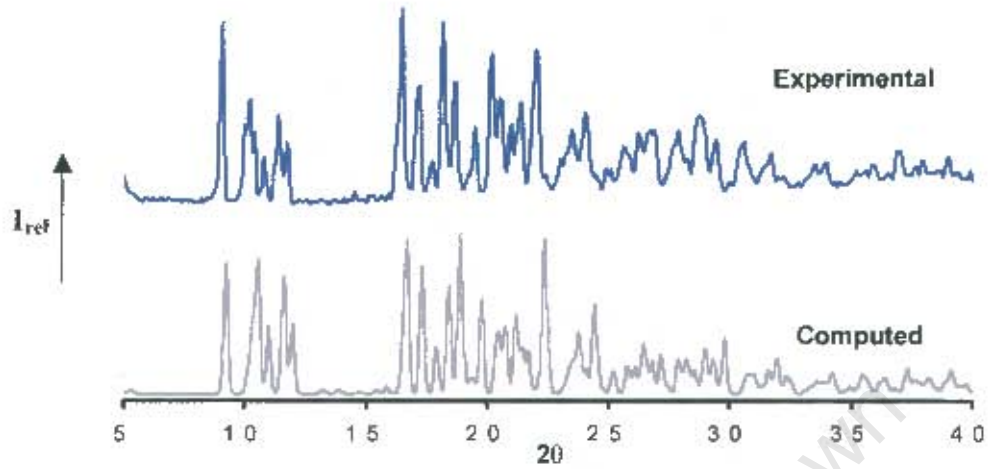

Figure 6.8 Computed [203K] and experimental [295K] PXRD patterns for **TULTAR**

X-ray Crystallographic Analysis of TULSUC

Single Crystal X-ray Diffraction

Data-collection and space group determination

Diffraction intensity data for the salt formed between tulobuterol and succinic acid were collected on a Nonius Kappa CCD diffractometer at 203K. A suitable crystal was mounted under paratone oil to glue the crystal to the glass fibre on freezing. Inspection of the intensity-weighted reciprocal lattice revealed Laue *2/m* symmetry, indicating the monoclinic system. XPREP[109] indicated the space group $P2_1/n$ [standard setting $P2_1/c$, space group No.14, unique axis *b*] as the only possible space group. The reflection conditions were investigated with LAYER[117] and found to be h0l: h + l = 2n; 0k0: k = 2n which uniquely identify this space group.

Structure solution and refinement

Direct methods in SHELXS-97[110] were used to solve the **TULSUC** structure. The asymmetric unit comprises one tulobuterol cation and half a succinate anion. The atoms identified in the E-map were refined in SHELXL-97[112] with isotropic temperature factors. This was followed by anisotropic refinement provided that isotropic temperature factors behaved satisfactorily. Hydrogen atoms were placed in fixed geometric positions and were, unless stated otherwise, refined using a riding model with isotropic thermal parameters 1.2 times those of their parent atoms. The two amino hydrogen atoms as well as the hydroxyl hydrogen atom were located in the difference Fourier map. The location of two amino hydrogen atoms, together with the near equality of the two C-O bonds at the terminus of the succinate anion, was proof for salt formation and the site of protonation on the tulobuterol molecule. Even though the amino hydrogen atoms were located in the difference Fourier map they were placed in idealised positions with tetrahedral geometry [AFIX 23]. The hydroxyl and methyl hydrogen atoms were placed using a rotating refinement strategy [AFIX 147 and AFIX 137 respectively] with the methyl hydrogen atoms refined with isotropic temperature factors 1.5 times those of their parent atoms. The crystal data and refinement parameters are presented in Table 6.7.

Table 6.7 Crystal and refinement parameters for **TULSUC**

Parameter	
Formula unit	$C_{12}H_{19}ClNO^{+}\cdot 0.5(C_4H_4O_4)^{2-}$
Formula weight / g mol^{-1}	286.7
Crystal system	Monoclinic
Space group	$P2_1/n$
a / Å	10.377(2)
b / Å	10.207(2)
c / Å	14.855(3)
α / °	90
β / °	106.23(3)
γ / °	90
Volume / Å^3	1510.8(5)
Z	4
Density$_{calc}$ / g cm^{-3}	1.261
μ(MoKα) / mm^{-1}	0.257
F(000)	612
Crystal size / mm^3	0.30x0.40x0.40
Temperature / K	203
Range scanned θ / °	$1 \leq \theta \leq 28$
Index ranges	h ; -13, 13 k ; -13, 13 l ; -13, 19
ϕ scan angle / °	1.0
ϕ scan range / °, no. of frames	10, 10 ; 10, 10
ω scan angle / °	1.0
ω scan ranges / °, no. of frames	245, 245 ; 94, 94 ; 46, 46
Dx / mm	33
No. of measured reflections	18716
No. of unique reflections	3581
No. of reflections with $I > 2\sigma(I)$	3136
No. of least-squares parameters	176
No. of reflections omitted	17
R_{int}, R_σ	0.0101, 0.0204
S	1.041
R_1 ($F_o > 4\sigma(F_o)$)	0.0373
wR_2 (all reflections)	0.1047
Weighting scheme parameters	a = 0.0489, b = 0.54
$(\Delta/\sigma)_{mean}$	< 0.001
Δρ excursions / e Å^{-3}	0.31, -0.43

Description of the structure

TULSUC crystallises in a 2:1 tulobuterol cation:succinate anion ratio in the monoclinic space group $P2_1/n$ with $Z = 4$ formula units per unit cell. The tulobuterol cations were located in general positions and the succinate anions on the centres of inversions at Wyckoff positions (0, 0, 0) and (½, ½, ½). An ORTEP[120] diagram of the asymmetric unit [which is also the empirical formula unit] consisting of one tulobuterol cation and half a succinate anion is presented in Figure 6.9(a), whilst Figure 6.9(b) illustrates one of the centres of inversion on which the succinate anions are located.

(a)

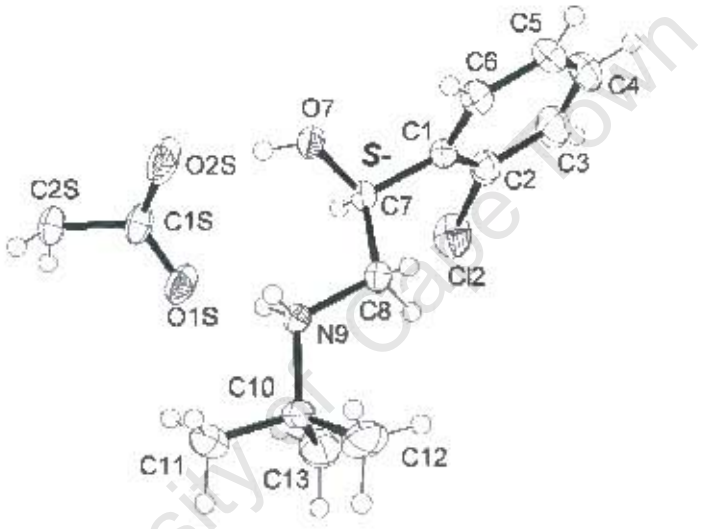

(b)

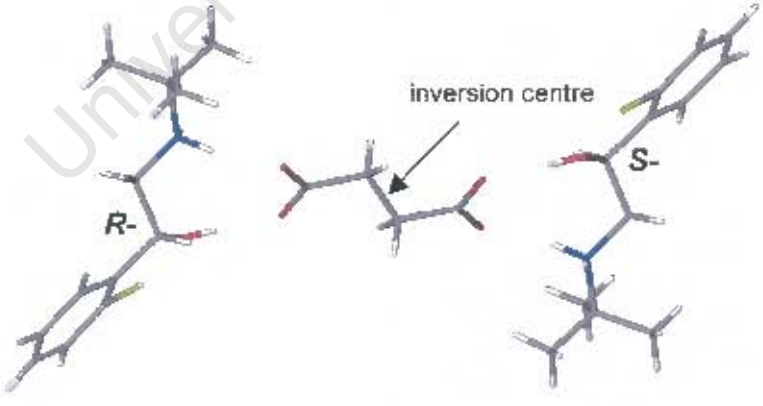

Figure 6.9 (a) ORTEP diagram of the asymmetric and formula unit of **TULSUC**. The succinate atoms are labelled with the suffix 'S'. Thermal ellipsoids are drawn at the 50% probability level. Hydrogen atoms are drawn as spheres with arbitrary radii.

(b) Diagram illustrating one of the inversion centres on which a succinate anion is located.

Hydrogen bonding and C-H···π-ring interactions

PLATON[121] revealed several O-H···O, N-H···O and C-H···Cl hydrogen bonding interactions which are presented in Table 6.8.

Table 6.8 Hydrogen-bonding interactions for **TULSUC**

D-H···A	H···A / Å	D···A / Å	D-H···A / °	Symmetry Code
O7-H7A···O2S	1.70(3)	2.525(1)	175(3)	x, y, z
N9-H9A···O1S	1.81(4)	2.703(1)	165(4)	x, y, z
N9-H9B···O7	1.97(2)	2.871(1)	171(3)	1-x, -y, 1-z
C7-H7···Cl2 (intramolecular)	2.66(3)	3.085(1)	106(3)	x, y, z

There are three unique intermolecular hydrogen bonds all of which are inverted through a crystallographic centre of symmetry to form the basic hydrogen-bonding motif consisting of six hydrogen bonds, as illustrated in stereo in Figure 6.10. The O7-H7A···O2S and N9-H9A···O1S hydrogen bonds connect the succinate and tulobuterol ions within the same formula unit whilst the third hydrogen bond, N9-H9B···O7, connects tulobuterol molecules of different formula units. C7-H7···Cl2 is the only intramolecular hydrogen bond and contributes to the stabilisation of the cation conformation. No other types of hydrogen bonds were observed for this structure.

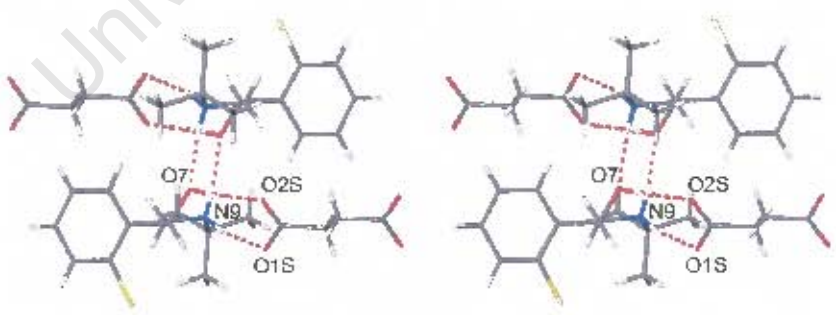

Figure 6.10 Stereo view of the basic hydrogen bonding motif in **TULSUC**

Two C-H···π-ring interactions were indicated by PLATON[121] and these are presented in Table 6.9.

Table 6.9 C-H···π-ring interactions for **TULSUC**

Interaction	H···Cg / Å	C···Cg / Å	C-H···Cg / °	Symmetry code
C13-H18···Cg*	3.32(3)	3.769(2)	110(3)	1/2-x, 1/2+y, 1/2-z
C13-H19···Cg	3.32(3)	3.769(2)	110(3)	1/2-x, 1/2+y, 1/2-z

* Cg = Centre of gravity of the aromatic ring of the tulobuterol cation

The identical symmetry codes for the two interactions indicate that the H18 and H19 atoms interact with the same π-ring as is illustrated in Figure 6.11. The interactions are between cations that are related by the screw axis parallel to the *b*-axis.

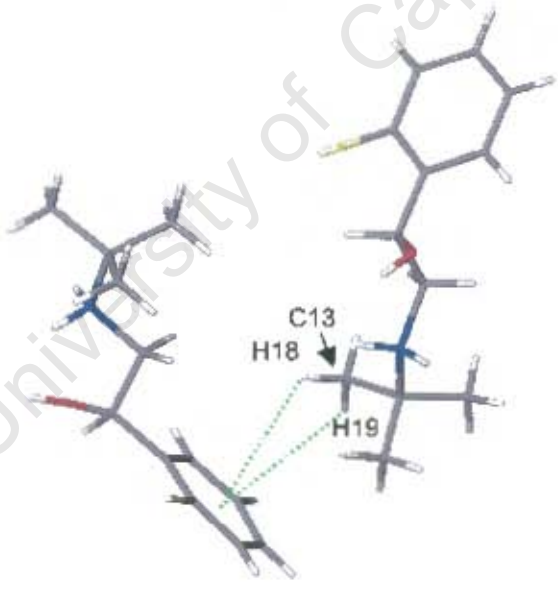

Figure 6.11 C-H···π-ring interactions for the **TULSUC** structure. For clarity only the cations are shown.

The observed π···π-ring distances are considered to be too long [>5Å] to qualify as significant interactions of this type.

Conformation and configuration of the tulobuterol cation

The principal torsion angles η_1, η_2, η_3, η_4 and η_5 for the tulobuterol cation in **TULSUC** are compared with those of the tulobuterol molecules in **Form 1** and **Form 2** in Table 6.10. The reader is referred to Figure 6.6 for a graphical illustration of the torsion angle definitions. Torsion angles in Table 6.10 are discussed in terms of their magnitudes only.

Table 6.10 Principal torsion angles for the **TULSUC** cation and polymorph molecules

Compound	η_1	η_2	η_3	η_4	η_5
TULSUC [(S-)]	91.0(2)	-147.0(1)	-177.2(1)	56.0(1)	157.6(1)
Form 1					
Molecule **A** [(R-)]	87.0(2)	-153.8(2)	-175.7(2)	62.2(2)	-170.5(2)
Molecule **B** [(R-)]	-81.4(2)	160.2(2)	-179.6(2)	-58.2(2)	173.7(2)
Molecule **C** [(R-)]	-77.8(2)	163.2(2)	178.1(2)	-60.1(2)	169.4(2)
Form 2					
Molecule **A** [(S-)]	84.0(2)	-157.2(2)	-174.0(2)	64.3(2)	-166.0(2)
Molecule **B** [(R-)]	-83.9(2)	157.1(2)	-175.2(2)	-54.1(2)	167.2(2)
Molecule **C** [(R-)]	-81.5(2)	159.9(2)	178.9(1)	-59.7(2)	172.6(2)

The η_1 torsion angle for the **TULSUC** cation is slightly larger than those for the **Form 1** and **Form 2** molecules, only just moving into the anticlinal region from synclinal. On the other hand, the η_2 torsion angle is slightly smaller indicating that the O7 and Cl2 atoms for **TULSUC** are closer together and anticlinal with respect to each other. The η_1 and η_2 torsion angles respectively indicate that the aromatic ring plane is nearly orthogonal to the backbone of the tulobuterol cation and that the Cl2 and O7 atoms are *trans*, as is the case for the **Form 1** and **Form 2** molecules.

The η_3 torsion angle is within the range of those for **Form 1** and **Form 2**, also being close to 180° and thus indicating that the backbone is in the 'extended' conformation with the aromatic ring *trans* to the N9 atom. The η_4 torsion angle for the **TULSUC** cation is also similar to those for the **Form 1** and **Form 2** molecules with the O7 atom *gauche* to the N9 atom.

As in the case of the **TULTAR** cations [previous section], the η_5 torsion angle for the **TULSUC** cation is significantly smaller than those for the **Form 1** and **Form 2** molecules, indicating that the backbone tail is slightly more 'bent' and 'swung' away from the O7 side of the tulobuterol backbone. All the torsion angles show that the **TULSUC** cation conformation is similar to those for the **Form 1** and **Form 2** molecules, except for the slight deviations mentioned above.

For the chosen asymmetric unit in the **TULSUC** structure the configuration at the C7 atom of the tulobuterol cation is (S-), but the centrosymmetric space group $P2_1/n$ requires the presence of a counterpart in the crystal with the opposite configuration. Thus tulobuterol was not resolved on salt formation with succinic acid.

Crystal packing

Stereo views of the crystal packing in the **TULSUC** structure are presented in Figures 6.12(a) and (b), which include the hydrogen bonding and C-H···π-ring interactions to present a clearer picture of closely associated ions. The view down the *a*-axis [Figure 6.12(a)] clearly shows that adjacent motifs [as in the case for the adjacent **TULTAR** hydrogen bond motifs] share a common anion thus forming an infinite chain of N-H···O and O-H···O hydrogen bonded ions, which in this case is along the *b*-axis. The view down the *b*-axis [Figure 6.12(b)] shows that the axes of these chains coincide with the centre and corners of the unit cell and that the C13-H18···Cg and C13-H19···Cg interactions [indicated in green] link these chains diagonally along the *xz*-plane.

Powder X-ray Diffraction

The computed and experimental PXRD patterns for **TULSUC** presented in Figure 6.13 show a close match [barring the slight mismatch of relative intensities due to preferred orientation effects] indicating that **TULSUC** did not transform on grinding and that the computed pattern can serve as a reference for **TULSUC** identification. The slight shift of the experimental trace relative to the computed trace to lower 2θ values is due to the different temperatures at which the information was obtained for the respective traces.

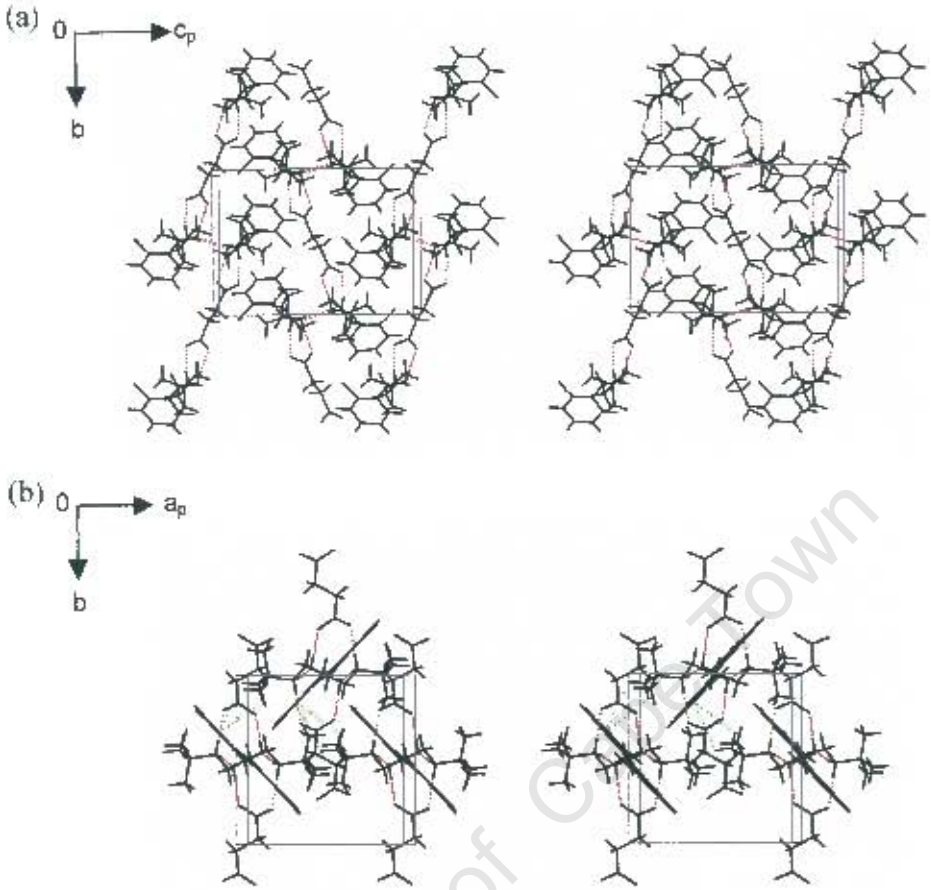

Figure 6.12 Stereo packing diagrams of **TULSUC** down the (a) *a*-axis and (b) *c*-axis. Hydrogen bond and C-H···π-ring interactions are shown in red and green respectively.

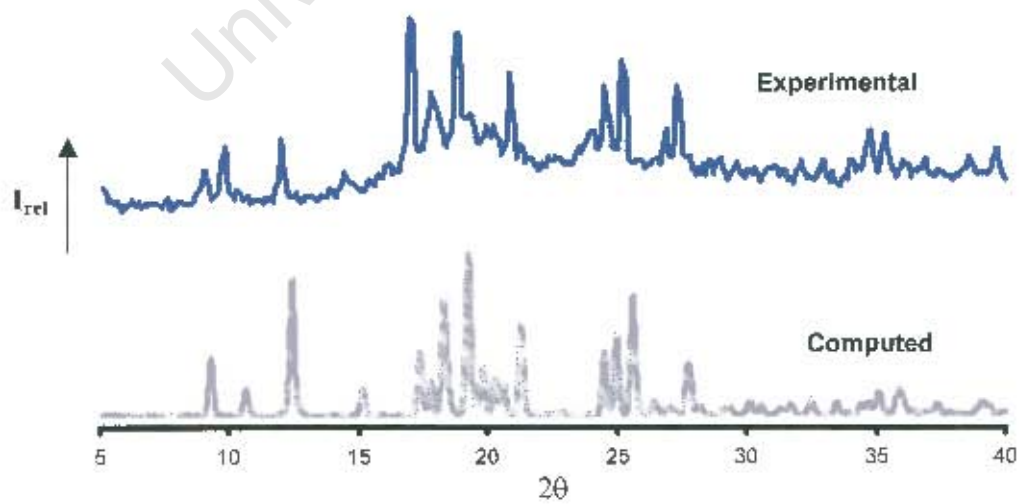

Figure 6.13 Computed [203K] and experimental [295K] PXRD traces for **TULSUC**

X-ray Crystallographic Analysis of TULBEN

Single Crystal X-ray Diffraction

Data-collection and space group determination

Diffraction intensity data for the salt formed between tulobuterol and benzoic acid were collected on a Nonius Kappa CCD diffractometer at 293K. A suitable crystal was mounted under paratone oil and glued to a glass fibre. XPREP[109] indicated the monoclinic space group $P2_1/c$ as the only possible choice. LAYER[117] was used to inspect the reflection conditions which were found to be h0l: l = 2n, 0k0: k = 2n which indicate the space group $P2_1/c$ unequivocally.

Structure solution and refinement

The asymmetric unit consists of one tulobuterol cation and one benzoate anion. The structure was solved in SHELXS-97[110] using direct methods, which revealed the peak positions of all the non-hydrogen atoms. These were placed and refined in SHELXL-97[112] with isotropic temperature factors and subsequently, subject to satisfactory behaviour of the latter, refined with anisotropic temperature factors. Hydrogen atoms were placed in fixed geometric positions and refined using a riding model with isotropic temperature factor 1.2 times those of their parent atoms. Two amino hydrogen atoms were located in the difference Fourier map, which together with the equalisation of the C-O bonds on the benzoate anion indicated salt formation and the site of protonation on the tulobuterol molecule. The hydroxyl hydrogen atom was also located in the difference Fourier map. The methyl hydrogen atoms were refined using a rotating refinement strategy [AFIX 137] with isotropic temperature factors 1.5 times those of their parent atoms. Crystal and refinement parameters are presented in Table 6.11.

Table 6.11 Crystal and refinement parameters for **TULBEN**

Parameter	
Formula unit	$C_{12}H_{19}ClNO^{+}\cdot C_3H_5O_2^{-}$
Formula weight / g mol^{-1}	349.8
Crystal system	Monoclinic
Space group	$P2_1/c$
a / Å	8.9587(3)
b / Å	18.9875(9)
c / Å	11.0801(5)
α / °	90
β / °	94.008(3)
γ / °	90
Volume / Å^3	1880.1(1)
Z	4
Density$_{calc}$ / g cm^{-3}	1.236
μ(MoKα) / mm^{-1}	0.219
F(000)	744
Crystal size / mm^3	0.60x0.50x0.15
Temperature / K	293(2)
Range scanned θ / °	$4 \leq \theta \leq 27$
Index ranges	h : 0, 11 k : -24, 24 l : -14, -14
ϕ scan angle per frame / °	1.0
ϕ scan range / °, no. of frames	181, 181
ω scan angle / °	1.0
ω scan ranges / °, no. of frames	36, 36; 99, 99; 24, 24; 57, 57
Dx / mm	50
No. of measured reflections	13507
No. of unique reflections	4251
No. of reflections with $I > 2\sigma(I)$	2849
No. of least-squares parameters	232
R_{int}, R_σ	0.0421, 0.0652
S	1.022
R_1 ($F_o > 4\sigma(F_o)$)	0.0582
No. of reflections omitted	18
wR_2(all reflections)	0.1829
Weighting scheme parameters	a – 0.0138, b 0.16
$(\Delta/\sigma)_{mean}$	< 0.001
Δρ excursions / e Å^{-3}	0.34, –0.36

Description of the structure

TULBEN crystallises in a 1:1 tulobuterol cation:benzoate anion ratio in the monoclinic space group $P2_1/c$ with $Z = 4$ formula units per unit cell. The asymmetric unit consists of one tulobuterol cation and one benzoate anion and is illustrated in the ORTEP[120] diagram in Figure 6.14.

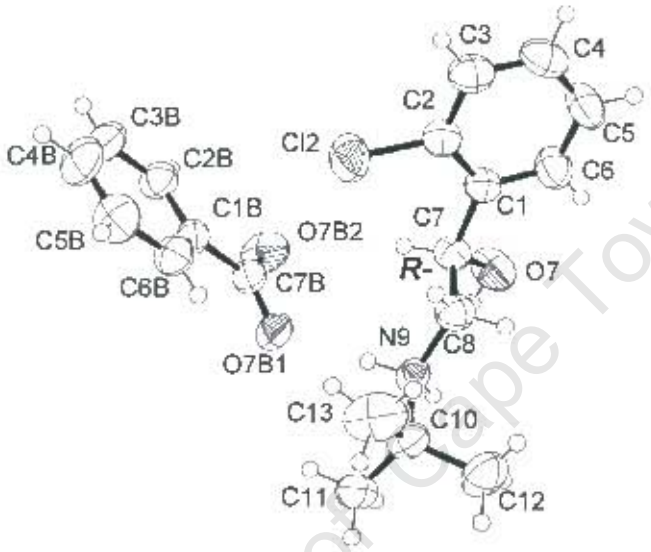

Figure 6.14 ORTEP diagram of the asymmetric unit of **TULBEN**. The benzoate atoms are labelled with the suffix 'B'. Thermal ellipsoids are drawn at the 50% probability level. Hydrogen atoms are drawn as spheres with arbitrary radii.

Hydrogen bonding and C-H···π-ring interactions

PLATON[121] calculated O-H···O, N-H···O, C-H···O and C-H···Cl hydrogen bonds for **TULBEN** which are presented in Table 6.12. There are three unique strong intermolecular hydrogen bonds that are inverted through a crystallographic centre of symmetry to yield the basic hydrogen-bonding motif consisting of six hydrogen bonds, which is illustrated in Figure 6.15.

Table 6.12 Hydrogen bonding interactions for the **TULBEN** structure

D-H···A	H···A / Å	D···A / Å	D-H···A / °	Symmetry Code
N9-H9A···O7B1	1.87(2)	2.776(2)	174(2)	x, y, z
O7-H7A···O7B1	1.84(3)	2.765(2)	164(3)	1-x, 1-y, -z
N9-H9B···O7B2	1.78(2)	2.722(2)	174(2)	1-x, 1-y, -z
C12-H15···O7B2	2.54(3)	3.298(3)	135(3)	1-x, 1-y, -z
C6-H6···O7 (intramolecular)	2.37(2)	2.703(3)	101(2)	x, y, z
C7-H7···Cl2 (intramolecular)	2.72(2)	3.078(2)	102(3)	x, y, z

The N9-H9A···O7B1 hydrogen bond connects ions within the same asymmetric unit, whilst the O7-H7A···O7B1 and N9-H9B···O7B2 hydrogen bonds are between two adjacent asymmetric units that are related by the crystallographic inversion centre. The fourth unique intermolecular hydrogen bond C12-H15···O7B2 [not shown] connects the same asymmetric units as the N9-H9B···O7B2 hydrogen bond and is thus also inverted through the centre of symmetry to yield two C-H···O hydrogen bonds that strengthen the association of the ions. The C6-H6···O7 and C7-H7···Cl2 hydrogen bonds are the only two intramolecular hydrogen bonds and contribute to the stabilisation of the tulobuterol cation conformation.

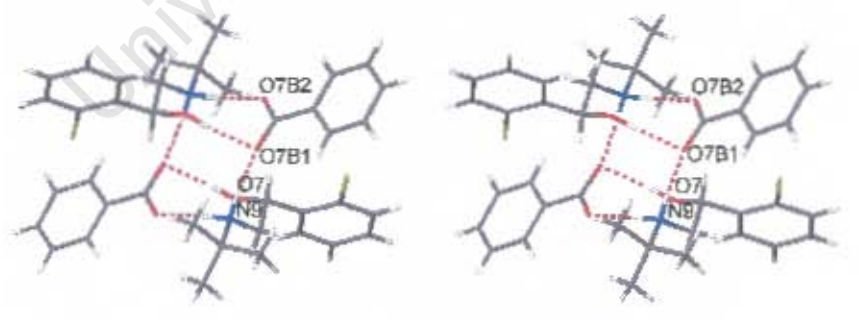

Figure 6.15 Stereo view of the basic hydrogen bonding motif in **TULBEN**

PLATON[121] was used to calculate two unique C-H···π-ring interactions for the **TULBEN** structure and these are presented in Table 6.13.

Table 6.13 C-H···π-ring interactions for the **TULBEN** structure

Interaction	H···Cg / Å	C···Cg / Å	C-H···Cg / °	Symmetry code[b]
C5B-H5B···Cg[a]	2.92(3)	3.773(3)	154(3)	1-x, 1-y, 1-z
C12-H16···Cg	3.17(4)	3.803(3)	125(3)	1+x, y, z

[a] Cg – Centre of gravity of the aromatic ring of the tulobuterol cation
[b] Symmetry code is applied to the second unit of the interaction

The two C-H···π-ring hydrogen bond symmetry codes indicate that these bonds link ions of different asymmetric units and will be discussed in further detail in the section titled **Crystal packing.**

The π···π-ring distances observed are considered to be too long [>5Å] to qualify as significant interactions of this type.

Conformation and configuration of the tulobuterol cation

The principal torsion angles η_1, η_2, η_3, η_4 and η_5 for the tulobuterol cation in **TULBEN** are compared with the corresponding parameters for the tulobuterol molecules in **Form 1** and **Form 2** in Table 6.14. The reader is referred to Figure 6.6 for an illustration of the torsion angle definitions. The torsion angles in Table 6.14 will be discussed in terms of their magnitudes only.

The η_1 and η_2 torsion angles for the **TULBEN** cation are similar to those for **Form 1** and **Form 2** molecules, indicating that the aromatic ring plane is also nearly perpendicular to backbone of the tulobuterol cation and that the Cl2 and O7 atoms are *trans* to each other.

The η_3 torsion angle for the **TULBEN** cation is slightly less than those for the **Form 1** and **Form 2** molecules, indicating that the backbone of the **TULBEN** cation is slightly more 'bent' but with the aromatic ring still being approximately *trans* to the N9 atom.

The η_4 torsion angle for the **TULBEN** cation is slightly larger but with the O7 atom still being *gauche* to the N9 atom.

Table 6.14 Principal torsion angles for the **TULBEN** cation and polymorph molecules

Compound	η_1	η_2	η_3	η_4	η_5
TULBEN [(R-)]	-81.8(2)	156.8(2)	167.9(2)	-73.8(2)	-177.6(2)
Form 1					
Molecule **A** [(S-)]	87.0(2)	-153.8(2)	-175.7(2)	62.2(2)	-170.5(2)
Molecule **B** [(R-)]	-81.4(2)	160.2(2)	-179.6(2)	-58.2(2)	173.7(2)
Molecule **C** [(R-)]	-77.8(2)	163.2(2)	178.1(2)	-60.1(2)	169.4(2)
Form 2					
Molecule **A** [(S-)]	84.0(2)	-157.2(2)	-174.0(2)	64.3(2)	-166.0(2)
Molecule **B** [(R-)]	-83.9(2)	157.1(2)	-175.2(2)	-54.1(2)	167.2(2)
Molecule **C** [(R-)]	-81.5(2)	159.9(2)	178.9(1)	-59.7(2)	172.6(2)

In contrast to the previously discussed salts, the η_5 torsion angle for the **TULBEN** cation is larger than in the case of the **Form 1** and **Form 2** molecules indicating that the cation tail is more 'extended' in the **TULBEN** structure, but is still found on the side of the backbone opposite to that of the O7 atom.

The overall conformation of the **TULBEN** cation is close to that for the **Form 1** and **Form 2** molecules, except for the small differences mentioned above.

The configuration at the C7 atom of the tulobuterol cation for the chosen asymmetric unit is (R-), but there is a counterpart with the opposite configuration in the crystal, as required by the centrosymmetric space group.

Crystal packing

The crystal packing of the **TULBEN** structure is presented as stereo views in Figures 6.16(a) and (b), which include the strong intermolecular hydrogen bonding as well as the C-H···π-ring interactions to present a clearer picture of closely associated ions in the

crystal. The view down the *a*-axis [Figure 6.16(a)] shows that adjacent motifs, contrary to the situation in the two previously discussed salts, do not share a common anion nor do they have strong intermolecular hydrogen bonds connecting them. Thus, isolated strongly hydrogen bonded clusters of ions are formed. The view also shows that these clusters coincide with the inversion centres at the midpoints of the *b* and *c* cell edges and that the C5B-H5B···Cg interactions connect adjacent clusters along the *c*-axis. The view down the *c*-axis shows that the C12-H16···Cg interactions connect the clusters along the *a*-axis.

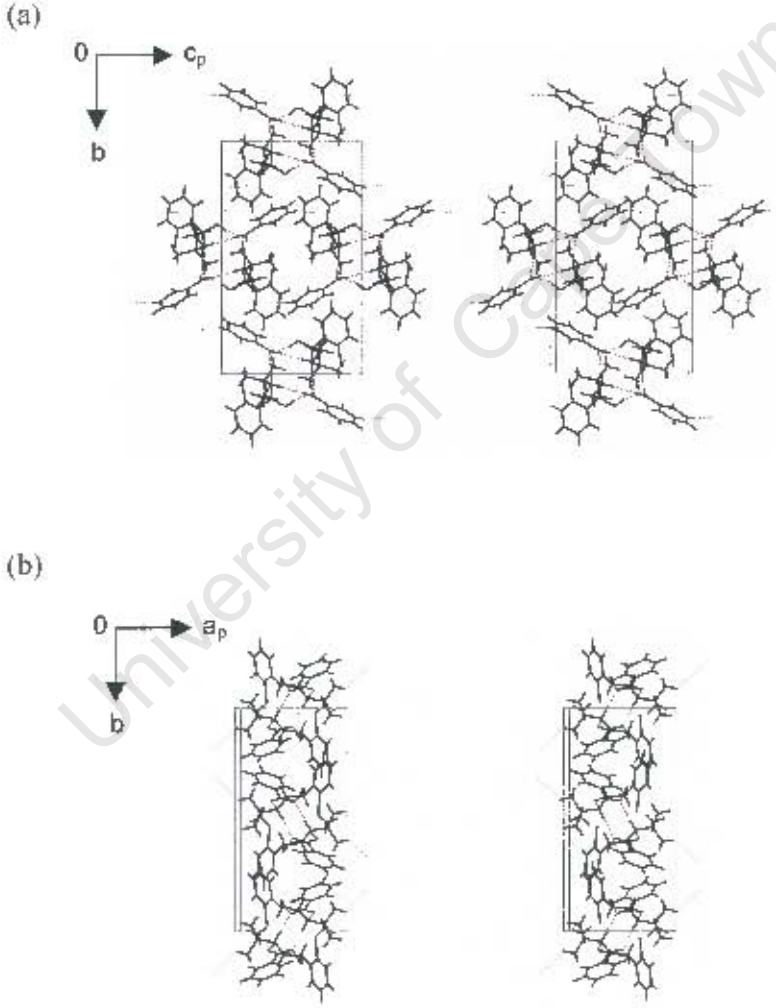

Figure 6.16 Stereoviews of the crystal packing down the (a) *a*- and (b) *c*-axes. Strong intermolecular hydrogen bonding interactions are shown in red whilst C-H···π-ring interactions are shown in green [only the C5B-H5B···Cg and C12-H16··· Cg interactions are shown in (a) and (b) respectively].

Powder X-ray Diffraction

The experimental and computed traces for the **TULBEN** structure are presented in Figure 6.17. These traces agree closely with each other and thus show that **TULBEN** did not transform on grinding and that the computed trace can serve as reference for **TULBEN** identification. The information for the traces were obtained at approximately the same temperatures and thus the shift to lower 2θ of the experimental trace that was observed for **TULTAR** and **TULSUC** is not evident here.

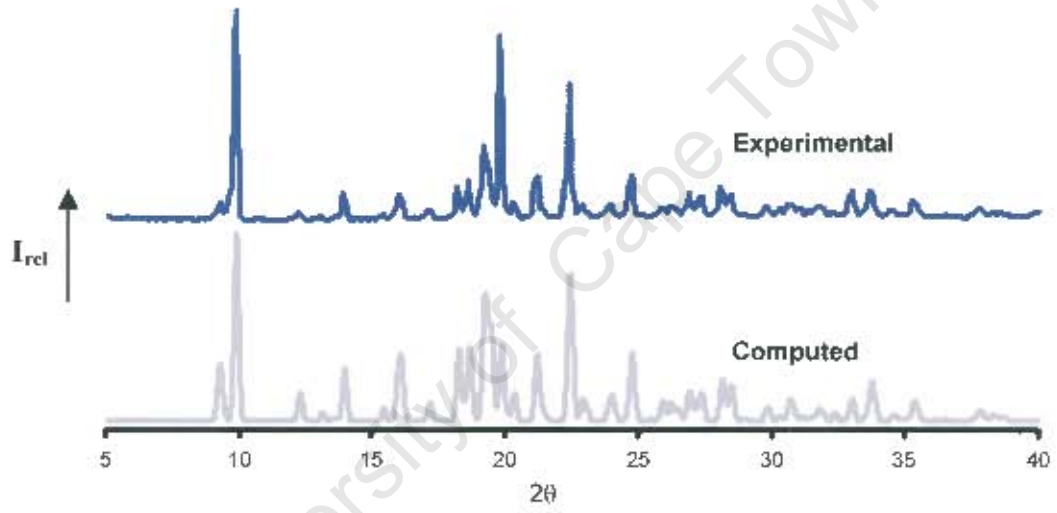

Figure 6.17 Computed [293K] and experimental [295K] PXRD traces for **TULBEN**

Discussion

This section will aim to compare the structures of **TULTAR**, **TULSUC** and **TULBEN** in terms of the conformation of their common tulobuterol cations, hydrogen bonding and C-H···π-ring interactions and crystal packing and then relate these to their thermal behaviour. Finally the structural features of the salts prepared in this study will be compared with those for the polymorphs of the hydrochloride salt.[102]

Conformations of the tulobuterol cations

Table 6.15 presents the torsion angles of the tulobuterol cations found in **TULTAR**, **TULSUC** and **TULBEN**. The differences in conformations of the cations between the respective salt structures are minor. This is indicated by the ranges in the torsion angles given at the bottom of Table 6.15. The η_5 torsion angle displays the widest range at 25.0° but this still does not indicate any major changes in the stereostructure such as a *trans* to a *gauche* rotation. So for all the cations of the respective salts the aromatic ring plane is nearly orthogonal to the backbone and *trans* to the amino nitrogen [backbone in extended conformation], whilst the hydroxyl group is nearly *trans* to the chlorine atom and *gauche* to the amino nitrogen atom. The tail of the tulobuterol cation also always adopts an extended conformation but with the tertiary butyl group slightly 'swung away' from the hydroxyl side of the backbone.

Table 6.15 Principal torsion angles for tulobuterol cations in **TULTAR**, **TULSUC**, and **TULBEN**

Compound	η_1	η_2	η_3	η_4	η_5
TULTAR					
Cation **A** (*R*-)	-81.1(4)	158.3(3)	-168.8(3)	-48.8(4)	-162.6(3)
Cation **B** (*S*-)	81.3(4)	-159.6(3)	170.5(3)	50.6(4)	156.7(3)
Cation **C** (*R*-)	-100.2(4)	137.6(3)	-173.7(3)	-51.2(4)	-155.1(3)
Cation **D** (*S*-)	99.5(4)	-139.6(3)	174.4(3)	53.9(4)	154.9(3)
TULSUC (*S*-)	91.0(2)	-147.0(1)	-177.2(1)	56.0(1)	157.6(1)
TULBEN (*R*-)	-81.8(2)	156.8(2)	167.9(2)	-73.8(2)	-177.6(2)
Δ(torsion angle)*	19.1	22.0	23.3	25.0	22.7

* The sign of the torsion angles for opposite enantiomers was accounted for by inverting the sign of that of the (S)-enantiomer [arbitrarily chosen] before calculating the range

Comparison of hydrogen bonding and C-H···π-ring interactions

In the **TULTAR** and **TULSUC** structures adjacent hydrogen bond motifs share a common anion resulting in the formation of infinite chains of N-H···O and O-H···O hydrogen bonded ions in both structures along the direction in which they share the common anions. Adjacent motifs in the **TULBEN** structure neither share a common ion nor have N-H···O or O-H···O hydrogen bonds linking them and therefore form isolated clusters. Table 6.16 presents the number of hydrogen bonding and C-H···π-ring interactions within and between the chains or clusters found in the respective structures. The interactions for the chains will be discussed in terms of the number per repeating unit.

There are four N-H···O and two O-H···O interactions contained in each of the hydrogen bonded units of **TULTAR**, **TULSUC** and **TULBEN**. A comparison of the hydrogen bonding motifs found in each structure is presented in Figure 6.18. It shows that a strong topological homology exists between the hydrogen-bonding motifs. All the O-H and N-H groups of the tulobuterol cations as well as the terminal oxygens of the anions are involved in the hydrogen bonding.

Table 6.16 Type and number of interactions for **TULTAR**, **TULSUC** and **TULBEN**

Interaction per unit	TULTAR chain	TULSUC chain	TULBEN cluster
Within chain/cluster			
N-H···O	4	4	4
O-H···O	2	2	2
C-H···O	1*	0	2
C-H···π-ring	2.5*	0	0
Between chain/cluster			
C-H···O	1[ab]	0	0
C-H···π-ring	0	4[ac]	2[a] and 2[c]

*Averaged over the two independent motifs, [ab] links chains diagonally along the *ab*-plane, [ac] links chains diagonally along the *ac*-plane, [c] links clusters along the *c*-axis

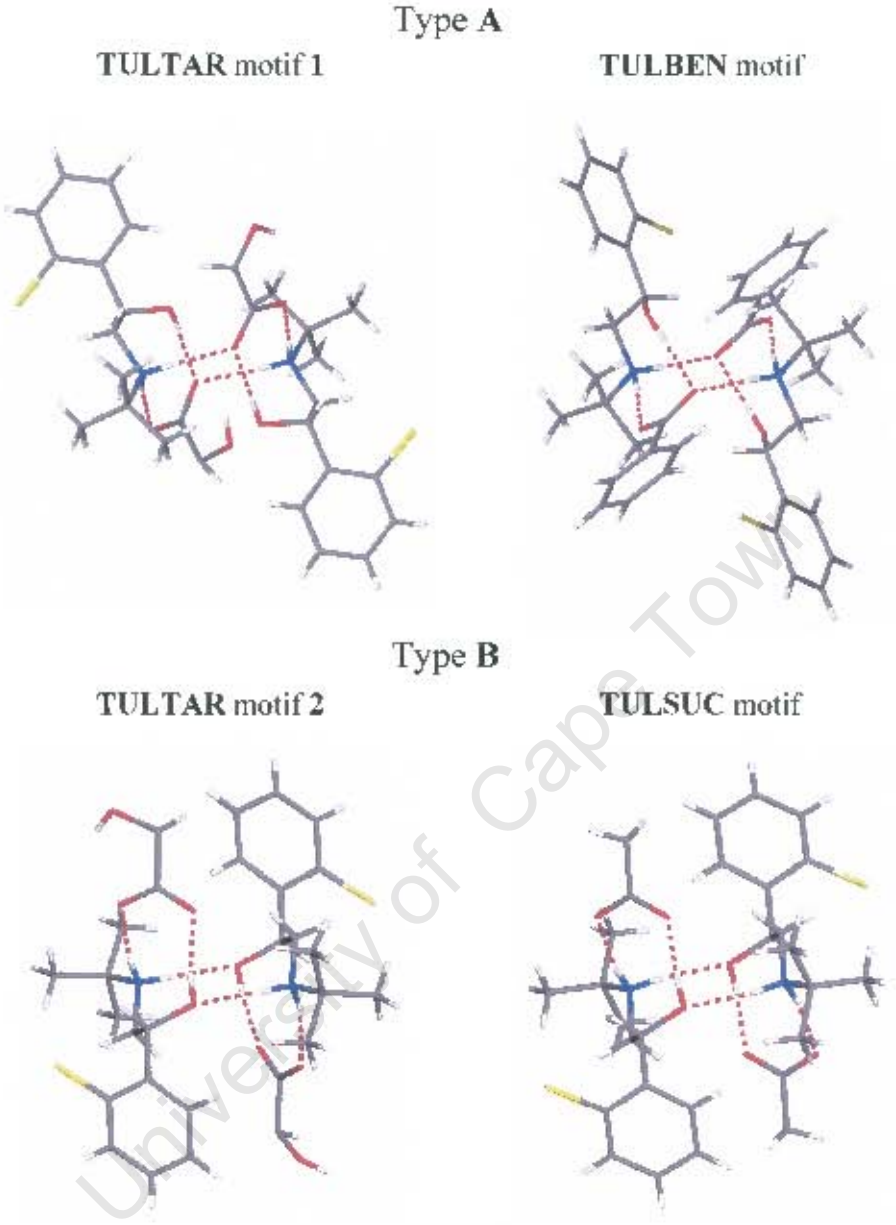

Figure 6.18 Comparison of the hydrogen-bonded motifs in **TULTAR**, **TULSUC** and **TULBEN**

The hydrogen bonding distances, and thus strengths, are also similar among the structures, as indicated in Tables 6.4, 6.8 and 6.12. In each structure the motif possesses either a pseudocentre [**TULTAR** motifs 1 and 2] or a crystallographic centre of inversion [**TULSUC** and **TULBEN** motifs]. However, certain features of the hydrogen bonding motifs subdivide them into two groups. In the type **A** motifs [**TULTAR** motif 1 and the **TULBEN** motif] each cation links to both anions but not to the other cation that makes

up the motif. The O-H group on the tulobuterol cation is also involved only as a hydrogen bond donor. In the type B motifs [**TULTAR** motif **2** and **TULSUC**] the cations link to each other as well as to one anion each, with the O-H group involved in both a hydrogen bond donating and accepting capacity.

The other types of hydrogen bonds found in the respective structures either reinforce the chains or clusters, or connect them to each other. In the **TULTAR** structure an average of one C-H···O and two and a half C-H···π-ring interactions per unit reinforce the chains, whilst an average of one C-H···O hydrogen bond per unit links adjacent chains. In the **TULSUC** structure no other hydrogen bonds further reinforce the chain but four C-H···π-ring interactions per unit link adjacent chains. In the **TULBEN** structure two C-H···O hydrogen bonds strengthen the association of the ions within the cluster, whilst adjacent clusters are connected by C-H···π-ring interactions along two directions [two interactions per direction]. Thus, two-dimensional sheets are formed in all three structures but which differ in the architecture of their constituent interactions. The order of the sheet strength, as determined by their constituent hydrogen bond types described above, is **TULTAR** > **TULSUC** > **TULBEN**, corresponding with the decreasing melting point order of the salts.

Crystal packing

C-H···π-ring interactions are common to all three structures and highlight a common trait of the packing amongst the three structures. For all these interactions, tertiary butyl hydrogen atoms of one cation interact with the chlorophenyl rings of another cation, indicating that these groups form hydrophobic 'pockets' in all the structures. An exception occurs in the case of the specific C-H···π-ring interaction in the **TULBEN** structure where it is an aromatic hydrogen atom interacting with another chlorophenyl ring, but which nevertheless also leads to the formation of a hydrophobic 'pocket'.

Comparison with the HCl salt structures

The salts prepared in this study will now be compared with the polymorphic HCl salt structures.[102] The principal torsion angles for the hydrochloride salt polymorphs are presented in Table 6.17. As for Table 6.15 the signs of the torsion angles for enantiomers of opposite chirality were accounted for by inverting the signs of the torsion angles for the (S)-enantiomer [arbitrarily chosen] before calculating the range. The latter also includes the torsion angles for the cations of the salts prepared in this study.

Table 6.17 Torsion angles for the tulobuterol cations in the HCl salt modifications[102]

Crystal form	η_1	η_2	η_3	η_4	η_5
Form I					
Cation 1 [(R-)]	-91.2	147.8	171.4	-70.8	-177.0
Cation 2 [(S-)]	96.5	-143.6	-169.6	71.7	-171.8
Cation 3 [(S-)]	84.2	-156.3	-169.8	72.1	179.8
Form II [(S-)]	107.7	-132.7	-172.0	71.6	-145.8
Form III [(S-)]	102.7	-138.3	-173.7	68.4	-163.1
Hydrate [(S-)]	87.2	-155.9	-177.9	61.7	-179.7
Δ(angle)[a]	|26.6|	|26.9|	|23.9|	25.0|	|59.3|

[a] Range includes the torsion angles for the cations in **TULTAR**, **TULSUC** and **TULBEN** given in Table 6.15

The fact that the ranges for the torsion angles given in Table 6.17, whose calculation includes all the cations in the hydrochloride salt polymorphs as well as the salts prepared in this study, are similar to those found in Table 6.15, indicates that conformations of the tulobuterol cations in the hydrochloride,[102] **TULTAR**, **TULSUC** and **TULBEN** salts are similar. The η_5 torsion angle range in Table 6.17 does, however, increase substantially relative to that found in Table 6.15 as a result of the Form II η_5 angle of –145.8°. A comparison, in a previous study, of torsion angles [η_1, η_3, η_4] of the tulobuterol HCl salts and other related adrenergic agents having an ethanolamine side chain, showed these to be similar.[155] The steric arrangement of the functional groups is consistent with rotamer **II** illustrated in Figure 6.19. In this rotamer the aromatic group is *trans* to the amino nitrogen, whilst the hydroxyl group is *gauche* to it. The comparison of the η_1 angles also

showed that the aromatic ring planes are nearly orthogonal to the ethanolamine side chain. The conformations of the cations in **TULTAR, TULSUC** and **TULBEN** thus also follow this general trend. This arrangement of functional groups is believed to be necessary for the activity of these compounds as adrenergic agents.[155]

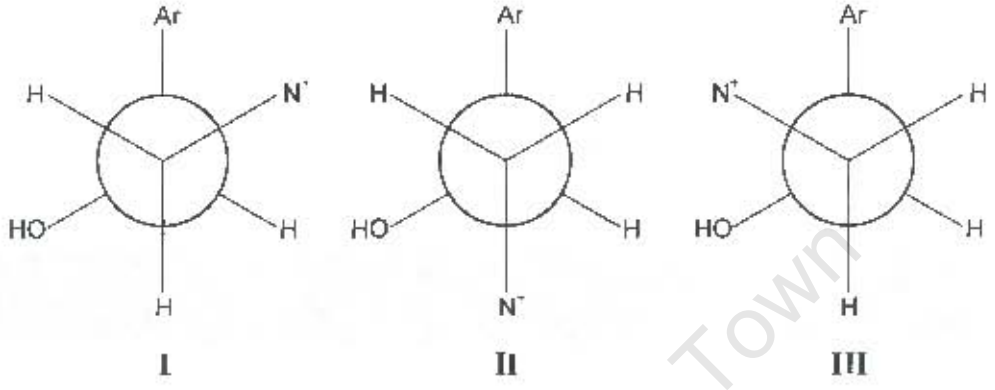

Figure 6.19 Possible rotamers for the η_3 and η_4 torsion angles. [adapted from reference 155]

As in the case of the salts prepared in this study, the hydrogen bonding in the HCl salt modifications determines the architecture of the crystal structures. Hydrogen-bonded motifs are also formed consisting of cations and anions related by pseudo- or true crystallographic symmetry elements. However, in the **TULTAR, TULSUC** and **TULBEN** structures the hydrogen bonding motifs consist of six hydrogen bonds as opposed to the four found in the HCl salt polymorphs. This is due to the anions in this study possessing more hydrogen bond donor and acceptor sites. The crystal packing is also characterised by the tertiary butyl and chlorophenyl groups forming hydrophobic 'pockets'.

Conclusion

In this chapter, three novel salts of tulobuterol prepared by its reaction with (R,R)-tartaric acid, succinic acid and benzoic acid respectively, were described. These have been characterised by thermal and X-ray diffraction techniques.

All three salts were established by TGA to be anhydrous with DSC analysis indicating one thermal event for each, viz. fusion at extrapolated melting points of 191, 163, 147°C for **TULTAR**, **TULSUC** and **TULBEN** respectively.

X-ray diffraction analysis established that **TULTAR** crystallises in the triclinic space group P1 with a = 9.665(2), b = 10.685(2), c = 16.923(3)Å, α = 94.06(3), β = 93.80(3), γ = 115.46(3)° and Z = 2 formula units per unit cell. **TULSUC** crystallises in the monoclinic space group $P2_1/n$ with a = 10.377(2), b = 10.207(2), c = 14.855(3)Å, β = 106.23(3)° and Z = 4 formula units per cell. **TULBEN** crystallises in the same space group as **TULTAR** but in a different setting [$P2_1/c$] with a = 8.9587(3), b = 18.9875(9), c = 11.0801(5)Å, β = 94.008(3)° and Z = 4 formula units per unit cell. An extensive and intricate hydrogen bonding arrangement of ions was found in all three structures, which were discussed separately as well as in terms of their common features and dissimilarities. The melting point order of the salts could be related to these common features and dissimilarities in their hydrogen-bonding interactions.

The structural features of the salts prepared in this study were also compared with the structural features of the known hydrochloride salt polymorphs. These were found to have many common features, e.g. the conformations of the cations of the salts prepared in this study were found to be similar to those of the hydrochloride salt polymorphs reported earlier[102] and generally consistent with those of adrenoreceptor agonists with an ethanolamine side chain.[155]

Chapter 7 - Conclusion

In this study a number of novel species of tulobuterol have been prepared. These include a second polymorphic form, four cyclodextrin inclusion complexes and three salts of tulobuterol. Identification and characterisation of these crystalline phases were afforded by elemental analysis, thermal, X-ray diffraction and spectroscopic techniques. A summary of the application of the above techniques to the identification and characterisation of the species prepared follows.

Polymorphs

Polymorph identification

Two polymorphic forms of tulobuterol, **Form 1** and **Form 2** [novel form], were prepared by recrystallisation from different solvent systems. Hot stage microscopy was a quick, inexpensive technique to assess different thermal behaviours that possibly indicated polymorphism. Microanalysis was then used to determine that the two crystal forms had the same elemental content, establishing them as polymorphs and not solvates.

Thermal analyses

Form 1 and **Form 2** were confirmed as polymorphs by their lack of mass loss on TGA. DSC established that **Form 1** has the higher melting point and enthalpy of fusion implying that monotropy described the stability relationship of the dimorphic pair and that **Form 1** is the thermodynamically more stable form at all temperatures below the melting points of the polymorphs. This was confirmed by using the accurately determined enthalpies of fusion of the polymorphs to calculate the stability transition temperature of the dimorphic system, which was found to lie well above the melting points of the polymorphs.

The DSC analysis of the polymorphs revealed a single thermal event for each, namely fusion. However, certain batches of **Form 2** crystal exhibited three thermal events, namely fusion at the **Form 2** melting temperature, immediate recrystallisation and subsequent fusion of the recrystallised material at the **Form 1** melting temperature. This was interpreted as being due to contamination of these batches of **Form 2** with small amounts of **Form 1**, which apparently acted as seeds for the recrystallisation of the

molten material into **Form 1**. The existence of a third form, **Form 3**, was implied by the appearance of a new peak on the DSC trace of the reheat of molten tulobuterol, but unfortunately this was its only form of characterisation. Finally, it was established that sample grinding prior to DSC analysis could affect the thermal behaviour of the polymorphs and thus that identification of ground forms should always be corroborated by powder X-ray diffraction.

X-ray diffraction

The crystal structures of the polymorphs were successfully determined. Apart from differences in crystal packing, as expected for polymorphs, single crystal X-ray diffraction revealed a common asymmetric unit with a highly conserved topology. This consists of three tulobuterol molecules associated by three homodromic O-H···N hydrogen bonds as a cyclic trimer. The polymorphs thus basically differ only in the way these trimers pack in their respective unit cells. Differences were observed for the inter-trimer interactions; specifically **Form 2** was found to have fewer C-H···π-ring interactions, which is consistent with its lower melting point. The presence of only soft C-H···π-ring and van der Waals interactions in the polymorphic crystals is consistent with their relatively low melting points. Powder X-ray diffraction indicated that these forms do not transform on grinding and that the computed PXRD traces can serve as references for their identification.

Spectroscopic studies

The FTIR spectra of the polymorphs proved to be indistinguishable, especially in the -NH and -OH frequency range, which is often diagnostic for polymorphs. This is consistent with the identical hydrogen bonding environments revealed by the single crystal X-ray analyses. However, solid-state NMR spectroscopy did prove to be diagnostic for the two forms, the differences correlating with short intermolecular contacts identified in their crystal structures.

Cyclodextrin inclusion complexes

Complex identification and determination of the stoichiometry

Complexation of tulobuterol with β-CD, γ-CD, DIMEB and TRIMEB was proved using a combination of techniques. Microanalysis proved that each analysed sample contained nitrogen and thus tulobuterol, whilst thermal analysis suggested complexation by the disappearance of the bulk crystalline properties of the drug molecule. However, unequivocal proof for complexation was afforded single crystal X-ray diffraction which revealed the three-dimensional structures of the complexes.

The stoichiometries of the complexes were determined by the combined information from microanalysis and TGA. Microanalysis was used to determine the host:guest ratios of dehydrated complexes, whilst TGA was used to determine the water content of the fully hydrated complexes. In the case of hygroscopic complexes, TGA was performed simultaneously in order to ascertain their water content at the time of microanalysis. The host:guest ratios are 1:1 for the DIMEB and TRIMEB inclusion complexes of tulobuterol, whilst the β-CD and γ-CD inclusion complexes of tulobuterol have host:guest ratios of 2:1 and 3:2 respectively.

Thermal analyses

Thermal analysis of the CD complexes involved HSM, DSC and TGA, which were used in a complementary and corroborative manner in the characterisation of the physical properties of the CD complexes.

HSM was used to characterise visually the thermal events indicated by DSC and TGA. The presence of included water was indicated by bubble formation on heating the complexes under silicone oil. Included water was indicated for the β-CD and γ-CD inclusion complexes only. This was evident from an initial mass loss and an endothermic peak from TGA and DSC respectively. TGA was also used to quantify the water present in the hydrated complexes, proving reproducible in its assessment. Thus this technique is more reliable than the single crystal structure solution where the disorder and high

thermal motion of water molecules made their quantitation and placement difficult. DSC was used to determine the onset temperatures of melting [TRIMEB complex] and decomposition [β-CD, γ-CD and DIMEB complexes]. These temperatures are higher than the respective melting temperatures of the polymorphs of the uncomplexed drug, indicating that the complexed tulobuterol remains intact in the solid phase at higher temperatures.

X-ray diffraction

The structures of the γ-CD and TRIMEB inclusion complexes were solved using isomorphous replacement, whilst the β-CD inclusion complex structure was solved from *ab initio* methods using SHELXD. Attempts at solving the structure of the DIMEB inclusion complex failed.

Host geometry

The geometries of the host molecules were mainly described in terms of their macrocyclic symmetries as defined by certain parameters of the O4-polygon as well as the tilt angles of the individual glucopyranose units. The O4-polygon parameters included the radius of the polygon, the deviation of each O4 atom from the O4 atom mean plane as well as the distances, angles and torsion angles defined by adjacent O4 atoms.

In the β-CD inclusion complex, the host molecules form a head-to-head dimer with O3-H···O3' hydrogen bonds implicated as the major interactions that bind the dimer. The glucopyranose units of the β-CD molecules have relatively small positive values, which results in their being fairly 'round'. The low tilt angles are attributed to the intramolecular O2···O3' and O3···O2' hydrogen bonds on the secondary side of the β-CD molecules. Conformational parameters of the host molecules agree well with those for other β-CD dimeric structures. The intermolecular O3···O3' hydrogen bonds that bind the dimer further restrict these tilt angles so the host molecules of dimeric β-CD structures show less deviation from ideal seven-fold symmetry than their monomeric counterparts.

The geometries of the γ-CD complex host molecules also agree well with those of other γ-CD inclusion complexes, which all form part of one isostructural series. The tilt angles

for the glucopyranose units are relatively low which results in the fairly 'round' shapes of the γ-CD molecules. This is attributed to the intramolecular O2···O3' and O3···O2' hydrogen bonding on their secondary sides. The γ-CD molecules stack on top of one another forming columns with intermolecular hydrogen bonding observed between the γ-CD molecules that further restrict the tilt angles.

The macrocyclic symmetry of TRIMEB [permethylated β-CD] molecules deviates significantly from that of native β-CD molecules as a result of the lack of O2-H···O3' and O2···H-O3' hydrogen bonding. Nevertheless, the TRIMEB complex was found to be a member of an existing TRIMEB complex isostructural series and thus its host conformational parameters agree closely with other members of this series.

Guest inclusion

Due to the severe disorder of the guest molecules that prevailed in the β-CD and γ-CD complexes, these could not be modelled. The only information regarding the guest molecules could be obtained from microanalysis, which indicated that one tulobuterol per β-CD dimer and two per three crystallographically independent γ-CD molecules are included.

The only successfully modelled guest molecule was that of the TRIMEB inclusion complex. In this case the tertiary butyl group of the tulobuterol molecule includes from the secondary side of the TRIMEB molecule. This host-guest interaction is stabilised not only by hydrophobic and van der Waals interactions but by a O-H···O, N-H··O and C-H···π-ring interaction. A significant portion of the tulobuterol molecule protrudes from the secondary side of the TRIMEB molecule, which is a common feature for the majority of the members of the isostructural series to which the complex belongs. The chlorophenyl ring of the tulobuterol molecule is located on the secondary face of the TRIMEB molecule as was found for other guest molecules of TRIMEB inclusion complexes that contain a chlorophenyl moiety. The conformations of the uncomplexed and complexed tulobuterol molecules were found to be essentially the same, except for the tertiary butyl group that is 'swung away' from its *trans* position in the uncomplexed

state in order to allow for a better fit in the TRIMEB cavity. The included tulobuterol molecule was found to have the (R-) configuration, which indicated a resolution of the drug, at least for the chosen crystal.

Host hydrogen bonding interactions

The non-covalently bonded interactions in the β-CD and γ-CD inclusion complexes are characterised by extensive hydrogen bonding networks that exclusively involve host atoms. The strong O-H··O hydrogen bonding interactions were found to have marked effects on the geometries of the host molecules. Both intra- and intermolecular hydrogen bonding restricted the host molecules of these complexes to relatively 'round' shapes as a result of the low tilt angles of their glucopyranose units. In the β-CD inclusion complex the O-H···O hydrogen bonding is divided into secondary and primary hydroxyl-mediated hydrogen bonding interactions. The former were found to be consistent with those observed in other β-CD dimeric structures, whereas the latter differed from the majority of β-CD dimeric structures in that they connected host molecules between adjacent dimeric layers rather than within the same dimeric layer. Host molecules within a dimeric layer were mainly connected by weaker C-H···O hydrogen bonds. In the γ-CD complex the host molecules within a channel are connected to each other mainly via O-H···O hydrogen bonds with C-H···O hydrogen bonds connecting host molecules of adjacent channels.

In the case of the TRIMEB molecules, the lack of hydroxyl groups meant that strong hydrogen bonds exclusively involving host atoms were precluded. Thus this complex contains only weaker C-H···O hydrogen bonds, which were nevertheless arranged in a systematic manner. Thus they contribute in a definite manner to the stabilisation of the host conformation as well as the extended structure of the complex.

Water interactions

The water molecules in the β- and γ-CD inclusion complexes were found to have a high degree of disorder as indicated by the larger number of water sites than molecules calculated from TGA, as well their partial site occupancy factors and close proximity to

other water molecules. Despite this, they formed quasi-invariant water networks that were found to be similar to those in other β- and γ-CD complexes.

Crystal packing

All the CD complexes with tulobuterol, except that with DIMEB, were found to be isostructural with known complexes of their hosts. The crystal packing arrangements were thus consistent with those observed in the isostructural series to which they belong. The β-CD inclusion complex with tulobuterol belongs to the subset of β-CD dimeric species that pack in the channel mode. Unlike the situation within a channel in the β-CD inclusion complex, where neighbouring host molecules are arranged anti-parallel, the host molecules in the γ-CD inclusion complex are arranged both parallel and anti-parallel with their neighbours. In the TRIMEB complex the host molecules are stacked parallel on top of one another, with slight lateral offsets between adjacent units resulting in the formation of a screw-channel.

Tulobuterol salts

Salt identification and determination of the stoichiometry

Salt formation of tulobuterol with (R,R)-tartaric acid, succinic acid and benzoid acid was established by microanalysis which also yielded the cation:anion ratios.

Thermal analyses

DSC revealed a single thermal event for each salt, namely fusion. TGA yielded negligible mass loss, which confirmed the lack of included solvent. These results were corroborated by HSM.

X-ray diffraction

The crystal structures of the three salts were determined by single crystal X-ray diffraction. Even though the constitutions of the salts differ in their anionic component, many similarities were found amongst the three structures. Firstly, the conformations of the cations were found to be similar in all the salts. Furthermore, the arrangements of

functional groups are similar to those of the hydrochloride salt and other adrenergic agents having an ethanolamine side chain, which have been compared in a previous study.[155] This arrangement is believed to be necessary for activity of these compounds. Secondly, extensive hydrogen bonding networks were found in all the salt structures and common motifs were identified that involve strong O-H···O and N-H···O hydrogen bonds. The nature in which these interactions connect ions in the respective salt structures, together with the presence/absence of weaker C-H···O and C-H···π-ring interactions, was found to be consistent with the melting point order of the salts. The packing arrangements of all three salts prepared in this study, as well as polymorphs of the hydrochloride salt, were found to have a common feature, namely that the tertiary butyl and chlorophenyl groups of neighbouring tulobuterol cations cluster together, forming hydrophobic 'pockets'.

Final remarks

All the species prepared in this study are novel, except for the higher melting polymorph of tulobuterol. The latter form had not, however, been characterised to the extent that it has in this study, especially in terms of the determination of its crystal structure. The feasibility of the inclusion of tulobuterol within a variety of cyclodextrins, as well as its ability to form a number of salts, have been amply demonstrated. Thus, the objectives of generating polymorphs, cyclodextrin inclusion complexes and salts of tulobuterol have been successfully addressed.

The range of techniques applied gave a comprehensive solid-state characterisation of all the species. Thermal analysis was key in the determination of the stability relationship of the polymorphs, which is important for future practical considerations with respect to manipulation of the drug. From a crystallographic point of view the polymorphs yielded very interesting features, such as unusually high numbers of molecules in the respective unit cells, and even more interestingly, the commonality of their asymmetric units, which are hydrogen bonded trimers. The similarity of the structural features of the salts, even when compared to the hydrochloride salt and other β-adrenergic agents with an ethanolamine side chain, is remarkable, especially in terms of the conformations of the

active components. In fact, all the tulobuterol molecules and cations successfully modelled in this study were found to have similar conformations. This not only suggests that the species prepared may be viable alternatives in that the required conformation for β-adrenergic activity is exhibited,[155] but it highlights the importance of structural studies in characterising possible alternatives to currently used drugs. Each solid species has unique physical properties, thus presenting each of these as a possible alternative to the currently marketed hydrochloride salt, depending on the specific application intended. In addition, physicochemical characterisation of the novel species prepared in this study was successful in relating their molecular scale and bulk properties. Knowledge of these relationships will be essential for future assessment of these species as viable alternatives to the hydrochloride salt.

Tulobuterol is proving to be an important bronchodilator in the long-term treatment of severe childhood asthma. It has recently been introduced as a transdermal patch which has been recommended for the treatment of the 'severe morning dip',[100] as effective tulobuterol levels are maintained by its transdermal application.[156] The polymorphs, cyclodextrin complexes and tulobuterol salts prepared in this study may also serve as viable alternatives to the hydrochloride salt in this respect as, in particular, the suitability of cyclodextrins as drug carriers in transdermal administration has been demonstrated.[157]

References

References

1. Lehn, J-M., *Angew. Chem. Int. Ed. Engl.*, **1988**, 27, 89-112.
2. Davy, H., *Trans. R. Soc. London.*, **1811**, 101, 1.
3. Dunitz, J. D., In: The Crystal as a Supramolecular Entity: Perspectives in Supramolecular Chemistry, Desiraju, G. R. (Ed.), **1996**, Wiley, New York, 2, 2.
4. Corradini, P., *Chem. Ind. (Milan)*, **1973**, 55, 122-129.
5. Bernstein, J., Polymorphism in Molecular Crystals - IUCr monographs on Crystallography, No. 14, **2002**, Clarendon Press, Oxford, 4-5.
6. Bernstein, J., Polymorphism in Molecular Crystals - IUCr monographs on Crystallography, No. 14, **2002**, Clarendon Press, Oxford, 8.
7. Bernstein, J., Polymorphism in Molecular Crystals - IUCr monographs on Crystallography, No. 14, **2002**, Clarendon Press, Oxford, 27.
8. Mitscherlich, E., *Ann. Chim. Phys.*, **1822**, 19, 350.
9. Amici, G. B., *Ann. Chim. Phys.*, **1844**, Ser. 3, 12, 114-120.
10. Lima-de-Faria, J. (Ed.), In: *Historical Atlas of Crystallography*, **1990**, Kluwer Academic Publishers, Dordrecht, The Netherlands, 68-69.
11. Lehmann, O., PhD thesis, Die Krystallanalyse oder die Chemische Analyse durch Beobachtung der Krystallbildung mit Hülfe des Mikroskps., Wilhelm Englemann, Leipzig, **1891**.
12. Ostwald, W. F., *Z. Phys. Chem.*, **1897**, 22, 289-330.
13. Tammann, G., *The States of Aggregation (trans. F. F. Mehl)*, **1926**, Constable Company, Ltd., London, 116-157.
14. Knapman, K., *Modern Drug Discovery*, **2000**, 3, 57.
15. Bernstein, J., Polymorphism in Molecular Crystals - IUCr monographs on Crystallography, No. 14, **2002**, Clarendon Press, Oxford, 27-28.
16. Bernstein, J., Polymorphism in Molecular Crystals - IUCr monographs on Crystallography, No. 14, **2002**, Clarendon Press, Oxford, 298-304.
17. Buerger, M. J., In: *Phase Transformations in Solids*, Smoluchowski, R., Mayer, J. E., Weyl, W. A. (Eds.), **1951**, John Wiley and Sons, New York, U.S.A., 183-211.

18. Grunenberg, A., Henck, J-O., Siesler, H. W., *Int. J. Pharm.*, **1996**, 129, 147-158.
19. Bernstein, J., Polymorphism in Molecular Crystals - IUCr monographs on Crystallography, No. 14, **2002**, Clarendon Press, Oxford, 38.
20. Burger, A., Ramberger, R., *Mikrochim. Acta*, **1979**, *II*, 259-272.
21. Burger, A., Ramberger, R., *Mikrochim. Acta*, **1979**, *II*, 273-316.
22. Burger, A., *Pharm. Int.*, **1982**, 3, 158-163.
23. Yu, L., *J. Pharm. Sci.*, **1995**, 84, 966-974.
24. Volmer, M., *Kinetic der Phasenbildung*, Stankopf, Leibzig, **1939**.
25. Bernstein, J., Davey, R. J., Henck, J-O., *Angew. Chem. Int. Ed.*, **1999**, 38, 3440-3361.
26. McCrone, Jr, W.C., *Fusion Methods in Chemical Microscopy*, **1957**, Interscience, New York.
27. Guillory, J.K., In: *Polymorphism in Pharmaceutical Solids*, Brittain, H. G. (Ed.), **1999**, Marcell Dekker, New York, 183-226.
28. Caira, M. R., In: *Topics in Current Chemistry*, **1998**, Springer-Verlag, Berlin, Heidelberg, 198, 164-208.
29. Bernstein, J., Polymorphism in Molecular Crystals - IUCr monographs on Crystallography, No. 14, **2002**, Clarendon Press, Oxford, 72-74.
30. Weissbuch, I., Popovitz-Biro, R., Lahav, M., Leiserowitz, L., *Acta Crystallogr.*, **1995**, B51, 115-148.
31. Ngooi, T-K, McGolrick, J. D., Antczak, C., Tindall, J. L. A., *CA*, **1994**, 121, 263,659e.
32. Maryanoff, *CA*, **1995**, *CA*, 122, 240,076k.
33. Ibragimov, B. T., Talipov, S. A., *J. Inclusion Phenom. Mol. Recognit. Chem*, **1994**, 17, 325.
34. Bernstein, J., Polymorphism in Molecular Crystals - IUCr monographs on Crystallography, No. 14, **2002**, Clarendon Press, Oxford, 94-149.
35. Brittain, H. G., In: *Polymorphism in Pharmaceutical Solids*, Brittain, H. G. (Ed.), **1999**, Marcell Dekker, New York, 227-278.
36. Threlfall, T. L., *Analyst*, **1995**, 120, 2435-2460.

37. Lehmann, M. S., Koetzle, T.F., Hamilton, W. J., *Cryst. Mol. Struct.*, **1972**, 2, 225-233.

38. Bernstein, J., Polymorphism in Molecular Crystals - IUCr monographs on Crystallography, No. 14, **2002**, Clarendon Press, Oxford, 49-50.

39. Etter, M. C., Macdonald, J. C., Bernstein, J., *Acta Crystallogr*, **1990**, B46, 256-262.

40. Bernstein, J., Davis, R. E., Shimoni, L., Chang, N-L., *Angew. Chem., Int. Ed. Engl.*, **1995**, 34, 1555-1573.

41. Szejtli, J., In: *Topics in Inclusion Science – Cyclodextrin Technology*, Davies, J. E. D. (Eds.), **1988**, Kluwer Academic Publishers, Dordrecht, The Netherlands.

42. Cramer, F., *Einschlussverbindungen (Inclusion Compounds)*, **1954**, Springer-Verlag, Berlin.

43. Takaha, T., Yanase, M., Takata, S., Okada, S., Smith, S. M., *J. Biol. Chem.*, **1996**, 271, 2902.

44. Sundararajan, P. R., Rao, V. S. R., *Carbohydrate Res.*, **1970**, 13, 351.

45. Nakagawa, T., Ueno, K., Kashiwa, M., Watanabe, J., In: *Proceedings of the 7th International Symposium on Cyclodextrins, Tokyo, April 25-28, 1994*, Osa, T. (Ed.), **1994**, Publ. Office, Acad. Soc. Japan, Tokyo, 114.

46. Villiers, A., *Compt. Rend.*, **1891**, 112, 536.

47. Schardinger, F., *Z. Untersuch. Nahr. u. Genussm.*, **1903**, 6, 865.

48. Schardinger, F., *Wien. klin. Wochschr.*, **1904**, 17, 207.

49. Schardinger, F., *Zentralbl. Bakteriol. Parasintenkd.*, **1905**, 14, 772.

50. Schardinger, F., Zentralbl. Bakteriol. Parasintenkd., Infektionskrankh. Hyg. Abt. 2 Naturwiss: Mikrobiol. Landwirtsch. Technol. Umweltschutzes, **1911**, 29, 188.

51. Freudenberg, K., Rapp, W., *Ber. Dtsch. Chem. Ges.*, **1936**, 69, 2041.

52. Freudenberg, K., Boppel, H., Meyer-Delius, M., *Naturwissenschaften*, **1938**, 26, 23.

53. Freudenberg, K., Meyer-Delius, M., *Ber. Dtsch. Chem. Ges.*, **1938**, 71, 1596.

54. Karrer, P., Nägeli, C., *Helv. Chim. Acta*, **1921**, 4, 169.

55. Miekeley, A., *Ber. Dtsch. Chem. Ges.*, **1932**, 65, 69.

56. Freudenberg, K., Blomquist, G., Ewald, L., Soff, K., *Ber. Dtsch. Chem. Ges.*, **1936**, 69, 1258.

57. French, D., *Adv. Carbohydrate Chem.*, **1957**, 12, 189.
58. Szejtli, J., In: *Comprehensive Supramolecular Chemistry - Cyclodextrins*, Szejtli, J., Osa, T. (Eds.), **1996**, 3, 2.
59. Saenger, W., *Angew. Chem., Int. Ed. Engl.*, **1980**, 19, 344.
60. Saenger, W., In: *Inclusion Compounds*, Atwood, J. L., Davies, J. E. D., MacNicol, D. D. (Eds.), **1984**, Oxford University Press, London, 2, Ch 8.
61. Harata, K., In: *Inclusion Compounds*, Atwood, J. L., Davies, J. E. D., MacNicol, D. D. (Eds.), **1984**, Oxford University Press, London, 5, Ch 9.
62. Saenger, W., Betzel, C., Hingerty, B. E., Brown, G. M., *Nature*, **1982**, 296, 581.
63. Saenger, W., Betzel, C., Hingerty, B. E., Brown, G. M., *Angew. Chem., Int. Ed. Engl.*, **1983**, 22, 883.
64. Harata, K., Uekama, K., Otagiri, M., Hirayama, F., *J. Inclusion Phenom.*, **1984**, 1, 279.
65. Lipkowitz, K., B., Green, K., Yang, J., *Chirality*, **1992**, 4, 205.
66. Lichtenthaler, F.W., Immel, S., *Starch*, **1996**, 48, 225.
67. Lichtenthaler, F.W., Immel, S., *Liebigs Ann.*, **1996**, 27.
68. Harata, K., *Bull. Chem. Soc. Jpn.*, **1979**, 52, 2451.
69. Manor, P. C., Saenger, W., *J. Am. Chem. Soc.*, **1976**, 96, 3630.
70. Lindner, K., Saenger, W., *Carbohydr. Res.*, **1982**, 99, 103.
71. Harata, K., *Bull. Chem. Soc. Jpn.*, **1987**, 60, 2763-2767.
72. Szejtli, J., *Chem. Rev.*, **1998**, 98, 1743-1753.
73. Bender, M. I., Komiyama, M., *Cyclodextrin Chemistry*, **1976**, Springer-Verlag, Berlin.
74. Rekharsky, M. V., *Inoue, Y., Chem. Rev.*, **1998**, 98, 1875.
75. Liu, L., Guo, Q-X., *J. Inclusion Phenom. Macrocyclic Chem.*, **2002**, 42, 1-14.
76. Kitagawa, M., Hoshi, H., Sakurai, M., Inoue, Y., Chûjô, R., *Bull. Chem. Soc. Jpn.*, **1988**, 61, 4225.
77. Sakurai, M., Kitagawa, M., Hoshi, H., Inoue, Y., Chûjô, R., *Chem. Lett.*, **1988**, 895.
78. Lichtenthaler, F. W., Immel, S., *Starch*, **1996**, 48, 145.

79. Frömming, K-H., Szejtli, J., In: *Topics in Inclusion Science – Cyclodextrins in Pharmacy*, **1993**, Kluwer Academic Publishers, Dordrecht, The Netherlands, Vol. 5.

80. Caira, M. R., *Revue Roumaine de Chemie*, **2001**, 46, 371-386.

81. Kálmán, A., Párkányi, L., In: *Advances in Molecular Structure Research*, JAI Press Inc., **1997**, 189-226.

82. Fábián, L., Kálmán, A., *Acta Crystallogr.*, **1999**, B55, 1039-1049.

83. Dodds, D. R., PhD Thesis, Physicochemical Study of Inclusion of Drug Molecules in Cyclodextrins, **1999**, University of Cape Town, South Africa.

84. Cambridge Structural Database and Cambridge Structural Database System, Version 5.25, November **2003** (updates April 2004), Cambridge Crystallographic Data Centre, University Chemical Laboratory, Cambridge, England.

85. Caira, M. R., Bourne, S.A., Vilakazi, S. L., Reddy, L., *Supramol. Chem.*, **2004**, 16, 279-285.

86. Caira, M.R., Hunter, R., Bourne S.A., Smith V.J., *Supramol. Chem.*, (in press **2004**).

87. Uekama, K., Irie, T., In: *Comprehensive Supramolecular Chemistry - Cyclodextrins*, Szejtli, J., Osa, T. (Eds.), BPC Wheatons Ltd., Exeter, U.K., **1996**, 3, Ch. 15.

88. Duchêne, D., In: *Cyclodextrins and Their Industrial Uses*, de Santé (Ed.), **1987**, Paris, France.

89. Brewster, M. E., In: Duchêne, D. (Ed), *New Trends in Cyclodextrins and Derivatives*, Editions de Santé, Paris, France, **1991**.

90. Ohtani, Y., Uekama, K., Fukunaga, K., Pitha, J., *Eur. J. Biochem.*, **1989**, 186, 117.

91. Waldeck, B., *Eur. J. Pharmacol.*, **2002**, 445, 1-12.

92. Bullowa, J. G. M., Kaplan, D. M., *Med. News*, **1903**, 83, 787–790.

93. Konzett, H., *Naunyn-Schmiedeberg's Arch.*, **1940**, 127, 27-40.

94. Brittain, R. T., Farmer, J. B., Jack, D., Martin, L. E., Simpson, W. T., *Nature (London)*, **1968**, 219, 862–863.

95. Cullum, V. A., Farmer, J. B., Jack, D., Levy, G. P., *Br. J. Pharmacol.*, **1969**, 35, 141–151.

96. Bergman, J., Persson, H., Wetterlin, K., *Experientia*, **1969**, 25, 899-901.

97. Persson, H., Olsson, T., *Acta Med. Scand.*, **1970**, 512, 11-19.

98. *The Merck Index*, 12th edition, S. Budavari (Ed.), **1996**, Merck & Co., Inc., Whitehouse Station, NJ, U.S.A., 9940.

99. Kubo, S., Kasé, Y., Miyata, T., Kito, G., Uesaka, I., *Arzneim. Forsch.*, **1975**, 25, 1028–1037.

100. Yoshihara, S., Yamada, Y., Abe, T., Arisaka, O., *Allergology International*, **2004**, 53, 69.

101. Saito, M., Yabu, H., Yamazaki, M., Matsumura, K., Kato, H., *Chem. Pharm. Bull.*, **1982**, 30, 652-658.

102. Harada, Y., Saito, M., Matsumura, K., Kato, H., Iitaka, Y., *Chem. Pharm. Bull.*, **1982**, 30, 2301-2312.

103. Soft Imaging System GmbH, *Digital Solutions for Imaging and Microscopy*, Version 3.1 for Windows (Copyright **1987-2000**).

104. Bernstein, J., Polymorphism in Molecular Crystals - IUCr monographs on Crystallography, No. 14, **2002**, Clarendon Press, Oxford, 144-146.

105. Bernstein, J., Polymorphism in Molecular Crystals - IUCr monographs on Crystallography, No. 14, **2002**, Clarendon Press, Oxford, 133.

106. Paratone N oil (Exxon Chemical Co., Texas, U.S.A.)

107. Stout, G. H., Jensen, L. H., *X-ray Structure Determination: a Practical Guide*, © **1989**, John Wiley & Sons, Inc., Ch 5.

108. Otwinowski, Z., Minor, W., In: *Processing of X-ray Diffraction Data in Oscillation Mode in Methods in Enzymology*, Carter, C. W., Sweet, R. M (Eds.), **1996**, Academic Press, New York, 276, 307.

109. *Data Preparation and Reciprocal Space Exploration*, Version 5.1, (Copyright Bruker Analytical X-ray Systems, **1997**).

110. Sheldrick, G. M., *SHELXS-97, Program for Crystal Structure Solution*, Institüt für Anorganische Chemie der Universität, Tammanstrasse 4, D-3400 Göttingen, Germany, **1997**.

111. Sheldrick, G. M., In: *Direct Methods for Solving Macromolecular Structures*, Dordrecht (Ed.), Kluwer Academic Publishers, **1998**, 401-411.

112. Sheldrick, G. M., *SHELXL-97, Program for the Refinement of Crystal Structures*, Institüt für Anorganische Chemie der Universität, Tammanstrasse 4, D-3400 University of Göttingen, Germany, **1997**.

113. Barbour, L.J., *X-SEED, A graphical interface to SHELX*, University of Missouri, Columbia, U.S.A., **1999**.

114. Miller, R., Weeks, C. M., In: *Direct Methods for Solving Macromolecular Structures*, Dordrecht (Ed.), Kluwer Academic Publishers, **1998**, 389-400.

115. Usón, I., Sheldrick, G. M., *Curr. Op. Struct. Biol.*, **1999**, 9, 643-648.

116. Yvon, K., Jeitschko, W., Parthé, E., *J. Appl. Cryst.*, **1977**, 10, 73.

117. Barbour, L. J., LAYER, A computer program for the graphic display of intensity data as simulated precession photographs, J. Appl. Cryst., **1999**, 32, 351.

118. *Pov-Ray for Windows*, Version 3.1e.watcom.win32, The persistence of vision development Team, © **1991-1999**.

119. *Weblab Viewer Pro*, Version 3.5, Molecular Simulations Inc., ©**1999**, San Diego, CA.

120. Farrugia, L. J., *Ortep-3 for Windows, J. Appl. Cryst.*, **1997**, 30, 565.

121. Spek, A. L., *PLATON*, A multipurpose crystallographic tool, Version 10500 © **1980-2000**.

122. Bernstein, J., Polymorphism in Molecular Crystals - IUCr monographs on Crystallography, No. 14, **2002**, Clarendon Press, Oxford, 41.

123. Herbstein, F. H., Marsh, R. E., *Acta Crystallogr.*, **1998**, B54, 677-686.

124. Marsh, R. E., Kapon, M., Hu, S., Herbstein, F., H., *Acta Crystallogr.*, **2002**, B58, 62-77.

125. Mentzafos, D., Mavridis, I. M., le Bas, G., Tsoucaris, G., *Acta Crystallogr.*, **1991**, B47, 746-757.

126. Makedonopoulou, S., Mavridis, I. M., *Acta Crystallogr.*, **2000**, B56, 322-331.

127. De Vries, *PhD Thesis, Inclusion of Alkylparabens in Cyclodextrins*, **2003**, University of Cape Town, South Africa.

128. le Bas, G., Tsoucaris, G., *Supramol. Chem.*, **1994**, 4, 13.

129. Saenger, W., *J. Inclusion Phenom.*, **1984**, 2, 445.

130. le Bas, G., Tsoucaris, G., *Mol. Cryst. Liq. Cryst.*, **1986**, 137, 287-301.

131. le Bas, G., Rysanek, N., Tsoucaris, G., *Minutes: International Symposium on Cyclodextrins*, de Santé (Eds.) **1990**, Paris, 114.

132. Steiner, T., Saenger, W., *Acta Crystallogr.*, **1998**, B54, 450-455.

133. Caira, M. R., Bourne, S. A., Mvula, E., *J. Therm. Anal. Calorim.*, **1999**, 56, 1329-1334.

134. Ding, J., Steiner, T., Saenger, W., *Acta Crystallogr.*, **1991**, B47, 731-738.

135. Giacovazzo, C., *SIR2002, Program for Crystal Structure Solution*, **2002**, Inst. di Ric. per lo Sviluppo di Metodologie Cristallografiche, CNR, Univ. of Bari, Italy.

136. Beurskens, P. T., Beurskens, G., de Gelder, R., Garcia-Granda, S., Gould, R. O., Israel, R. Smits, J. M. M., **1999**, *The DIRDIF-99 program system*, Technical Report of the Crystallography Laboratory, University of Nijmegen, The Netherlands.

137. Egert, E, Sheldrick, G., *Acta Crystallogr*, **1985**, A41, 262-268.

138. Mvula, E. N., MSc Thesis, Preparation and Solid State Properties of Cyclodextrin Complexes of Selected Drug Molecules, **1999**, University of Cape Town, South Africa.

139. Caira, M. R., Griffith, V. J., Nassimbeni, L. R., van Oudtshoorn, B., *Supramol. Chem.*, **1996**, 7, 119-124.

140. Caira, M. R., Bourne, S. A., Mhlongo, W. T., Dean, P. M, *Chem. Commun.*, **2004**, Advance Article., DOI: 10.1039/b408660k.

141. Harata, K., Uekama, K, Otagiri, M., Hirayama, F., *Bull. Chem. Soc. Japan.*, **1983**, 56, 1732-1736.

142. Saenger, W., In: *Inclusion Compounds*, Atwood, J.L., Davies, J. E. D., MacNicol, D. D (Eds.), Oxford University Press, London, **1984**, 2, 231.

143. Caira, M. R., Griffith, V. J., Nassimbeni, L. R., van Oudtshoorn, B., *J. Chem. Soc. Perkin Trans. 2*, **1994**, 2071-2073.

144. Rontoyianni, A., Mavridis, I. M, *J. Inclusion Phenom. Macrocyclic Chem.*, **2001**, 32, 415-428.

145. Makedonopoulou, S., Yannakopoulou, K, Mentzafos, D., Lamzin, V., Popov, A., Mavridis, I. M., *Acta Crystallogr.*, **2001**, B57, 399-409.

146. Cardinael, P., Peulon, V., Perez, G., Coquerel, G., Toupet, L., *J. Inclusion Phenom. Macrocyclic Chem.*, **2001**, 39, 159-167.

147. Harata, K., Uekama, K., Imai, T., Hirayama, F., Otagiri, M., *J. Inclusion Phenom.*, **1988**, 6, 443-460.

148. Harata, K., Hirayama, F., Arima, H., Uekama, K., Miyaji, T., *J. Chem. Soc., Perkin Trans. 2*, **1992**, 1159-1166.

149. Mentzafos, D., Mavridis, I. M., Schenk, H., *Carbohydr. Res.*, **1994**, 253, 39-50.

150. Brown, G., Caira, M. R., Nassimbeni, L. R., *J. Inclusion Phenom. Mol. Recognit. Chem.*, **1996**, 26, 281-294.

151. Caira, M. R., Griffith, V. J., Nassimbeni, L. R., van Oudtshoorn, B., *J. Inclusion Phenom. Mol. Recognit. Chem.*, **1995**, 20, 277-290.

152. Caira, M. R., Bourne, S. A., Mvula, E. N., *Biolog. J. Armenia, Special Issue: Cyclodextrins*, **2001**, 148-158.

153. Caira, M. R., Bourne, S. A., Giordano, F., Vilakazi, S. L., *Supramol. Chem.*, **2004**, in press.

154. Harata, K., *Chem. Rev.*, **1998**, 98, 1803-1827.

155. Saito, M., Harada, Y., Matsumura, K., Kato, H., Ito, Y., Hori, T., *Chem. Pharm. Bull.*, **1983**, 31, 1460-1468.

156. Horiguchi, T., Kondo, R., Miyazaki, J., Fukumokto, K., Torigoe, H., *Arzneim. Forsch.*, **2004**, 54, 280-285.

157. Matsuda, H., Arima, H., *Advanced Drug Delivery Reviews*, **1999**, 36, 81-99.

Appendix

Appendix

Supplementary crystallographic information on each of the solved structures in this thesis has been stored in the folder 'Appendix A' on a compact disk, attached to the inside cover of this thesis. The files pertaining to a particular structure are stored in a subfolder that is named according to the structure abbreviation that was used in the thesis. Each subfolder contains seven text files that can be opened in a text editor such as Windows98 WORDPAD. The files contain the following information.

File	Information
.HKL	Reflection data
.RES	SHELX type coordinate file
.CIF	Crystallographic Information File
.FCF	Structure factor tables
.XL	SHELX output file
.LIS	PLATON output file listing all geometric parameters of a structure
.SUP	PLATON output file summarising selected information from .LIS file in tabulated form